

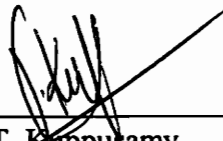
# MULTIPHASE FLOW AND MASS TRANSPORT THROUGH POROUS MEDIA

by

Kevin P. Snyder

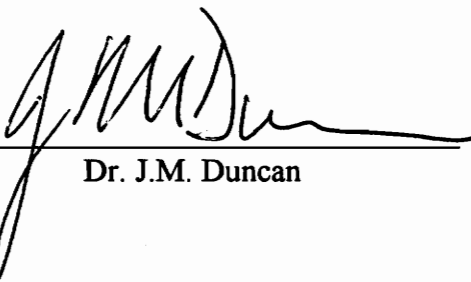
Thesis submitted to the Faculty of the  
Virginia Polytechnic Institute and State University  
in partial fulfillment of the requirements for the degree of  
Master of Science  
in  
Civil Engineering

APPROVED:



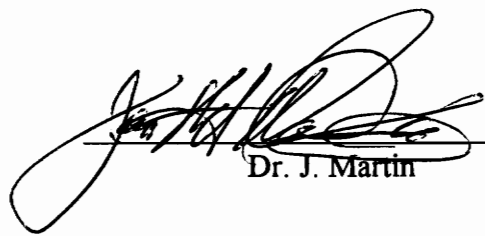
---

Dr. T. Ruppusamy



---

Dr. J.M. Duncan



---

Dr. J. Martin

June, 1993

Blacksburg, Virginia

C.2

LD  
5655  
V855  
1993  
5669  
C.2



# **MULTIPHASE FLOW AND MASS TRANSPORT THROUGH POROUS MEDIA**

by

Kevin P. Snyder

Dr. T. Kuppusamy

Civil Engineering

(ABSTRACT)

The migration of organic contaminants in the subsurface, due to leaking underground storage tanks, includes both discrete and dissolved phase plume movements through the porous media. Such problems always involve the multiphase flow and mass transport through three phases, namely air, oil, and water. A finite element model is developed in this thesis based on the theory of multiphase flow weakly-coupled with the theory of mass transport, in a three-dimensional setting. Galerkin's method is employed to derive the finite element formulations for multiphase flow and mass transport based on the appropriate governing differential equations. The equations for multiphase flow are based on van Genuchten's model for unsaturated flow for air and water. In this model, the saturation-pressure-conductivity relations are used to obtain the constitutive behavior. The solution procedure of the resulting time dependent nonlinear equation involves using a general  $\theta$ -scheme, for time integration, and a modified Picard's method, for nonlinear iteration. The governing equation for mass transport in a three-phase system is derived based on the assumption of linear partitioning between the air, oil, water, and solid phases. The equations for flow and transport are weakly-coupled through the time lagged interphase mass transfer term. A computer program called IMFTP3D is developed. The program can solve problems related to (1) multiphase immiscible flow, (2) diffusion without flow, and (3) multiphase flow weakly-coupled with mass transport. The three-dimensional model is validated for all three options based on previous two-dimensional models and laboratory experiments present in the literature.

Laboratory experiments were conducted involving gasoline movements through both a one-dimensional column and a two-dimensional flume. The computer program, IMFTP3D, was then used to investigate the usefulness of the model in predicting water outflow in for the column problem and plume movements in the flume experiment.

## **ACKNOWLEDGMENTS**

I first wish to thank Professor Kuppusamy for his guidance, patience, and his encouragement. In addition, I would like to thank all of the faculty members for their help with course work and theoretical problems, with special thanks directed to Professor Duncan and Dr. Martin for serving as members on my committee.

I would also like to thank my parents Joan Adams, Tom Adams, and Richard Snyder, for their help and support throughout my college career.

# TABLE OF CONTENTS

CHAPTER 1: INTRODUCTION.....	1
CHAPTER 2: MULTIPHASE IMMISCIBLE FLOW .....	7
INTRODUCTION.....	7
DARCY'S LAW .....	10
FLUID-SOLID RELATIONS .....	15
FLUID CONTENT VS. PRESSURE HEAD .....	16
SCALING TWO-PHASE SYSTEMS .....	23
THEORY OF UNSATURATED FLOW .....	27
VAN GENUCHTEN'S MODEL FOR UNSATURATED FLOW .....	30
THEORY OF MULTIPHASE IMMISCIBLE FLOW.....	37
SATURATION-CAPILLARY HEAD RELATIONS .....	37
VERTICAL EQUILIBRIUM IN A THREE-PHASE SYSTEM .....	40
FLUID CONDUCTIVITY RELATIONS .....	43
GOVERNING EQUATIONS OF MULTIPHASE IMMISCIBLE FLOW .....	45
CONCLUSIONS .....	51
CHAPTER 3: FINITE ELEMENT MODEL FOR MULTIPHASE FLOW .....	53
INTRODUCTION.....	53
FORMULATION FROM GOVERNING EQUATIONS.....	53
TIME INTEGRATION TECHNIQUE.....	58
ITERATION FOR NONLINEARITY.....	59
INVESTIGATION OF CONVERGENCE .....	63
CONCLUSIONS .....	68
CHAPTER 4: VALIDATION OF 3-D MULTIPHASE FLOW MODEL.....	69
INTRODUCTION .....	69
EXAMPLE 4.1 .....	70

EXAMPLE 4.2 .....	76
SIMULATIONS OF A FULLY THREE-DIMENSIONAL PROBLEM.....	83
EXAMPLE 4.3 .....	83
CONCLUSIONS .....	94
CHAPTER 5: EXPERIMENTAL STUDY .....	96
INTRODUCTION .....	96
COLUMN TEST .....	97
PROCEDURE.....	97
COLUMN TEST RESULTS .....	101
FINITE ELEMENT SIMULATION OF THE COLUMN EXPERIMENT.....	104
FLUME TEST.....	108
PROCEDURE.....	108
FLUME TEST RESULTS.....	111
FINITE ELEMENT SIMULATION OF FLUME EXPERIMENT.....	115
VARIATION IN OUTFLOW DUE TO PARAMETER SELECTION.....	119
VARIATIONS DUE TO THE SELECTION OF VAN GENUCHTEN'S PARAMETER.....	122
CONCLUSIONS .....	124
CHAPTER 6: THREE-DIMENSIONAL MASS TRANSPORT .....	125
INTRODUCTION .....	125
MASS TRANSPORT PROCESSES.....	126
CONVECTION .....	130
EQUATION DEVELOPMENT FOR CONVECTION .....	131
DIFFUSION .....	133
EQUATION DEVELOPMENT FOR DIFFUSION .....	135
MECHANICAL DISPERSION .....	136
EQUATION DEVELOPMENT FOR MECHANICAL DISPERSION .....	139
COMBINED EQUATIONS OF CONVECTIVE-DISPERSIVE TRANSPORT .....	145

FINITE ELEMENT FORMULATION FOR DIFFUSION .....	147
TIME INTEGRATION METHOD .....	149
EXAMPLE 6.1 .....	150
CONCLUSIONS .....	153
CHAPTER 7: MULTIPHASE FLOW COUPLED WITH MASS TRANSPORT .....	154
INTRODUCTION .....	154
GOVERNING EQUATIONS FOR MULTIPHASE MASS TRANSPORT .....	156
COMPONENT PROPERTIES.....	161
LINEAR PARTITION COEFFICIENTS .....	161
RADIOACTIVE DECAY COEFFICIENTS .....	165
FINITE ELEMENT FORMULATION .....	165
TIME INTEGRATION SCHEME .....	167
ITERATION FOR NON LINEARITY .....	168
SOLUTION PROCEDURE .....	168
CONCLUSIONS .....	169
CHAPTER 8: VALIDATION OF WEAKLY-COUPLED FORMULATION .....	171
INTRODUCTION .....	171
EXAMPLE 8.1 .....	171
CONCLUSIONS .....	205
CHAPTER 9: SUMMARY AND CONCLUSIONS .....	207
REFERENCES .....	211

## LIST OF ILLUSTRATIONS

Figure 2.1 Relationship between wetting and nonwetting fluids in a pore space.....	17
Figure 2.2 Meniscus showing the principle radii of curvature (Bear 1972).....	20
Figure 2.3 Variation in contact angle due to movement direction of fluid-fluid interface (Bear 1972) .....	21
Figure 2.4 Water content versus capillary head for drainage and imbibition .....	22
Figure 2.5 Unscaled water content-pressure head relations (Parker et al. 1987) .....	25
Figure 2.6 Scaled water content-pressure head relations (Parker 1987).....	26
Figure 2.7 Elemental control volume for the flow of water through porous material .....	28
Figure 2.8 Saturation-pressure relation for various values of van Genuchten's parameter alpha .....	35
Figure 2.9 Saturation-pressure relation for various values of van Genuchten's parameter n .....	35
Figure 2.10 Relationship between wetting, intermediate, and nonwetting fluids in a pore space.....	39
Figure 2.11 Saturation distribution for a system in vertical equilibrium.....	42
Figure 2.12 Relative oil and water permeabilities (Sheng 1986) .....	44
Figure 3.1 Example depicting the solution technique used in the Picard's method .....	61
Figure 3.2 Example depicting the solution technique used in the modified Picard's method .....	62
Figure 3.3 Plot of unknowns converging vs. time step for the first output interval .....	66
Figure 3.4 Comparison of water outflow versus time for the different revised Picard's methods used in the simulation of the experimental column example .....	66
Figure 3.5 Comparison of water outflow versus time for the different revised Picard's methods .....	67
Figure 4.1 Three-dimensional finite element mesh for Example 4.1 .....	72
Figure 4.2 Comparison of water outflow versus time for two-and three-dimensional simulations with experimental data.....	73
Figure 4.3 Comparison of two- and three-dimensional models for time = 0.01 hours.....	74
Figure 4.4 Comparison of two- and three-dimensional models for time = 0.1 hours.....	74
Figure 4.5 Comparison of two- and three-dimensional models for time = 1.0 hours.....	75

Figure 4.6 Comparison of two- and three-dimensional models for time = 10 hours.....	75
Figure 4.7 Comparison of two- and three-dimensional models for time = 100 hours.....	76
Figure 4.8 Two-dimensional finite element mesh (Example 4.2) .....	77
Figure 4.9 Three-dimensional finite element mesh (Example 4.2) .....	78
Figure 4.10 2-D Mesh - Elements with greater than zero oil saturation after 153 days.....	79
Figure 4.11 2-D Mesh - Elements with greater than zero oil saturation after 535 days.....	79
Figure 4.12 2-D Mesh - Elements with greater than zero oil saturation after 1600 days.....	80
Figure 4.13 3-D Mesh - Elements with greater than zero oil saturation after 153 days.....	80
Figure 4.14 3-D Mesh - Elements with greater than zero oil saturation after 535 days.....	80
Figure 4.15 3-D Mesh - Elements with greater than zero oil saturation after 1600 days.....	81
Figure 4.16 Comparison of 2- and 3-dimensional models on Basis of oil inflow (Example 4.2) .....	82
Figure 4.17 Comparison of 2- and 3-dimensional models on Basis of water outflow (Example 4.2) .....	82
Figure 4.18 Three-dimensional finite element mesh (Example 4.3) .....	86
Figure 4.19 Oil plume at the end of 82.2 days .....	87
Figure 4.20-a Oil plume at the end of 153 days .....	88
Figure 4.20-b Oil plume at end of 153 days, center cross-section .....	89
Figure 4.20-c Oil plume at end of 153 days, rear cross-section .....	90
Figure 4.21-a Oil plume at end of 256 days .....	91
Figure 4.21-b Oil at end of 256 days, center cross-section.....	92
Figure 4.2-c Oil plume at end of 256 days, rear cross-section .....	93
Figure 5.1 Column testing device .....	98
Figure 5.2 Three-dimensional finite element mesh used to run simulations with experimental column outflow data.....	106
Figure 5.3 Plot of best fit finite element analysis for parameters shown in Table 5 with the experimental data from the column test.....	107
Figure 5.4 Experimental flume used to examine the movement of gasoline (Gibson 1991) .....	109



Figure 5.5 Picture taken of flume testing apparatus at initial condition.....	110
Figure 5.6 Picture of flume test during an early stage in the experiment.....	111
Figure 5.7 Picture of flume test during an intermediate stage in the experiment .....	112
Figure 5.8 Picture of flume test during a later stage in the experiment.....	112
Figure 5.9 Gasoline plume movement for a constant head water level during flume experiment (Gibson 1991).....	113
Figure 5.10 Gasoline plume movement for a water level caused by a hydraulic gradient in flume experiment (Gibson 1991).....	114
Figure 5.11 Finite element mesh for simulations based on the flume experiment .....	117
Figure 5.12 Results of finite element simulation for flume experiment at 15 seconds.....	118
Figure 5.13 Plot showing simulations for 5 cases involving variations in scaling parameters $\beta_{ow}$ and $\beta_{ao}$ .....	120
Figure 5.14 Plot showing simulations for 3 cases involving variations in scaling parameter $\beta_{ow}$ .....	120
Figure 5.15 Plot showing simulations for 3 cases involving variations in scaling parameter $\beta_{ao}$ .....	121
Figure 5.16 Comparison of water outflow for van Genuchten's parameter $\alpha$ .....	123
Figure 5.17 Comparison of water outflow for van Genuchten's parameter $n$ .....	123
Figure 6.1 Depiction of concentration breakthrough curve for plug flow and convection- dispersion (EPA 1989) .....	128
Figure 6.2 Two-dimensional depiction of convection and diffusion.....	129
Figure 6.3 Two-dimensional depiction of convection and dispersion (EPA 1989) .....	129
Figure 6.4 Three-dimensional finite element mesh (Example 6.1).....	152
Figure 8.1 Two-dimensional finite element mesh used for the multiphase flow and pollutant transport problem.....	173
Figure 8.2 Three-dimensional finite element mesh used in the multiphase flow and transport problem.....	173
Figure 8.3 Section of the two-dimensional domain used in comparing selected two- and three- dimensional simulations.....	174

Figure 8.4 Oil plume movement after 100 days .....175

Figure 8.5 Oil plume movement after 100 days (3-D simulation).....175

Figure 8.6 Dissolved plume movement after 100 days .....176

Figure 8.7 Dissolved Plume movement after 100 days (3-D simulation) .....176

Figure 8.8 Dissolved plume movement after 100 days .....177

Figure 8.9 Dissolved plume movement after 100 days (3-D simulation).....177

Figure 8.10 Dissolved plume movement after 100 days .....178

Figure 8.11 Dissolved plume movement after 100 days (3-D simulation).....178

Figure 8.12 Dissolved plume movement after 100 days .....179

Figure 8.13 Dissolved plume movement after 100 days (3-D simulation).....179

Figure 8.14 Dissolved plume movement after 100 days .....180

Figure 8.15 Dissolved plume movement after 100 days (3-D simulation).....180

Figure 8.16 Oil plume movement after 512 days.....181

Figure 8.17 Oil plume movement after 512 days (3-D simulation).....181

Figure 8.18 Dissolved plume movement after 512 days .....182

Figure 8.19 Dissolved plume movement after 512 days (3-D simulation).....182

Figure 8.20 Dissolved plume movement after 512 days .....183

Figure 8.21 Dissolved plume movement after 512 days (3-D simulation).....183

Figure 8.22 Dissolved plume movement after 512 days .....184

Figure 8.23 Dissolved plume movement after 512 days (3-D simulation).....184

Figure 8.24 Dissolved plume movement after 512 days .....185

Figure 8.25 Dissolved plume movement after 512 days (3-D simulation).....185

Figure 8.26 Dissolved plume movement after 512 days .....186

Figure 8.27 Dissolved plume movement after 512 days (3-D simulation).....186

Figure 8.28 Oil plume movement after 983 days.....187

Figure 8.29 Oil plume movement after 983 days (3-D simulation).....187

Figure 8.30 Dissolved plume movement after 983 days .....188

Figure 8.31 Dissolved plume movement after 983 days (3-D simulation)..... 188

Figure 8.32 Dissolved plume movement after 983 days ..... 189

Figure 8.33 Dissolved plume movement after 983 days (3-D simulation)..... 189

Figure 8.34 Dissolved plume movement after 983 days ..... 190

Figure 8.35 Dissolved plume movement after 983 days (3-D simulation)..... 190

Figure 8.36 Dissolved plume movement after 983 days ..... 191

Figure 8.37 Dissolved plume movement after 983 days (3-D simulation)..... 191

Figure 8.38 Dissolved plume movement after 983 days ..... 192

Figure 8.39 Dissolved plume movement after 983 days (3-D simulation)..... 192

Figure 8.40 Dissolved plume movement after 983 days ..... 192

Figure 8.41 Oil plume movement after 95 days ..... 193

Figure 8.42 Dissolved phase movement after 95 days ..... 194

Figure 8.43 Dissolved phase movement after 95 days ..... 194

Figure 8.44 Oil plume movement after 512 days..... 194

Figure 8.45 Dissolved phase movement after 512 days ..... 195

Figure 8.46 Dissolved phase movement after 512 days ..... 195

Figure 8.47 Dissolved phase movement after 512 days ..... 195

Figure 8.48 Dissolved phase movement after 512 days ..... 196

Figure 8.49 Oil plume movement after 983 days..... 196

Figure 8.50 Dissolved phase movement after 983 days: ..... 196

Figure 8.51 Dissolved phase movement after 983 days ..... 197

Figure 8.52 Dissolved phase movement after 983 days ..... 197

Figure 8.53 Dissolved phase movement after 983 days ..... 197

Figure 8.54 Oil plume saturation after 95 days ..... 198

Figure 8.55 Dissolved phase movement after 95 days ..... 199

Figure 8.56 Dissolved phase movement after 95 days ..... 199

Figure 8.57 Dissolved phase movement after 95 days ..... 200

Figure 8.58 Dissolved phase movement after 95 days .....200

Figure 8.59 Dissolved phase movement after 95 days .....200

Figure 8.60 Dissolved phase movement after 95 days .....201

Figure 8.61 Oil plume movement after 512 days.....201

Figure 8.62 Dissolved phase movement after 512 days .....201

Figure 8.63 Dissolved phase movement after 512 days .....202

Figure 8.64 Dissolved phase movement after 512 days .....202

Figure 8.65 Dissolved phase movement after 512 days .....202

Figure 8.66 Dissolved phase movement after 512 days .....202

Figure 8.67 Dissolved phase movement after 512 days .....203

Figure 8.68 Oil plume movement after 983 days.....203

Figure 8.69 Dissolved phase movement after 983 days .....203

Figure 8.70 Dissolved phase movement after 983 days .....204

Figure 8.71 Dissolved phase movement after 983 days .....204

Figure 8.72 Dissolved phase movement after 983 days .....204

Figure 8.73 Dissolved phase movement after 983 days. ....205

## LIST OF TABLES

Table 2.1 Comparison of measured and predicted scaling factors of two-phase systems .....	25
Table 2.2 Model parameters for an air-water system.....	36
Table 3.1 Comparison of convergence achieved for the different revised Picard's methods between time output levels of 1 and 60 seconds .....	67
Table 4.1 Material Properties and Parameters for Example 4.1.....	72
Table 4.2 Material Properties and Parameters for Example 4.2.....	78
Table 5.1 Material properties of Monterey #0/30 sand used in the column and flume experiments.....	96
Table 5.2 Conditions for column tests 1-10 .....	100
Table 5.3 Water/Gas/Vacuum Tests .....	101
Table 5.4 Water/Gas No Vacuum .....	102
Table 5.5 Gas/Gas/No Vacuum .....	103
Table 5.6 Water/Water/No Vacuum .....	103
Table 5.7 Results from lab experiment involving outflow of water due to a know head of oil applied to a saturated soil column.....	104
Table 5.8 Material parameters estimated from column tests on oil and water.....	105
Table 5.9 Parameters used in finite element analysis which resulted in a reasonable estimation with the experimental data obtained from the column experiment .....	107
Table 5.10 Parameters used in finite element analysis which resulted in a reasonable estimation with the experimental data obtained from the flume test.....	116
Table 5.11 Parameters used to investigate the effects of scaling parameters $\beta_{ow}$ and $\beta_{ao}$ .....	119
Table 5.12 Parameters used in investigating the effects of varying van Genuchten's parameters on the outflow of water.....	122
Table 6.1 Longitudinal dispersivity values from various scale experiments.....	138
Table 6.2 Comparison of concentrations from 2-D and 3-D simulations for 1.0 days .....	151
Table 6.3 Comparison of concentrations from 2-D and 3-D simulations for 10 days .....	151

Table 7.1 Properties of common organic contaminants..... 164

Table 7.2 Properties of organic compounds at 20 C ..... 164

Table 8.1 Material Properties/Parameters for multiphase flow portion of Example 8.1..... 172

Table 8.2 Coefficients for mass transport in Example 8.1 ..... 172

# CHAPTER 1

## INTRODUCTION

Contamination of aquifers is a serious problem confronting engineers and scientists today. Contamination can be a result of a variety of legal and illegal practices including: leakage from underground and above ground storage tanks, pipeline transport systems, landfills, industrial waste sites, septic systems, and illegal dump sites. Some of these hazardous wastes are organic fluids such as TCE, PCE, Benzene, Toluene, Xylene, Ethyl dibromide, etc., which are either insoluble or only slightly soluble in water.

Underground storage tanks (USTs) are used extensively in the US for the storage of gasoline. Many of these tanks are constructed of steel and are subject to corrosion if inadequately protected. Unfortunately, many of the existing tanks are not adequately protected and present an extensive environmental hazard. Tejada (1984) reported that about 16,000 of approximately 1.2 million steel underground storage tanks in the US are inadequately protected, and Lehman (1984) estimated that 100,000 storage tanks are presently leaking and another 350,000 will develop leaks in the next five years. Today, the number of failed underground storage tanks is over 1 million, and is a problem that is expected to increase in the future. An article in the Wednesday, March 17, 1993, edition of the USA Today cited examples of sites in which problems already exist. These include:

- (1) a 1-million-gallon leaking tank in East Austin, Texas which has already contaminated more than half of the nearby water wells tested;
- (2) a site in El Segundo, California, where 84 million to 254 million gallons of petroleum spilled at a local Refinery;
- (3) a spill in Tulsa that was estimated at over 38 million gallons; and

(4) a tank farm in Brooklyn, NY that has leaked 17 million gallons.

The ground water contamination problem caused generally involves a complex mixture of multiple organic constituents moving through the subsurface as discrete fluid phases (air, oil, and water). Along with these movements, contaminants may also undergo complex chemical and biodegradable reactions with time. These chemical reactions are important considerations, since many of these contaminants result in serious health problems even at very low concentrations.

The nature and the extent of the contaminant plume movements are relevant questions at the start of every ground water contamination project. Due to the behavior of pollutants in the subsurface environment, the cleanup of contaminated sites not only requires cleanup in the area near the contaminant source but also cleanup downstream and/or upstream from the point source. In order for the cleanup plan to be effective, cost efficient, and complete, it is important that engineers first predict the movement of the contaminant phase and the dissolved plume before remediation begins. The EPA (1989) outlines some of the valuable uses of transport models in the protection and cleanup of ground- and surface-water resources, these include:

- (1) predicting the time of arrival and the concentration of the contaminants at a monitoring well, surface water body, or water supply well;
- (2) designing safe and cost effective waste facilities;
- (3) installing effective monitoring systems; and
- (4) developing effective and cost efficient strategies for the remediation of contaminated aquifers.

Numerical models are generally used to simulate the transport of the contaminant through the different phases in the system, i.e., air, oil, and water. The movement of these contaminants, as a discrete phase or as a portion of the water phase,



throughout the subsurface environment is dependent on the relationships between the contaminant, water table, porous media, and the atmosphere. Until recently, the fundamental impediment has been the substantial lack of information concerning the constitutive relationships governing the movement of these contaminants. The recent development of these relationships, based on van Genuchten's model for unsaturated flow, and the advancements in numerical models have made it possible to predict movements of plumes in non homogeneous domains with complex spatial dimensions and boundary conditions (Parker et al. 1987, Kuppusamy et al. 1987, Kuppusamy and Lien 1987, Sheng 1986). The development of efficient numerical algorithms for such problems, especially the finite element technique, has become very useful in recent years in the attempt of solving the complex theory of multiphase flow and mass contaminant transport through soils.

The research presented in this thesis involves addressing the aspects of contaminant transport described above. The four specific areas that have not been previously studied but are currently being developed include:

- (1) the interphase mass transfer of the flow problem;
- (2) the validity of the linear partitioning, attempted in the previously formulated transport problem;
- (3) the mass balance calculations in the flow and transport problem with evaluation of the 'weak-coupled' flow-transport formulation; and
- (4) the extension of the method used to form two-dimensional problems to three-dimensional problems, including a computer program to aid in further research and analysis.

IMFTP3D is a three-dimensional finite element program that is developed based on the theory to be described in this thesis. The program is used to validate the

formulation presented in this thesis by describing the movement of contaminants via multiphase flow and mass transport. The models contained in IMFTP3D include:

- (1) a three-phase immiscible flow problem, considering the contaminant as a discrete phase;
- (2) a mass transport (diffusion only) problem; and
- (3) a three-phase flow problem weakly-coupled with the mass transport problem.

IMFTP3D utilizes the finite element method to model three-dimensional domains with homogeneous or non homogeneous soil matrix conditions. The program uses eight-noded brick elements and solves the nonlinear and time dependent differential equations for multiphase immiscible flow using a modified version of Picard's Method. The program also solves multiphase flow coupled with mass transport. This is accomplished by first solving for the primary unknowns, oil and water heads, and the corresponding velocity vectors. The velocity vectors are then used in the convective transport portion of the mass transfer equation. Also, an option involving contaminant transport through molecular diffusion without flow calculations is available. The program has been tested on both the IBM RISC 6000 and the IBM Mainframe System.

A review of the current literature and the presentation of the general constitutive relationships for multiphase immiscible flow is presented in Chapter 2. This includes a review of Darcy's law, two-phase saturation-pressure-conductivity relations, and the theory of unsaturated flow based on van Genuchten's model. The two-phase relations are then extended to the theory of three-phase flow.

Chapter 3 reviews the three-dimensional finite element formulation based on the variational method. This chapter also includes a section on time integration, covering the techniques used to solve the time dependent equations for multiphase flow. The final

section in Chapter 3 addresses the basic technique for handling non linearity due to the fluid conductivity and capacity terms and an investigation into how convergence effects the results of finite element simulations.

Validation of the three-dimensional finite element model is presented in Chapter 4 using two example problems. The three-dimensional model for multiphase flow is compared with experimental data taken from current literature in a one dimensional setting. The model is then compared to a previously validated two-dimensional model using a hypothetical UST example problem. A third example is presented to show the effectiveness of the model in a full three-dimensional setting.

Chapter 5 describes an experimental laboratory study involving the flow of gasoline and water through a column and a flume filled with soil. The results of the column and flume tests are compared to the results obtained from the three-dimensional finite element simulations. An investigation on how the multiphase flow scaling coefficients and van Genuchten's parameters effect the results of the three-dimensional simulations, based on outflow of water, is also presented.

In Chapter 6, mass transport with and without phase flow is addressed and the three-dimensional finite element formulation is presented for diffusion only problem. A comparison of the results from a hypothetical problem is used to validate the three-dimensional model based on a two-dimensional model previously presented by Sheng (1986).

Chapter 7 introduces the weakly-coupled formulation involving multiphase flow and mass transport. The theories presented in Chapters 2, 3 and 6 are combined and extended to the coupled formulation. A full discussion of the theory and the three-dimensional finite element formulation is presented. Aspects related to the time integration scheme and the iteration technique for non linearity are also discussed.

In Chapter 8, an example comparing the two- and three-dimensional models for multiphase flow and multicomponent mass transport is presented to validate the three-dimensional formulation. This example includes an investigation into the effects of the partitioning coefficients, used in the transport of contaminant between the air and water phases and between the oil and water phases, on the dissolved and discrete phase plume movements.

The final chapter, Chapter 9, summarizes the work and presents the conclusions of this thesis. Also presented are recommendations for further research and a summary of research planned for the next phase of the study.

## **CHAPTER 2**

### **MULTIPHASE IMMISCIBLE FLOW**

#### **INTRODUCTION**

Multiphase immiscible flow is the study of the behavior of fluids that do not change phase when in contact with each other but instead flow as separate and discrete phases within a porous media. In this thesis, the system considered is an air-oil-water system.

As discussed in the introduction, initially the contaminant may originate from a spill or a leaking underground storage tank. In cases where the volume of the contaminant is small compared to the surface area over which it is traveling, the contaminant will migrate through the unsaturated zone until a residual saturation is reached and contaminant flow as a discrete phase discontinues. The movements in this zone are mainly in the vertical direction, accompanied by some lateral movement, and are governed by capillary forces. In the near vicinity, a gaseous plume may also develop if the contaminant is volatile. This plume can move over a great distance in a short time, due to the low conductivities of gases. Many of these vapors will eventually migrate out of the ground and escape into the atmosphere. In cases where the contaminant vapors are denser than the surrounding air, new and complex conditions may need to be considered. In the present model, the effects of the gaseous phase on the other fluid phases are disregarded, due to the negligible head loss in the gaseous phase as compared to the liquid phases (pressure head for the air phase is considered constant and equal to zero or the

atmospheric pressure). These aspects are discussed further in the section on equation development, later in this chapter.

In situations where the volume of the contaminant spilled or leaking is of sufficient size, the lighter than water non aqueous phase liquid (LNAPL) travels through the unsaturated zone to the vadose zone and possibly down to the water table. Depending on the amount of contaminant, the contaminant then flows in the lateral direction within the vadose zone possibly depressing the water table. This flow is governed by the pressure gradients within the discrete phase and by the capillary forces between the fluids in the system. If the contaminant is denser than water, dense non aqueous phase liquid (DNAPL), the contaminant will migrate through the saturated zone and will flow according to the topography of the subsurface. In either case, a residual saturation of contaminant will be left behind the traveling discrete plume. The residual volume may further contaminate the aquifer by dissolving into the water phase over time. This chapter deals with the discrete movement of the LNAPL and does not cover equations or models related to the transport of the contaminant to the aqueous phase. The mass transport problem relating contaminant transport between the oil phase and other phases in the system is covered in Chapters 6 and 7. The model is not intended for the tracking of DNAPL contaminants, which display an erratic fingering path movement through both the unsaturated and saturated zones (EPA 1989).

The study of multiphase immiscible flow originated in the area of oil exploration engineering. During the twenty year period before analysis was extended to pollutant transport, researchers such as Corey et al. (1956), Snell (1962), Saraf (1966), and Stone (1970, 1973) developed models and measuring techniques to determine the effective saturation for the multiphase flow system as it is encountered in oil exploration.

An increasing concern over our nation's ground water system and the wide failures of underground storage facilities containing low solubility hydrocarbons lead to the extension of the theory of multiphase flow to the movement of discrete contaminants in the subsurface environment. The first detailed analysis of this type was presented by Van Dam (1967). This involved a two-phase analysis related to hydrocarbon pollution by examining contaminant infiltration. Later, Mull (1971) analyzed this infiltration phenomenon and developed a procedure for estimating the extent of lateral movement of hydrocarbons in the subsurface. In 1981, Hochmuth developed a two-dimensional model with the capillary pressure-saturation estimation simplified as a step function. Abriola and Pinder (1985a) derived equations, based on the basic conservation of mass principles, by the application of volume averaging techniques. These equations involve five unknowns: two capillary pressures and three mass fractions and consider the effects of matrix and fluid compressibilities, gravity, phase composition, interphase mass exchange, capillarity, diffusion, and dispersion. Later that year, Faust (1985) incorporated Richard's assumption in using a simplified subset of the three-phase flow equations previously used in petroleum engineering.

The following discussion is based on the research conducted by Parker et al. (1987), Kuppusamy et al. (1987), and Sheng (1986). Here, saturation-pressure-permeability relationships are extended from the unsaturated flow model developed by van Genuchten (1980). This model is used to construct a two-dimensional model for multiphase immiscible flow. Later, Parker and Lenhard (1987) extend the saturation-pressure and permeability-saturation relations to include hysteresis. This accommodates the effects of pore blocking and arbitrary saturation paths, which are not considered here. The model presented in this chapter is based on the theory of unsaturated flow and is an extension of Darcy's law and van Genuchten's model to the three-phase system. The

following discussion begins with a review of Darcy's law and a review of the fluid-solid, fluid-pressure head, and fluid-fluid relations. The discussion then involves a review of the theory of unsaturated flow in an air-water system, including an introduction to van Genuchten's model and the parameters  $\alpha$  and  $n$ . The unsaturated system is then extended to the multiphase flow system and the associated scaling parameters are presented.

## DARCY'S LAW

Ground water flows under two main subsurface conditions: (1) flow through porous materials, and (2) flow through fractured rock. The first condition involves movements through a variety of different materials, including coarse material, such as sand and gravel, and fine material, such as silts and clays. The description of ground water flow, under saturated conditions, was first described as a quantitative science by the French hydraulic engineer Henry Darcy. The well known Darcy's law, an empirical law, was proposed in 1856 based on experimental evidence. Since then, many attempts have been made to explain Darcy's law based on physics, with the most successful attempt being described by the Navier-Stokes Equations (Bear 1972). Darcy's law for an isotropic soil in three-dimensions is described by the following equation:

$$\begin{aligned} v_x &= -K_x \frac{\partial h}{\partial x}, \\ v_y &= -K_y \frac{\partial h}{\partial y}, \quad \text{and} \\ v_z &= -K_z \frac{\partial h}{\partial z}; \end{aligned} \tag{2.1}$$



where

$v_x$ ,  $v_y$ , and  $v_z$  = the Darcy's velocity in the x-, y-, and z-direction, respectively;  
 $K_x$ ,  $K_y$ , and  $K_z$  = the hydraulic conductivity in the x-, y-, and z-direction, which relates the macroscopic equation presented by Darcy to smaller scale behavior that is present in the pore spaces which make up the porous media;

$h$  = the pressure head,

$\frac{\partial h}{\partial x}$  = the hydraulic gradient in the x-direction,

$\frac{\partial h}{\partial y}$  = the hydraulic gradient in the y-direction, and

$\frac{\partial h}{\partial z}$  = the hydraulic gradient in the z-direction.

It is generally excepted that this equation holds for both saturated and unsaturated flow conditions and for both steady state and transient flow problems (Freeze and Cherry, 1979). The fluid conductivity ( $K$ ) is a function of the intrinsic permeability ( $k$ ), the density ( $\rho$ ), gravity ( $g$ ), and the fluid viscosity ( $\mu$ ). The relationship is as follows (Freeze and Cherry 1979):

$$K = \frac{k\rho g}{\mu}. \quad (2.2)$$

Freeze and Cherry (1979) explain that the intrinsic permeability is a function of the porous media, making the hydraulic conductivity a function of both the porous media and the fluid. As suggested by Parker (1989), a critical assumption in estimating the hydraulic conductivity based on the intrinsic permeability, lies in the validity of the intrinsic

permeability being a function of only the porous media and not the fluids moving through the porous media. Parker (1989) further explains that in a rigid granular material, not undergoing swelling or consolidation, the assumption that the intrinsic permeability is a unique tensorial quantity is valid. Acar (1985) shows, that in fine grained soils, this assumption may break down and the intrinsic permeability may differ by an order of magnitude for different fluids.

It has been found that Darcy's law, which specifies a linear relationship between discharge and hydraulic gradient, may break down for conditions in which the specific discharge increases beyond certain limits (Bear 1972). The upper limit is described by the dimensionless Reynolds number,  $R_e$ . This ratio of inertial forces to viscous forces, present in fluid flow, determines the validity of Darcy's law by estimating if the system is in a condition of laminar or turbulent flow. During laminar flow, low values of Reynolds's number, viscous forces are predominant and Darcy's law is valid (Bear 1972). As the value of Reynolds number increases, flow is governed by inertial forces and experimental results deviate from the results produced by Darcy's law. This is known as the upper limit for Darcy's law. Reynolds number is defined for flow in porous media by

$$R_e = \frac{qd}{\nu}, \quad (2.3)$$

where

$d$  = the length of flow in the porous media,

$q$  = the specific discharge, and

$\nu$  = the kinematic viscosity of the fluid.

Since Reynolds number was originally developed to analyze flow in pipes an analogy between the pipe length,  $d$ , and the flow channel length in the porous media must be made (Bear 1972). This is usually carried out by relating  $d$  to the grain size of the porous media. Researchers, such as Collins (1961) and Ward (1964) have developed such correlations. Bear (1972) suggests that Darcy's law is valid for flow in a porous media as long as Reynolds number, based on average grain size diameter, does not exceed some value between 1 and 10. It is assumed that this upper limit is dependent on the porous media and/or the viscosity of the fluid.

Darcy's law has also been found to have a lower limit of validity. Investigators, such as Von Engelhardt and Tunn (1955), Swartzendruber (1962), Kutilek (1969), Bolt and Groenevelt (1969), and Low (1961) have shown that as the hydraulic gradient decreases below a critical value (under very low flow conditions), Darcy's law is found to be invalid. Irmay (In chap. 5 of Bear et al. 1968), as described by Bear (1972), attributes this behavior to the rheological non-Newtonian (shear-rate dependent) behavior of water. Bear (1972) explains that other researchers attribute the diversion from Darcian flow to be a result of the streaming potential generated by flow. This occurs in fine grained soils, where counter currents are produced along the pore walls in the opposite direction to the direction of flow. The behavior fluids exhibit at low flow rates is referred to as non-Darcian laminar flow and describes the lower limit for the validity of Darcy's law.

It has also been found that in situations involving gas flow, a phenomenon called slip phenomenon or the Klinkenberg effect may take place (Bear 1972). This phenomenon suggests that the velocity at the solid-fluid or gas-liquid interface is not zero but instead is equal to some finite value.

The macroscopic velocity versus the microscopic velocity and the specific discharge are also important considerations when using Darcy's law. Freeze and Cherry

(1979) explain that Darcy's law produces a specific discharge based on the macroscopic dimensions of the porous media. Therefore, the pore water velocity or average linear velocity is equal to the Darcy velocity,  $v$ , divided by the porosity. This is given by

$$\bar{v} = \frac{v}{\phi}, \quad (2.4)$$

where  $\bar{v}$  is the average linear velocity, and  $\phi$  is the effective porosity. The effective porosity is defined as the volume of voids divided by the total volume,  $V_v/V_{\text{bulk}}$ , and is assumed to remain constant throughout the porous media. This implies that consolidation and compression are not considered in the calculations. If considered this would result in difficulties in estimating new fluid conductivities and effective saturations for the two- and three phase systems (Parker 1989). Other researchers, such as Biot (1941) have developed models for three-dimensional consolidation in soils.

Freeze and Cherry (1979) emphasizes that the velocity obtained through Equation 2.4 is not the actual velocity present in the pores, but is instead an approximation that assumes the pore channels in a porous media are linear, possessing no tortuosity. This is never true, making the actual pore water velocity greater than the average linear velocity. The approximation is not important in most areas of ground water flow, but in the area of pollutant transport this approximation may effect the mass transport results provided by the advection-dispersion mass transport analysis.

## FLUID-SOLID RELATIONS

Before tackling the complex relations between fluids in a multiphase flow system, it is important to understand the changes that fluids exhibit when in contact with a porous media. De Marsily (1986) discusses the different zones that exist in a water saturated porous media. The two major zones are distinguished as (1) an adhesive water zone and (2) a free water zone. The adhesive water zone is located within the first  $0.1\mu\text{m}$  of water next to the porous media surface. In this zone, attraction forces can reach several  $10^{12}$  Pa changing the properties of water, such as the viscosity, and density drastically (de Marsily 1986). This zone is followed by a transition zone where the water molecules are immobile, but are subjected to negligible attraction forces. Beyond this point, the water is free and movement is controlled by gravity or pressure gradients.

In the study of multiphase flow, only the free portion of the fluids will be considered in determining the movements of the different phases. Although other factors such as the adhesive water zone, the existence of unconnected pores and dead end pores, and fractured rock considerations will not be covered, it is important that researchers in the area of multiphase flow understand these factors and the possible limitations associated with certain porous media. The researcher must have an excellent knowledge of the porous media to insure that pores are interconnected and that channel flow can occur. An example of a porous media that does not permit flow would be a vesicular igneous rock, such as pumice or scoria which have high porosities but fluid conductivities of zero.

## FLUID CONTENT VS. PRESSURE HEAD

Due to difficulties in measuring the pressure heads of various fluids in a three-phase system, estimations of fluid pressures from two-phase systems are measured and applied to the theory of three-phase flow. In any two-phase system the saturation or water content of a given phase is a result of the pressure difference between the two fluids in the system.

In a system containing two fluid phases, one fluid will generally have a greater affinity for the porous media than for the other fluid. This fluid is referred to as the wetting phase and will occupy the smallest pore spaces in a porous media. The other fluid, the nonwetting phase, therefore occupies the larger pores. Figure 2.1 shows the relationship between the wetting and nonwetting phases in a section of a pore contained in any porous media. The fluid-fluid interface shown in Figure 2.1 determines the magnitude of the pressure difference between the two fluids in the system. This pressure difference or capillary pressure is related to the interface curvature at a point (the microscopic point inside the void space) and is defined as (Bear 1972)

$$P_c = P_{nw} - P_w, \quad (2.5)$$

where

$P_{nw}$  = the pressure of the nonwetting fluid,

$P_w$  = the pressure of the wetting fluid, and

$P_c$  = the capillary pressure between the fluids.

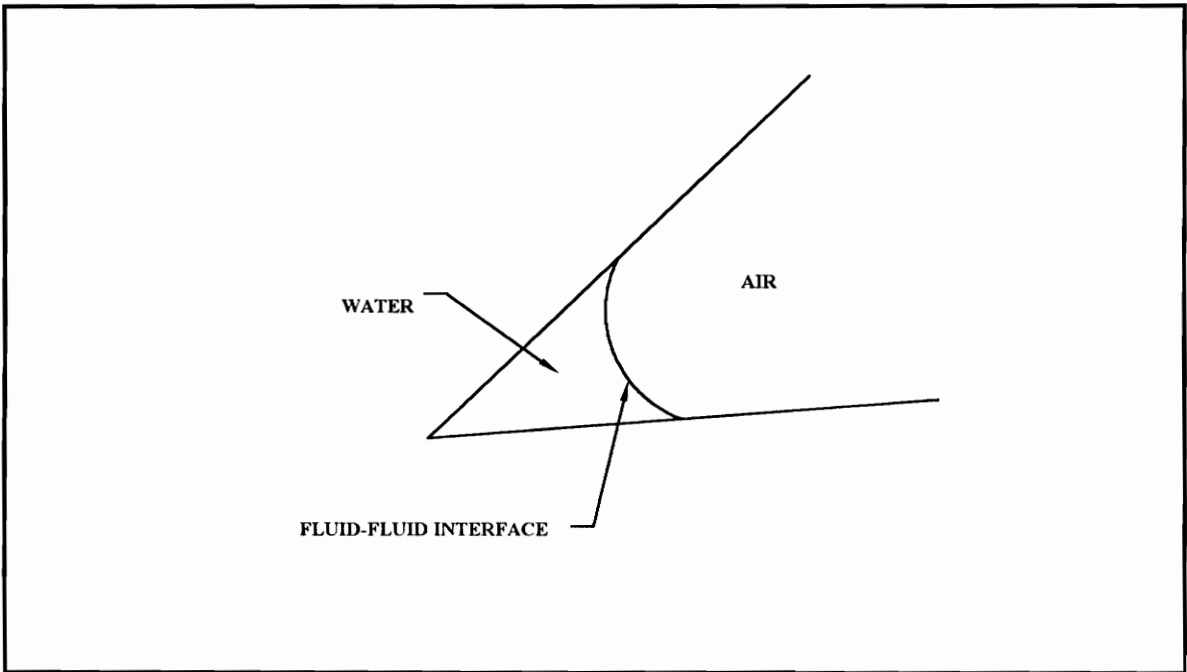


Figure 2.1 Relationship between wetting (water) and nonwetting (air) fluids in a pore.

The capillary pressure is the tendency of the porous media to suck the wetting phase and to repel the nonwetting phase; this is referred to in soil science as the capillary suction or capillary tension (Bear 1972). The capillary pressure is always positive, since the nonwetting phase pressure must always exceed the wetting phase pressure to insure the correct shape of the interface. Since the equations of fluid flow are based on heads, rather than pressures, we may similarly define the capillary head as

$$h_c = h_{nw} - h_w, \quad (2.6)$$

where

$h_c$  = the capillary head,

$h_{nw}$  = the head of the nonwetting phase, and

$h_w$  = the head of the wetting phase.

Parker (1989) explains that the heads of the wetting and nonwetting phase fluids must be defined by a reference fluid that is usually selected as water.

Bear (1972) shows that the capillary pressure is obtained by considering two principal radii of curvature,  $r'$  and  $r''$ , in two orthogonal planes (Figure 2.2). From this, it is shown that the capillary pressure is related to the mean radius of curvature by the Laplace equation for capillarity,

$$P_c = \frac{2\sigma}{R}, \quad (2.7)$$

where  $R$  is the mean radius of curvature ( $2/R = 1/r' + 1/r''$ ) and  $\sigma$  is the interfacial tension between the two fluids (Bear 1972).

Considering now an air-water system, as the water pressure (wetting phase pressure) becomes more negative relative to the air pressure (nonwetting phase pressure which is assumed to be zero), the capillary pressure between the two phases increases. The water phase moves out of the larger pores as the radius of curvature between the water and air phases becomes smaller than the pore size in that portion of the porous media. As the radius of curvature further decreases, the capillary pressure increases and the air phase progressively enters the system (Parker 1989). Bear (1972) explains that the capillary pressure relations in an actual porous media are taken as a statistical average over the void space in the vicinity of a considered point in the porous media. Since the capillary pressure is a function of the radius of curvature and the interfacial tension, it depends on the geometry of the void space; the nature of the fluid and the solid phases; and the degree of saturation of the fluids in the pore spaces (Bear 1972). Since the



geometry of porous media is too complex to actually measure the two principal radii of curvature, idealized models of the pore space must be adopted for which the relationship  $P_c = P_c(S_w)$  can be defined, where  $S_w$  is the saturation of the wetting phase (Bear 1972). The degree of saturation,  $S$ , for any phase in the system is defined as the volume of the fluid phase divided by the volume of the total void space,  $S = V_{\text{fluid}}/V_{\text{voids}}$ . The value of saturation for a given fluid may vary from 0 to 1, with the summation of all the fluids in the system equal to one,  $\sum_i^n S_i = 1$ . Therefore, in considering two immiscible fluids,  $S_{nw}(h_c) = 1 - S_w(h_c)$ . Furthermore, the fluid content equals the porosity times the saturation,  $\theta = \phi S$ . Several empirical and semi-empirical formulas exist which approximate the porous media as capillary tubes, spheres of constant radii, or bundles of parallel circular rods (Bear 1972).

Using experimental data, Brooks and Corey (1964) developed an effective saturation function relating the residual saturation of the wetting fluid and the actual saturation in the system. The effective saturation is given by

$$S_e = \frac{(S_w - S_m)}{(1 - S_m)}, \quad (2.8)$$

where

$S_e$  = the effective saturation,

$S_w$  = the saturation of the wetting phase in the system, and

$S_m$  = the residual saturation for the porous media.

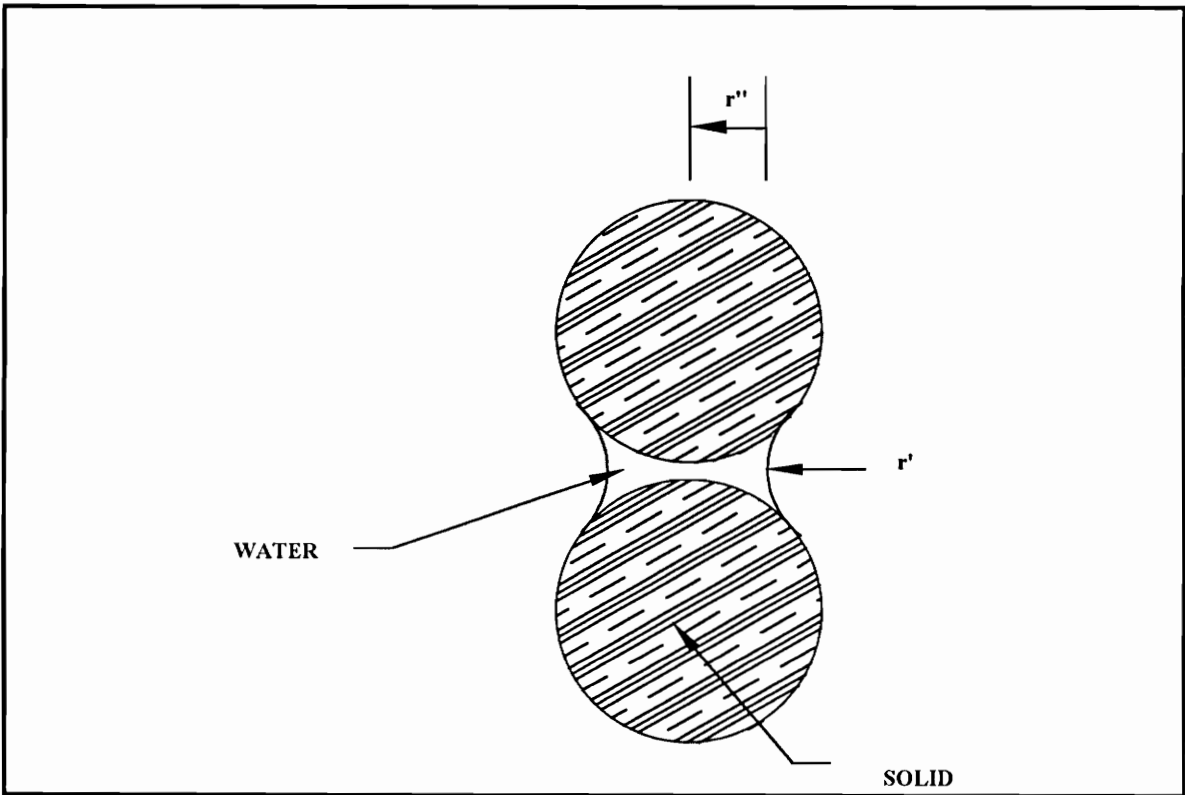


Figure 2.2 Meniscus showing the principle radii of curvature (after Bear 1972).

For the purpose of this thesis, the residual saturation of the wetting phase is defined as the quantity of wetting fluid left in the porous media at a high capillary pressure. This is the lowest value of saturation that can be obtained once the wetting phase has entered the system. The residual saturation of the nonwetting phase is similarly defined as the saturation of the nonwetting fluid at a capillary head of zero, after imbibition. Imbibition is defined as the displacement of a nonwetting phase by a wetting phase due solely to capillary forces and is in the opposite direction of drainage.

Since the contact angle,  $\theta$ , between the fluid-fluid interface and the porous media is a function of the direction of displacement, hysteresis in capillary pressure-saturation relations is experienced depending on whether drainage or imbibition is occurring (Bear

1972). Figure 2.3 shows how the direction of movement effects the contact angle in an oil-water system. A greater angle of contact occurs when the nonwetting fluid is being displaced by a wetting fluid, and a smaller angle of contact occurs when the wetting fluid is displaced by the nonwetting fluid (Bear 1972). For the static condition, the angle of contact will fall in-between these two extremes.

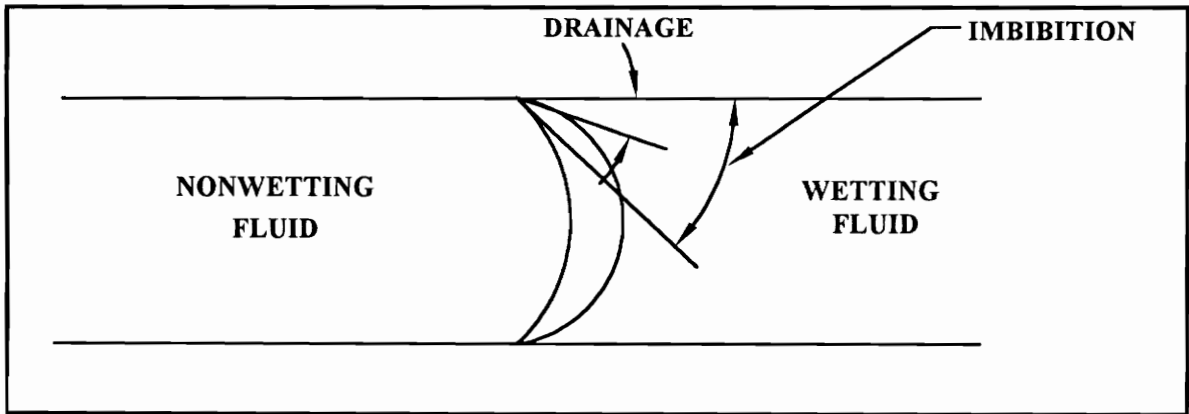


Figure 2.3 Variation in contact angle due to movement direction of fluid-fluid interface (after Bear 1972)

For a situation in which a wetting fluid is being displaced, drainage condition, it can be expected that the saturation of the wetting phase will be greater within a given range of capillary pressure heads. Figure 2.4 shows the different curves relating water content to pressure head for either drainage or imbibition.

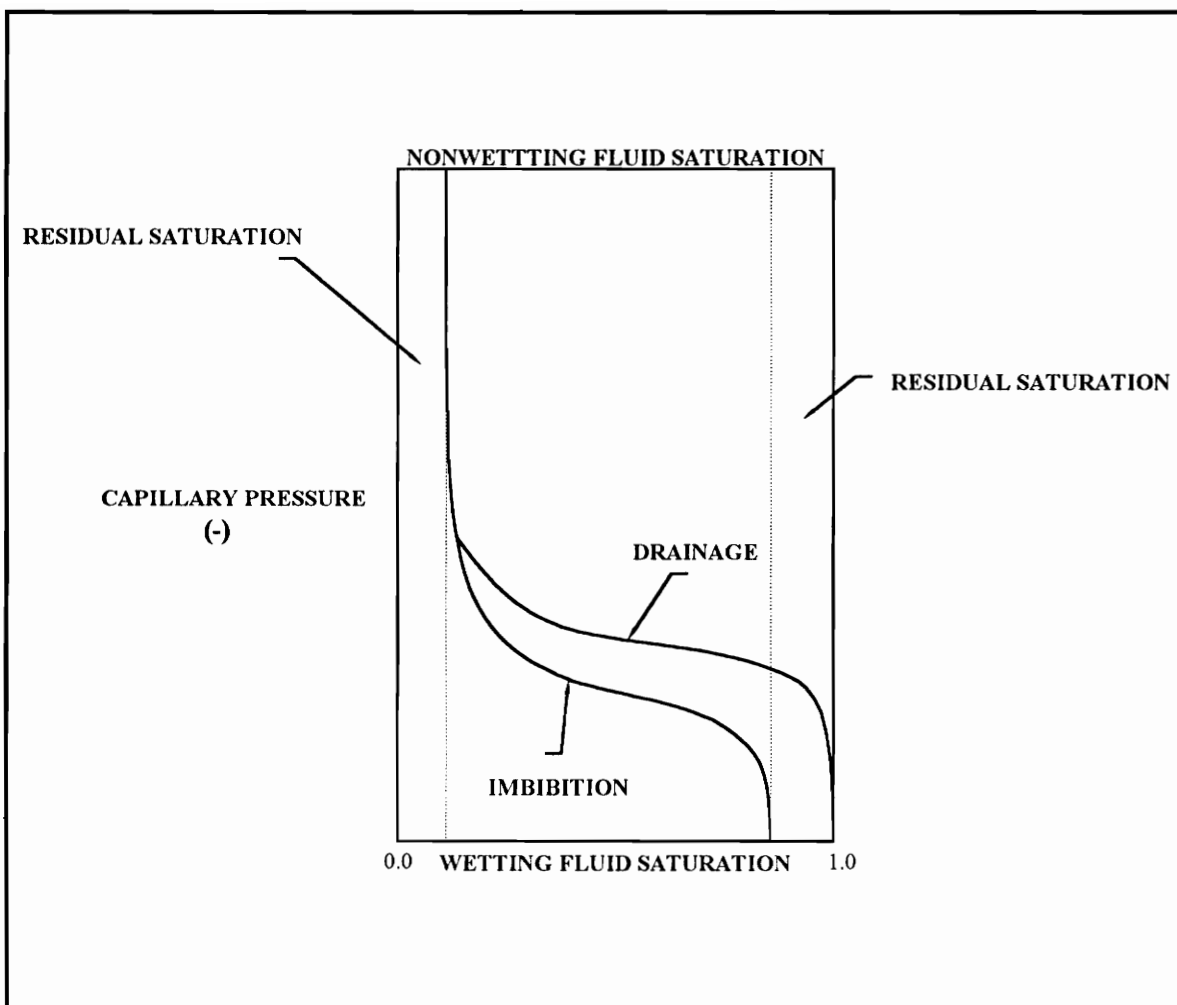


Figure 2.4 Water content versus capillary head for drainage and imbibition.

## SCALING TWO-PHASE SYSTEMS

The Laplace equation (Equation 2.7) defines the relationship between fluid pairs in a porous media. If we rewrite the Laplace equation as

$$R = \frac{2\sigma}{P_c}, \quad (2.9)$$

and assume that  $S_w(R)$  represents the pore size distribution, then Corey (1986) suggests that the saturation-capillary pressure relations may be scaled from the interfacial tension between the fluid-fluid interface. This scaling relation can be written as

$$S_w(\beta_{nw}h_c) = S^*(h_c^*), \quad (2.10)$$

where

$S_w$  = the effective saturation of the wetting phase,

$\beta_{nw}$  = the fluid-fluid dependent scaling factor (here n represents the nonwetting fluid and w represents the wetting fluid),

$h_c$  = the capillary head, and

$S_*(h_c^*)$  = the effective wetting fluid saturation versus capillary head relation for the reference two-fluid system (usually taken as the air-water system).

The scaling parameter  $\beta_{nw}$  can be approximated as

$$\beta_{nw} = \frac{\sigma^*}{\sigma_{nw}}, \quad (2.11)$$

where

$\sigma^*$  = the interfacial tension of the reference fluid pair and

$\sigma_{nw}$  = the interfacial tension between the n-fluid (nonwetting fluid) and w-fluid (wetting fluid) for a fluid-fluid pair.

Examples relating the unscaled and scaled saturation-capillary pressure relations for an air-oil and oil-water system in a porous media where taken from Parker et al. (1987) and are shown in Figures 2.5 and 2.6. The scaling factors used to obtain Figure 2.6 from Figure 2.5 are fit using nonlinear regression. These figures show that using the scaling factor,  $\beta_{nw}$ , a two phase system can be fit to the reference air-water system. Later in this chapter, the same process is extended to a three-phase system using two-phase measurements.

Table 2.1 shows a comparison of the scaling parameters determined by the direct curve-fitting method described above to the estimated values based on the interfacial tension relations for the fluid-fluid pairs referenced to the air-water interfacial tension (Lenhard and Parker 1987a). It is noted that the interfacial tension is a function of the porous media as well as the fluid-fluid pair. Further calculations show that estimations based on interfacial tension deviate from the measured predictions by 10-20% for the systems that were considered.

Table 2.1 Comparison of measured and predicted scaling factors of two-phase systems

Fluid	Measured $\beta_{ao}$	Predicted $\beta_{ao}$	Measured $\beta_{ow}$	Predicted $\beta_{ow}$
Benzene	21.8	1.94	1.85	2.12
o-xylene	2.11	2.12	1.91	2.27
p-cymene	1.90	1.97	2.11	2.14
Benzl alcohol	1.22	1.26	5.59	5.87

After Lenhard and Parker (1987a).

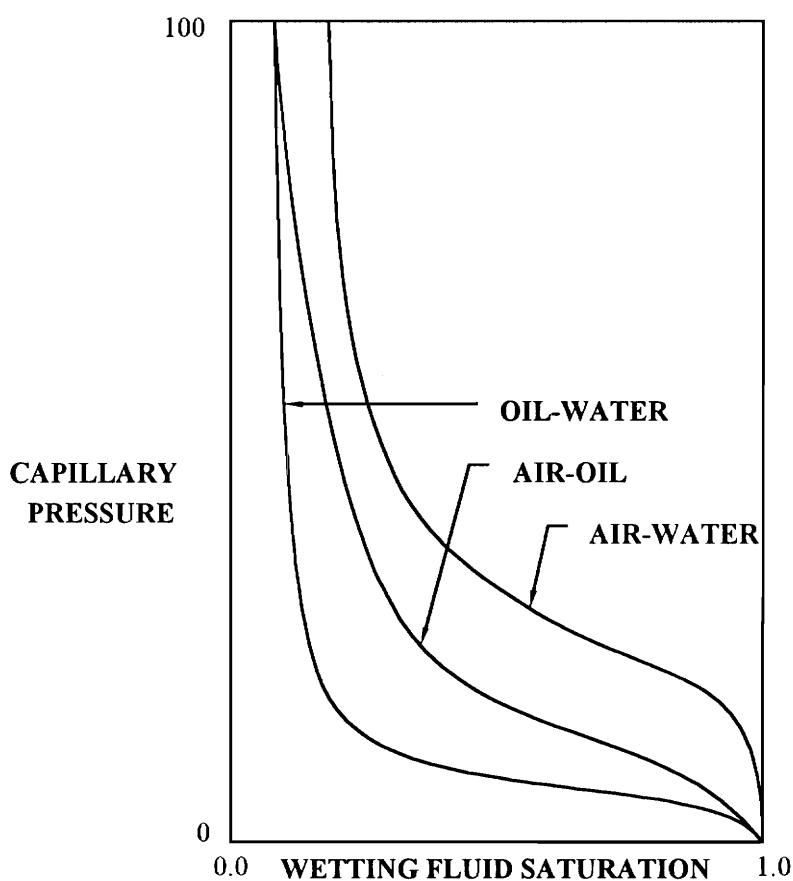


Figure 2.5 Unscaled water content-pressure head relations (after Parker et al 1987)

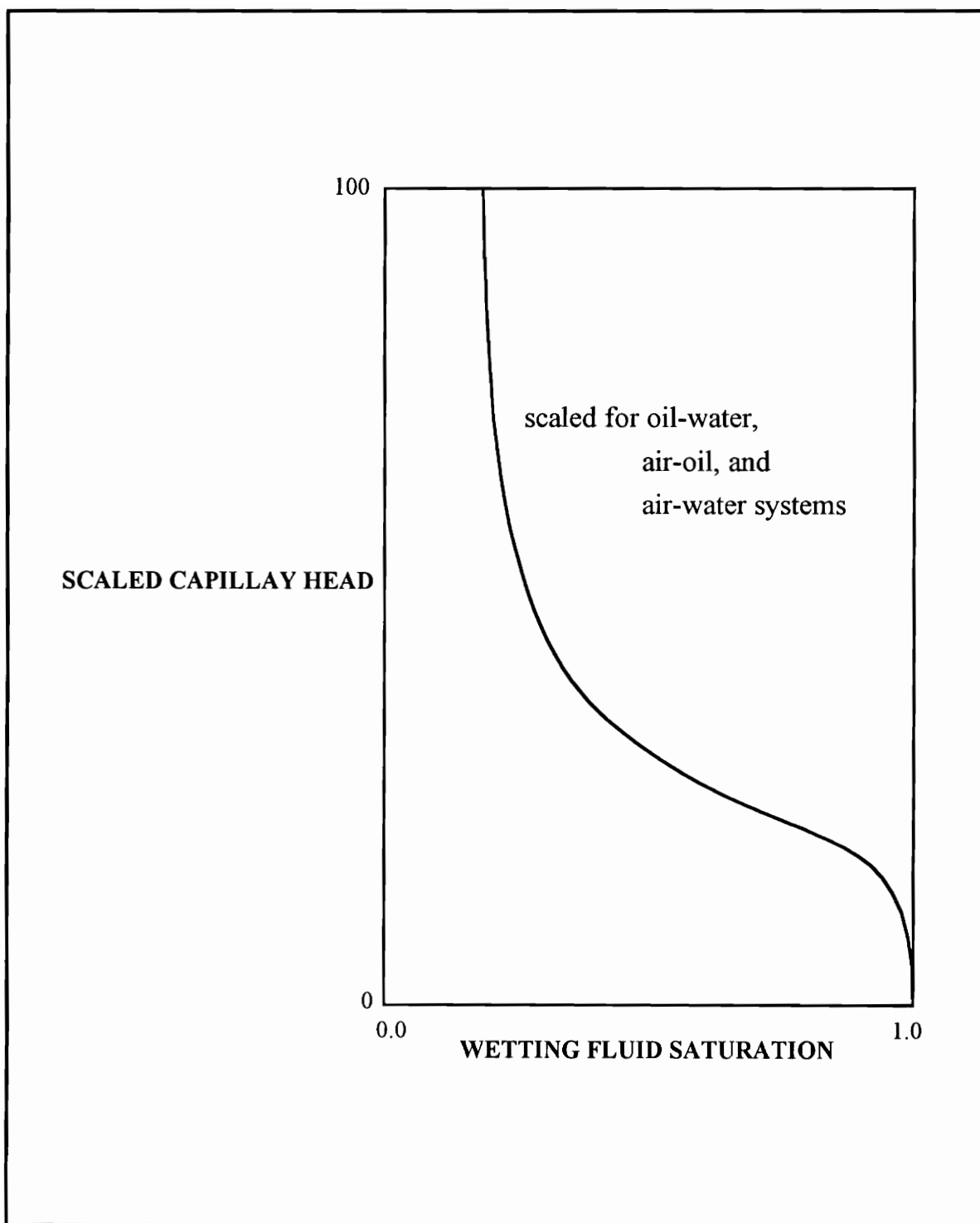


Figure 2.6 Scaled water content-pressure head relations (after Parker et al. 1987)



The previous predictions do not account for the effects of hysteresis which occur due to the saturation history, irregularities in the pore geometry, contact angle hysteresis, nonwetting fluid entrapment, or other phenomenon (Parker 1989). Models which address effects of hysteresis in two-phase and three-phase systems have been presented by Haverkamp and Parlange (1986), Kool and Parker (1987), and Parker and Lenhard (1987). Kaluarachchi and Parker (1987) found that the effects of hysteresis are relatively small for air-water systems controlled by a flux-type boundary condition, and Kool and Parker (1988) suggest that the effects of hysteresis are insignificant as compared to the uncertainty related to measurement errors and model calibration. Therefore, Parker (1989) explains that for a two-phase system in which the wetting phase is the only phase of significant importance hysteresis may be disregarded, but for situations in which the nonwetting phase is of great concern, such as in aquifer contamination by a hydrocarbon in an air-oil-water system, the effects of hysteresis may be significant.

## **THEORY OF UNSATURATED FLOW**

Unsaturated flow is merely a specific case of immiscible flow involving two fluids, air and water. Here the air phase is assumed to be the stagnant nonwetting phase occupying the portions of the void space not occupied by the water phase (wetting phase). The previous equation for Darcy's law (Equation 2.1) for saturated flow can be extended to conditions above the water table, unsaturated conditions, by developing unsaturated fluid conductivities for the water phase. If we now consider an elemental control volume, such as that in Figure 2.7, the continuity equation can be written as (Freeze and Cherry 1979)

$$-\frac{\partial(\rho V_x)}{\partial x} - \frac{\partial(\rho V_y)}{\partial y} - \frac{\partial(\rho V_z)}{\partial z} = \phi \theta' \frac{\partial \rho}{\partial t} + \rho \theta' \frac{\partial \phi}{\partial t} + \phi \rho \frac{\partial \theta'}{\partial t}, \quad (2.12)$$

where

$\rho$  = the density;

$\theta'$  = the volumetric water content divided by the porosity,  $\theta/\phi$ ; and

$V_x$ ,  $V_y$ , and  $V_z$  = the Darcy velocity.

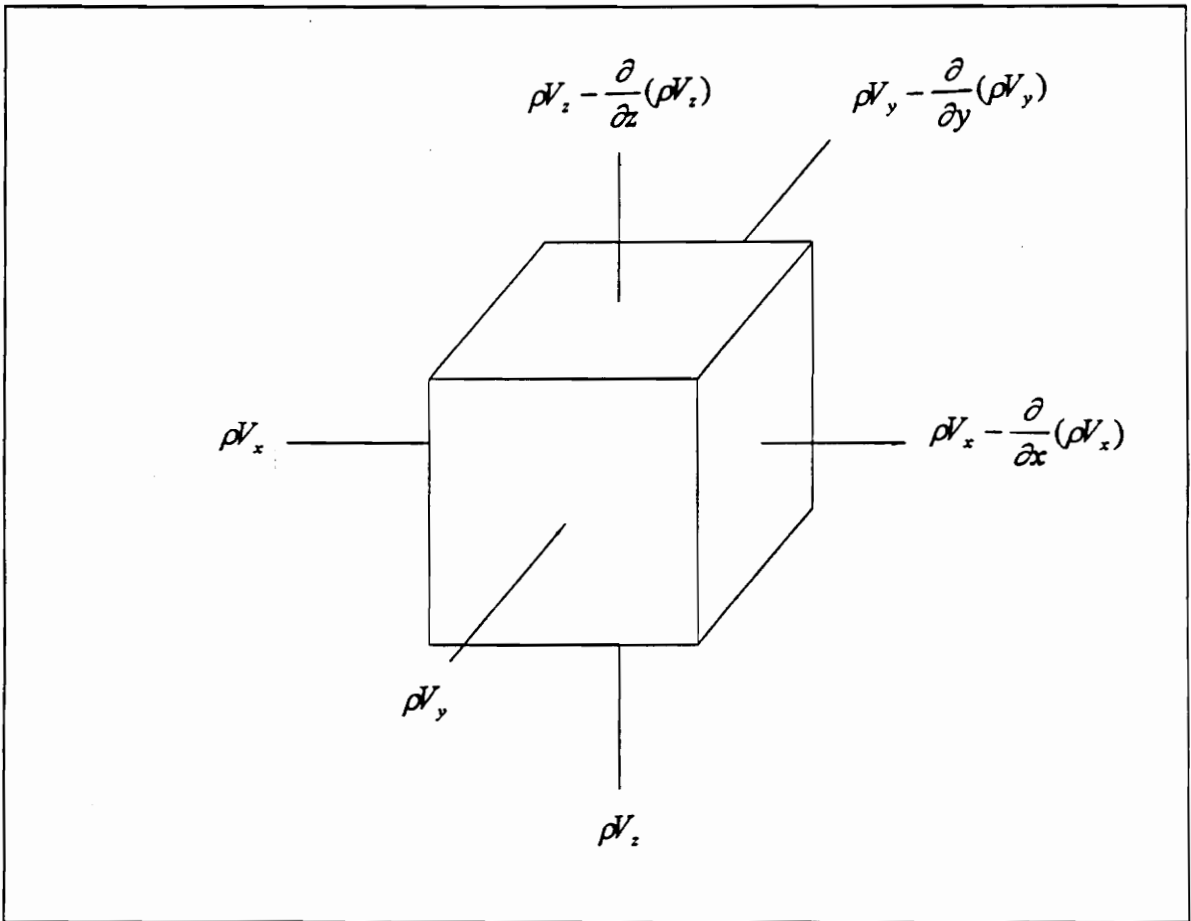


Figure 2.7 Elemental control volume for the flow of water through porous material.

Since Equation 2.12 represents continuity for unsaturated flow it must incorporate the time rate of change of moisture content as well as the time rate of change of storage due to water expansion and compaction. It is found that the first two terms on the right-hand side of Equation 2.12 are small as compared to the third term and can be disregarded. If the fluid is considered incompressible in all three directions, then the density term,  $\rho$ , can be factored out of the relationship. If we recognize that  $\phi \partial\theta' = \partial\theta$ , then the control volume can be represented, for an isotropic material in three-dimensions, by the following (Freeze and Cherry 1979):

$$\frac{\partial}{\partial x} \left( K(h) \frac{\partial h}{\partial x} \right) + \frac{\partial}{\partial y} \left( K(h) \frac{\partial h}{\partial y} \right) + \frac{\partial}{\partial z} \left( K(h) \frac{\partial h}{\partial z} \right) = \frac{\partial \theta}{\partial t}, \quad (2.13)$$

where

$K(h)$  = the relative fluid conductivity and is dependent on the pressure head,  $h$ ;

$\frac{\partial \theta}{\partial t}$  = the change in water content per unit time; and

$\theta$  = the volumetric water content.

Using the chain rule, the right hand side of Equation 2.13 can be expanded to  $\frac{\partial \theta}{\partial h} \frac{\partial h}{\partial t}$ , with the coefficient of moisture capacity being defined as  $C_h = \frac{\partial \theta}{\partial h}$ . Therefore, Equation 2.13 can be represented by the following equation:

$$\frac{\partial}{\partial x} \left( K(h) \frac{\partial h}{\partial x} \right) + \frac{\partial}{\partial y} \left( K(h) \frac{\partial h}{\partial y} \right) + \frac{\partial}{\partial z} \left( K(h) \frac{\partial h}{\partial z} \right) = C_h \frac{\partial h}{\partial t}, \quad (2.14)$$

where  $K(h)$  and  $C_h$  are functions of the pressure head,  $h$ , making the equation for unsaturated flow both nonlinear and time dependent for transient flow conditions. These parameters are obtained by constructing a soil-water retention curve, which is a plot of the water content versus the pressure head for an air-water system in a given porous media (Figure 2.4). The unsaturated hydraulic conductivity,  $K_u$ , can then be approximated based on the relative hydraulic conductivity,  $K_r$ , and the saturated hydraulic conductivity,  $K_s$  by the following relationship:

$$K_u = K_r K_s \quad (2.15)$$

Researchers such as Mualem (1976), Brooks and Corey (1964), Burdine (1953) and van Genuchten (1980) have determined or revised methods for obtaining the relative hydraulic conductivity in unsaturated soils from effective saturation, or pressure head and water content relations (Mualem 1976). It is important to note that there is question as to whether the relative permeability is a tensor quantity, as used in Equation 2.15, or a scalar quantity similar to the hydraulic conductivity (Parker 1989).

## **VAN GENUCHTEN'S MODEL FOR UNSATURATED FLOW**

A continuous empirical function relating the effective saturation to the pressure head was developed by van Genuchten (1980) based on Mualem's model for relative permeability and knowledge of the soil-water retention curve. Mualem's equation which relates the hydraulic conductivity to water content versus pressure head relations is given by (Mualem 1976)

$$K_r = S_e^{0.5} \left[ \frac{\int_0^\theta \frac{\partial \theta}{h}}{\int_0^{\theta_s} \frac{\partial \theta}{h}} \right]^2. \quad (2.16)$$

The power, 0.5, on the effective saturation term was determined by conducting experiments on 45 soils, making the above equation semi-empirical. The effective saturation  $S_e$  is related to the pressure head and scaling parameters  $\alpha$  and  $n$  by (van Genuchten 1980)

$$S_e = [1 + |\alpha h|^n]^{-m} \quad \text{for } h < 0 \quad (2.17)$$

$$S_e = 1.0 \quad \text{for } h \geq 0,$$

where  $\alpha$  and  $n$  are parameters which control the slope and position of the saturation-pressure curve and  $m = 1 - 1/n$ . The parameters  $\alpha$  and  $n$  are inversely related to the air entry pressure and the pore size distribution (van Genuchten 1978a). The soil-water retention curve can be constructed using the following equation which is obtained by relating the effective saturation to the water content:

$$\theta = \theta_r + \frac{\theta_s - \theta_r}{[1 + |\alpha h|^n]^m} \quad \text{for } h < 0, \quad (2.18)$$

$$\theta = \theta_s \quad \text{for } h \geq 0.$$

where

$\theta_r$  = the residual water content

$\theta_s$  = the saturated water content, and

$h$  = the pressure head.

The coefficient of moisture capacity,  $C_h$ , used in unsaturated flow is

$$C_h = \frac{\partial \theta}{\partial h} = \frac{-\alpha m (\theta_s - \theta_r)}{1 - m} \theta_e^{1/m} (1 - \theta_e^{1/m})^m, \quad (2.19)$$

where  $\theta_e = \frac{\theta - \theta_r}{\theta_s - \theta_r}$  is the dimensionless water content. In terms of effective saturations,

Equation 2.19 can be expressed as

$$C_h = -\alpha m (\theta_s - \theta_r) S_e^{1/m} (1 - S_e^{1/m})^m. \quad (2.20)$$

The relationship for relative hydraulic conductivity is (van Genuchten 1980)

$$K_r(S_e) = S_e^{0.5} [1 - (1 - S_e^{1/m})^m]^2. \quad (2.21)$$

This equation can be written in terms of pressure heads as

$$K_r(h) = \frac{[1 - |\alpha h|^{n-1} \{1 + |\alpha h|^n\}^{-m}]^2}{[1 + |\alpha h|^n]^{m/2}}. \quad (2.22)$$

Equation 2.22 is extended to the theory of multiphase flow in a later section.

The above equations presented by van Genuchten are based on five parameters which describe the shape and position of the curve for saturation versus pressure head relations. The parameters  $K_s$ , the saturated hydraulic conductivity, and  $\theta_s$  (saturation,  $S = 1.0$ ), the saturated water content, are both material property parameters. The residual water content,  $\theta_r$ , is an empirical relation based on test data for a given soil media and is a function of the soil-fluid relations which are different for most porous mediums. This is the lowest water content that can be achieved once water has reached a residual saturation in the system. Recall, the residual water content is directly related to the residual saturation by  $\theta_r = \phi S_r$ , where  $\phi$  = the porosity. The final two parameters  $\alpha$  and  $n$  are referred to as van Genuchten's parameters. These parameters define the slope and shape of the curve defined by Equation 2.17.

Figures 2.8 and 2.9 show the effects of varying van Genuchten's parameters (Ahmad 1991). Figure 2.8 shows that increasing the value of  $n$  results in an increase the slope of the curve describing the saturation-pressure relationship. Figure 2.9 shows that for a constant value  $n$ , the parameter  $\alpha$  effects the slope of the curve but also drastically changes the position of the curve as well, shifting the curve towards the vertical axis for increasing values.

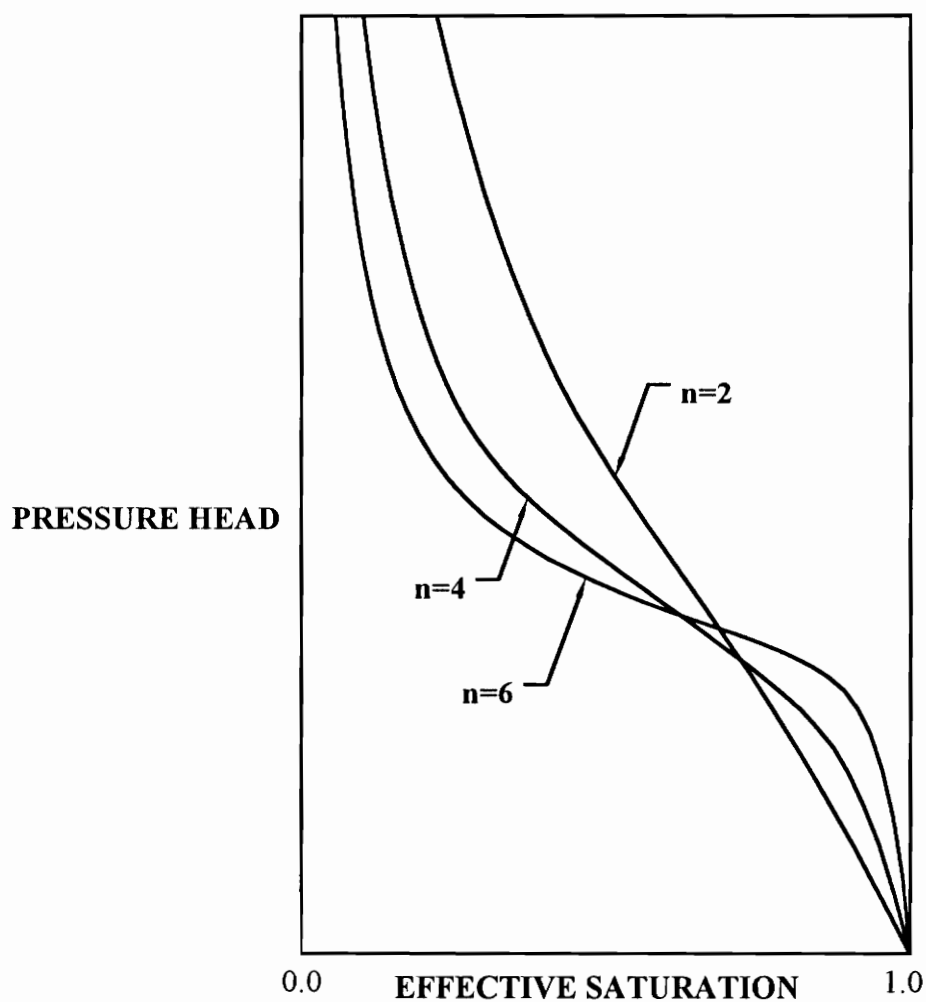


Figure 2.8 Saturation-pressure relation for various values of van Genuchten's parameter  $\alpha$  (after Ahmad 1991).



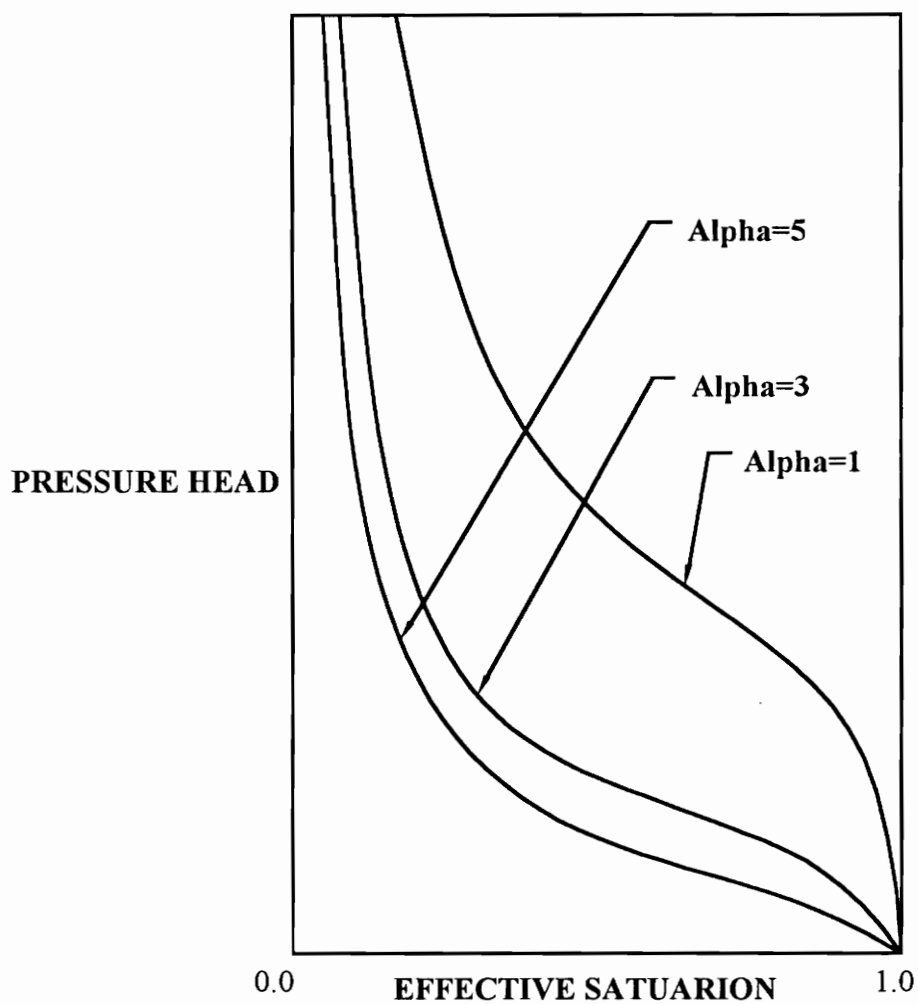


Figure 2.9 Saturation-pressure relation for various values of van Genuchten's parameter  $n$  (after Ahmad 1991).

Kool et al. (1985) developed a range of values for which van Genuchten's parameters usually apply in an air-water system. According to his study, values of  $\alpha$  generally range from 1.6 to 16 ft<sup>-1</sup>, with the lowest value of  $\alpha$  corresponding to a heavy clayey soil being equal to 0.5 ft<sup>-1</sup>. The study also concluded that values of  $n$  normally range from 1.1 to 3.5 with the upper limit equal to 10 for sandy soils with extremely narrow pore size distributions. In general, values of both  $\alpha$  and  $n$  are found to be high in sandy soils and low in fine textured soils. The relationship shown in Figures 2.8 and 2.9 is similar for both air-oil and oil-water systems. In an extensive literature review no correlations between oil and water flow in a three-phase flow system based on the effects of van Genuchten's parameters were found. Correlations of this type is presented in Chapter 5, based on an experimental column test conducted with air, gasoline, and water. Model parameters based on an air-water system are shown in Table 2.2 (Parker et al. 1985 and van Genuchten 1980).

Table 2.2 Model parameters for an air-water system.

Soil	$\alpha$ (m <sup>-1</sup> )	$n$	$S_{wr}$	$K_{ws}$ (m/day)
<b>Parker et al (1985):</b>				
Sandy loam	1.53	1.265	0.208	0.06
Silt loam	3.46	1.289	0.265	1.296
Sandy clay loam	0.82	1.275	0.276	0.095
Clay	0.07	1.419	0.185	0.00019
<b>van Genuchten (1980):</b>				
Hygiene sandstone	0.790	10.40	0.612	1.08
Touchet silt loam	0.500	7.09	0.405	3.03
Silt loam G.E.3	0.423	2.06	0.311	0.05
Beit Netofa clay	0.152	1.17	0.0	0.00082

After Sheng (1986).

## **THEORY OF MULTIPHASE IMMISCIBLE FLOW**

Immiscible non aqueous phase liquids (NAPLs) are liquids other than water that are considered essentially insoluble in water. For the current discussion of multiphase flow systems, the assumption of immiscible fluids will be considered without interphase mass transport. The interphase mass transport movements are described in Chapters 6 and 7 for the mass transport and weakly-coupled multiphase flow problems.

### **SATURATION-CAPILLARY HEAD RELATIONS**

As previously discussed, the saturation-capillary head relations control the flow of immiscible liquids in a two-phase system. This theory will now be extended to the three-phase system, air-oil-water, in which the capillary head between the different phases in the system determines the flow of the contaminant (referred to here as the oil phase) and the other phases in the system (water and air phases). Due to the difficulty in measuring the relationships between the three different phases in a multiphase system, researchers have developed the three-phase relationships based on two-phase measurements and applied them to three-phase systems (Parker et al. 1987, Kuppusamy et al. 1987). In this section, the relationships between the fluid pressures, saturations, and permeabilities for the two-phase system will be extended to the three-phase system. Again, the soil matrix's effective porosity, and the fluid density and viscosity are the variables that control the relative permeability-saturation-pressure relations in the two- and three-phase flow problems.

In the three-phase system, oil is the wetting phase with respect to air and the nonwetting phase with respect to water. This relationship between air, oil, and water,

controls their interaction and restricts contact between the air and water phase whenever oil is present in the system (Figure 2.9). The capillary head relations between the air, oil, and water phases control the saturation of each of the phases and the total saturation in the three-phase system. From Figure 2.10, it can be seen that the saturation of the water phase is dependent on only the oil-water interface and resulting capillary head ( $h_{ow}$ ), while the oil phase saturation is a function of both the oil-water and air-oil capillary heads:  $S_o = f(h_{ow}, h_{ao})$ . Furthermore, the total saturation in the system ( $S_t$ ) is dependent on the air-oil interface and equals the oil phase saturation plus the water phase saturation,  $S_t = S_o + S_w$  (Leverett 1941).

By extending the saturation-pressure relations developed for the two-phase system to the three-phase system, Parker et al. (1987) developed the scaling parameters relating the phase saturations to the reference system (air-water) as follows:

$$\begin{aligned}\bar{S}_w(\beta_{ow}h_{ow}) &= S^*(h^*) \\ \bar{S}_t(\beta_{ao}h_{ao}) &= S^*(h^*),\end{aligned}\tag{2.23}$$

where  $\bar{S}_w = \frac{(S_w - S_r)}{(1 - S_r)}$  is the effective saturation of the water phase and

$\bar{S}_t = \frac{(S_w + S_o - S_{or} - S_{wr})}{(1 - S_{or} - S_{wr})}$  is the effective total fluid saturation. The terms  $S_{or}$  and  $S_{wr}$  ✓

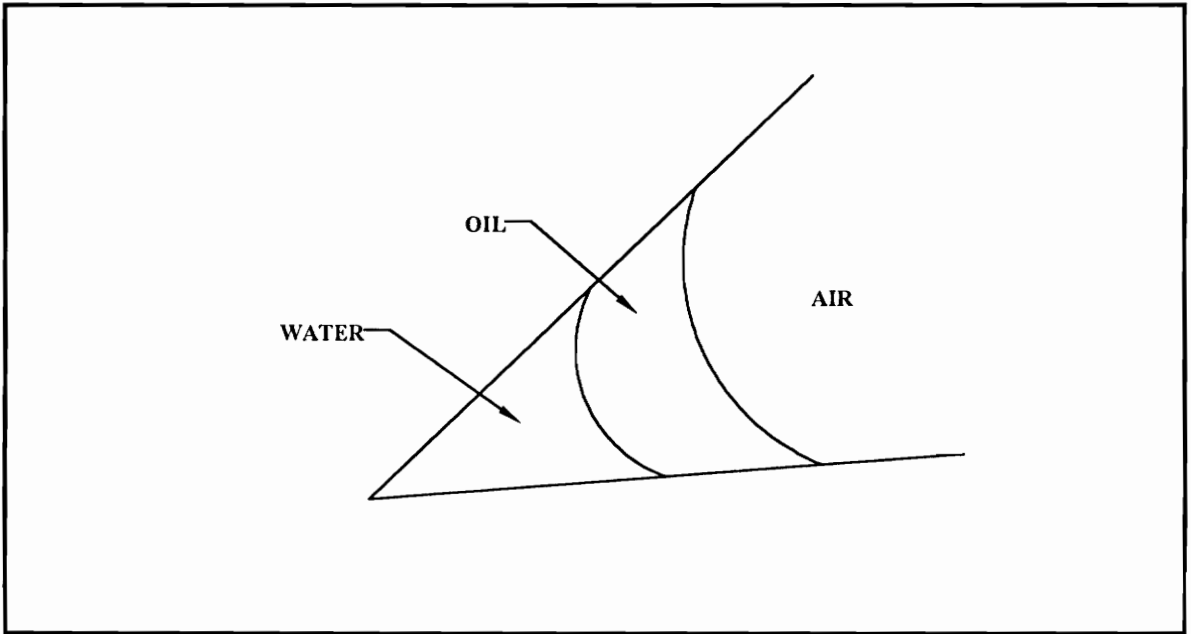


Figure 2.10 Relationship between wetting (water), intermediate phase (oil), and nonwetting (air) fluids in a pore space.

refer to the residual saturations of the oil and water phases, respectively. Similarly, the subscripts  $ow$  and  $ao$  on the capillary head and fluid-fluid scaling parameter terms in Equation 2.23 represent the oil-water and air-oil systems, respectively. Note, the scaling parameters in Equation 2.23 are referenced to the air-water system with the coefficient  $\beta_{aw} = 1.0$ . The capillary heads used in the multiphase flow analysis are defined in a similar manner to those in the two phase flow analysis, with

$$\begin{aligned}
 h_{ao} &= h_a - h_o \\
 h_{ow} &= h_o - h_w \\
 h_{aw} &= h_a - h_w.
 \end{aligned}
 \tag{2.24}$$

The scaling parameters  $\beta_{ao}$  and  $\beta_{ow}$  can be determined from laboratory tests conducted with different fluid-fluid pairs or through the interfacial tension relationships previously presented for the two-phase system.

## VERTICAL EQUILIBRIUM IN A THREE-PHASE SYSTEM

Parker (1989) and Hochmuth and Sunada (1985) describe fluid distributions in a three-phase system to clarify the significance of saturation-capillary head pressure relations. If we assume a contaminant volume is of large proportions, the contaminant will first migrate through the unsaturated zone to the water table. After a sufficient amount of time, the movement of the contaminant in the vertical direction will essentially cease and the pressure distribution in the vertical direction will reach hydrostatic conditions (Parker 1989). This will result in two interface elevations, an air-oil interface at some distance  $Z_1$ , measured from the datum, and an oil-water interface at elevation  $Z_2$ . Figure 2.11 shows the saturation distributions for a system in vertical equilibrium. At elevation  $Z_1$  the oil pressure is equal to the atmospheric pressure and at elevation  $Z_2$  the oil and water pressures are equal (Parker 1989). Equations for the two interface elevations can now be described as a function of the piezometric heads and capillary pressures within and between each fluid-fluid pair (Hochmuth 1981). The equation at the air-oil interface, elevation  $Z_1$ , is (Hochmuth and Sunada 1985)

$$Z_1 = H_o + \frac{(P_c)_o^a}{\gamma_o}, \quad (2.25)$$

while the equation for the oil-water interface is

$$Z_2 = \frac{\gamma_w}{\Delta\gamma} H_w - \frac{\gamma_o}{\Delta\gamma} H_o + \frac{(P_c)_w^o}{\Delta\gamma}, \quad (2.26)$$

where

$H_o$  = the piezometric head of the oil phase,

$H_w$  = the piezometric head of the water phase,

$\gamma_o$  = the specific weight of the oil phase (the oil density times the gravitational constant),

$\gamma_w$  = the specific weight of the water phase,

$\Delta\gamma = \gamma_w - \gamma_o$ ,

$(P_c)_o^a$  = the capillary pressure at the air-oil interface, and

$(P_c)_w^o$  = the capillary pressure at the oil-water interface.

Furthermore, the piezometric head equals the pressure head plus the elevation head,

$H_w = h_w + z$  and  $H_o = h_o + \rho_o z$ . Note, that the piezometric heads or total heads are the driving force in the equations for flow. The  $h$  terms represent the pressure heads for the water and oil phases, respectively. From examination of Figure 2.11 and manipulation of the previous relations, Parker (1989) shows that the various table elevations are related by the following equation:

$$Z_2 = \frac{(Z^* - \rho_o Z_1)}{(1 - \rho_o)}, \quad (2.27)$$

where  $\rho_o$  is the density of the oil phase and  $Z^*$  is the air-water interface, when no oil is present in the system. Relationships for the air-oil and oil-water capillary heads are (Parker 1989)

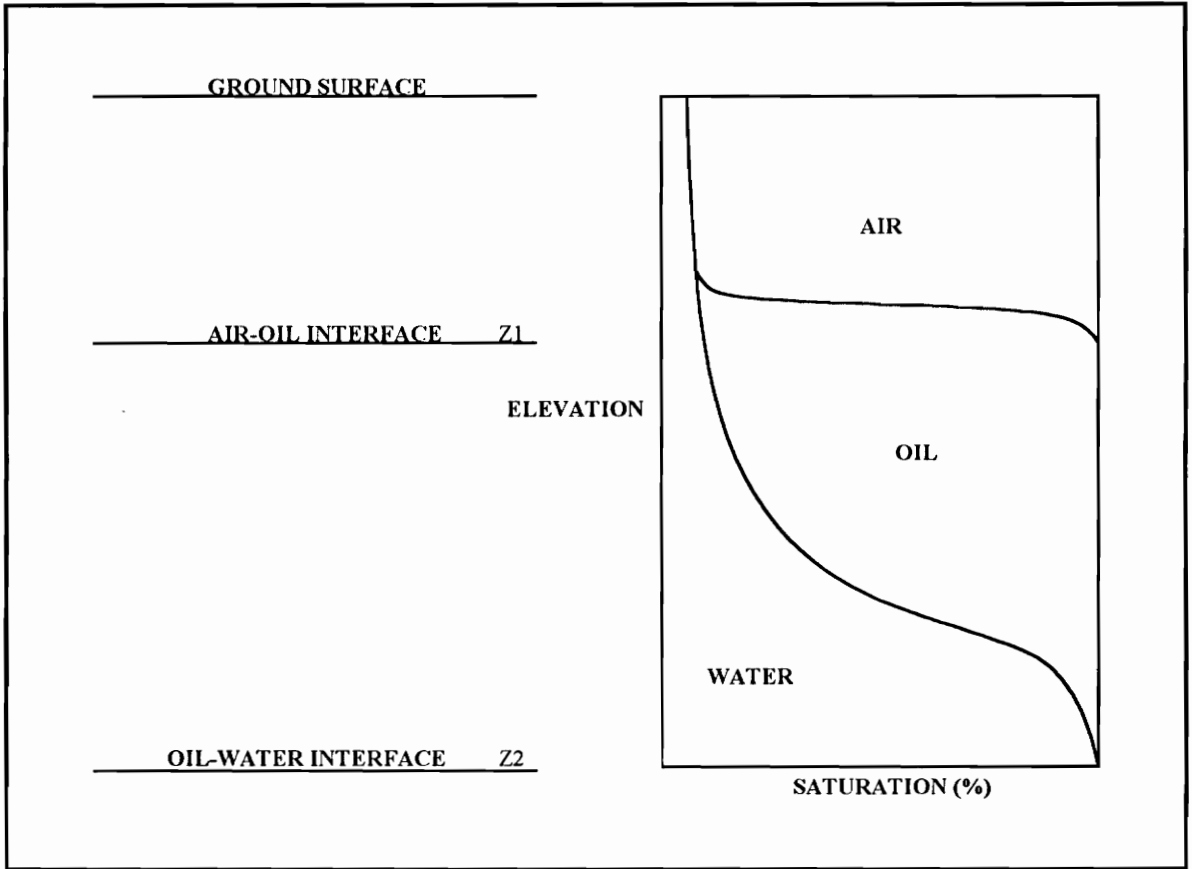


Figure 2.11 Saturation distribution for a system in vertical equilibrium.

$$h_{ao} = h_a - h_o = \rho_o(Z_1 - Z), \text{ and}$$

(2.28)

$$h_{ow} = h_o - h_w = (1 - \rho_o)(Z - Z_2),$$



where  $Z$  is the distance measured from the datum. Given these relations and recalling the relations  $S_w(h_{ow})$  and  $S_t(h_{ao})$ , the vertical distribution of the water and oil saturations can be determined for any system in equilibrium (Parker 1989). Parker (1989) notes that the thickness of the oil layer in an observation well is represented by the piezometric head,

but the actual oil specific volume,  $V_o = \int_{Z_1}^{\text{soil surface}} \phi S_o dz$  will be significantly less than this representation.

## FLUID CONDUCTIVITY RELATIONS

The fluid conductivity for each phase in a porous media is dependent on the degree of saturation of the given phase. Since the saturation of each phase is dependent on the capillary head, the fluid conductivity is also dependent on the capillary head between any two phases in the system. Since oil (the nonwetting phase) displaces water (the wetting phase) from the largest pores in a system, the fluid conductivity of water is effected more drastically as displacement occurs. Since fluid conductivity is dependent on the pore size of the soil media, as well as the phase saturation, an abrupt change in the water conductivity occurs as it is displaced by the oil phase. These relationships assume a monatomic displacement of the water phase by the oil phase, with no residual air phase present during the infiltration of oil. Figure 2.12 shows the relationship between oil and water relative permeabilities in a two-phase system. Figure 2.12 shows that an exponential reduction in the relative permeability of the water phase is observed along with an exponential increase in the oil phase permeability. This is due to the relationship between the wetting and nonwetting phases and the size of the pore spaces they are

contained in. Other researchers such as Stone (1970, 1973) and Baker (1988) have developed two- and three-phase models which relate relative hydraulic permeability through empirical predictions. The model presented in this chapter does not account for the hysteretic effects encountered due to varying movement directions of the different phases in the system, nor does it account for occluded air, oil, or water phases. A discussion and a model describing the entrapment of the oil phase, due to an advancing oil-water interface, and air entrapment, due to an advancing air-oil interface is presented by Parker and Lenhard (1987).

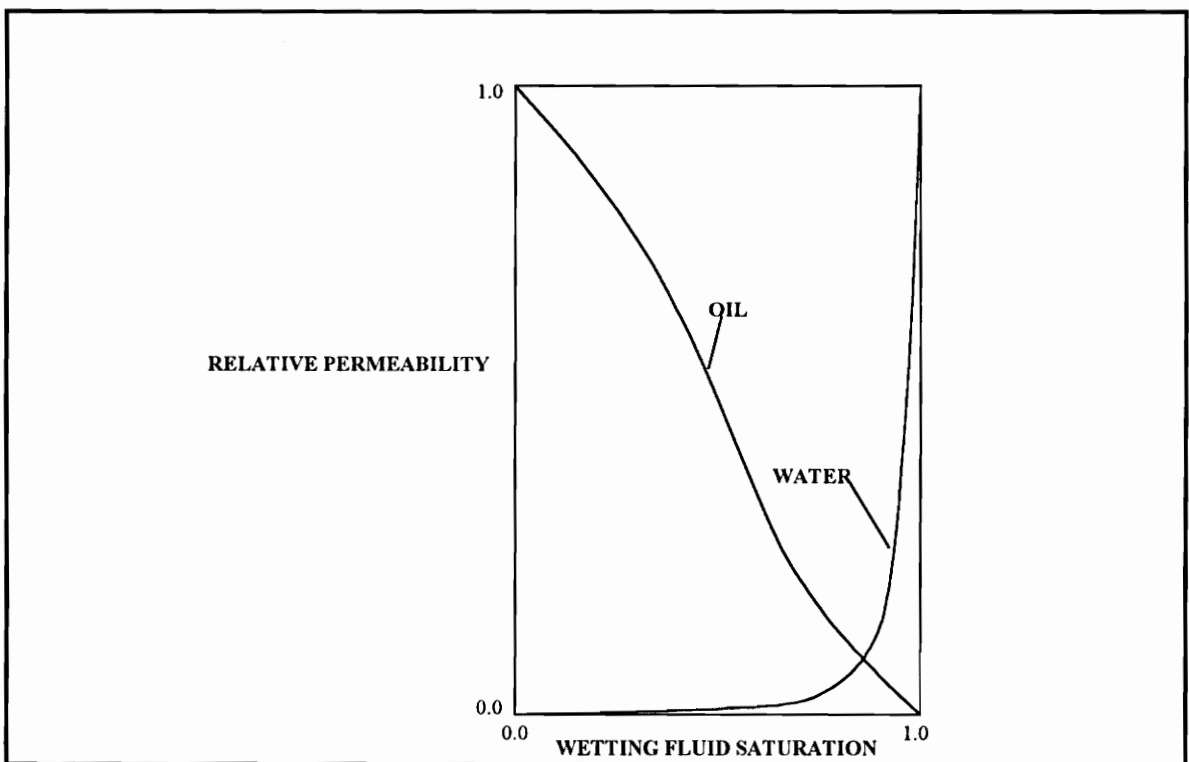


Figure 2.12 Relative oil and water permeabilities (after Sheng 1986)

## GOVERNING EQUATIONS OF MULTIPHASE IMMISCIBLE FLOW

By considering the specific case of a three-fluid phase system, consisting of air, oil, and water phases, and substituting Darcy's law,  $q = Ki$ , for each fluid phase into the equation for general mass conservation, the following general flow equation is developed:

$$\phi \frac{\partial \rho S}{\partial t} = - \frac{\partial \rho q_x}{\partial x} - \frac{\partial \rho q_y}{\partial y} - \frac{\partial \rho q_z}{\partial z} + \gamma, \quad (2.29)$$

where  $\gamma$  is a source-sink term due to the transfer of mass between phases, not considered in this chapter. The equations for each phase in the x-direction are:

$$\phi \frac{\partial \rho_w S_w}{\partial t} = \frac{\partial}{\partial x} \rho_w K_w \left[ \frac{\partial h_w}{\partial x} + \rho_w z \right] + \gamma_w, \quad (2.30)$$

$$\phi \frac{\partial \rho_o S_o}{\partial t} = \frac{\partial}{\partial x} \rho_o K_o \left[ \frac{\partial h_o}{\partial x} + \rho_o z \right] + \gamma_o, \text{ and} \quad (2.31)$$

$$\phi \frac{\partial \rho_a S_a}{\partial t} = \frac{\partial}{\partial x} \rho_a K_a \left[ \frac{\partial h_a}{\partial x} + \rho_a z \right] + \gamma_a, \quad (2.32)$$

where

$\rho$  = the fluid density,

$S$  = the fluid saturation, and

$\phi$  = the porosity. The subscripts a, o, and w refer to the air, oil and water phases, respectively.

In the multiphase flow system considered here, it is assumed that the fluids are flowing in a porous media with the gas phase equal to the atmospheric pressure. Since the fluid conductivity of the gas phase is considerably higher than that of the liquid phases, head loss in the gas phase is also neglected. Therefore, Equation 2.32 is eliminated from the analysis. Hysteresis due to wetting and drying of different phases in the system will not be taken into account and no interface mass transfer between the phases is considered in this section. By using saturation-head relations, the time dependent portion of the governing equations can be written in terms of the total oil and water heads and the capacity coefficients. These equations describe the movement of the oil and water phases in the multiphase immiscible flow system and can be written in three-dimensions as (Kuppusamy et al. 1987)

$$\frac{\partial}{\partial x} \left( K_{xw} \frac{\partial H_w}{\partial x} \right) + \frac{\partial}{\partial y} \left( K_{yw} \frac{\partial H_w}{\partial y} \right) + \frac{\partial}{\partial z} \left( K_{zw} \frac{\partial H_w}{\partial z} \right) = e_{wo} \frac{\partial H_o}{\partial t} + e_{ww} \frac{\partial H_w}{\partial t} \quad (2.33)$$

for the water phase, and

$$\frac{\partial}{\partial x} \left( K_{xo} \frac{\partial H_o}{\partial x} \right) + \frac{\partial}{\partial y} \left( K_{yo} \frac{\partial H_o}{\partial y} \right) + \frac{\partial}{\partial z} \left( K_{zo} \frac{\partial H_o}{\partial z} \right) = e_{oo} \frac{\partial H_o}{\partial t} + e_{ow} \frac{\partial H_w}{\partial t} + R \quad (2.34)$$

for the oil phase, where

H = the total head,

e = the moisture capacity coefficients,

K = the fluid conductivity, and

R = the interphase mass transfer. R is equal to zero for the multiphase immiscible

flow system, without mass transport. The term will have a value based on mass transport when considered in the weakly-coupled analysis described in Chapter 7.

In the above equations, the subscripts o, and w refer to the oil and water phases, respectively. The moisture capacity is the derivative of the volumetric fluid content with respect to the fluid pressure. The subscripts au, ow and WW refer to the oil-oil, oil-water, and water-water capacity coefficients. The capacity coefficients for the air-oil-water system are given by

$$e_{ww} = \frac{\partial \theta_w}{\partial h_w} = \phi \frac{\partial S_w}{\partial h_w} = \phi(1 - S_{rw} - S_{ro}) \frac{\partial \bar{S}_w}{\partial h_w}, \quad (2.35)$$

$$e_{oo} = \frac{\partial \theta_o}{\partial h_o} = \frac{\partial \theta_t}{\partial h_o} - \frac{\partial \theta_w}{\partial h_o} = \phi \frac{\partial S_t}{\partial h_o} - e_{wo}, \text{ and} \quad (2.36)$$

$$e_{wo} = e_{ow} = -e_{ww}, \quad (2.37)$$

where

S = the saturation,

$\phi$  = the porosity, and

h = the pressure head.

In Equations 2.35 and 2.36 the subscript r refers to the residual saturation for the given phase, and the subscript t refers to the total saturation of the system. The effective

saturations for a given phase in Equations 2.35 and 2.36, denoted as  $\bar{S}$ , are nondimensionalized saturations and are found by conducting static head tests that relate capillary pressure head to the degree of saturation of the wetting phase under static conditions (Sheng 1986). Normalizing the relations obtained for the two-phase flow systems to the three-phase system, the following equations for effective saturations are developed:

$$\bar{S}_w = \frac{S_w - S_{rw}}{1 - S_{rw} - S_{ro}}, \quad (2.38)$$

$$\bar{S}_o = \frac{S_o - S_{ro}}{1 - S_{rw} - S_{ro}}, \text{ and} \quad (2.39)$$

$$\bar{S}_t = \frac{S_w + S_o - S_{rw} - S_{ro}}{1 - S_{rw} - S_{ro}}. \quad (2.40)$$

The notation used in Equations 2.38-2.40 is the same as previously described. The residual saturations,  $S_{ro}$  and  $S_{rw}$  in these Equations are independent of the change in capillary pressure heads and  $S_{ro}$  is assumed to vary linearly with the oil saturation,  $S_o$ , so that

$$S_{ro} = \frac{S_o (S_{ro}^{ao} - S_{rw}^{ow})}{1 - S_{rw}^{ow}}. \quad (2.41)$$

In Equation 2.41, the superscripts ao and ow refer to the air-oil and oil-water systems for the residual oil and water saturations.

The effective saturations in the two- and three-phase systems are (Kuppusamy et al., 1987):

(1) for the air-oil-water system:

$$\bar{S}_w = \left[ 1 + (\beta_w^{ow} \alpha h_{ow})^n \right]^{-m}; \quad (2.42)$$

$$\bar{S}_t = \left[ 1 + (\beta_o^{ao} \alpha h_{oa})^n \right]^{-m}; \text{ and} \quad (2.43)$$

$$\bar{S}_o = \bar{S}_t - \bar{S}_w. \quad (2.44)$$

(2) for the air-oil system:

$$\bar{S}_t = \bar{S}_o = \left[ 1 + (\beta_o^{ao} \alpha h_{oa})^n \right]^{-m}, \text{ and} \quad (2.45)$$

(3) for the air-water system, the parameter  $\beta_a^{aw} = 1$  and the equation reduces to the form of the original equation for unsaturated flow (van Genuchten 1980):

$$\bar{S}_t = \bar{S}_w = \left[ 1 + (\alpha h_{aw})^n \right]^{-m}, \quad (2.46)$$

These equations describe the relationship between capillary head and effective saturation for any combination of fluids in the three-phase system. Taking the partial derivative of the effective saturations with respect to the water and oil heads, respectively, Equations 2.35 and 2.36 can be expressed as:

$$e_{ww} = \Phi(1 - S_{rw} - S_{ro})\beta_w^{ow}\alpha(n-1)\bar{S}_w^{1/m}(1 - \bar{S}_w^{1/m})^m \quad (2.47)$$

$$e_{oo} = \Phi(1 - S_{rw} - S_{ro})\beta_o^{ao}\alpha(n-1)\bar{S}_t^{1/m}(1 - \bar{S}_t^{1/m})^m + e_{ww}. \quad (2.48)$$

Note that before oil enters the system,  $S_{ro}$  equals zero, but once oil has entered the system, the term  $S_{ro}$  will not fall below the residual saturation value. Therefore, if oil is not present in the system, Equation 2.48 reduces to the moisture capacity coefficient for water, which is the time dependent portion of the unsaturated flow equation for the air-water system, this can be expressed as:

$$e_{ww} = \Phi(1 - S_{rw})\alpha(n-1)\bar{S}_w^{1/m}(1 - \bar{S}_w^{1/m})^m. \quad (2.49)$$

The  $\beta$  terms, in Equations 2.47 and 2.48, are scaling parameters which relate the given phase (denoted by the subscript) in a two-phase system (denoted by the superscripts) to the original relationship for unsaturated flow, described by van Genuchten (1980). Here the subscripts o and w represent the oil and water phases, while the ow and ao superscripts represent the oil-water and air-oil systems. These parameters  $\beta$ ,  $n$ , and  $\alpha$  are not material parameters but are curve-fitting parameters that can all be determined through laboratory column tests. It is important to note, that if  $S_o \leq S_{ro}$  then  $e_{ow} = e_{wo} = e_{oo}$  and when no oil is present in the system.

The fluid conductivity,  $K(h)$ , in Equations 2.33 and 2.34, which describes the multiphase flow system, is based on the saturated hydraulic conductivity and the relative permeability, as previously shown in Equation 2.15,  $K_u = K_r K_s$  (Parker et al., 1987). For the multiphase flow system, the model previously presented by Mualem can be extended



to each of the phases in the system. Parker (1989) explains that this can be accomplished by considering that the Laplace equation indicates an inverse relationship between pore radius and capillary pressure, resulting in the effective saturation of each phase being a function of an aggregate constant which is then factored out of each equation. For the non-hysteretic van Genuchten model, the equations which relate the unsaturated fluid conductivities for the water and oil phase to the effective saturations are (Parker et al. 1987):

$$K_w = K_{sw} \bar{S}_w^{0.5} \left[ 1 - \left( 1 - \bar{S}_w^{1/m} \right)^m \right]^2, \text{ and} \quad (2.50)$$

$$K_o = K_{so} \bar{S}_o^{0.5} \left[ 1 - \left( 1 - \bar{S}_w^{1/m} \right)^m - \left( 1 - \bar{S}_t^{1/m} \right)^m \right]^2, \quad (2.51)$$

where  $K_o$  and  $K_w$  represent the fluid conductivities for the oil and water phases, respectively and  $K_{so}$  and  $K_{sw}$  represent the saturated fluid conductivities for the oil and water phases, respectively.

## CONCLUSIONS

Chapter 2 presents the governing equations related to multiphase flow. The theory is based on research conducted by Parker et al. (1987), Kuppusamy et al. (1987), and Sheng (1986). The model is directly related to the theory of unsaturated flow, which is a simplified case of multiphase flow for a two-phase system. The present model is based on van Genuchten's model (1980), relating water content to pressure head in an unsaturated

air-water system. Here, van Genuchten's model is extended to the three-phase system consisting of air, oil, and water.

Chapter 2 includes a complete discussion of the curve-fitting parameters related to van Genuchten' model and the scaling parameters which extend this model to the multiphase flow model. A complete discussion of unsaturated flow and other aspects such as fluid-fluid and fluid-solid relations are also presented.

## **CHAPTER 3**

### **FINITE ELEMENT MODEL FOR MULTIPHASE FLOW**

## INTRODUCTION

The governing differential equations for multiphase immiscible flow are applied to arbitrary domains with heterogeneous and nonlinear materials. Due to these complexities, numerical methods are the only convenient and effective way of solving these problems. IMFTP3D utilizes the finite element method, which has been proved to be both elegant and effective in solving fluid flow problems with conditions such as those described in Chapter 2.

## FORMULATION FROM GOVERNING EQUATIONS

For a trilinear, isoparametric, eight-noded brick element (hexahedral), the total heads within each element expressed as:

$$H_w = [N] \{H_n\}_w^T = [N_1 \ N_2 \ N_3 \ N_4 \ N_5 \ N_6 \ N_7 \ N_8] \{H_{w1} \ H_{w2} \ H_{w3} \ H_{w4} \ H_{w5} \ H_{w6} \ H_{w7} \ H_{w8}\}^T \quad (3.1)$$

$$H_o = [N] \{H_n\}_o^T = [N_1 \ N_2 \ N_3 \ N_4 \ N_5 \ N_6 \ N_7 \ N_8] \{H_{o1} \ H_{o2} \ H_{o3} \ H_{o4} \ H_{o5} \ H_{o6} \ H_{o7} \ H_{o8}\}^T \quad (3.2)$$

where

$H_{wi}$  and  $H_{oi}$  = the unknown nodal heads for the water and oil phases at node  $i$ ,  
respectively, and

$N_i$  = the trilinear shape functions for the three-dimensional brick element.

The shape functions for elements 1-8 are (Hughes, 1987)

$$\begin{aligned}
N_1 &= \frac{1}{8}(1-s)(1-t)(1+r), & N_5 &= \frac{1}{8}(1-s)(1-t)(1-r), \\
N_2 &= \frac{1}{8}(1+s)(1-t)(1+r), & N_6 &= \frac{1}{8}(1+s)(1-t)(1-r), \\
N_3 &= \frac{1}{8}(1+s)(1+t)(1+r), & N_7 &= \frac{1}{8}(1+s)(1+t)(1-r), \\
N_4 &= \frac{1}{8}(1-s)(1+t)(1+r), & N_8 &= \frac{1}{8}(1-s)(1+t)(1-r),
\end{aligned} \tag{3.3}$$

where s, t, and r are the coordinates in the natural coordinate system. The derivatives of the shape functions with respect to the spatial coordinates in each direction are

$$[B] = \left[ \frac{\partial N_i}{\partial x} \quad \frac{\partial N_i}{\partial y} \quad \frac{\partial N_i}{\partial z} \right]^T. \tag{3.4}$$

By using the variational approach, the functional for the oil and water phases is constructed in three-dimensions as (Kuppusamy et al. 1987):

$$\begin{aligned}
\Pi_w &= \frac{1}{2} \iiint_{x,y,z} \left[ K_{xw} \left( \frac{\partial H_w}{\partial x} \right)^2 + K_{yw} \left( \frac{\partial H_w}{\partial y} \right)^2 + K_{zw} \left( \frac{\partial H_w}{\partial z} \right)^2 \right] dx dy dz \\
&+ \iiint_{x,y,z} \left( e_{wo} H_w \frac{\partial H_o}{\partial t} + e_{ww} H_w \frac{\partial H_w}{\partial t} \right) dx dy dz - \int_l H_w \bar{q}_w dl,
\end{aligned} \tag{3.5}$$

and

$$\begin{aligned} \Pi_o = & \frac{1}{2} \iiint_{x,y,z} \left[ K_{xo} \left( \frac{\partial H_o}{\partial x} \right)^2 + K_{yo} \left( \frac{\partial H_o}{\partial y} \right)^2 + K_{zo} \left( \frac{\partial H_o}{\partial z} \right)^2 \right] dx dy dz \\ & + \iiint_{x,y,z} \left( e_{oo} H_w \frac{\partial H_o}{\partial t} + e_{ow} H_w \frac{\partial H_w}{\partial t} \right) dx dy dz - \int_1 H_o \bar{q}_o dl. \end{aligned} \quad (3.6)$$

Now the element equations in matrix form can be written as

$$[K]_w \{H_n\}_w + [K_{tw}]_w \{\dot{H}_n\}_w + [K_{tw}]_o \{\dot{H}_n\}_o = \{Q\}_w, \text{ and} \quad (3.7)$$

$$[K]_o \{H_n\}_o + [K_{to}]_w \{\dot{H}_n\}_w + [K_{to}]_o \{\dot{H}_n\}_o = \{Q\}_o, \quad (3.8)$$

where the overdot represents differentiation with respect to time. The fluid conductivity matrix for the water phase is

$$[K]_w = \iiint_{x,y,z} [B]^T [K_w] [B] dx dy dz, \quad (3.9)$$

where

$$[K_w] = \begin{bmatrix} K_{xw} & 0 & 0 \\ 0 & K_{yw} & 0 \\ 0 & 0 & K_{zw} \end{bmatrix}. \quad (3.10)$$

The capacity matrices for the water, with respect to the water and oil phases, are given as

$$[K_{tw}]_w = \iiint_{x,y,z} e_{ww} [N]^T [N] dx dy dz, \text{ and} \quad (3.11)$$

$$[K_{to}]_w = \iiint_{x,y,z} e_{wo} [N]^T [N] dx dy dz . \quad (3.12)$$

Similarly, for the oil phase, the conductivity matrix is

$$[K]_o = \iiint_{x,y,z} [B]^T [K_o] [B] dx dy dz , \quad (3.13)$$

where

$$[K_o] = \begin{bmatrix} K_{xo} & 0 & 0 \\ 0 & K_{yo} & 0 \\ 0 & 0 & K_{zo} \end{bmatrix} . \quad (3.14)$$

The capacity matrices for oil, with respect to the water and oil phases, are

$$[K_{tw}]_o = \iiint_{x,y,z} e_{ow} [N]^T [N] dx dy dz , \text{ and} \quad (3.15)$$

$$[K_{to}]_o = \iiint_{x,y,z} e_{oo} [N]^T [N] dx dy dz . \quad (3.16)$$

The load vectors for the water and oil phases are represented, respectively, by

$$\{Q\}_w = \{\bar{q}_{w1} \ \bar{q}_{w2} \ \bar{q}_{w3} \ \bar{q}_{w4}\}^T \quad (3.17)$$

$$\{Q\}_o = \{\bar{q}_{o1} \bar{q}_{o2} \bar{q}_{o3} \bar{q}_{o4}\}^T + \{Q^*\}, \quad (3.18)$$

where

$$\{Q^*\} = \int R\{N\}^T dx dy dz. \quad (3.19)$$

This term is set equal to zero for the case of discrete phase flow, but is used in the weakly-coupled mass transport model presented in Chapter 7. By combining the equations for oil and water flow into a fully-coupled formulation, where the unknown oil and water heads are solved simultaneously, the following relationship is developed:

$$[K]\{H_n\} + [K_t]\{\dot{H}_n\} = \{Q\}, \quad (3.20)$$

where the conductivity and capacity matrices are

$$[K] = \begin{bmatrix} [K]_w & [0] \\ [0] & [K]_o \end{bmatrix}, \text{ and} \quad (3.21)$$

$$[K_t] = \begin{bmatrix} [K_{tw}]_w & [K_{to}]_w \\ [K_{tw}]_o & [K_{to}]_o \end{bmatrix}. \quad (3.22)$$

The unknown head and velocity vector terms are

$$\{H_n\} = \{H_{w1} H_{w2} H_{w3} H_{w4} H_{w5} H_{w6} H_{w7} H_{w8} H_{o1} H_{o2} H_{o3} H_{o4} H_{o5} H_{o6} H_{o7} H_{o8}\}^T, \quad (3.23)$$

and

$$\{\dot{H}_n\} = \{\dot{H}_{w1} \dot{H}_{w2} \dot{H}_{w3} \dot{H}_{w4} \dot{H}_{w5} \dot{H}_{w6} \dot{H}_{w7} \dot{H}_{w8} \dot{H}_{o1} \dot{H}_{o2} \dot{H}_{o3} \dot{H}_{o4} \dot{H}_{o5} \dot{H}_{o6} \dot{H}_{o7} \dot{H}_{o8}\}^T, \quad (3.24)$$

The load vector is

$$\{Q\} = \{\bar{q}_{w1} \bar{q}_{w2} \bar{q}_{w3} \bar{q}_{w4} \bar{q}_{w5} \bar{q}_{w6} \bar{q}_{w7} \bar{q}_{w8} \bar{q}_{o1} \bar{q}_{o2} \bar{q}_{o3} \bar{q}_{o4} \bar{q}_{o5} \bar{q}_{o6} \bar{q}_{o7} \bar{q}_{o8}\}^T. \quad (3.25)$$

Evaluation of all integrals is employed using the two-point Gauss-quadrature technique.

## TIME INTEGRATION TECHNIQUE

IMFTP3D uses the finite difference method to handle the time dependent differential equations. Applying the general ' $\theta$ ' algorithm (Belytschko and Liu, 1983), to the equation

$$[K]\{H_n\} + [K_t]\{\dot{H}_n\} = \{Q\}, \quad (3.26)$$

the general form of the  $\theta$ -method, as it is used in the multiphase flow portion of IMFTP3D, is given as



$$\begin{aligned} & \left( \frac{[K_t]_{t+\Delta t}}{\Delta t} + \theta [K]_{t+\Delta t} \right) \{H_n\}_{t+\Delta t} \\ &= \left( \frac{[K_t]_{t+\Delta t}}{\Delta t} - (1-\theta) [K_t]_{t+\Delta t} [K_t]^{-1} [K]_t \right) \{H_n\}_t + (1+\theta) [K_t]_{t+\Delta t} [K_t]^{-1} \{Q\}_t + \theta \{Q\}_{t+\Delta t} \quad (3.27) \end{aligned}$$

where  $\theta$  is referred to as the time-weighting factor ( $0 \leq \theta \leq 1$ ),  $\Delta t$  is the time increment, and the subscripts denote the time at which the variables are evaluated. Here,  $[K_t]_t \neq [K_t]_{t+\Delta t}$  and  $\{Q\}_t$  is not necessarily equal to  $\{Q\}_{t+\Delta t}$ . IMFTP3D allows the user to input the desired value of  $\theta$  to be used in the problem. The fully-implicit backwards difference method corresponds to a value of  $\theta = 1$ , and is unconditionally stable. Other methods such as the fully-explicit forwards difference method ( $\theta = 0$ ), the Crank-Nicholson method ( $\theta = 1/2$ ), and the Galerkin method ( $\theta = 2/3$ ) may give more accurate solutions than the backwards difference method, but often lead to oscillatory solutions for large time steps. It is recommended that a value of  $\theta \geq 0.6$  be used.

## ITERATION TECHNIQUE FOR NONLINEARITY

In the governing differential equations, the damping and stiffness matrices,  $[K_t]_{t+\Delta t}$  and  $[K]_{t+\Delta t}$ , are functions of the head terms,  $\{H_n\}_{t+\Delta t}$ , which are unknown for the initial iteration. Thus the problem is nonlinear and requires an iterative technique to handle this nonlinearity numerically. Commonly employed methods to handle nonlinear problems include the direct iteration method (Picard's method) and the tangent iteration method (Newton-Ralphson method). Direct iteration methods are numerically simple, but may not be as efficient as the tangent iteration methods for problems that involve severe

nonlinearities. Figure 3.1 depicts how nonlinear problems are solved using the direct iteration method. The figure shows that oscillations can result for some solutions.

IMFTP3D uses a modified direct iteration method based on a relaxation factor,  $\lambda$  (Sheng, 1986). Figure 3.2 depicts how this method is used to solve nonlinear problems. It can be seen by comparing Figures 3.1 and 3.2 that the modified method provides faster convergence in cases where the solution is oscillating about a given value. The modified Picard's method presented here is further revised and presented in the following section.

Initially, estimated values of the conductivity and capacity matrices are made based on the initial values of the oil and water heads in the system. After this, a new value of head is computed and the new stiffness and damping matrices for further iterations are computed based on

$$\{H_n\}^* = \lambda\{H_n\}_t + (1 - \lambda)\{H_n\}_{t-1}, \quad (3.28)$$

where

$\lambda$  is the relaxation factor (recommended values  $0.3 \leq \lambda \leq 0.7$ ), and

$\{H_n\}^*$  is the head value used to compute the stiffness and damping matrices for the next iteration.

$(H_n)_t$  is the value of head computed in the current iteration, and

$\{H_n\}_{t-1}$  is the value of head computed in the previous iteration.

This process continues for the number of iterations, input by the user, or until all unknown oil and water head terms converge according to the following criteria:

$$\left| H_i^j - H_i^{j-1} \right|_{t+1} \leq \varepsilon \left| H_i^j \right|_{t+1}. \quad (3.29)$$

The superscript  $j$  represents the solution for the current iteration and the subscript  $i$  represents the different degrees of freedom for oil and water heads. The term  $\epsilon$  defines the convergence criteria desired and is a value input by the user (recommended range from 0.05 - 0.10).

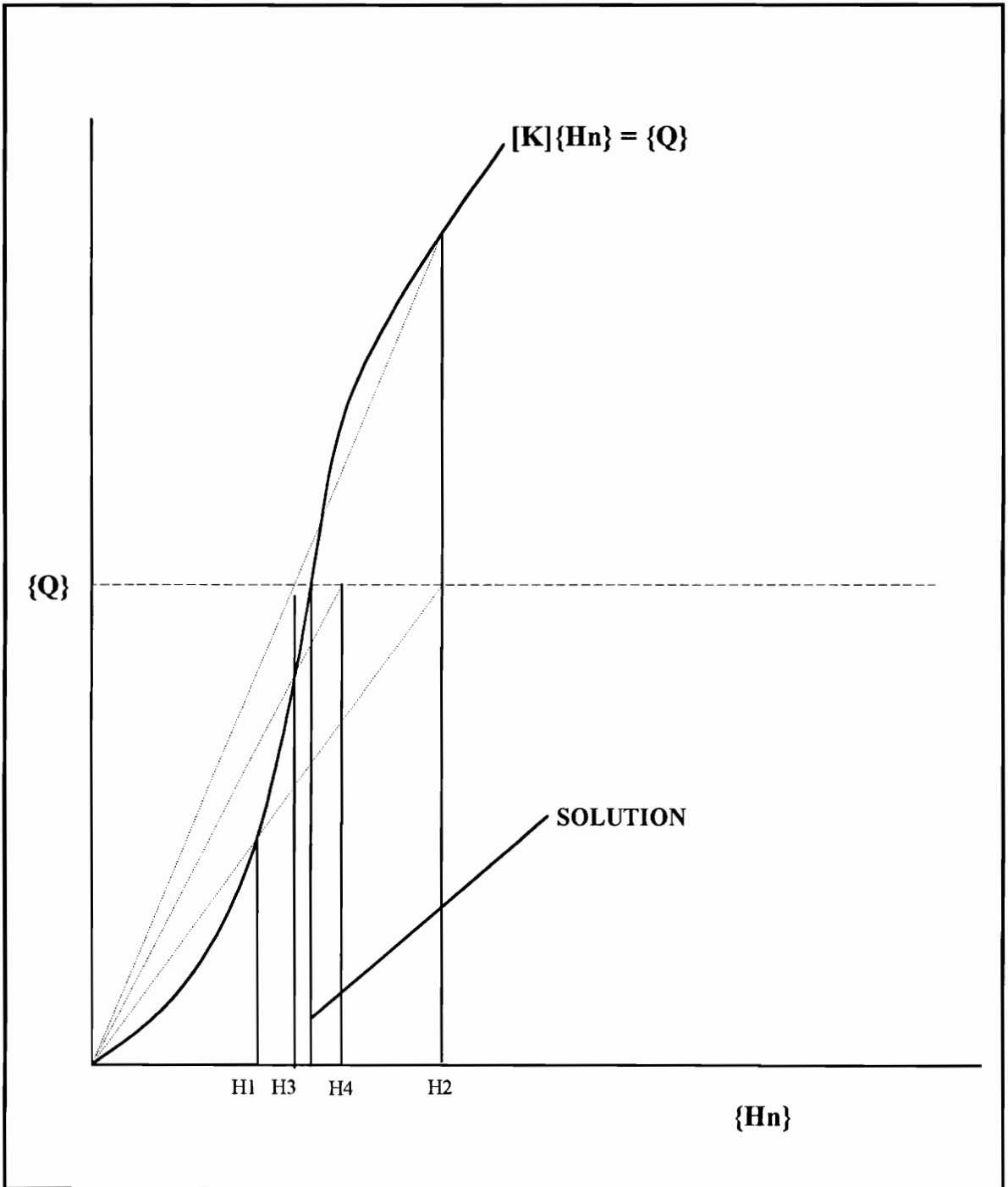


Figure 3.1 Example depicting the solution technique used in the Picard's method.

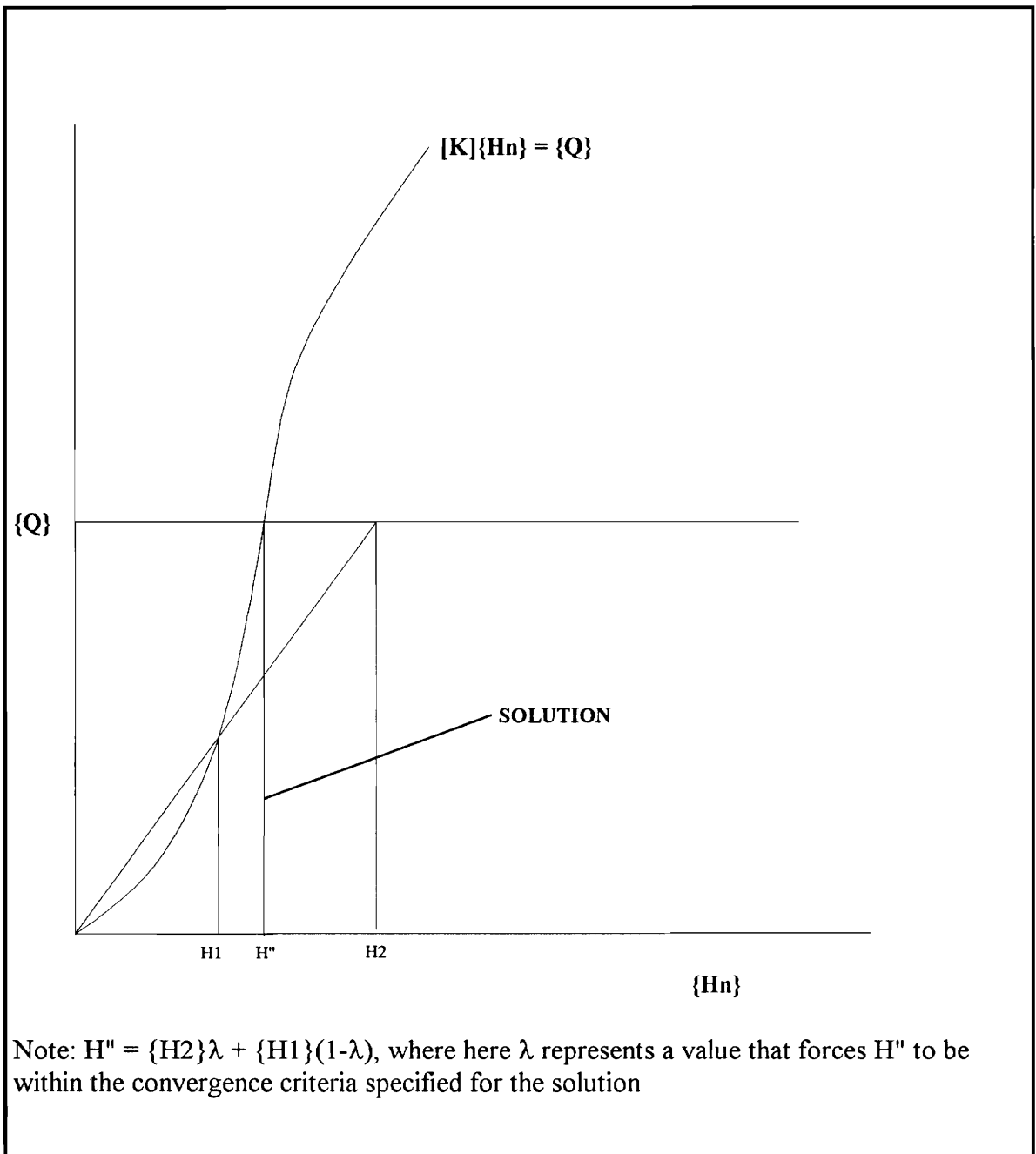


Figure 3.2 Example depicting the solution technique used in the modified Picard's method (After Sheng 1986).

## INVESTIGATION OF CONVERGENCE

Huyakorn and Pinder (1983) explains that both the direct and tangent iteration techniques face numerical difficulties in the multiphase flow problem. This is due to nonlinearities that arise, caused by variations in the fluid conductivities and the moisture capacities, before equilibrium is reached (Sheng 1986). Sheng (1986) investigated convergence in a multiphase flow formulation, similar to the one presented here, using a modified Picard's method, presented above.

In this discussion a comparison between the modified Picard's method and three variations of this method will be presented. The original modified Picard's method will be referred to as case 1, while the three other cases are presented below.

Case 2: The first revision made to the modified Picard's method involves increasing the tuning factor throughout the simulation process. The tuning factor, as previously described, controls the convergence by determining the degree of emphasis placed on the previous solution in the estimation used to update the stiffness and damping matrices for the next iteration. The initial value of the tuning factor is chosen by the user (recommended as 0.10) and is increased by 0.10 until convergence is achieved, the iteration limit is exceeded, or the tuning factor itself exceeds 1.0. For an iteration limit of 10 ( $ITR = 10$ , input by the user), the program will run 10 iterations for each tuning factor (0.1, 0.2, 0.3, ..., 1.0, if the convergence criterion is not satisfied) until the convergence criteria previously described is satisfied.

Case 3: This revision is an extension of the revision described in case 2, but includes further iterations if the convergence criterion has not been satisfied after the previous

process has taken place. In case 3, iterations are carried out at the tuning factor that gave the best results in the process referred to here as case 2. The new iteration limit for this procedure is ten times the value input by the user. The solution used to update the stiffness and damping matrices are the values corresponding to the last iteration (tuning factor of 1.0). Therefore, an iteration limit of 10 would result in 10 iterations per tuning factor and then 100 iterations at the most effective tuning factor if convergence is not complete.

Case 4: The final revision is similar to case 3. The difference is that the solution used to update the stiffness and damping matrices, after the process described in case 2 has taken place, is equal to the best solution at the most effective corresponding tuning factor.

Figure 3.3 is a plot of the number of unknowns converging versus time for the four convergence cases described above. The simulation results are based on analyses conducted on an experimental column problem, further described in Chapter 5. Since convergence was found to be poor in all cases before one second, for a time step of 0.1 seconds, convergence was only plotted up to this time level. Figure 3.3 shows the difference in the results due to the different convergence levels reached in each of the simulations. Figure 3.4 and 3.5 are plots of the simulated water outflow versus the output time levels for the four methods using two sets of parameters. It is important to note that convergence for each of these time levels was complete and the differences in the results are a function of poor convergence in the initial time steps. Figures 3.3-3.5 suggest that even if convergence is complete in later time levels, convergence of previous time levels is still critical. This is due to the time dependent nature of the problem.

Table 3.1 compares the four cases studied on the basis of convergence after the first time output level (1 second) through the last time output level (60 seconds). Here, it is shown that the original Modified Picard's method results in questionable convergence throughout the simulation, while the further modified versions result in better convergence and similar solutions (shown in Figures 3.4 and 3.5). Further simulations confirm that cases 3 and 4 result in the most consistent and similar answers. The disadvantage to the revised simulations is related to the time involved in continuing the program for an increased number of iterations. Therefore, for problems in which a tuning factor is known to produce good results, this type of simulation may not be necessary, but for simulations in which convergence is poor in various time steps, the procedure described in cases 3 and 4 will actually reduce the run time by providing quicker convergence in later time steps with a more reliable answer.

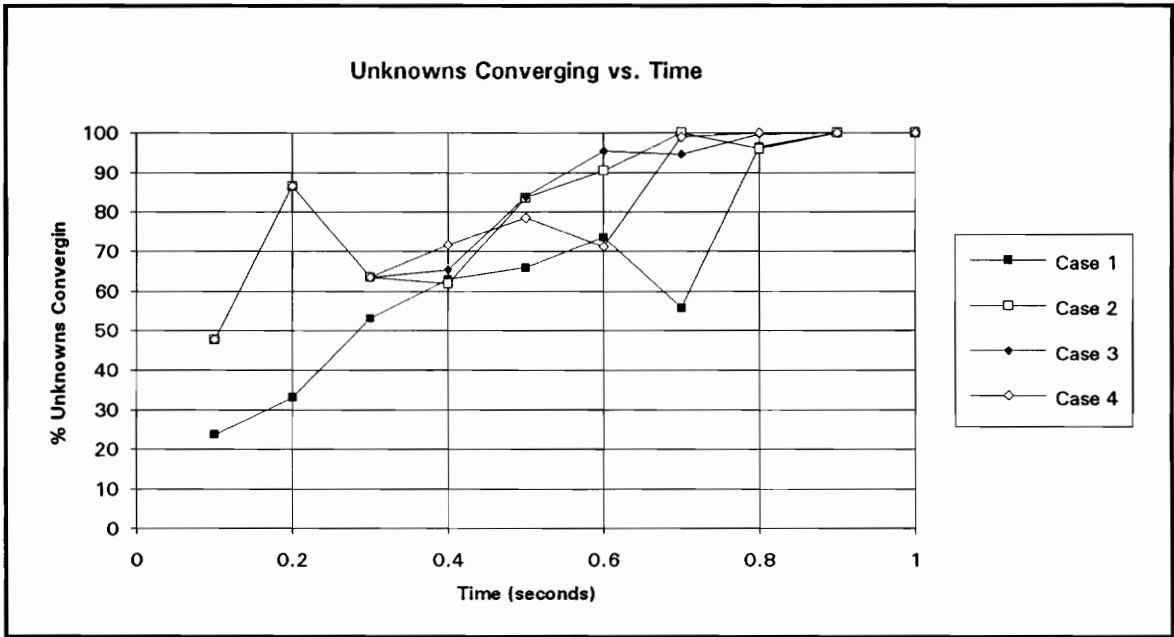


Figure 3.3 Plot of unknowns converging versus time step for the first output time interval.



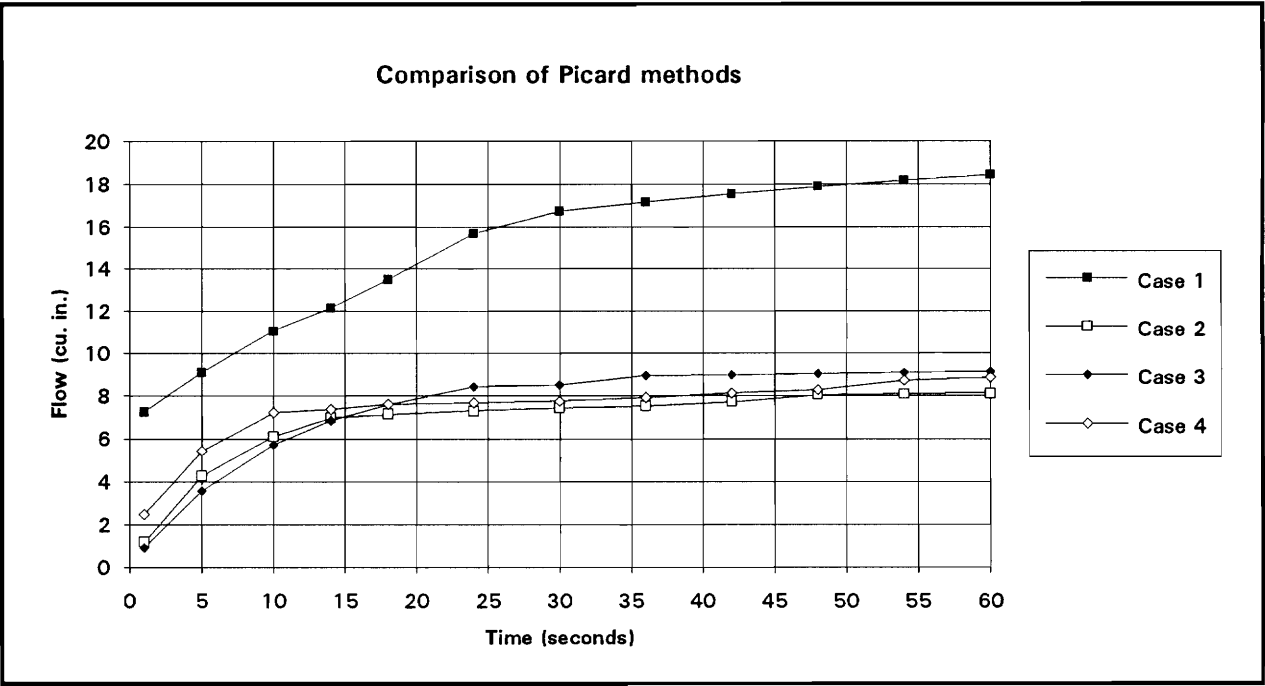


Figure 3.4 Comparison of water outflow versus time for the different revised Picard's methods used in the simulation of the experimental column example.

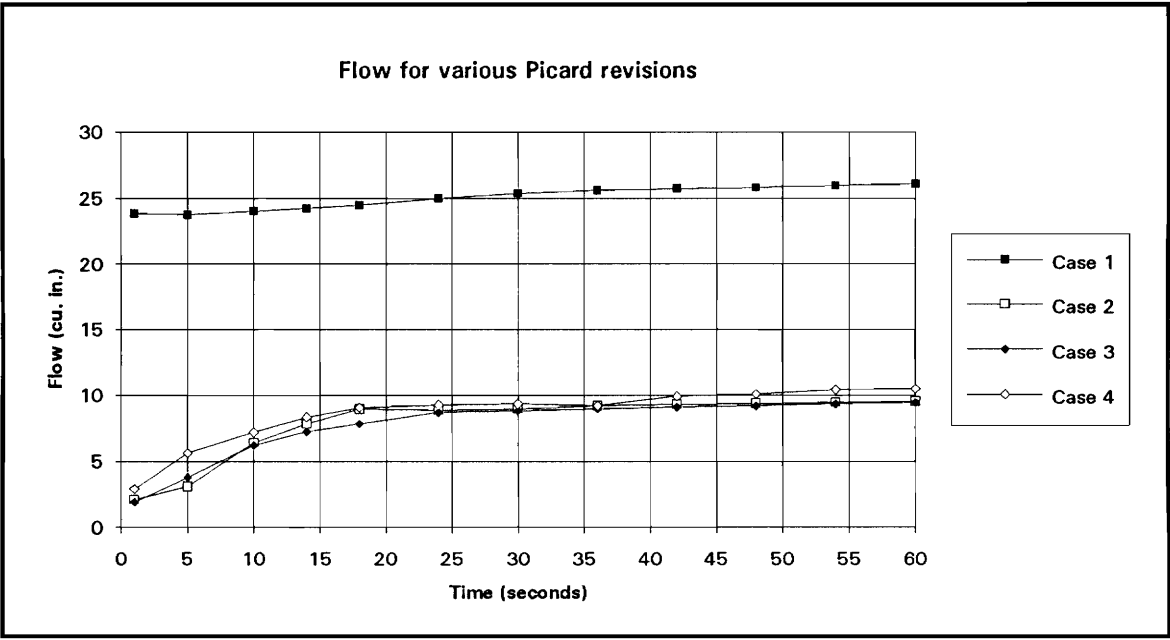


Figure 3.5 Comparison of water outflow versus time for the different revised Picard's methods used in the simulation of the experimental column example

Table 3.1 Comparison of convergence achieved for the different revised Picard's methods between time output levels of 1 and 60 seconds.

Case	No. of time steps not converging	percentage of avg. convergence
1	20	97.9
2	5	99.2
3	4	99.2
4	1	98.9

## CONCLUSIONS

Chapter 3 presents the finite element formulation for the multiphase flow problem based on Galerkin's method. The problem is both time dependent and nonlinear and therefore requires both a time integration scheme and an iteration technique to handle these aspects numerically. The Time integration scheme used in the multiphase flow portion of the model is the general  $\theta$ -scheme and the iteration for nonlinearity is based on the modified Picard's method.

An evaluation of the effects of convergence, on the results of the three-dimensional finite element simulations, is made based on the modified Picard's method and further modified methods that show better convergence for more time steps throughout the simulations. It is found that the results of later time steps can be drastically effected by the convergence of previous time steps during the simulation.

## **CHAPTER 4**

### **VALIDATION OF THREE-DIMENSIONAL MULTIPHASE IMMISCIBLE FLOW MODEL**

#### **INTRODUCTION**

Validation of the numerical simulations has been one of the concerns of many researches since the complex conditions in the field environment coupled with the complexity of the theory make the comparison of field data with numerical simulations difficult or impossible to understand. Researchers have compared numerical solutions to both approximate analytical solutions and lab investigations. Hochmuth and Sunada (1985) developed a two-phase model using the finite element method to track horizontal movement and validated their model using an approximate analytical solution developed by Shamir and Dagan (1971). Other researchers have compared two-dimensional simulations with previously validated one-dimensional models. Osborne and Sykes (1986) developed a two-phase flow finite element model, based on a generalized method of weighted residuals and linear isoparametric elements, to simulate the movements of contaminants at the Hyde Park Landfill located in Niagara Falls, New York. The model was validated by comparison with existing one-dimensional models for two-phase flow. The three-dimensional model presented in this thesis is validated based on a comparison with a previously validated two-dimensional model and experimental data contained in the existing literature.

The validation of the three-dimensional multiphase immiscible flow model is accomplished by comparing the model solution to experimental data and also with the

previously validated two-dimensional model using two example problems. Both of the example problems are taken from Kuppusamy et al. (1987) and compared the models for previously studied one- and two-dimensional simulations.

#### **EXAMPLE 4.1**

The first example problem is a comparison of a transient laboratory test on a soil column with two- and three-dimensional multiphase immiscible flow finite element simulations. The experiment involves 5.06 cm long by 5.33 cm diameter columns of well-graded sand. Initially, the columns are at an equilibrium condition with the pressure head for water,  $h_w$ , equal to 2.0 cm at the bottom of the sample and the pressure head for oil (p-cymene),  $h_o$ , equal to 1.0 cm at the top of the sample. This condition will also be present in the finite element model as the initial condition throughout the domain. The sample is then subjected to an injection of oil, resulting in a constant oil pressure head ( $h_o$ ) of 30 cm at the top of the sample. This will represent a continuous oil boundary condition in the finite element model. The contaminant used in the example is p-cymene, which has a density of 0.86 g/cm<sup>3</sup>. The lower end of the column is maintained at a constant pressure head of 2.0 cm above the bottom of the soil core and is the water boundary condition in the finite element model. The burette controlling this condition is separated from the soil core by a 0.64 cm thick porous plate, having a sufficiently high bubbling pressure to remain water saturated throughout the experiment.

The model parameters and material properties used in the finite element models are shown in Table 4.1. The parameters used for the porous stone are selected to minimize any oil from penetrating this section of the domain during the simulation.

The finite element meshes used in comparing the two- and three-dimensional models are similar to those used by Sheng (1986). The three-dimensional finite element mesh used in the simulation is shown in Figure 4.1. The mesh is constructed of 36 elements and 90 nodes, with 4 elements contained in each vertical layer of the mesh. To compare the three-dimensional simulation results with the two-dimensional simulation, a similar mesh is also used for the two-dimensional analysis. The two-dimensional mesh is constructed using 18 elements and 30 nodes, with 2 elements contained in each vertical layer of the mesh. The meshes are uniform 4.72 cm wide by 0.633 cm high elements with a thickness of 4.72 cm. This makes the cross-sectional area of each element equivalent to the cross-sectional area of the testing apparatus ( $22.3 \text{ cm}^3$ ). The bottom most layer of elements in the finite element mesh is used to represent the porous stone.

Figure 4.2 shows the comparison of the two- and three-dimensional finite element simulations with the experimental data based on the outflow of water at different time levels. The figure shows an excellent correlation between the two- and three-dimensional finite element models and a good correlation with the experimental results. The results of the two- and three-dimensional simulations are so close that it is impossible to distinguish them separately at this scale. The slight deviations between the finite element simulations and the experimental analysis resulted as either a deficiency in the general parametric model for the constitutive properties or are due to an inadequate representation of the porous media initial and boundary conditions. It is extremely difficult to determine the exact initial conditions of the oil and water contents at various points in the column. Also, the porous stone representation can be questioned. However, the predictions are within reasonable limits.

Table 4.1 Material Properties and Parameters for example 4.1

Material Properties	Well-Graded Sand	Porous Stone
Hydraulic Conductivities in x-, y-, z-directions for water	23.3 cm/hr	1.02
Hydraulic Conductivities in x-, y-, z-directions for oil	41.3 cm/hr	$1.02 \times 10^{-10}$
Porosity	0.42	0.10
Residual saturation for air-water, air-oil, and oil-water systems	0.0	0.0
Model Parameters		
van Genuchten parameter, $\alpha$	$0.052 \text{ m}^{-1}$	0.0001
van Genuchten parameter, $n$	1.84	10
Scaling Factor, $\beta_{ao}$	.91	$1.0 \times 10^{+8}$
Scaling Factor, $\beta_{ow}$	2.10	1

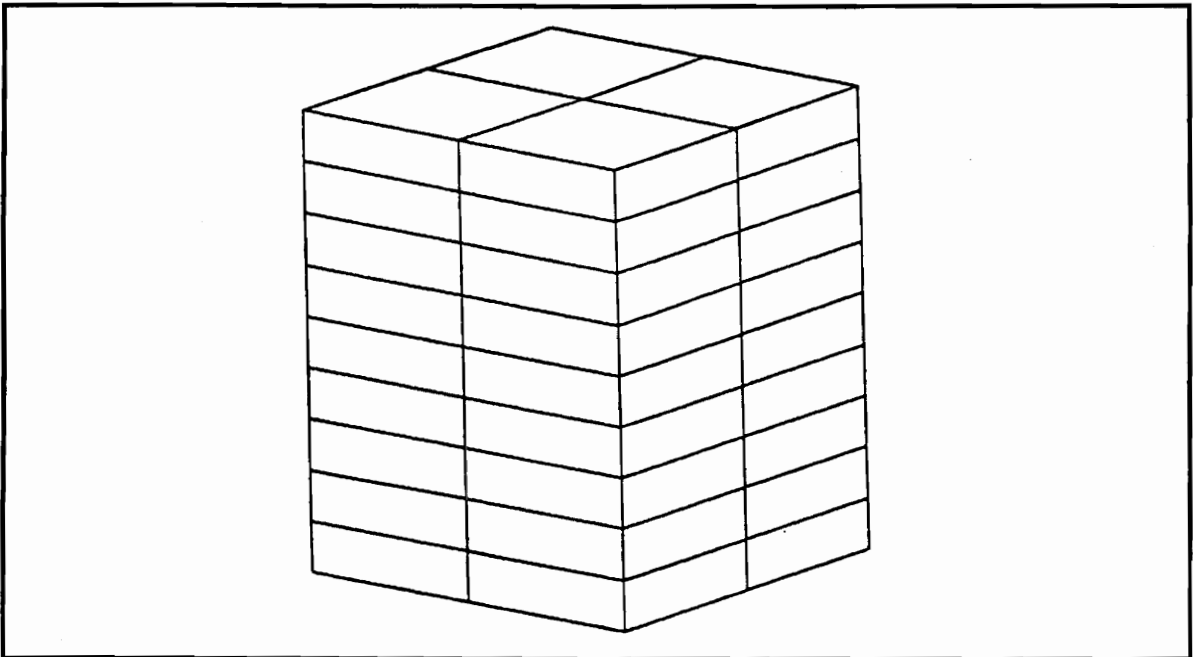


Figure 4.1 Three-dimensional finite element mesh for example 4.1

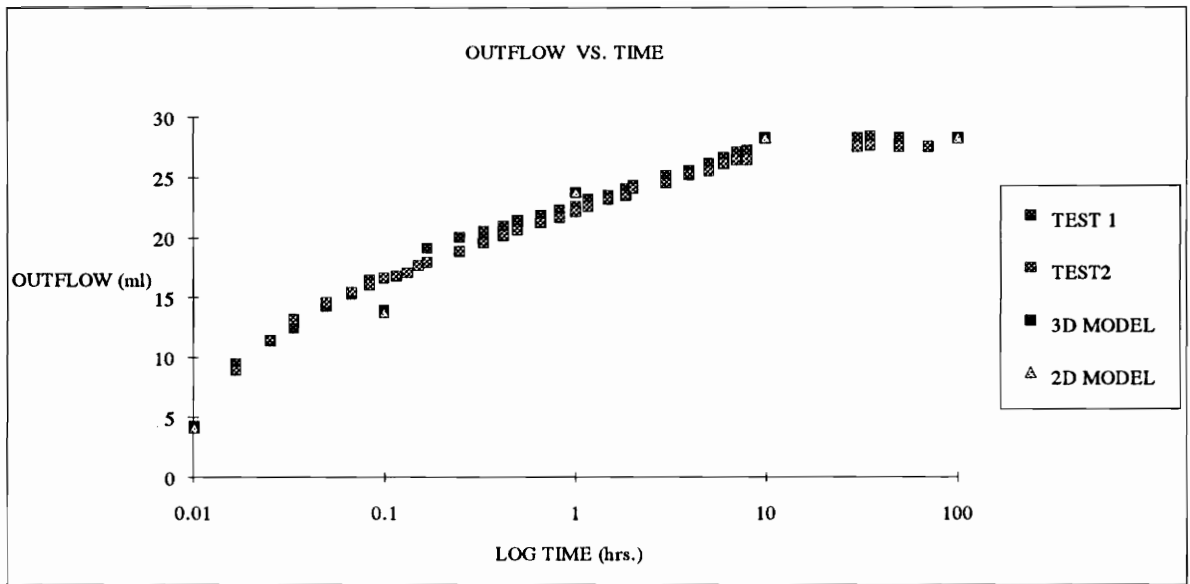


Figure 4.2 Comparison of water outflow versus time for two-and three-dimensional simulations with experimental data

Figures 4.3-4.7 show the comparison of the two- and three- dimensional simulations based on the element saturation in different vertical levels at different points in time (0.01-100 hours). The horizontal axis of the graphs in these figures, labeled element level, represents the distance from the bottom of the sample to the top of the sample in 0.633 cm intervals. Hence, element level 1 represents the bottom layer of elements in the finite element mesh (the porous stone) and element level 9 represents the top layer of elements in the mesh. These figures also show the excellent correlation between the two- and three-dimensional simulations, where again points between the two- and three-dimensional model results are difficult to distinguish. The fluctuation in saturation near the base of the mesh is attributed to the nonexistence of a boundary condition for the oil phase in the base of the specimen. This causes the oil head to be larger than the water

head in the base of the sample, since the oil head is not constrained in this region while the water head is constrained by the 2 cm boundary condition.

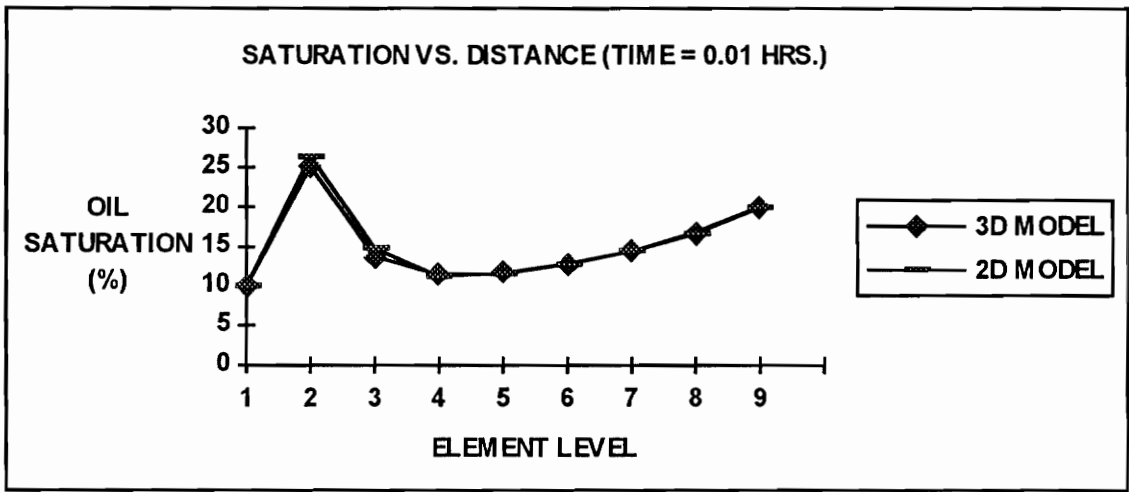


Figure 4.3 Comparison of two- and three-dimensional models for time = 0.01 hours

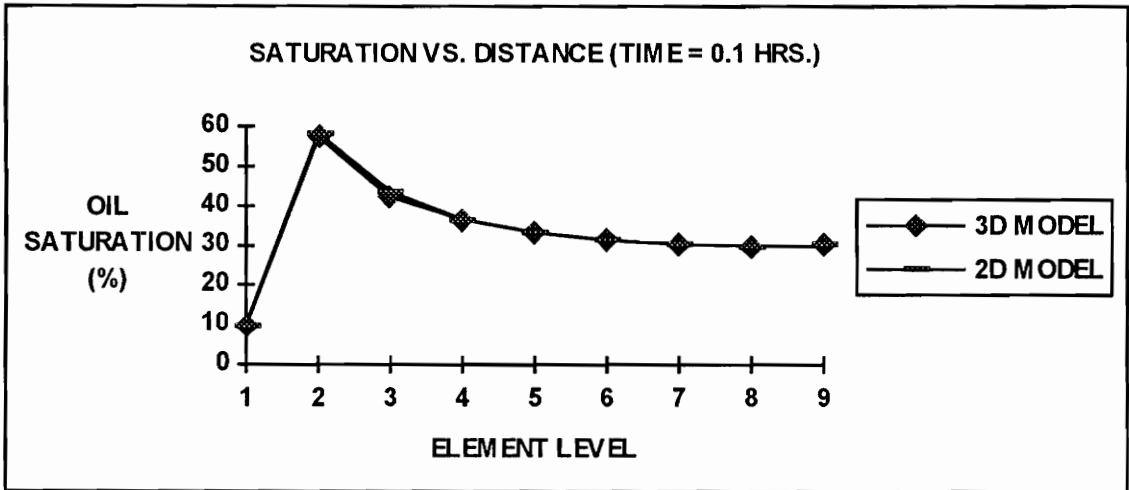


Figure 4.4 Comparison of two- and three-dimensional models for time = 0.1 hours



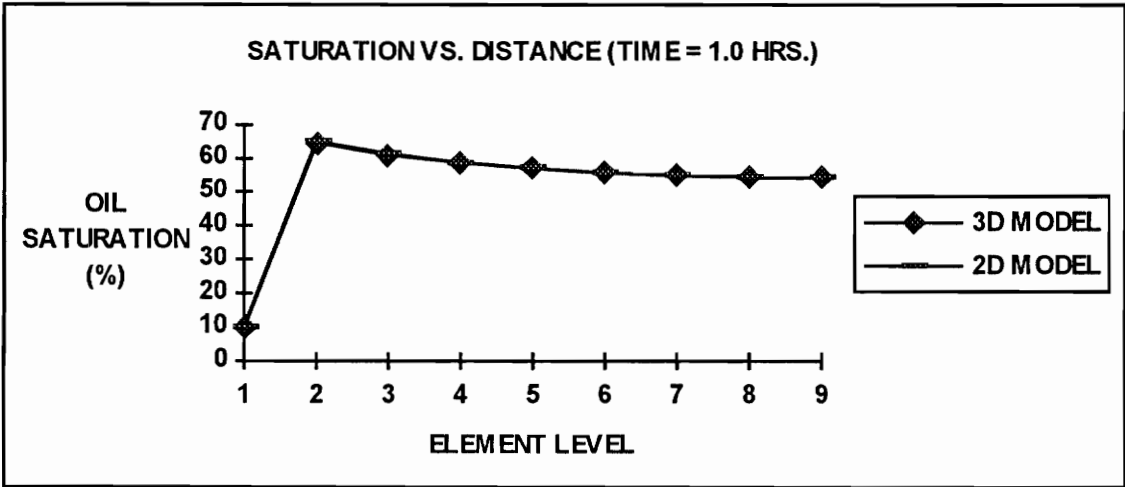


Figure 4.5 Comparison of two- and three-dimensional models for time = 1.0 hours

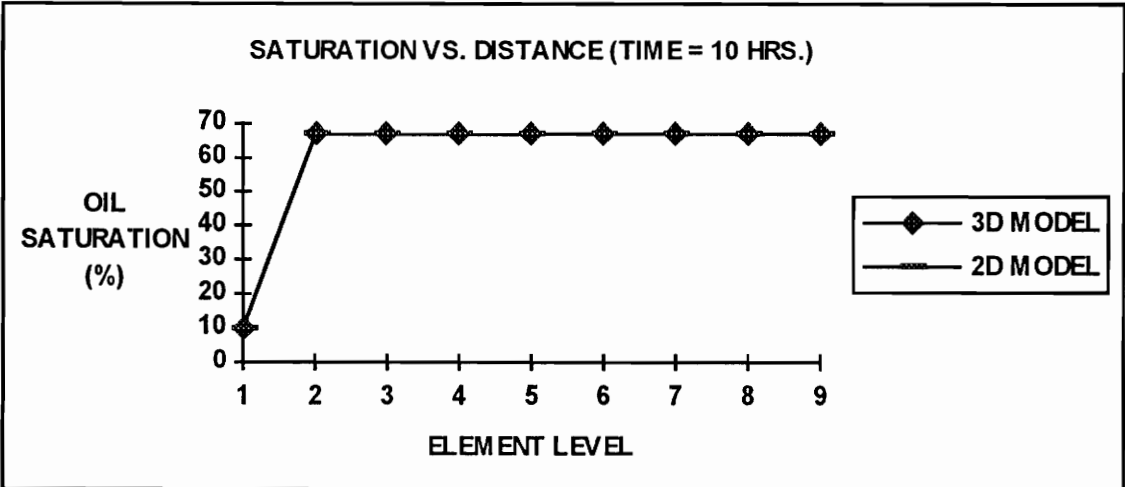


Figure 4.6 Comparison of two- and three-dimensional models for time = 10 hours

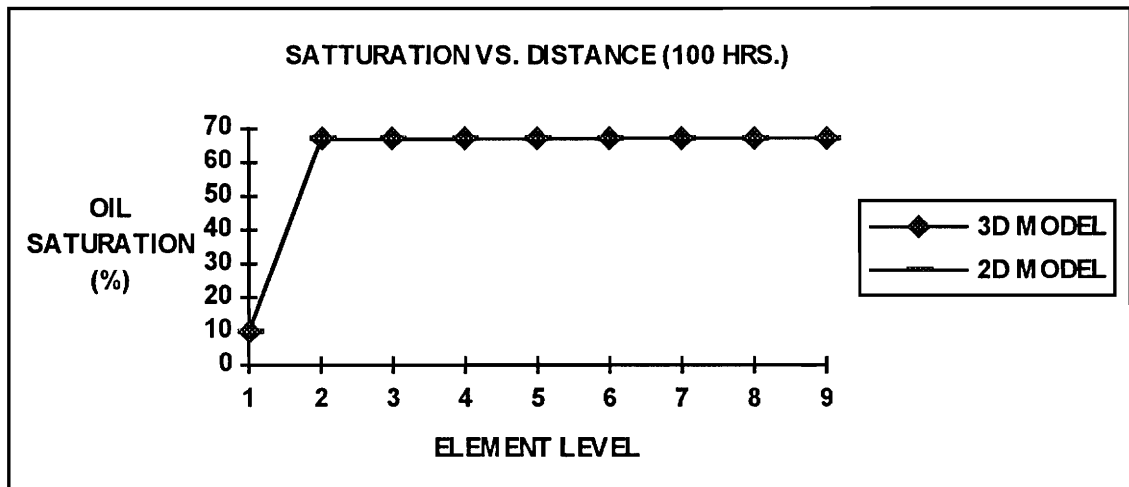


Figure 4.7 Comparison of two- and three-dimensional models for time = 100 hours

Based on the above comparisons, it is concluded that the three-dimensional model developed here shows an excellent correlation with the earlier two-dimensional model and a reasonable correlation with the experimental soil column test data for the one-dimensional column test.

#### EXAMPLE 4.2

To further examine the relationship between the two- and three-dimensional finite element models, a two-dimensional example problem is analyzed. The hypothetical problem involves a storage tank 10 meters wide by 2 meters deep, located within the subsurface of the given domain. Figure 4.8 shows the two-dimensional finite element mesh, which is discretized into 140 elements and 169 nodes (Kuppusamy et al. 1987). The three-dimensional finite element mesh is modeled after the original two-dimensional finite element mesh, shown in Figure 4.9. The three-dimensional mesh is discretized into

338 nodes and 140 elements. The domain consists of a well graded sand, 210 meters long by 16 meters deep and 10 meters thick. The base of the domain is chosen as the datum for the problem. The boundary conditions for the NAPL are all natural boundary conditions, except at the base of the leaking storage tank, where a total NAPL head of 12.8 meters (oil density = 0.899 g/cm<sup>3</sup>) is applied and held constant throughout the simulation. Initially the water table elevation is at equilibrium, with an elevation of 16 meters at the left boundary and 8 meters at the right boundary. This water condition initially displays no flux along the boundary surface. The initial condition imposed for the NAPL corresponds to no saturation in the system, which is operationally achieved by setting the total NAPL head equal to -1.0 meter. The material properties and parameters used in this example are presented in Table 4.2. The time step used in the simulation was initially set equal to 25 days.

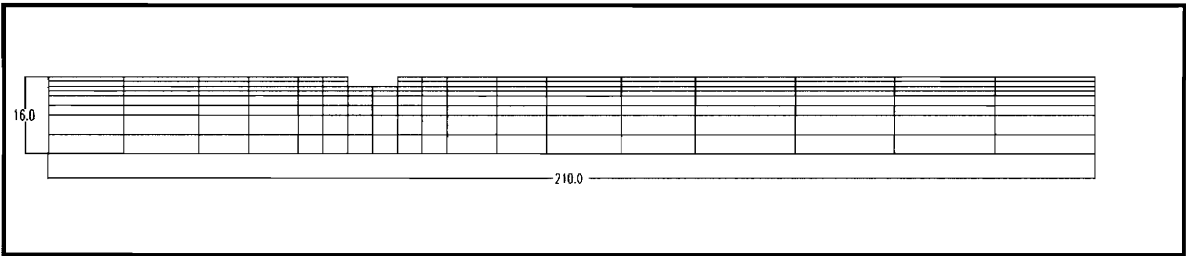


Figure 4.8 Two-dimensional finite element mesh (Example 4.2)

Table 4.2 Material Properties and Parameters for example 4.2

Material Properties	Well-Graded Sand
Hydraulic Conductivities in x-, y-, z-directions for water	2 m/day
Hydraulic Conductivities in x-, y-, z-directions for oil	1.5 m/day
Porosity	0.40
Residual saturation for air-water, air-oil, and oil-water systems	0.0
<b>Model Parameters</b>	
van Genuchten parameter, $\alpha$	5.0 m <sup>-1</sup>
van Genuchten parameter, n	1.84
Scaling Factor, $\beta_{ao}$	2.0
Scaling Factor, $\beta_{ow}$	2.2

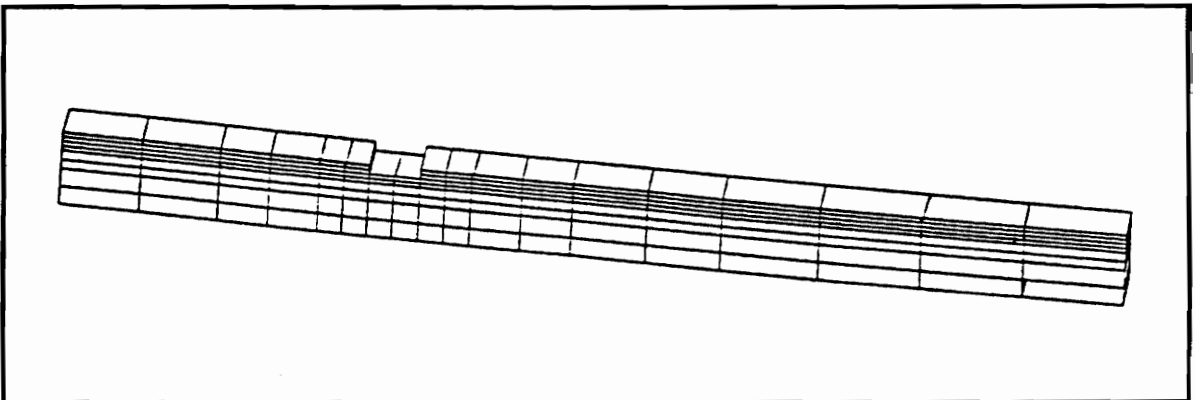


Figure 4.9 Three-dimensional finite element mesh (example 4.2)

Figures 4.10-4.12 show the two-dimensional model's prediction of the oil movement through each element. The shaded areas in these figures represent elements which contain an oil saturation greater than zero ( $S_o > 0.0$ ). The figures are for the same domain and represent time output levels of 153, 535, and 1600 days. Figures 4.13-4.15 show the three-dimensional model's prediction of the movement of oil saturation for the

same output time levels and conditions as the two-dimensional model. Examination and comparison of these figures suggest that the three-dimensional model predicts plume movements very similar to the two-dimensional simulation for a given time level, with the three-dimensional simulation predicting slightly slower movements.

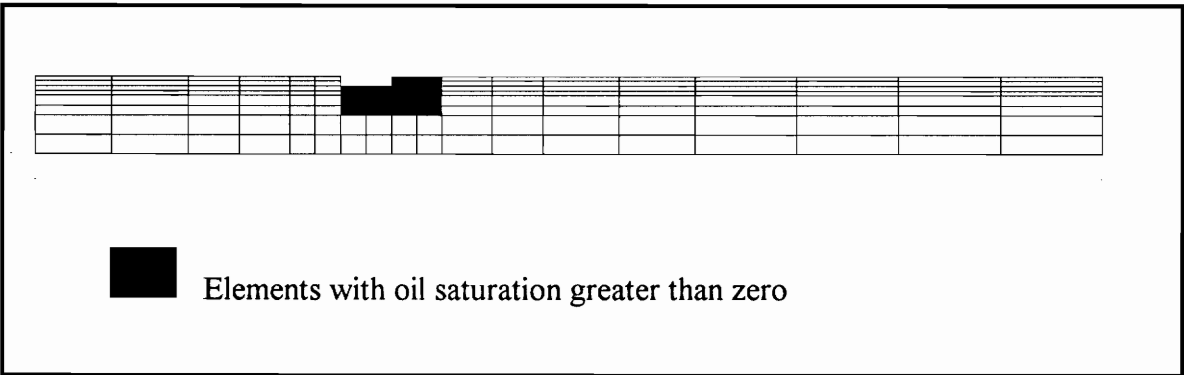


Figure 4.10 2-D Mesh - Elements with greater than zero oil saturation after 153 days.

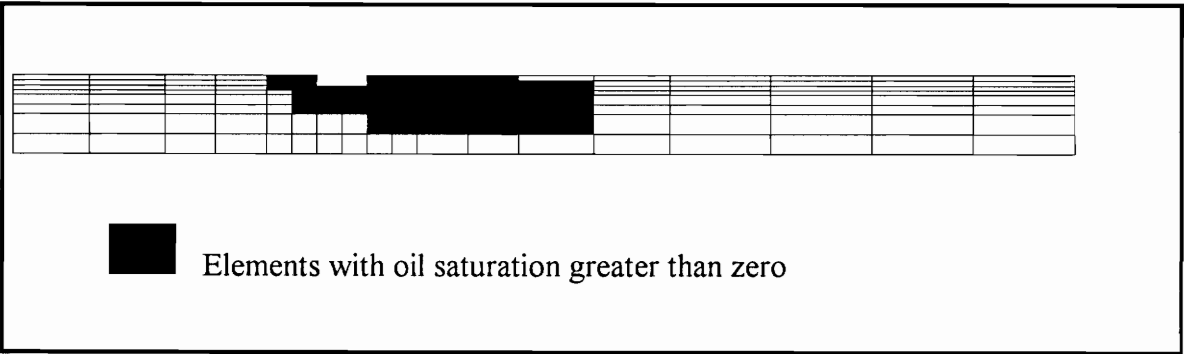


Figure 4.11 2-D Mesh - Elements with greater than zero oil saturation after 535 days.

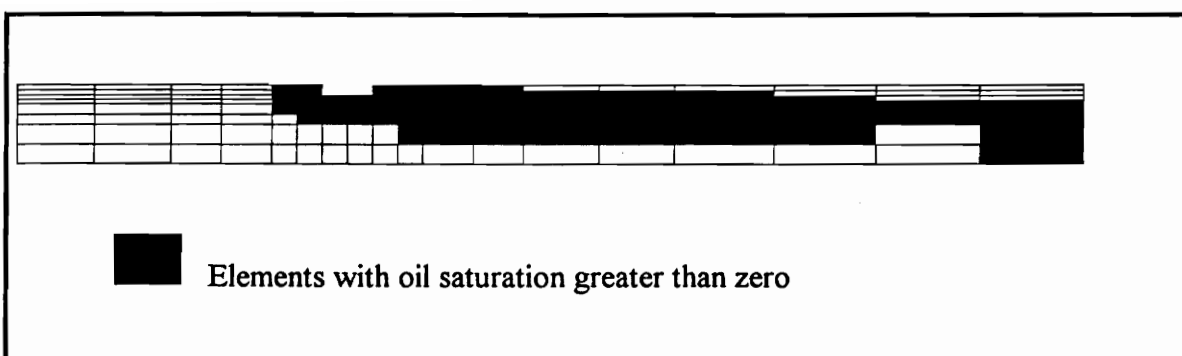


Figure 4.12 2-D Mesh - Elements with greater than zero oil saturation after 1600 days.

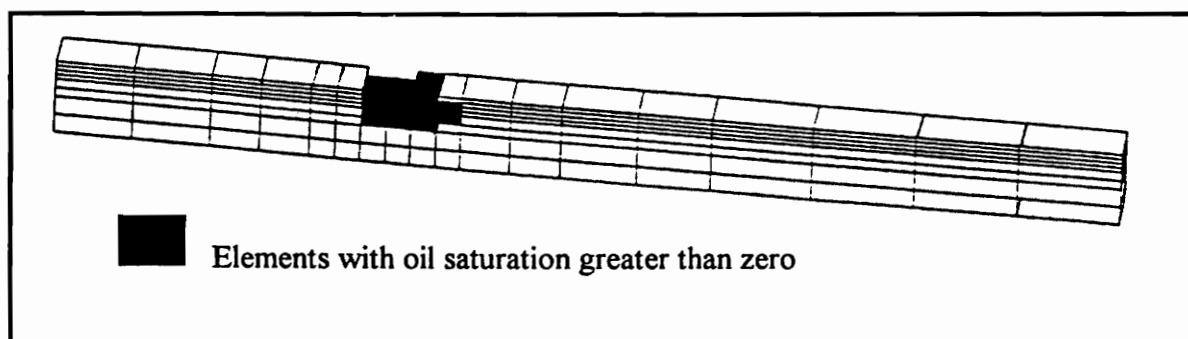


Figure 4.13 3-D Mesh - Elements with greater than zero oil saturation after 153 days.

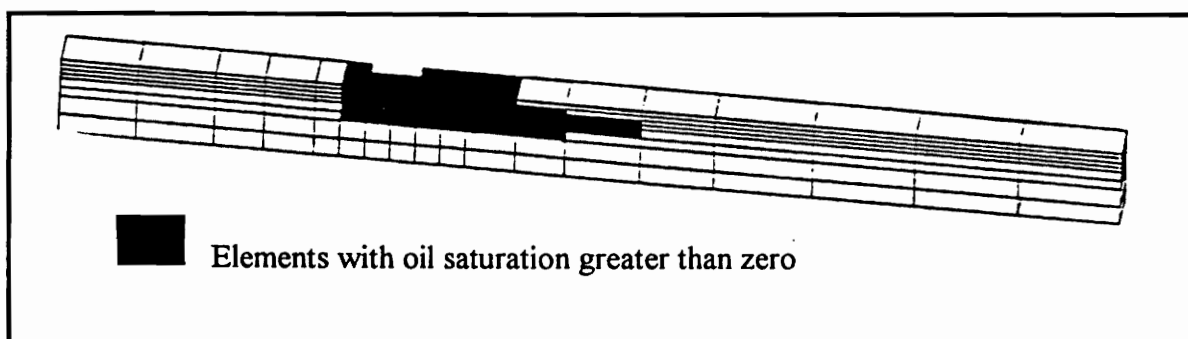


Figure 4.14 3-D Mesh - Elements with greater than zero oil saturation after 535 days.

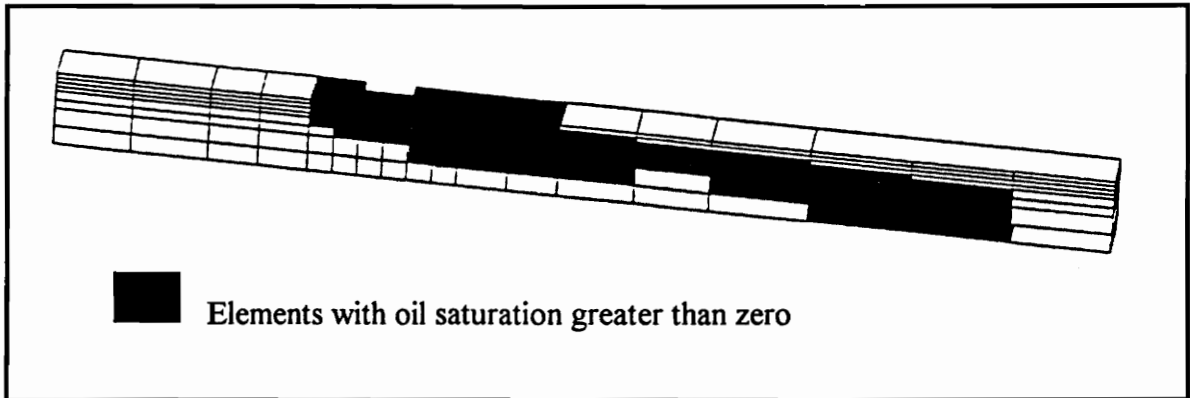


Figure 4.15 3-D Mesh - Elements with greater than zero oil saturation after 1600 days.

Figures 4.16 and 4.17 compare the two- and three dimensional models based on the inflow of oil into the soil domain and the outflow of water from the soil domain. These figures again show an excellent correlation between the two- and three-dimensional finite element simulations. Figure 4.16 shows a steady increase in oil inflow into the domain over time for both models, while figure 4.17 shows the outflow of water from the domain. However, it is noted from the computer output, in the initial stages there is a slight increase in water content with the domain. The initial inflow of water is due to the capillary forces present at the beginning of the simulation, which causes water to rise from its initial condition at the water table.

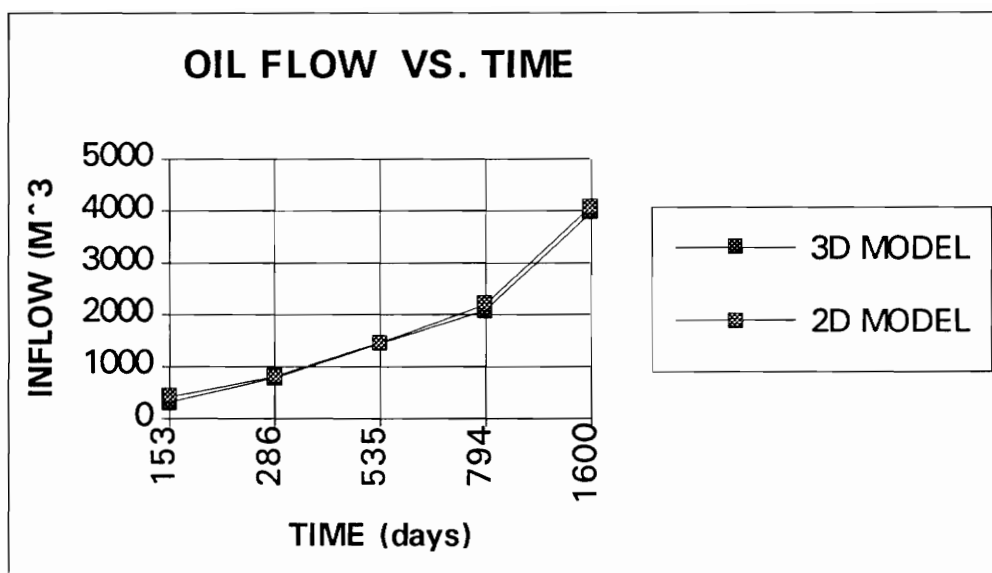


Figure 4.16 Comparison of two- and three-dimensional models on basis of oil inflow for Example 4.2.

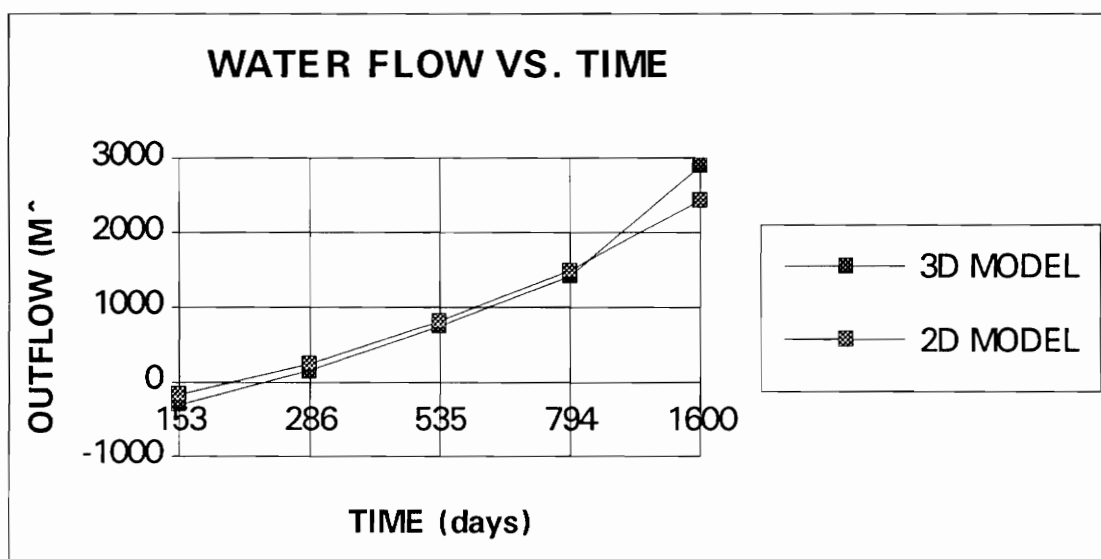


Figure 4.17 Comparison of two- and three-dimensional models on basis of water outflow for Example 4.2.



Validation of the three-dimensional model is now complete based on the excellent correlation this model displayed in comparison with the two-dimensional model. The models are found to give similar results for both oil inflow and water outflow as well as oil saturation and movement throughout the soil domain for both one- and two-dimensional problems. Furthermore, the three-dimensional simulation for the one-dimensional column test problem showed a good correlation with experimental results. Now that validation of the three-dimensional model is complete, the model can be used to independently to simulate problems related to a full three-dimensional domain.

## **SIMULATIONS OF A FULLY THREE-DIMENSIONAL PROBLEM**

Now that the three-dimensional finite element model for multiphase flow has been validated, an additional example is simulated to investigate the movement of contaminants in a fully three-dimensional domain.

### **EXAMPLE 4.3**

This example is very similar to Example 4.2, used to validate the three-dimensional model. The example uses the same soil domain and soil properties with one significant change. This problem in this example will be treated as a three-dimensional problem in which the oil tank will be located in the center of a 30 m thick soil domain. The 210 m long by 16 m deep portions of the domain will remain the same as Example 4.2, with an initial water table present throughout the domain. The oil tank will again be 10 m long and 2 m deep and will also have a thickness of 10 m. This tank is located on the ground surface of a 30 m thick soil domain. Here, the lateral movement in the three-dimensional

plume is investigated. The finite element mesh for the three-dimensional simulation is shown in Figure 4.18. The mesh is discretized into 504 elements and 860 nodes.

The three-dimensional finite element mesh has been divided into three sections in the lateral direction. These three sections are used to show the lateral movement of the oil phase into the 30 m wide soil domain.

Results of the simulation are shown in Figures 4.19-4.21 for time steps of 82.8, 153, and 286 days, with the elements containing an oil saturation greater than zero darkened. These figures show the movement of the oil phase in both the down stream and lateral directions. Figure 4.19 shows the results for the first time level, 82.8 days. Here, oil is present only in the upper most layer of the domain and is confined to the elements adjacent to the nodal oil sources.

Figures 4.20a, b, and c show the movement of the oil phase at a time level of 153 days. Figure 4.20a shows the results of the simulation in three-dimensions, looking at just the outer surface of the domain, while Figures 4.20b, and c show the results of the simulation in three-dimensions for the vertical cross-sectional view of the center and rear slices of the mesh. Close examination of the results shows that the movement of the oil phase through the subsurface is not completely symmetrical. Further examination of Figure 4.20c, the rear vertical cross-section of the domain, exemplifies this point. Since the subsurface properties are the same in all three directions, the answer should be symmetric in horizontal plane. This unsymmetric answer could result from many different sources including: (1) a deficiency in the general parametric model for the constitutive properties, (2) error in the computer implementation, (3) error in the data input, or a result of (4) poor convergence in the finite element simulation. The first two sources of error are disregarded based on the previous examples which validated the three-dimensional model and the computer code based on the two-dimensional simulations.

Although the data file for this example is extensive, containing over 1000 lines, an error such as this one would most likely result from input boundary conditions or mesh connectivity, both of which have been examined closely. Therefore, the error is believed to be a function of the convergence. Convergence will therefore need to be examined more closely in future simulations. It is noted that convergence, for a given time interval, does not necessarily secure a correct answer for that time interval, since previous convergence can effect later solutions in time dependent problems (see Chapter 5).

Figures 4.21a, b, and c show the elements in the domain which have an oil phase saturation greater than zero for time output level of 286 days. These figures show the movement of the oil phase throughout the three-dimensional domain. Figure 4.21a shows the movement of the oil phase on the boundary of the domain, while 4.21b and 4.21c show movement through the center and rear vertical cross-sections respectively. Examination of these figures again reveals that the simulation is unsymmetric in the horizontal plane, which is not consistent with theory. A comparison of Figures 4.21a-c with Figures 4.20a-c, shows that more symmetric results are achieved with higher convergence at the latter time output level. This again suggests that convergence at is the key to the unsymmetric oil phase movement in the horizontal direction for the earlier time levels.

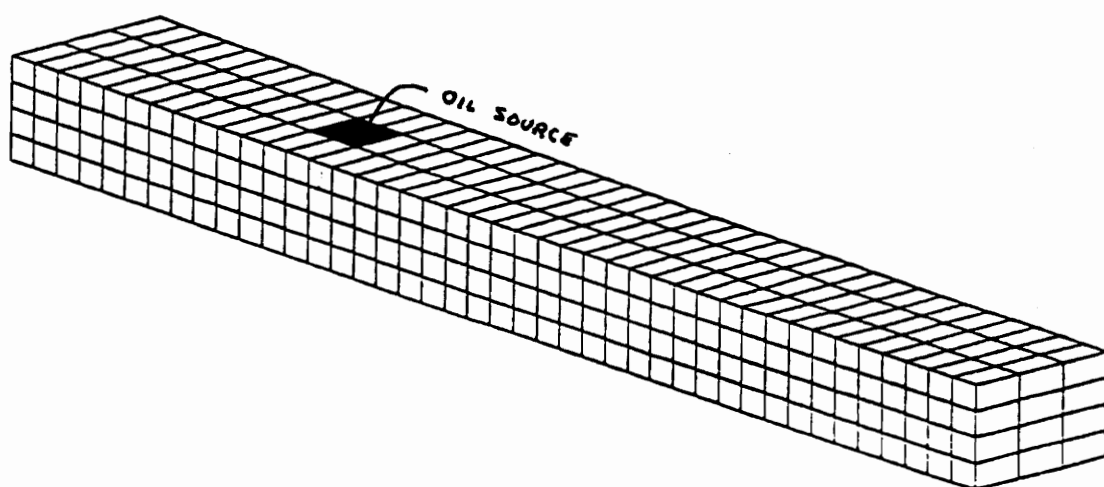
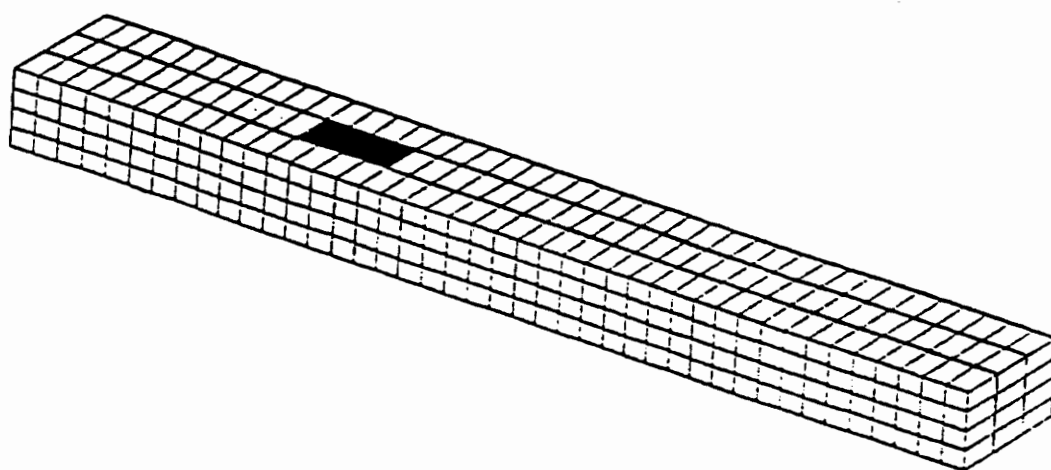


Figure 4.18 Three-dimensional finite element mesh (example 4.3)




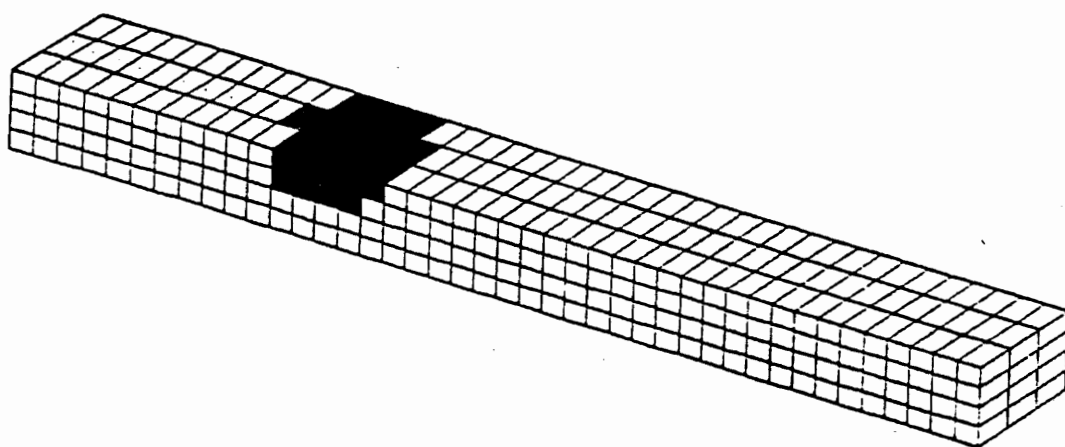
 oil saturation greater than zero

Figure 4.19 Oil plume at the end of 82.2 days.




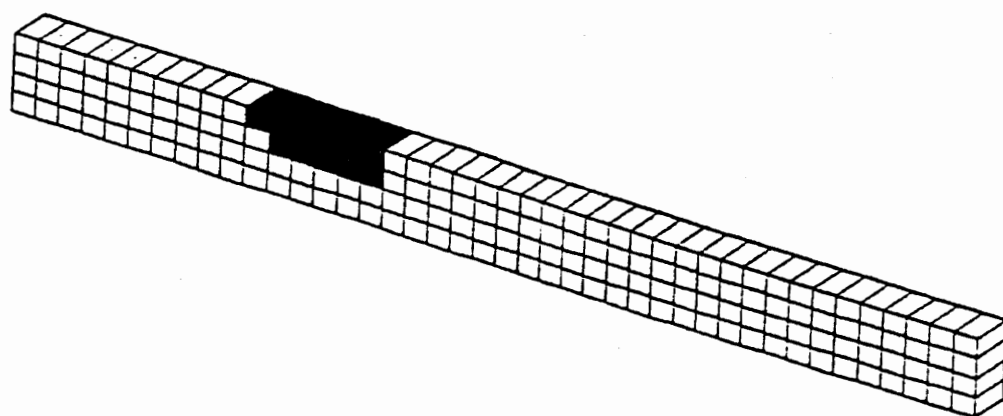
 oil saturation greater than zero

Figure 4.20-a Oil plume at the end of 153 days.




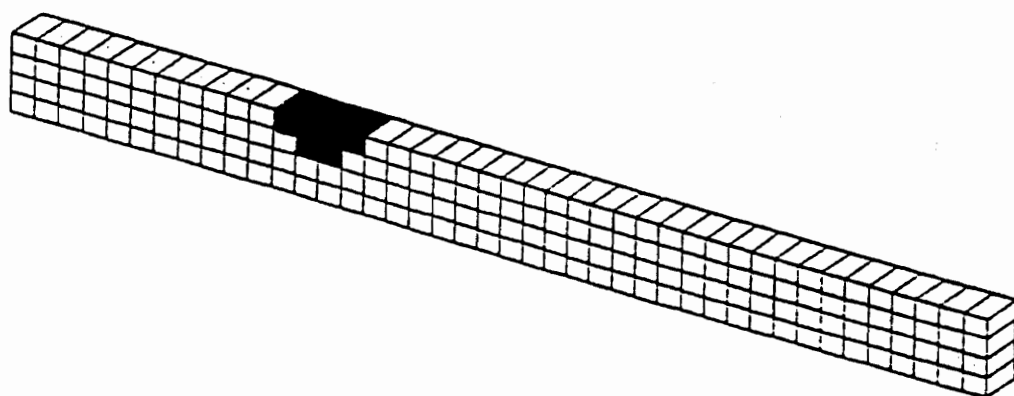
 oil saturation greater than zero

Figure 4.20-b Oil plume at end of 153 days, center cross-section.




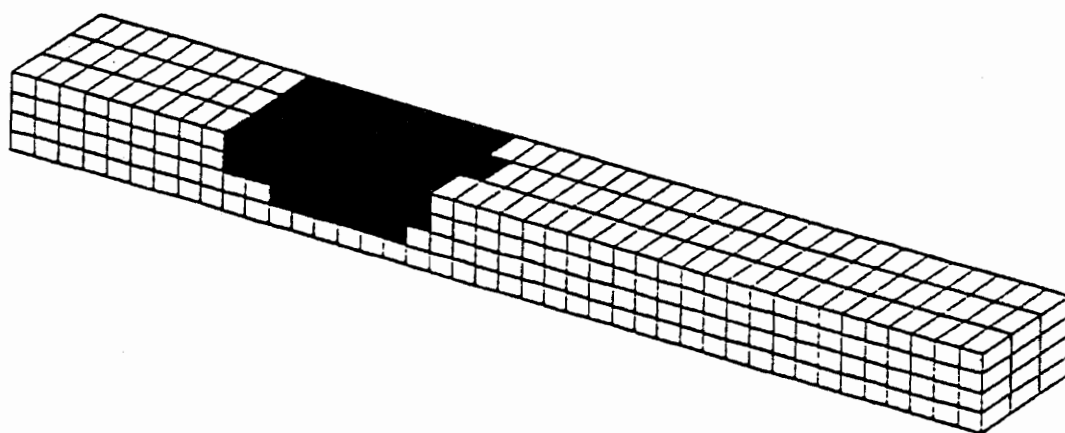
 oil saturation greater than zero

Figure 4.20-c Oil plume at end of 153 days, rear cross-section.






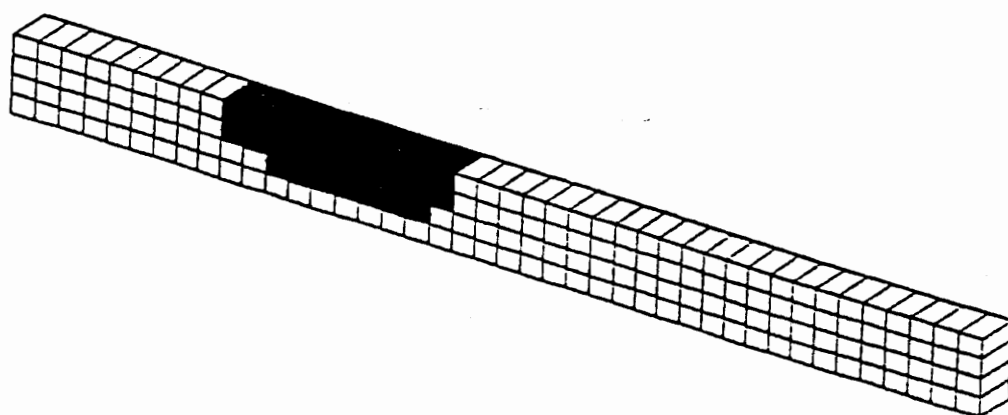
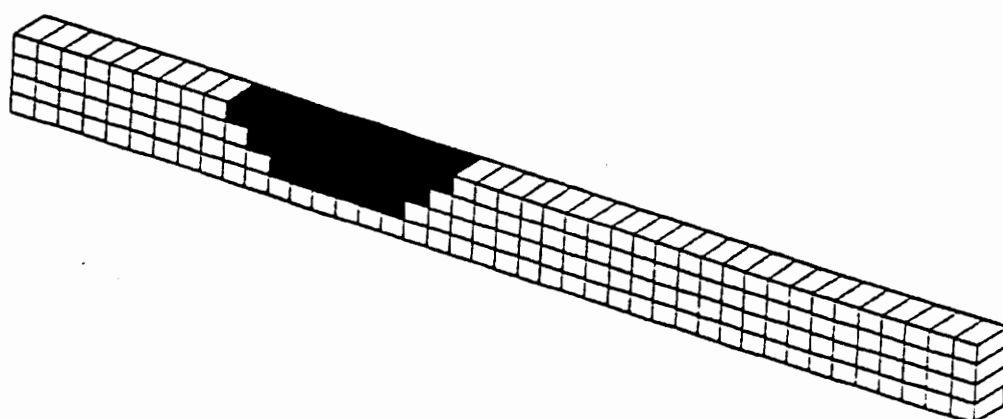
 oil saturation greater than zero

Figure 4.21-a Oil plume at end of 256 days.



■ oil saturation greater than zero

Figure 4.21-b Oil at end of 256 days, center cross-section.




 oil saturation greater than zero

Figure 4.21-c Oil plume at end of 256 days, rear cross-section

## CONCLUSIONS

Chapter 4 introduces the concept of multiphase immiscible flow and gives a brief description of the background related to this complex theory, which originated in the area of oil exploration engineering. The methodology developed by current researchers (Parker et al. 1987, Kuppusamy et al. 1987, Sheng 1986) is used to develop a three-dimensional finite element model for multiphase immiscible flow. The model is compared with a previously validated two-dimensional model and experimental data taken from current literature. The conclusions of these simulations are presented as follows:

- (1) the three-dimensional model shows very similar results to the two-dimensional model for simulations conducted on a one-dimensional column problem,
- (2) the three-dimensional model shows a reasonable correlation with experimental data from column test results from current literature,
- (3) the three-dimensional model simulation results are similar to the two-dimensional model simulation results for a two-dimensional domain, with slightly slower plume movements for a given time step. This effect becomes greater in later time output levels

After validation of the three-dimensional model, a fully three-dimensional domain similar to the one used in the two-dimensional simulation (Example 4.2) is used to investigate plume movements in three-dimensions. The simulations show similar but decreased plume movement as compared with the results of three-dimensional simulations in a two-dimensional setting. The three-dimensional simulations result in poor convergence in initial and intermediate time steps during the simulations. It has been

reported widely in the literature that this is often true for the time integration schemes used in numerical modeling (Belytschko and Liu 1983).

## CHAPTER 5

### EXPERIMENTAL STUDY

#### INTRODUCTION

Series of tests were performed in the laboratory to determine the gasoline and water conductivities and the flow patterns of gasoline through a sandy soil. Two types of tests were performed: (1) a column test and (2) a flume test (Gibson 1992).

The sand used in all tests was Montaerey #0/30 sand. Montaerey sand is a commercially available clean uniform sand which classifies as a poorly graded sand under the USCS guidelines. The index properties of the sand are shown in Table 5.1 (Milestone 1985). The contaminant used in the experiment is ordinary gasoline and the properties are estimated based gasoline's major constituents. The specific density used for the gasoline phase was approximated as 0.8 (Corapcioglu and Baehr 1987, Ryan and Cohen, 1991). It is important to note that this is an estimate that may be off by as much as 10 %.

Table 5.1 Material properties of Montaerey #0/30 sand used in the column and flume experiments

Property	Value
$G_s$	2.65
$\gamma_{d\max}$	105.8 lbs/ft
$\gamma_{d\min}$	91.7
$e_{\max}$	0.803
$e_{\min}$	0.563
$d_{50}$	0.45
$C_u$	1.60
$C_c$	1.00

## **COLUMN TEST**

The column tests were conducted in a circular Plexiglas pipe. The apparatus used in these tests is shown in Figure 5.1. A graduated cylinder was used to measure the outflow of the liquid-phases from the base of the column. Ten sets of experimental tests involving gasoline and water were conducted using four different testing procedures. Tests 1-4 involved measuring the flow of gasoline and water as a two-phase flow system. This data was used to test the utility of the multiphase flow model by comparing the results of the finite element simulations (outflow of water) with the experimental results (measured water outflow). Tests 5-10 were used to estimate the hydraulic conductivity of the soil for both the gasoline and water phases. These values were used as a starting point in the finite element simulations.

## **PROCEDURE**

Sand was weighed and placed in the column to a height of 10 inches, resulting in a total volume of 71.27 in<sup>3</sup>. For each test, the approximate height and weight of the sand was kept constant to provide similar material property parameters. The soil was then carefully saturated through a valve located at the bottom of the column with the liquid to be used in the experiment. Care was taken not create a large head differential, which may have caused separation in the soil column. The soil was then saturated with either water or gasoline and a constant head of 6 inches of gasoline or water was then applied to the top of the soil sample. Tests were performed involving both gasoline and water under a near constant vacuum and under a free draining condition.

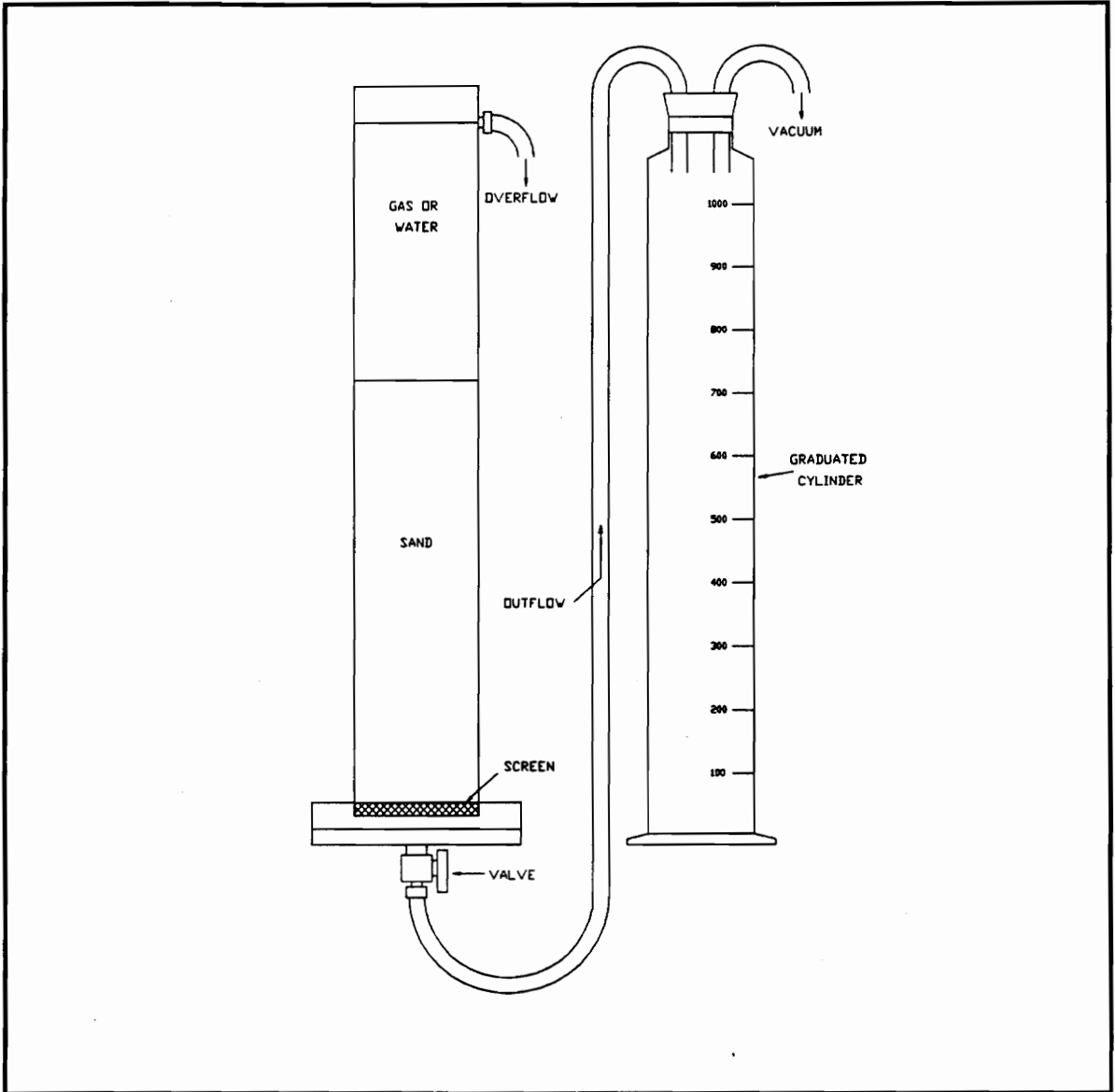


Figure 5.1 Column testing device



Tests 1-3 were conducted by first saturating the sample with water. These tests were conducted with a constant vacuum of 14.5 inches of mercury. This represents the boundary condition at the base of the cylinder. At the top of the cylinder a constant head of gasoline equal to six inches was maintained throughout the experiment by continuously replacing the gasoline phase as it flowed through the porous media. An outlet hole is located at six inches above the top of the soil sample to assist in maintaining the constant head. The tests conducted without a vacuum were initiated by opening the valve at the bottom of the column. If the test was performed under a vacuum, a vacuum of 14.5 inches of Hg is attained prior to opening the valve. As the test preceded, measurements of the outflow were taken as the cylinder of soil emptied into a graduated cylinder. The gasoline or water head was maintained at the top of the sample by continuously replacing any fluid which had entered the testing device. The test ended when the either graduated cylinder was full or sufficient time had passed.

The procedure used in test 4 is similar to tests 1-3. Like tests 1-3, test 4 involved both gasoline and water, the difference in the testing procedure involved the boundary condition at the base of the cylinder. In test 4 no vacuum was applied to the base of the sample, instead the sample was allowed to drain freely with water outflow resulting from the capillary forces caused by the infiltration of the gasoline phase.

Tests 5-7 were conducted using only gasoline. The tests were conducted by first saturating the sample with gasoline and by then applying a constant gasoline head of six inches to the top of the sample, this head was maintained throughout the experiment. For test 5-7 no vacuum was applied to the base of the sample, allowing the sample to drain freely.

Test 8-10 were conducted in a similar manner to tests 5-7. The only difference was that in tests 8-10 the fluid used was water. Once again, the sample was allowed to drain freely under no induced vacuum.

Table 5.2 outlines the ten tests. The table describes the fluids used to saturate the sample (fluid in soil) and the fluid used as the boundary condition at the top of the sample (fluid above soil). The table also provides information related to the application of the vacuum, the weight of the soil, the volume of the soil, and calculated porosity for each test.

Table 5.2 Conditions for column tests 1-10.

Test #	Fluid in soil	Fluid above soil	Vacuum (in Hg) at base	Weight of soil (lbs)	Volume of soil (ft <sup>3</sup> )	Porosity
1	Water	Gas	14.5	3.85	.0103	0.44
2	Water	Gas	14.5	4.02	.0104	0.42
3	Water	Gas	14.5	4.03	.0104	0.42
4	Water	Gas	0.0	4.03	.0104	0.42
5	Gas	Gas	0.0	4.02	.0104	0.42
6	Gas	Gas	0.0	4.02	.0104	0.42
7	Gas	Gas	0.0	4.02	.0104	0.42
8	Water	Water	0.0	4.02	.0103	0.41
9	Water	Water	0.0	4.02	.0104	0.42
10	Water	Water	0.0	4.02	.0104	0.42

## COLUMN TEST RESULTS

The results of the column tests described in the previous section are shown in Tables 5.3-5.6. Table 5.3 show the results of tests 1-3, involving the gasoline-water two-phase flow problem. The results are presented in terms of the volume of outflow measured in the graduated cylinder over a given time interval. Selected volumes, in Table 5.3, are in italics to represent the volume contained in the graduated cylinder once gasoline has percolated through the entire column and has exited the base of the sample into the graduated cylinder. The values given in italics are the best approximation of the true volume, given the gasoline foam obstructs accurate readings. Examination of Table 5.3 reveals that the outflow measurements became large over a short time period, with water being forced completely from the sample in approximately six seconds. The values of outflow are also fairly erratic due to the crude measuring techniques used in the experiment. The short time scale over which comparable results are taken coupled with the erratic nature of the results prohibit efficient comparison with finite element simulations. For future studies involving the use of a vacuum, it is recommended that a less permeable soil be used and that a more consistent vacuum be applied to the sample.

Table 5.3 Water/Gas/Vacuum Tests

Time (sec)	Volume Test #1 (ml)	Volume Test #2 (ml)	Volume Test #3 (ml)
2	110	230	150
4	210	375	275
6	330	<i>615</i>	<i>402.5</i>
8	<i>480</i>	<i>680</i>	<i>510</i>
10	<i>590</i>	<i>760</i>	<i>640</i>
12	<i>675</i>		<i>733</i>
14	<i>700</i>		<i>870</i>

Table 5.4 shows the results of test 4, gasoline-water under no vacuum. Again the values in italics represent volumes of outflow measured, after gasoline infiltration through the entire sample has occurred. The results in the first 60 seconds of the analysis provide a good base for comparing the outflow of water measured in the experiment with finite element simulations.

Table 5.4 Water/Gas No Vacuum

Time (sec)	Volume Test #4 (ml)	Time (sec)	Volume Test #4 (ml)	Time (sec)	Volume Test #4 (ml)
14	105	60	360	108	<i>670</i>
18	138	66	<i>403</i>	114	<i>720</i>
24	170	72	<i>438</i>	120	<i>763</i>
30	198	78	<i>478</i>	126	<i>803</i>
36	225	84	<i>510</i>	132	<i>843</i>
42	260	90	<i>548</i>	138	<i>890</i>
48	293	96	<i>585</i>	144	<i>940</i>
54	323	102	<i>628</i>	150	<i>983</i>

Table 5.5 shows the results of test 5-7, for column experiments involving the infiltration of gasoline under a constant head without a vacuum. The results of the test are used to calculate initial estimates of the fluid conductivity of gasoline to be used in the finite element analysis. The estimated value of the saturated hydraulic conductivity for the gasoline phase,  $K_{SO}$ , is 0.206 in/sec.

Table 5.5 Gas/Gas/No Vacuum

Time (sec)	Volume Test #5 (ml)	Volume Test #6 (ml)	Volume Test #7 (ml)
5	70	67	74
10	146	137	142
15	223	210	229
20	294	285	303
25	372	355	381
30	443	425	459

Table 5.6 shows the results of test 8-10, for column experiments involving the infiltration of water under a constant head without a vacuum. The results of the test are used to calculate initial estimates of the fluid conductivity of water to be used in the finite element analysis. The estimated value of the saturated hydraulic conductivity for the water phase,  $K_{sw}$ , is 0.166 in/sec.

Table 5.6 Water/Water/No Vacuum

Time (sec)	Volume Test #8 (ml)	Volume Test #9 (ml)	Volume Test #10 (ml)
5	49	61	60
10	100	115	117
15	152	174	179
20	206	235	240
25	257	292	297
30	309	350	360
35	361	412	415
40	409	466	472

## FINITE ELEMENT SIMULATION OF THE COLUMN EXPERIMENT

The recorded values used in the comparison with multiphase flow model, under the no vacuum condition are shown in Table 5.7

Table 5.7 Results from lab experiment involving outflow of water due to a know head of oil applied to a saturated soil column.

Time (seconds)	Experimental Outflow (in <sup>3</sup> )
14	6.41
18	8.42
24	10.37
30	12.08
36	13.73
42	15.87
48	17.87
54	19.71
60	21.97

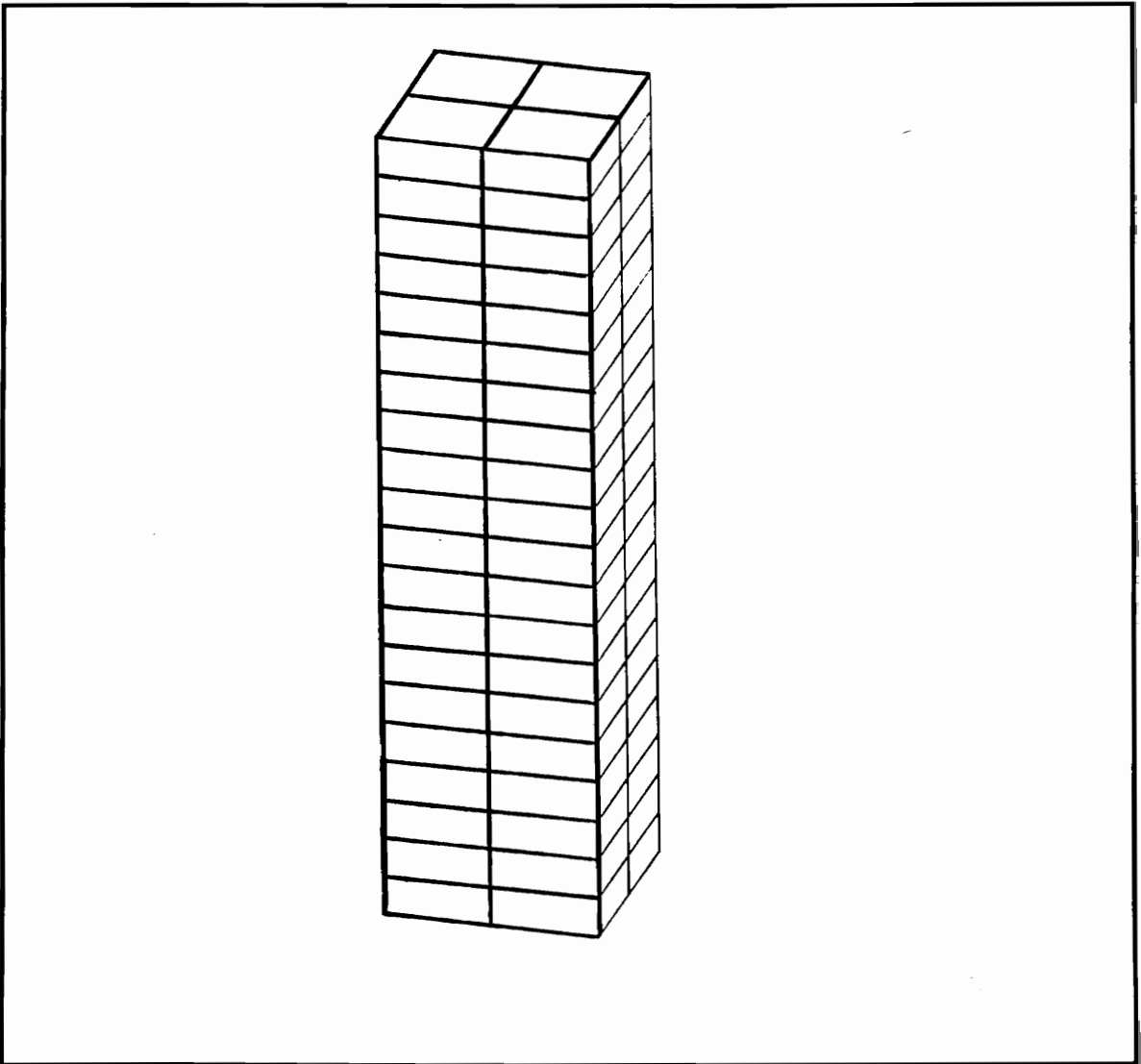
The material properties in Table 5.8 are estimated from column tests involving water and gasoline independently. The curve-fitting parameters describing the relationship between the water head and saturation in an air-water system are estimated using the two-dimensional finite element code developed by Sheng (1986). The simulations are used to investigate the effects of the scaling parameters, relating multiphase flow to unsaturated flow, and van Genuchten's parameters on the solutions at various time levels.

Table 5.8 Material parameters estimated from column tests on oil and water.

Parameter	Estimation
Saturated Water Hydraulic Conductivity, $K_{sw}$	0.166 in/sec
Saturated Oil Hydraulic Conductivity, $K_{so}$	0.206 in/sec
Porosity, $\eta$	0.42
van Genuchten's Parameter, $\alpha$	7.2 ft <sup>-1</sup>
van Genuchten's Parameter, $n$	5.0

The three-dimensional finite element model based on multiphase immiscible flow and mass transport, IMFTP3D, is used to simulate the outflow observed in the lab by varying the scaling parameters  $\beta_{ow}$  and  $\beta_{ao}$ , and the material property parameters  $K_{so}$  and  $K_{sw}$ , for constant values on van Genuchten's parameters  $\alpha$  and  $n$ . The three-dimensional code was compiled using FORTRAN77 on a UNIX based IBM RISC 6000 workstation. The mesh used in the gas/water column simulation is shown in Figure 5.2. The mesh consists of 80 elements and 189 nodes. Material property parameters for the simulations are initially estimated using a column test with the two fluids independently. These values are further revised to simulate the column experiment.

The values of outflow from the column experiment did not correspond to the outflow of water simulated in the finite element analysis, based on the estimated material property parameters. This difference in results may be due to incomplete convergence in early time steps of the simulation, causing an overestimation of both water and oil flow in the domain. Additional sources of error may arise from the difficulty in measuring water outflow for a given time, due to disturbance. For future studies, the investigator recommends that a soil media with a lower value of hydraulic conductivity be used, in order to get more accurate answers over a short time period. Variability between the finite-element model and the test data may also be a result of the natural variability that



**Figure 5.2** Three-dimensional finite element mesh used to run simulations with experimental column outflow data.

exists in values of hydraulic conductivity for any given soil. Table 5.9 shows the parameters used in the three-dimensional analysis that gave results which more closely simulate experimental data



Table 5.9 Parameters used in finite element analysis which resulted in a reasonable estimation with the experimental data

Parameter	Values used in F.E.A.
Saturated Water Hydraulic Conductivity, $K_{sw}$	0.025
Saturated Oil Hydraulic Conductivity, $K_{wo}$	0.25
Porosity, $\eta$	0.42
van Genuchten's Parameter, $\alpha$	0.6
van Genuchten's Parameter, $n$	10
Air-oil scaling parameter, $\beta_{ao}$	2.2
Oil-water scaling parameter, $\beta_{ow}$	4.5

Figure 5.3 shows a comparison of the "best fit" finite element analysis with the experimental data. The figure shows some variation between the results but a good correlation for the estimated parameters. These parameters will be used further to estimate movement in an experimental flume problem, containing the same soil.

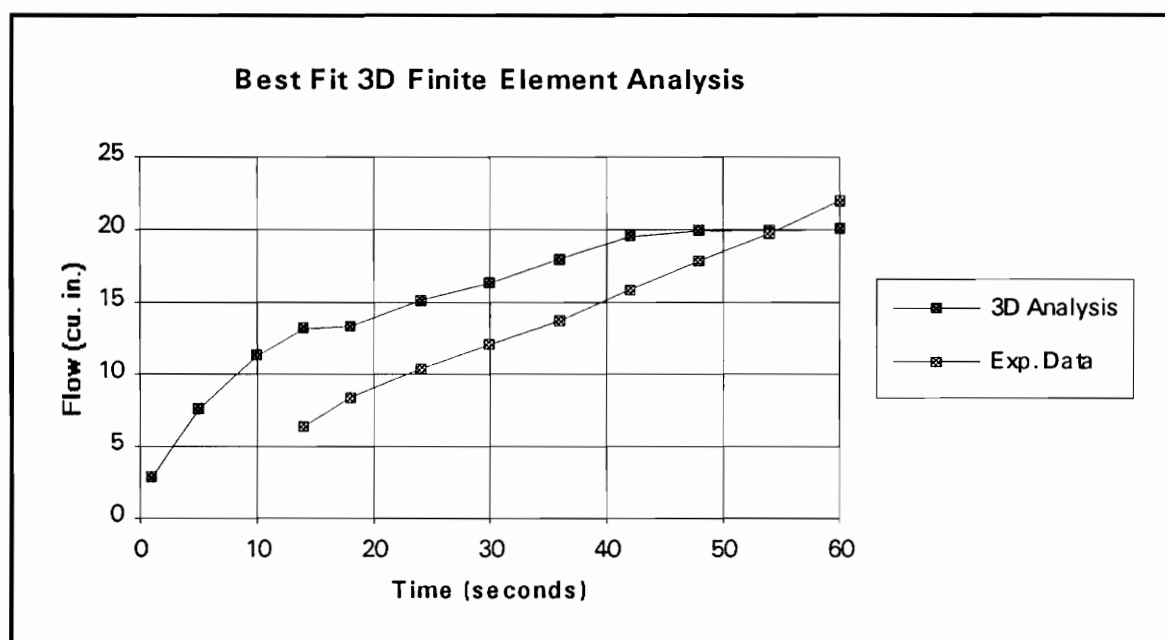


Figure 5.3 Plot of best fit finite element analysis for parameters shown in Table 5 with the experimental data from the column test.

## **FLUME TEST**

A flume test was performed to determine the nature of the flow of gasoline through Montaerey sand in a two-dimensional domain. The objective the flume experiment is to determine the accuracy of IMFTP3D in predicting discrete phase plume movements and to display the usefulness of the program in solving real problems. The tests were performed in a Plexiglas tank, shown in Figure 5.4. The flume consists of a Plexiglas tank containing soil of the following dimensions: 24 inches wide, 17.75 inches high, and 2.09 inches thick. Figure 5.4 is a depiction of the front and profile views of the flume experiment using a sloping hydraulic gradient through the Montaerey sand.

## **PROCEDURE**

Montaerey sand was first weighed and placed up to the rim of the tank, except where the square column is fixed to the top of the tank. To maintain constant material properties, efforts were made to mix the coarse and fine fractions of the soil evenly throughout the tank. Water was then siphoned into the tank through the two columns on the either side to the body of the tank. This water seeped into the soil by passing through holes drilled into the barrier between the main tank and the side columns. The holes are show in the profile view of Figure 5.4. The water was allowed to seep into the soil until a steady state condition is reached. The tests were run with a sloping hydraulic gradient as shown in Figure 5.4 and with a constant value of head and a horizontal water table throughout the domain. For the tests involving a sloping hydraulic gradient, glass tubes on each column controlled the water level and flow throughout the tank. An inlet used to infiltrate gasoline into the domain is located at the top-center of the flume. This was used

to apply a constant head of gasoline equal to three inches. The gasoline was then allowed to infiltrate into the apparatus under this constant head until the discrete plume reached the imposed water table. At this time, flow is controlled by the capillary pressure relations described previously for the multiphase flow problem. Figure 5.5 shows a picture of the flume testing apparatus before testing began.

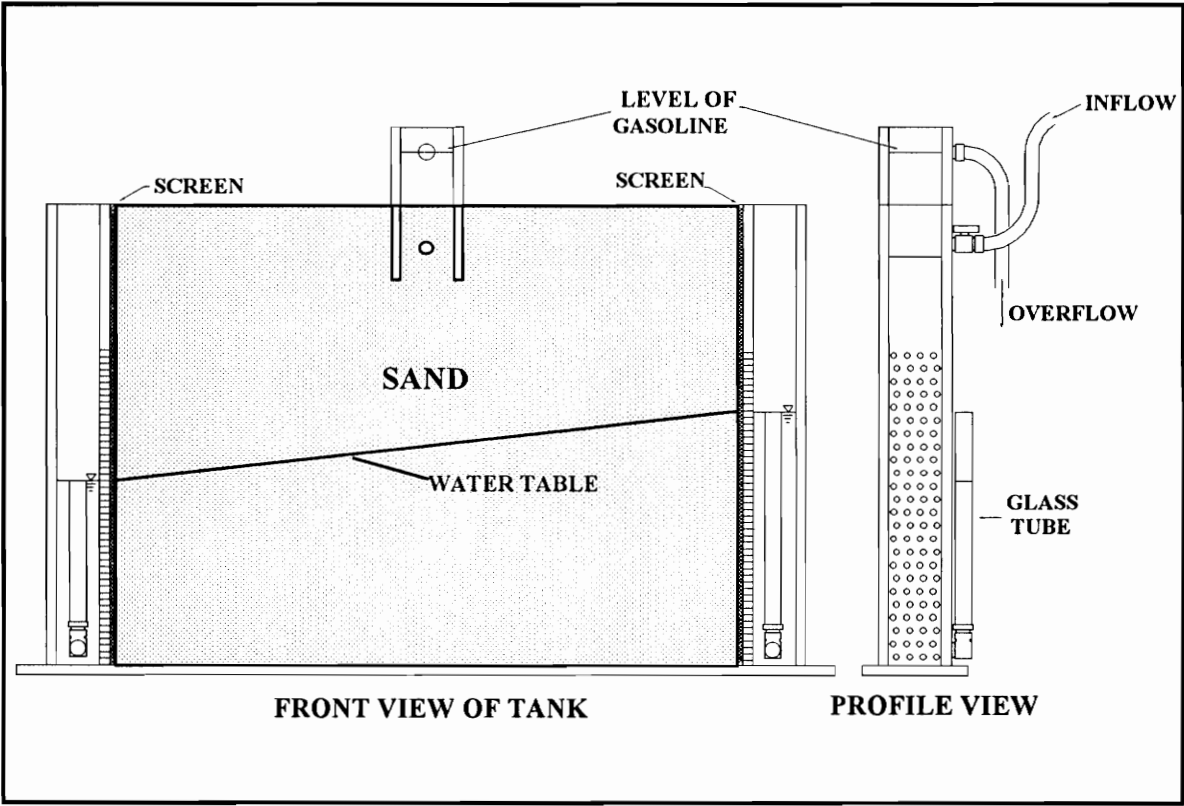


Figure 5.4 Experimental flume used to examine the movement of gasoline (After Gibson 1991).



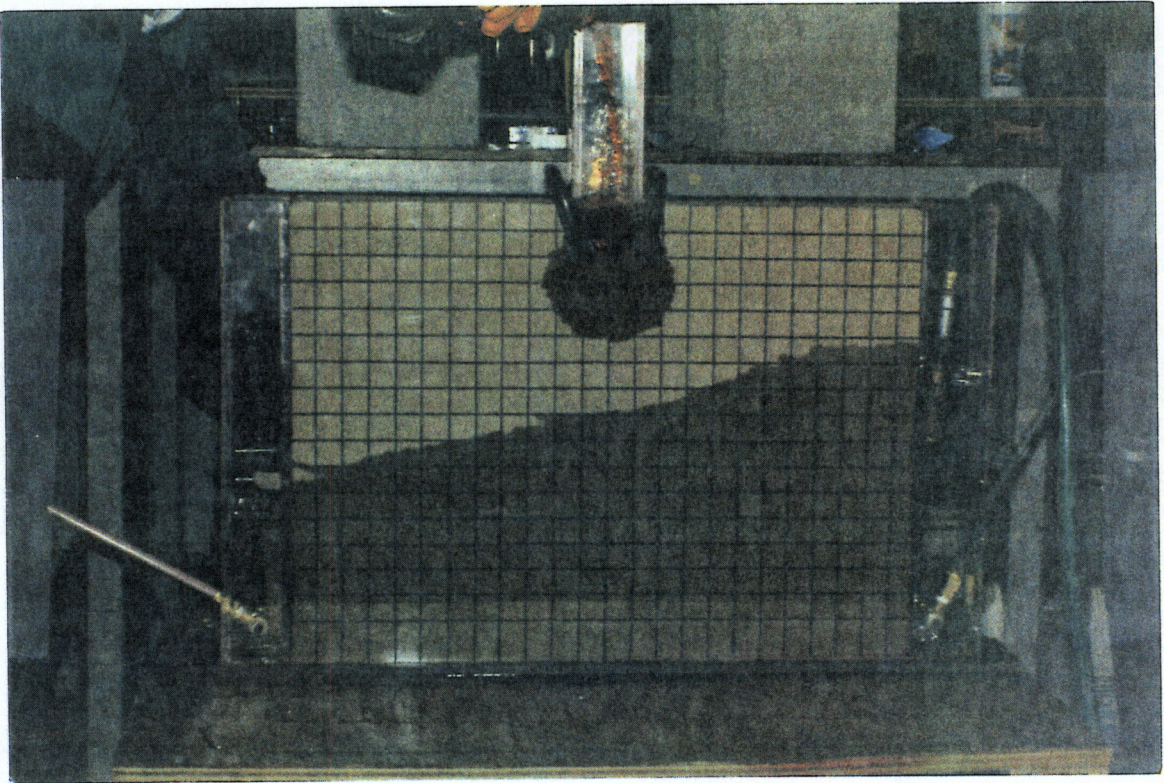


Figure 5.5 Picture taken of testing apparatus at initial condition

## FLUME TEST RESULTS

Figures 5.6-5.8 show pictures of the experiment in progress at arbitrary time levels. The results of the flume tests are shown in figures 5.9 and 5.10. The figures are plotted by estimating points on a grid on the face of a tank by viewing a video that taken during the experiment. The tape was paused every 5 to 10 seconds to estimate the gasoline plume movement at various time levels. Figure 5.9 shows the movement of the gasoline plume for a level water table, while figure 5.10 shows the movement of the gasoline plume for a water table with a sloping hydraulic head.



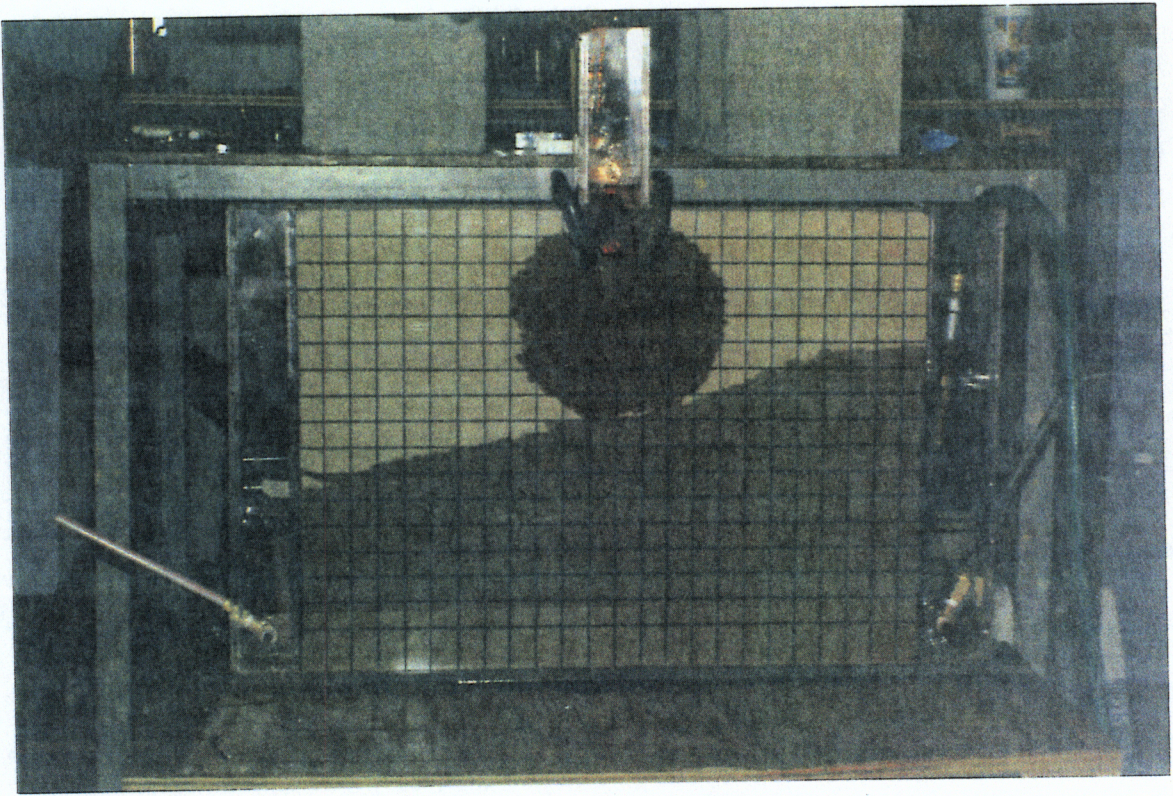


Figure 5.6 Picture of flume test during an early stage in the experiment.

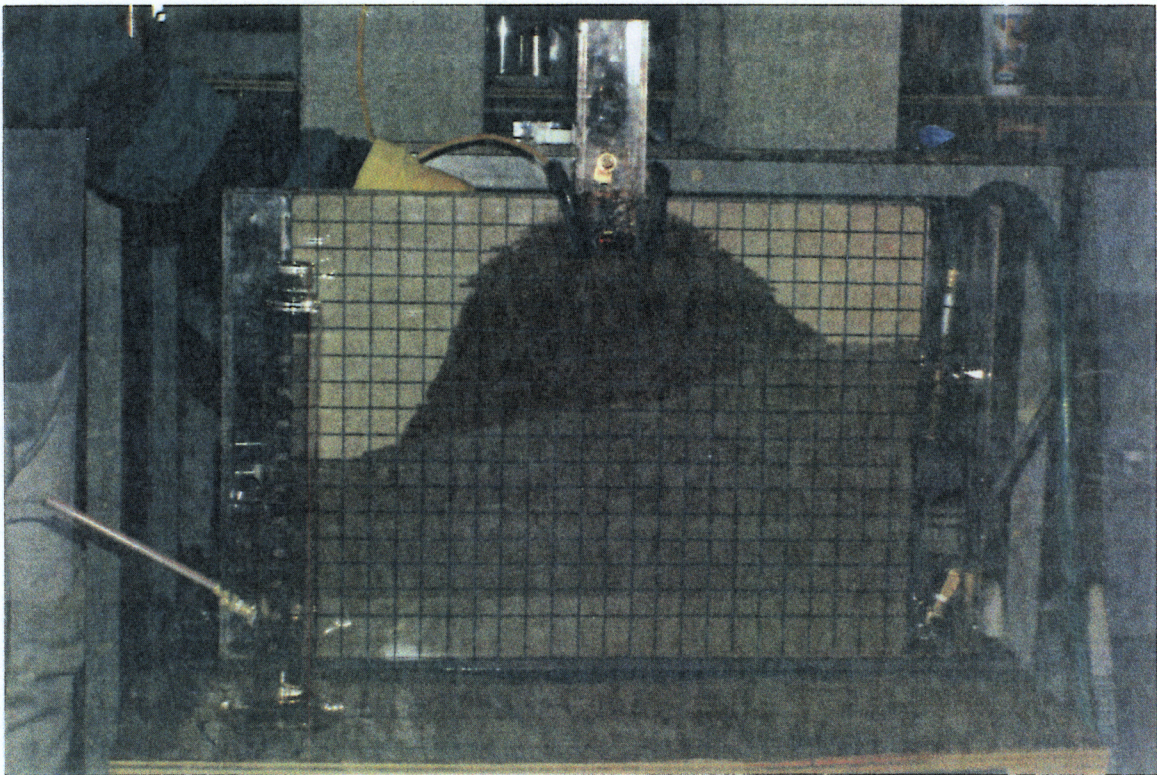


Figure 5.7 Picture of flume test during an intermediate stage in the experiment.



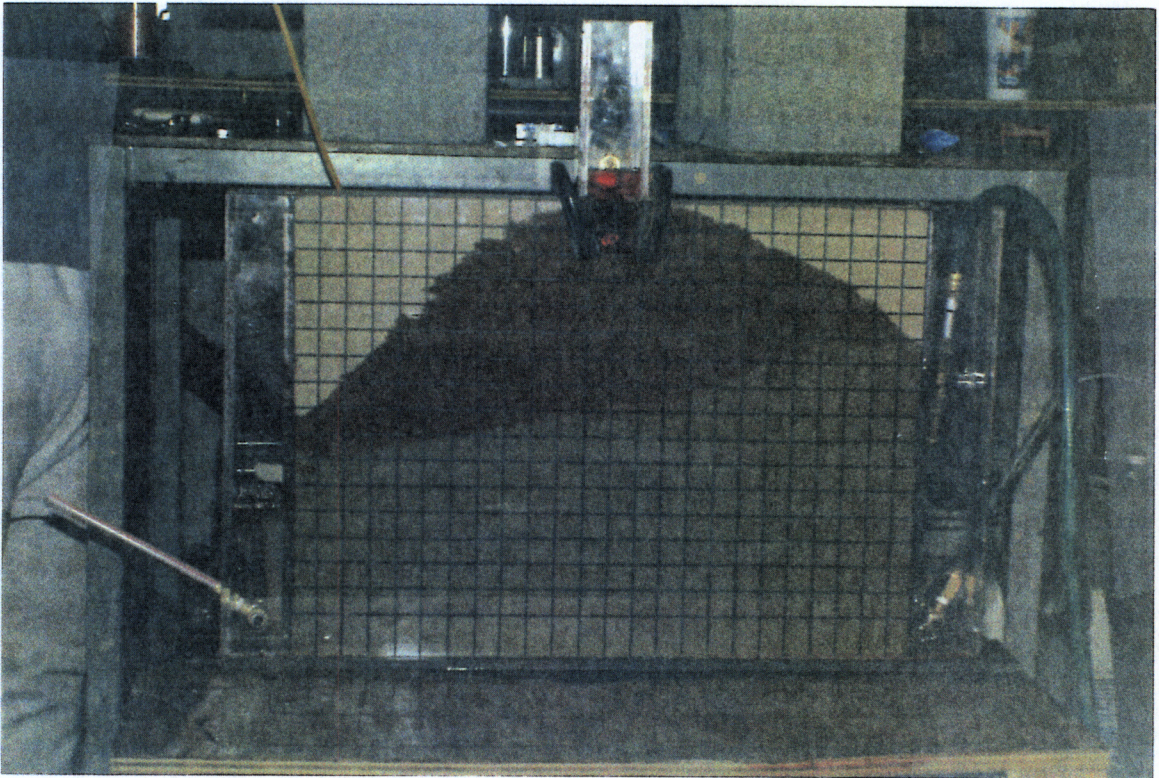


Figure 5.8 Picture of flume test during a later stage in the experiment.



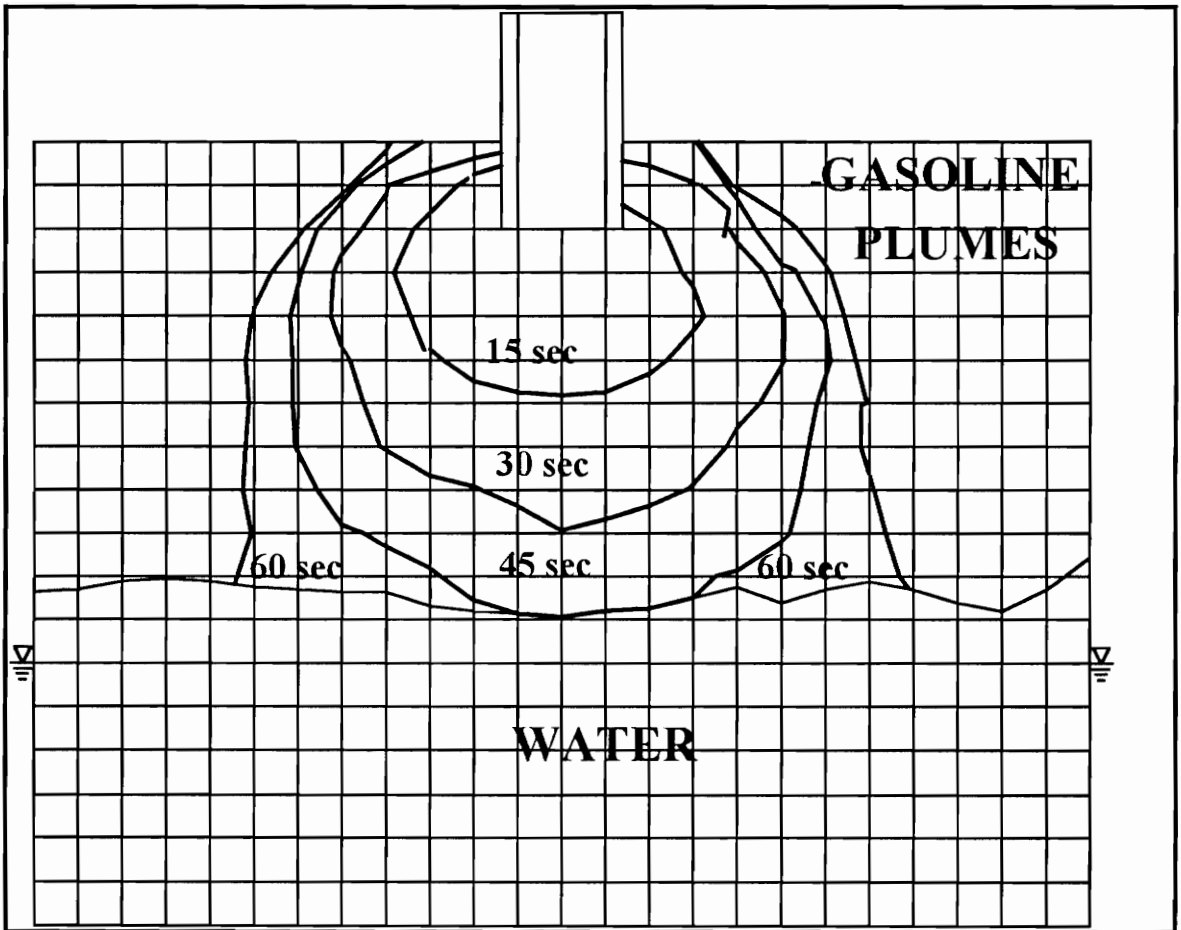


Figure 5.9 Gasoline plume movement for a constant head water level during flume experiment (After Gibson 1991).

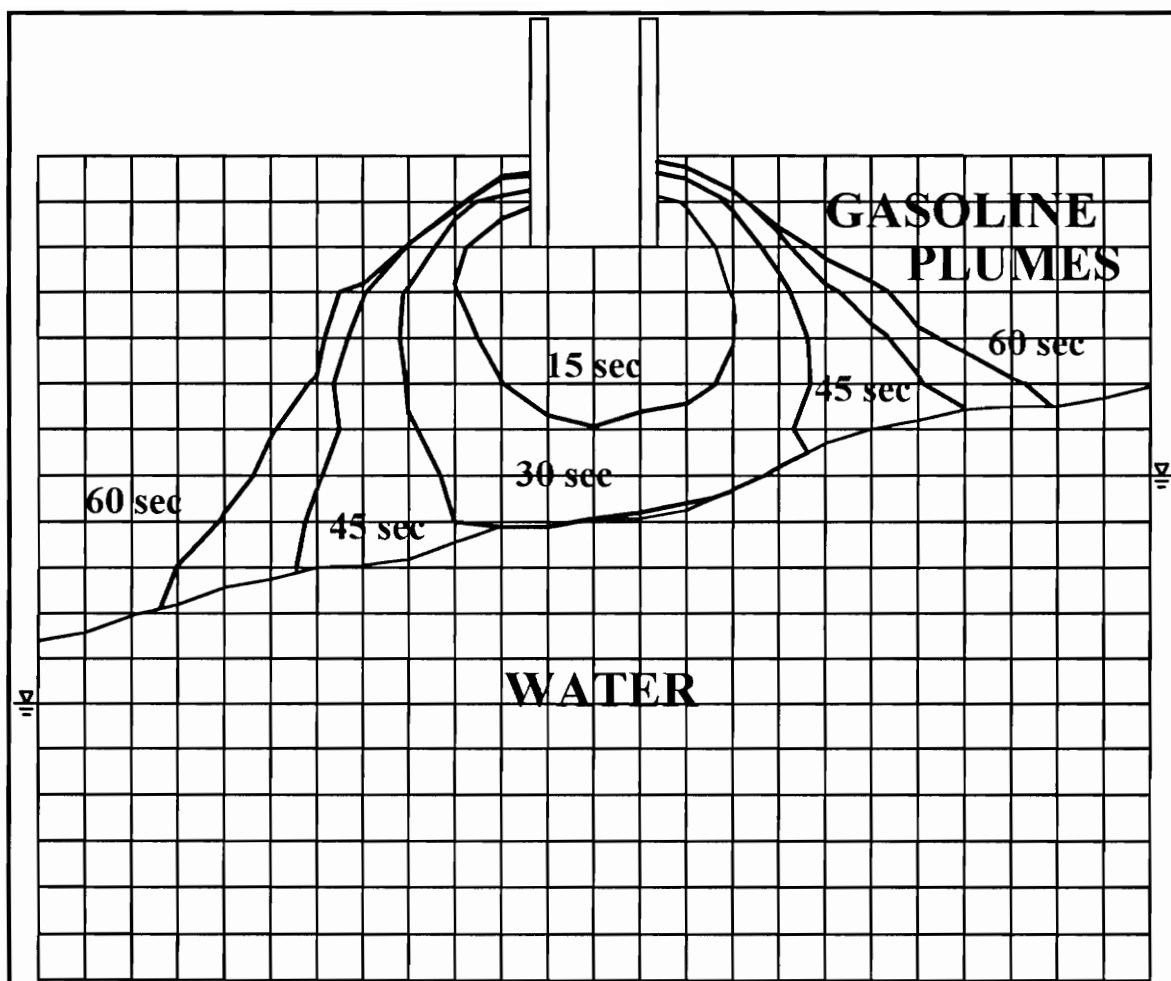


Figure 5.10 Gasoline plume movement for a water level caused by a hydraulic gradient in flume experiment (After Gibson 1991).



## FINITE ELEMENT SIMULATION OF FLUME EXPERIMENT

The values in Table 5.10 represent the parameters used in the finite element simulation that best describe the conditions portrayed in the flume experiment. The initial parameters were estimated based on the experimental data and the column problem simulations. These parameters were further revised to provide a reasonable fit. The comparison between the finite element simulation and the experimental data is based solely on estimated saturation contours. An important aspect to note is related to the degree of saturation required for a contaminant to be tracked using a laboratory experiment. Saturations obtained from the finite element simulations vary in magnitude from very small quantities, such as 0.0001, to large quantities, approaching a saturation of 1.0. For the current analysis it is assumed that a saturation of 0.5 must be achieved in a testing situation for tracking to be effective. This is an arbitrary value. The assumption is made based on the differences in residual concentrations of the water phase that may be present in the testing apparatus as compared with those values used in the data file. In the data file describing the problem to be simulated, a value of zero is used as the residual saturation for all phases in the system. This is the only assumption that could be made, since testing procedures to obtain a residual saturation were not made during the experiments. Obviously this is not true for the conditions in the experiment and the residual saturation for all phases in the system is actually greater than zero. The author feels that if the residual saturation were assumed to be equal to zero in the experiment than a value of saturation equal to 0.5 would likely produce traceable results.

The finite element mesh used for the flume simulations is shown in Figure 5.11. The mesh is modeled after Figure 5.2 and discretized into 950 nodes and 432 elements.

The finite element mesh was developed so that each element's dimensions are approximately equal to the mesh contained on the face of the testing apparatus.

Table 5.10 Parameters used in finite element analysis which resulted in a reasonable estimation with the experimental data obtained from the flume test.

Parameter	Values used in F.E.A.
Saturated Water Hydraulic Conductivity, $K_{sw}$	0.001
Saturated Oil Hydraulic Conductivity, $K_{wo}$	0.002
Porosity, $\eta$	0.42
van Genuchten's Parameter, $\alpha$	0.6
van Genuchten's Parameter, $n$	5
Air-oil scaling parameter, $\beta_{ao}$	2.2
Oil-water scaling parameter, $\beta_{ow}$	3.5

The results of the finite element simulations for the flume experiment are shown in Figure 5.12. Figure 5.12 shows the simulated discrete phase movement, in a two-dimensional cross-section, for a time level of 15 seconds. The darkened elements represent elements in which the oil saturation is greater than 0.5. Comparing this figure with Figure 5.10, it is found that a reasonable correlation exists between the experimental data and the results of the finite element simulation. The results for output levels of 30, 45, and 60 seconds resulted in little movement in the discrete phase. This is due to the boundary conditions in the finite element mesh. The lateral boundary conditions are too close to the area of interest and result in poor results for greater plume movements. The mesh is currently being revised, and future simulations are expected to give more reliable results. These results will be presented in the final report for this project.

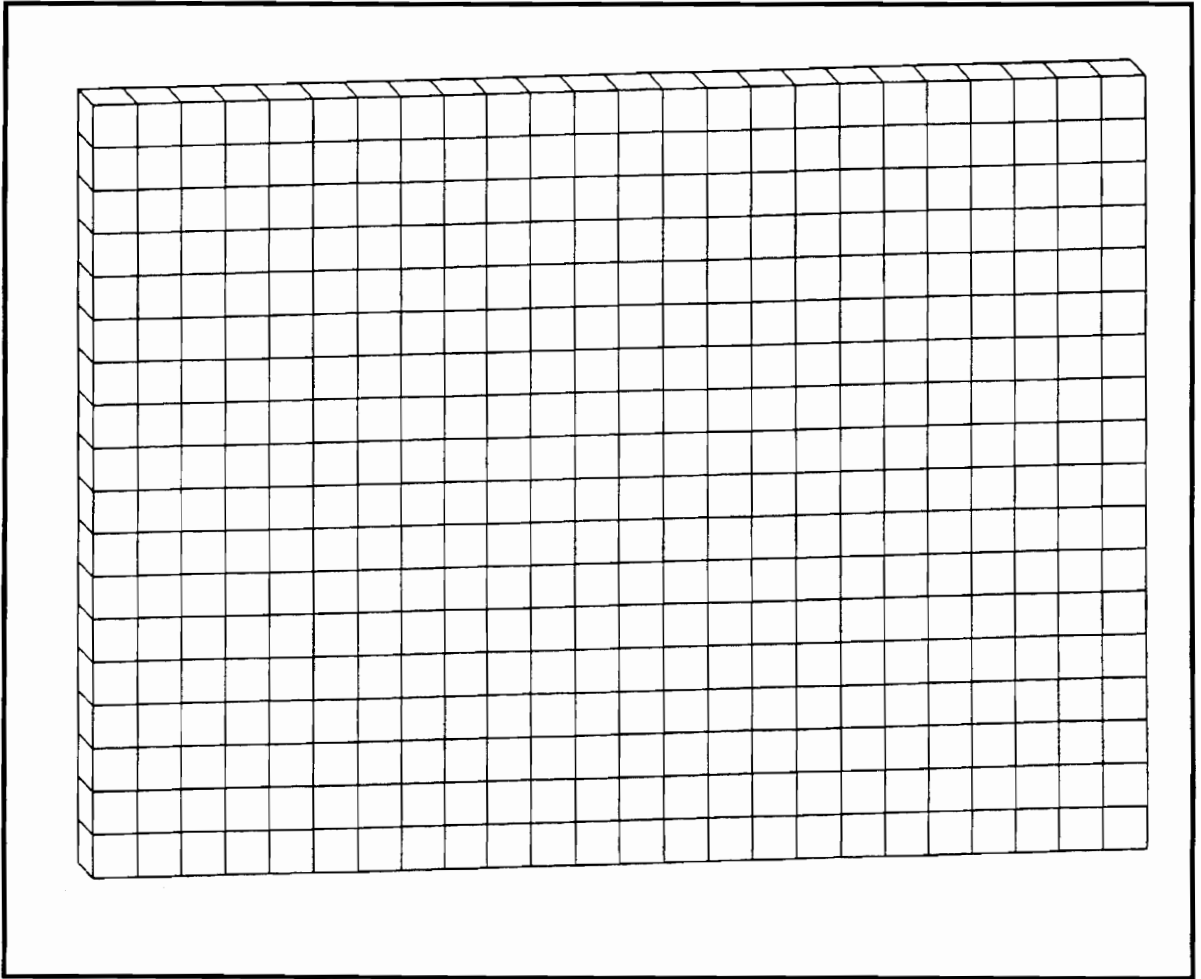


Figure 5.11 Finite element mesh for simulations based on the flume experiment

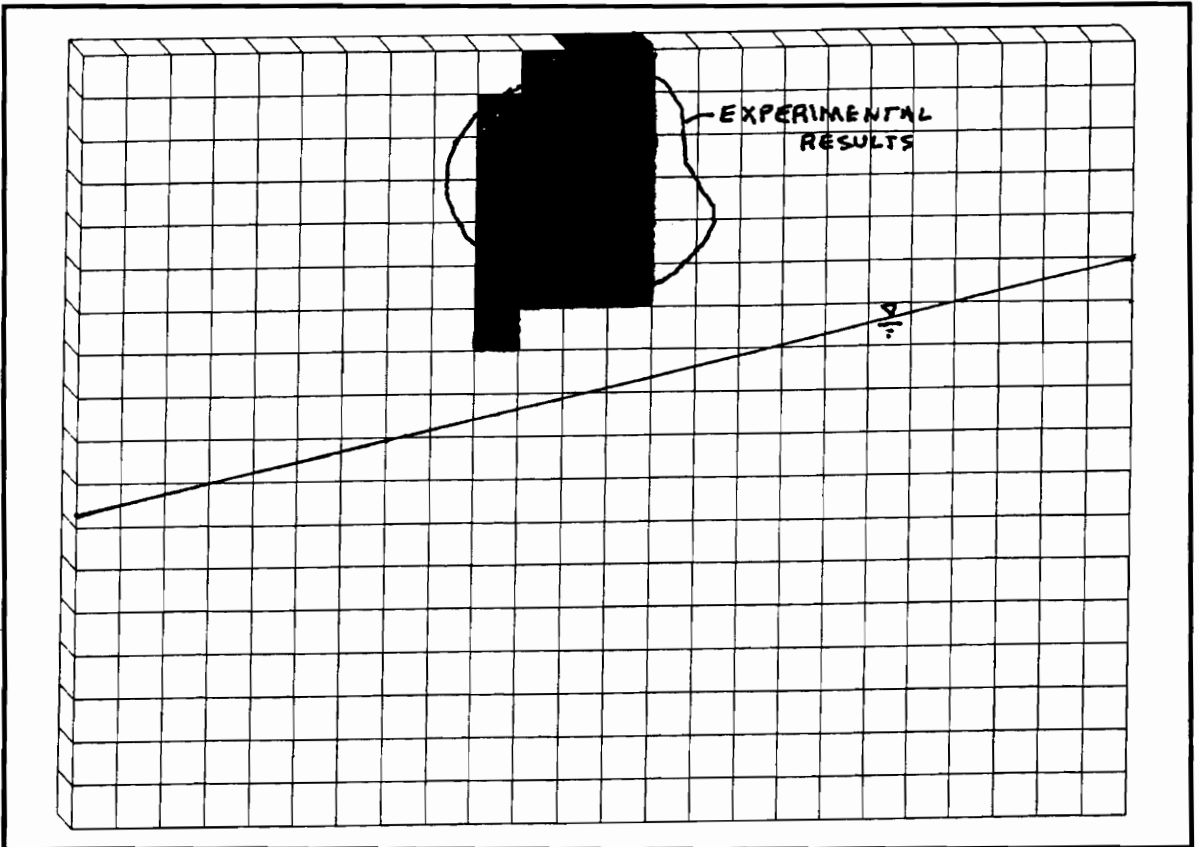


Figure 5.12 Results of finite element simulation for flume experiment at 15 seconds.

## VARIATION IN OUTFLOW DUE TO PARAMETER SELECTION

The results from the finite element simulations of multiphase immiscible flow are dependent on both material property parameters, such as the fluid conductivity and porosity, as well as scaling parameters. Van Genuchten's curve fitting parameters,  $\alpha$  and

$n$ , are related to the amount of head required to produce a given water content in an air-water system. Parker et al. (1987) related this unsaturated air-water system to a general system involving two or more immiscible fluids flowing simultaneously, introducing the scaling parameters  $\beta_{aw}$ ,  $\beta_{ow}$ , and  $\beta_{ao}$ . These three scaling parameters relate the system of immiscible fluids to the theory of unsaturated flow according to van Genuchten (1980).

In modeling the previously described column test, various simulations were made to determine the parameters that best simulate the lab results. The values of  $\alpha$  and  $n$  are selected based on two-dimensional finite element simulations using a similar mesh and effect the shape and slope of the curve describing unsaturated flow in the system (van Genuchten 1980). Here the results of various simulations are presented for constant values of  $\alpha$  and  $n$ , while the values of  $\beta_{ow}$  and  $\beta_{ao}$  are varied. Figures 5.13-5.15 show the results of the simulations as a plot of the water outflow versus time for the parameters listed in Table 5.11.

Table 5.11 Parameters used to investigate the effects of scaling parameters  $\beta_{ow}$  and  $\beta_{ao}$ .

Parameter	Case 1	Case 2	Case 3	Case 4	Case 5
$K_{sw}$	0.012	0.012	0.012	0.012	0.012
$K_{so}$	0.018	0.018	0.018	0.018	0.018
$\alpha$ (ft <sup>-1</sup> )	7.2	7.2	7.2	7.2	7.2
$n$	5.0	5.0	5.0	5.0	5.0
$\beta_{ow}$	1.2	3.2	2.2	2.2	2.2
$\beta_{ao}$	3.5	3.5	2.5	4.5	3.5

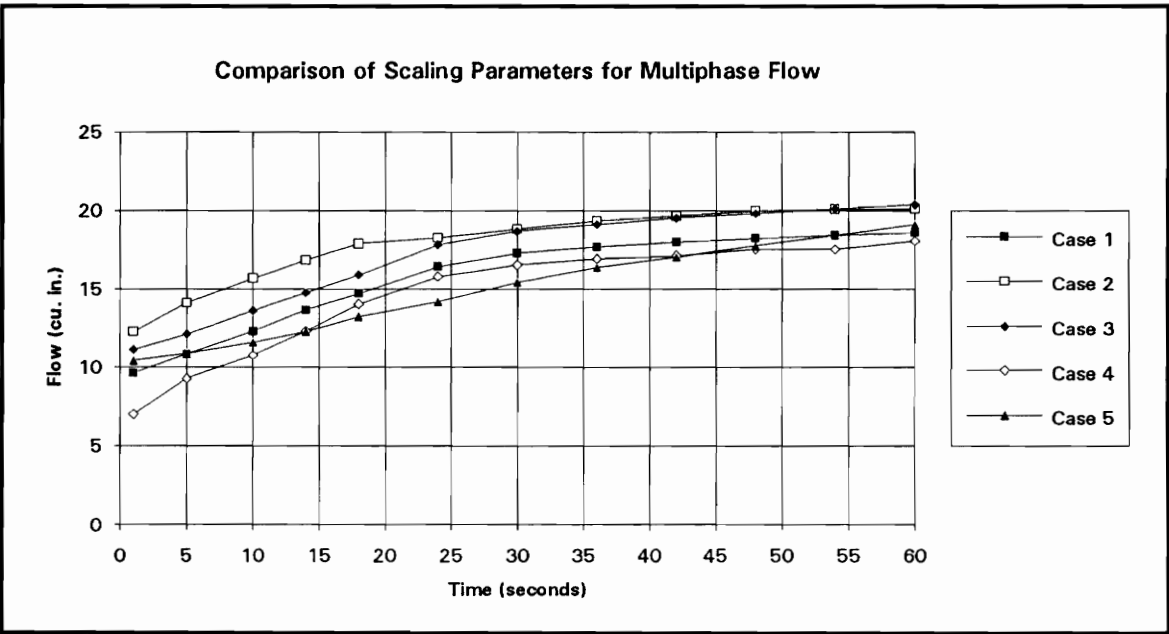


Figure 5.13 Plot showing simulations for 5 cases involving variations in scaling parameters  $\beta_{OW}$  and  $\beta_{AO}$ .

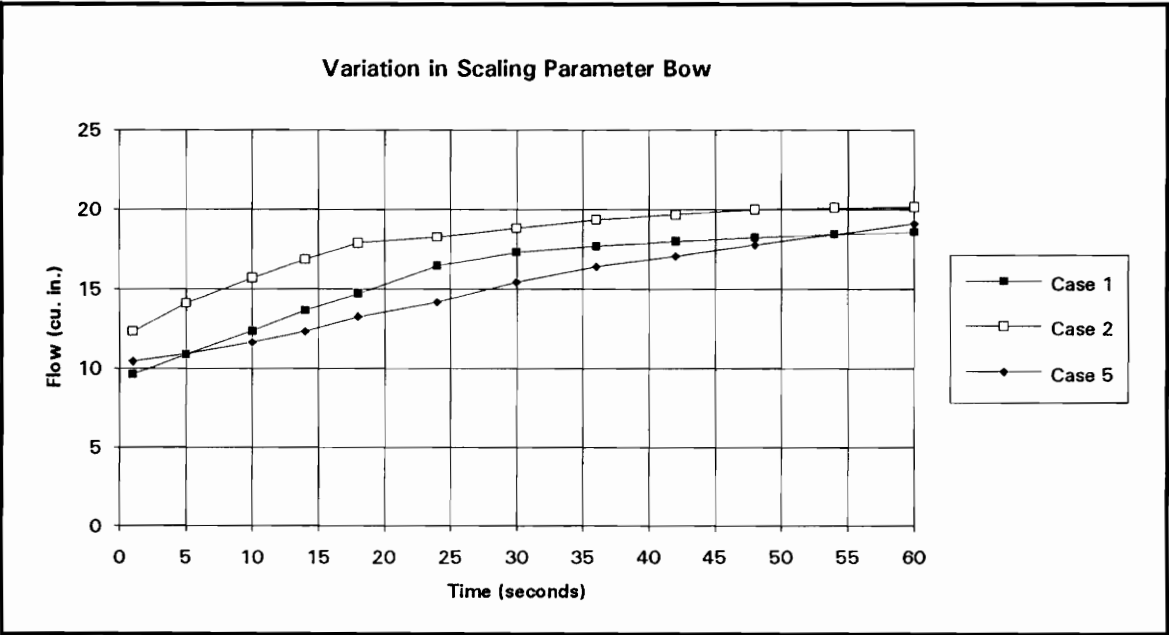


Figure 5.14 Plot showing simulations for 3 cases involving variations in scaling parameter  $\beta_{OW}$ .

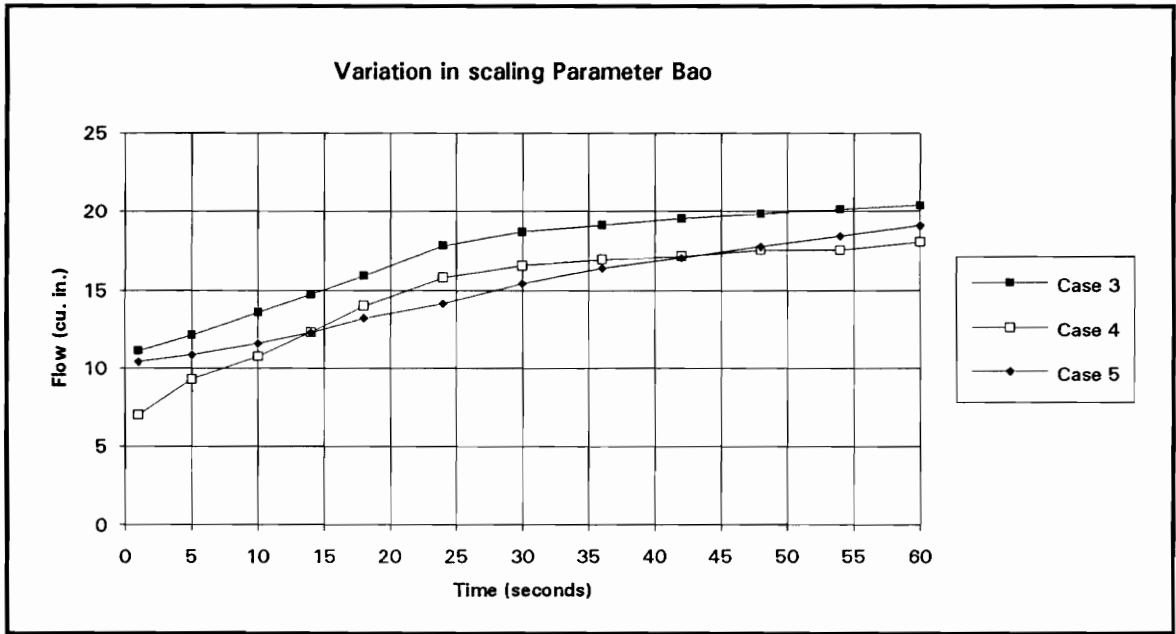


Figure 5.15 Plot showing simulations for 3 cases involving variations in scaling parameter  $\beta_{aO}$ .

Figure 5.14 shows that as the parameter  $\beta_{OW}$  is increased from 1.2 to 3.2, the value of outflow of water also tends to increase by 30 to 36 %. Figure 5.15 shows that as the parameter  $\beta_{aO}$  is decreased from 4.5 to 2.5, the value of water outflow for the simulations tends to increase by 10 to 30 %. Consistent results throughout the simulations for these parameters may be hidden by the effects of convergence at intermediate time levels.

**VARIATIONS DUE TO THE SELECTION OF VAN GENUCHTEN'S  
PARAMETERS**

In this section the column problem is used to investigate the effects' van Genuchten's parameters,  $\alpha$  and  $n$ , have on the outflow of water in a multiphase flow system. Table 5.12 shows the constant values of  $\beta_{ao}$  and  $\beta_{ow}$ , as well as the material property parameters used in the evaluation.

Table 5.12 Parameters used in investigating the effects of varying van Genuchten's parameters on the outflow of water

Parameter	Value
$K_{sw}$	0.025 in/sec
$K_{so}$	0.25 in/sec
$\beta_{ow}$	2.2
$\beta_{ao}$	4.5

Figures 5.16 and 5.17 show the variation in outflow due to the selection of van Genuchten's parameters  $\alpha$  and  $n$ . Figure 5.16 shows that for increasing values of van Genuchten's parameter  $\alpha$  there is a corresponding increase in the outflow of water in the three-phase air-gasoline-water column simulation. Figure 5.17 shows that for increasing values of van Genuchten's parameter  $n$ , there is a corresponding increase in water outflow for the two-phase column simulation. Comparing Figures 5.16 and 5.17 it is obvious that van Genuchten's parameter  $n$  effects the multiphase flow simulations to a greater extent than the parameter  $\alpha$ .



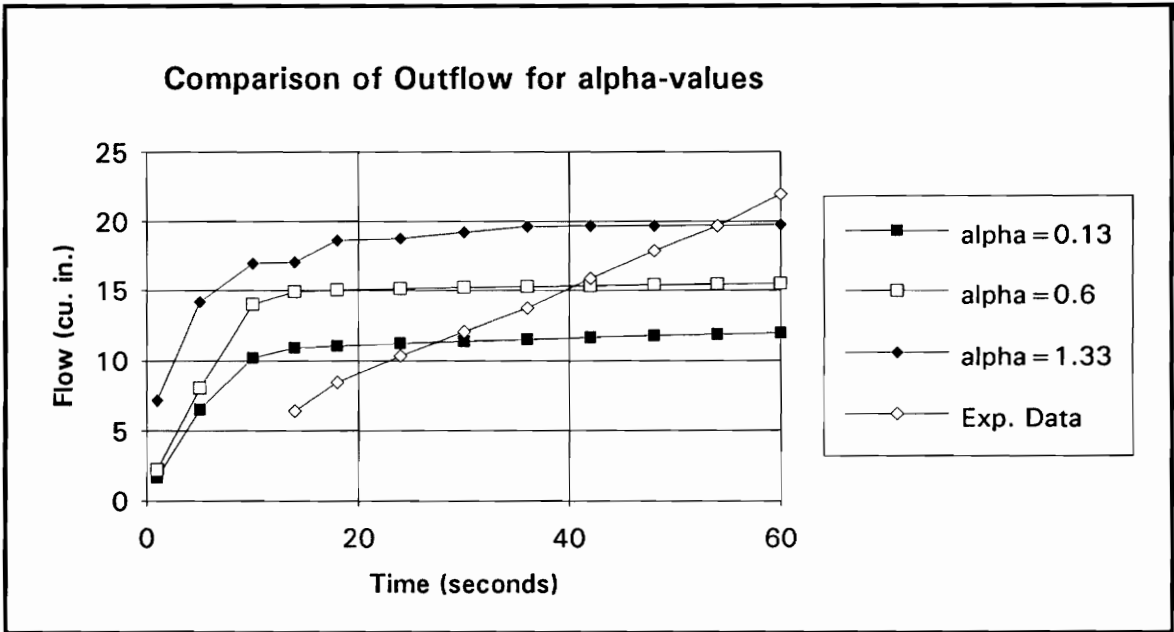


Figure 5.16 Comparison of water outflow for van Genuchten's parameter  $\alpha$ .

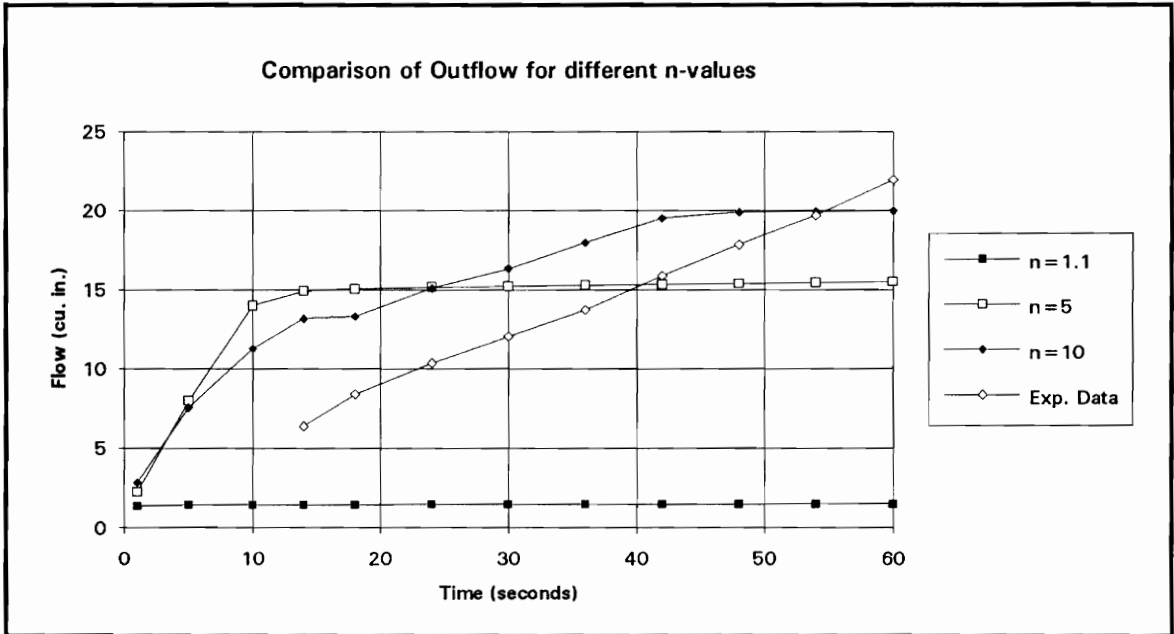


Figure 5.17 Comparison of water outflow for van Genuchten's parameter  $n$ .

## CONCLUSIONS

Chapter 5 presents an experimental study using a one-dimensional column test and a two-dimensional flume test. The results of the tests are presented in the preceding sections, with a comparison made between the multiphase flow column test under no suction with a finite element simulation. The results of the simulation show a good comparison with the experimental data, but only after the estimated parameters are changed to accommodate the simulation process. This difference in material property parameters is likely to be due the difficulty of effectively and accurately measuring fluid outflow during the testing procedure.

The effects of the scaling parameters developed by Parker et al. (1987) on the results of the three-dimensional simulation is made in the last section of Chapter 5. It is found that as the parameter  $\beta_{OW}$  is increased from 1.2 to 3.2, the value of outflow of water also tends to increase by 30 to 36 %. Similarly, as the parameter  $\beta_{aO}$  is decreased from 4.5 to 2.5, the value of water outflow for the simulations tends to increase by 10 to 30 %.

Varying van Genuchten's parameters  $\alpha$  and  $n$  also effected the water outflow results, for constant scaling and material parameters. It is found that increasing both parameters  $\alpha$  and  $n$  results in an increase in water outflow for the time scale studied. It is also noted, that varying the parameter  $n$  effects the results of the simulation to a much greater extent than varying the parameter  $\alpha$ .

## **CHAPTER 6**

### **THREE-DIMENSIONAL MASS TRANSPORT**

#### **INTRODUCTION**

Past researchers, such as Burnett and Frind (1987a, 1987b) have shown that the two-dimensional model simulations predict further plume movement than actually occurs in experiments. Up until recently, these formulations were still used in analysis, since three-dimensional analyses were often considered too expensive to warrant use. The increased accessibility to high speed computers, at a reduced cost, has enabled three-dimensional analyses to become more feasible and popular. This leads to simulations that no longer use spatially simplified domains, and provide a better approximation to the real life situations that must be analyzed.

As previously mentioned, three types of transport problems are covered in this thesis: (1) multiphase immiscible flow, (2) mass transport without flow (molecular diffusion), and (3) multiphase immiscible flow in a weak-coupled formulation with convective-dispersive mass transport. The three-dimensional finite element formulation for multiphase immiscible flow is validated in Chapter 4, based on laboratory test results and the simulations using a previously validated two-dimensional formulation. The coupled problem is addressed in Chapter 7. The objective of this chapter is three-fold. First the mechanisms that control mass transport are presented with a review of the relevant coefficients and their limitations. The second objective is to present the molecular diffusion portion of the mass transport equation and develop a three-dimensional finite element formulation. Only the equations for mass transport related to diffusion are used

directly in this chapter. The convection-dispersion equations for the three-phase system are presented in Chapter 7. Finally, the three-dimension formulation of the diffusion equation, without flow is validated based on a comparison with a two-dimensional model. This type of problem would relate to a situation in which no flow is present in the system, but mass transport still occurs due to the diffusive nature of the contaminants, such as in a clay landfill liner.

## **MASS TRANSPORT PROCESSES**

The study of the convective-dispersive process is important in predicting the plume spread, determining when cost effective remediation measures should be planned. Predicting the plume movements is a challenging and complex problem that involves many linear and nonlinear transport mechanisms. These mechanisms cause numerical difficulties in models used to estimate plume movements. In addition to this, concentrations of a given solute may be strongly dependent on the concentrations of other contaminants in the aquifer or the mineralogy of the porous media (National Research Council 1990). This may yield numerical simulations that are inadequate for predicting movements in a natural geological setting.

The three major modes of transport covered in this chapter include: (1) convection or advection, (2) mechanical dispersion, and (3) molecular diffusion. Other mechanisms that effect the concentration and movement of the contaminant in the aquifer include radioactive decay, retardation, and partitioning between the different phases in the system; namely the air, oil, water, and solid phases. Some of these mechanisms are discussed in Chapter 7 and are used to develop the mass transport formulation for the

three-phase system that is weakly-coupled with the multiphase flow formulation presented in Chapter 3.

Most experimental work involves representing the displacement of one substance by another substance through a concentration breakthrough curve, such as the one depicted in Figure 6.1. Figure 6.1 shows the concentration breakthrough curve (dotted line) based on contaminant transport through convection, plug flow situation. Convection is the phenomenon by which dissolved substances are carried along by the movement of fluid displacement. This is dependent on the amount of free or mobile fluid in the porous medium and the "real" velocity of the fluid (de Marsily 1986). If this were true in the field, then tracking a contaminant would be easy since the contaminant plume movement throughout the subsurface would be essentially a one dimensional problem.

Re-examination of Figure 6.1 helps explain the actual concentration movement. This shows that the actual shape of the breakthrough curve is not one of plug flow, but is instead S-shaped. This is caused by other mechanisms which effect mass transport such as molecular diffusion and mechanical dispersion. Molecular diffusion is the net transport of a molecule in a fluid due to intermolecular collisions (Lyman et al. 1982). Movement controlled by this mechanism is assumed to be constant in all directions and is a function of the concentration gradients present in different phases in the medium. The significance of this process is highly dependent on the media contained in the subsurface domain. For domains that contain silts or clays, where the permeability is very small, resulting in small velocity vectors, the effects of molecular diffusion can be relatively large. On the other hand, in a sandy or gravelly subsurface domain the effects of molecular diffusion are small as compared to the convection and mechanical dispersion terms and may often be neglected.

A uniform plume in a two-dimensional domain, as shown in Figure 6.2, is the result of a mass transport problem considering only convection and molecular diffusion. Figure 6.3 shows a more reasonable estimation of plume movements. Here the plume travels in a non-uniform manner and spreads in the transverse and lateral directions at different rates. This variation in movement over space and time is controlled by the mechanism referred to as mechanical dispersion. The spreading in the direction of ground water flow is caused by the longitudinal component of mechanical dispersion, while the spreading in the direction perpendicular to ground water flow is caused by the mechanism referred to as the transverse dispersion (EPA 1989). Mechanical dispersion is the process by which a contaminant moves through the subsurface domain according to the microscopic fluctuations of the velocity vectors in the flow path and macroscopic relations which are described in greater detail in the following sections.

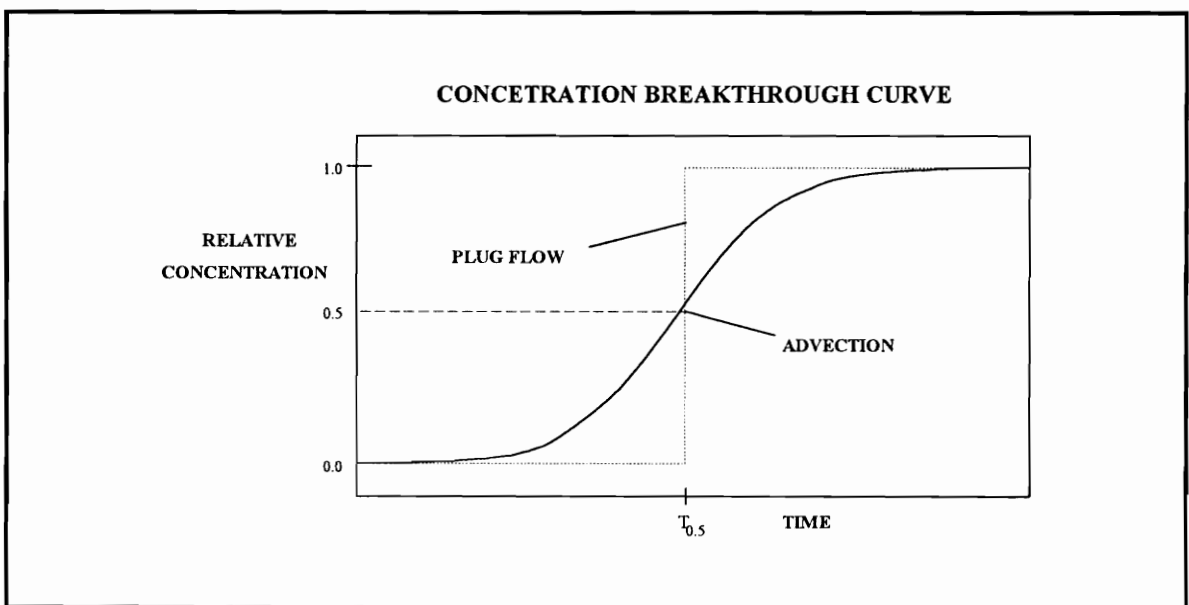


Figure 6.1 Depiction of concentration breakthrough curve for plug flow and convection-dispersion (After EPA 1989)

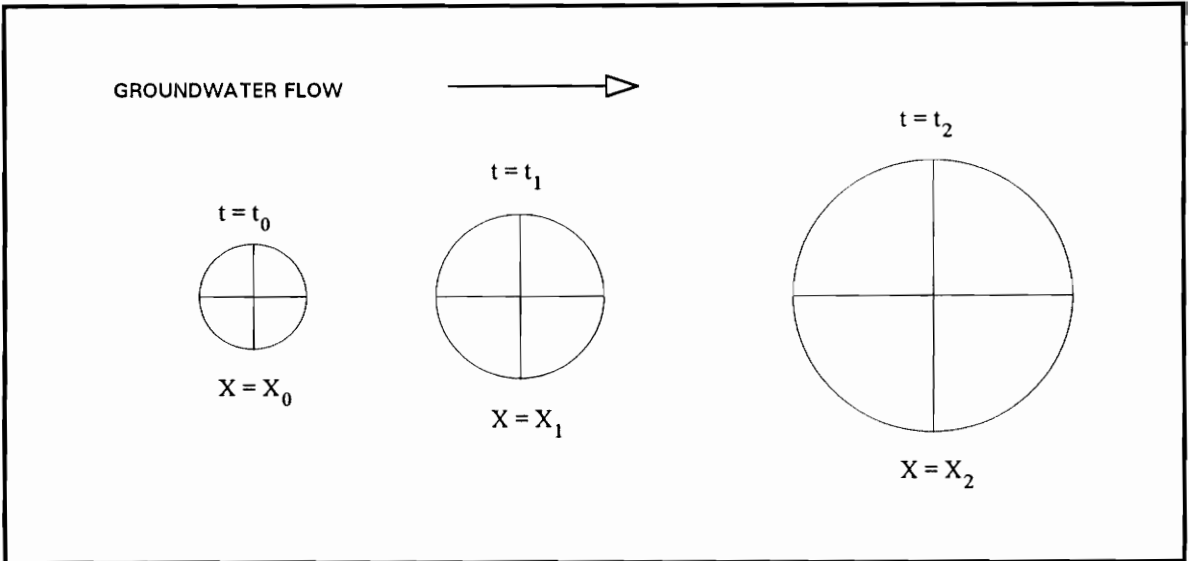


Figure 6.2 Two-dimensional depiction of convection and diffusion

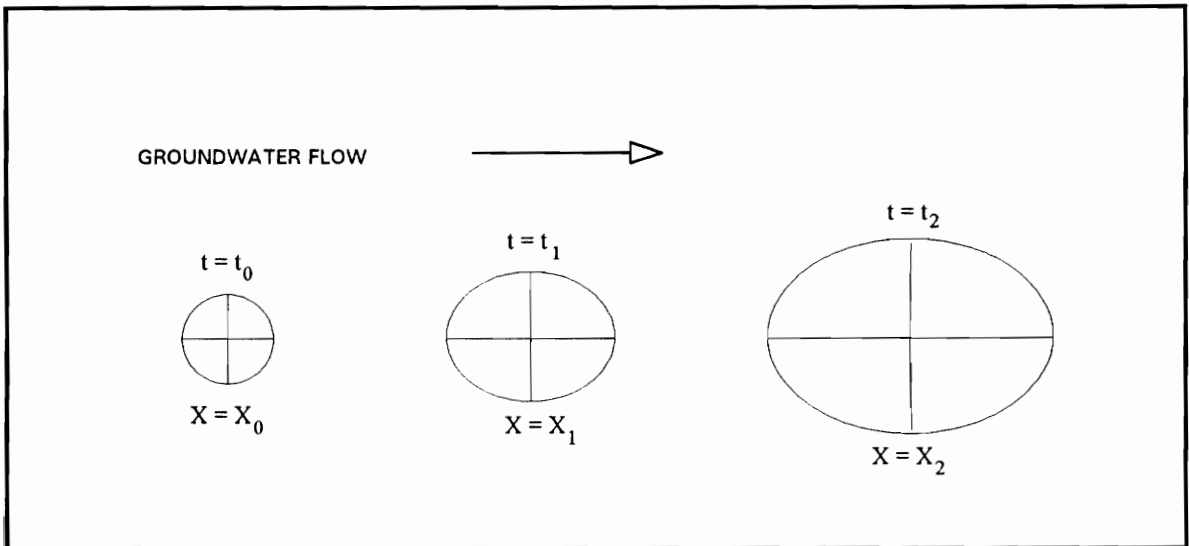


Figure 6.3 Two-dimensional depiction of convection and dispersion (after EPA 1989)

The following sections further describe the three processes mentioned above: convection, diffusion, and dispersion. These sections not only cover the theory and limitations related to each of the modes of transport but also develop the governing equations based on conservation of mass.

## **CONVECTION**

As stated in the previous section, convection is the process by which contaminant transport of solutes takes place as a result of the bulk motion of the ground water flow (Freeze and Cherry 1979). This is the best understood of the three processes that make up mass transport but limitations between the theory and field conditions still apply.

Recall the discussion presented in Chapter 2 on liquid solid relations. This section explains that not all of the fluid-phase contained in the pore spaces is "free." In fact there is an adhesive layer that does not flow but instead remains stagnant in the pore space. This brings up the discussion pertaining to what portion of the fluid phase is actually mobile and can be considered as a part of the convection portion of the transport equation. In reality, the significance of this problem is related to the permeability of the soil and the magnitude of the hydraulic gradient present in the aquifer (de Marsily 1986). This may become a problem in certain soils where the validity of Darcy's law is questionable and may result in invalid velocity vectors which are used in the convection portion of the mass transport equation.

Many researchers find it necessary to define the term constant kinematic porosity. This is the porosity corresponding to the void space in which fluid is flowing in a free state. It is important to note that this is highly dependent on the porous media and the hydraulic head in the aquifer system, but measurements of kinematic porosity have never



been made and must be estimated by the modeler based on experience (de Marsily 1986). This thesis will refer to only the porosity of a porous media, but the previous discussion should be considered when choosing this value for certain conditions.

## EQUATION DEVELOPMENT FOR CONVECTION

If we now consider, on a macroscopic scale, an elementary volume,  $V$ , similar to the one used in describing mass transfer in an unsaturated flow system, and a surface area,  $S$ , we can define the convection portion of the mass transport equation (de Marsily 1986). The volumetric flux of fluid crossing  $S$  is given by the Darcy velocity,  $U$  (note that the Darcy velocity in this section is represented by  $U$  to avoid confusion with the elemental volume,  $V$ ). This flux is transformed into a mass flux of contaminant through scalar multiplication of the Darcy velocity and the volumetric concentration,  $C$ , of the contaminant. Therefore the mass flow entering the elemental volume is (de Marsily 1986)

$$\int_s CU \cdot n \, d\sigma, \quad (6.1)$$

where  $n$  is the vector normal to the surface,  $S$ , of the elemental volume,  $V$ .

The mass of substance contained in the elemental volume,  $V$ , at any time,  $t$ , is the integral of the elementary volumes of the fluid,  $\phi \, dv$ , contained in the porous medium multiplied by the volumetric concentration,  $C$ , of the fluid contained in this medium (de Marsily 1986). This is given by

$$\int_v \phi C \, dv. \quad (6.2)$$

The variation of the mass contained in a given element per unit time can be obtained by taking the derivative of the previous expression with respect to time:

$$\frac{\partial}{\partial t} \int_V \phi C \, dv = \int_V \phi \frac{\partial C}{\partial t} \, dv. \quad (6.3)$$

de Marsily shows that by applying Leibnitz's rule, the passage between Equations 6.1 and 6.3 can be made, since the volume and porosity are considered constant for the element considered. Therefore the equation for mass balance related to mass transport becomes

$$\int_S CU \cdot n \, d\sigma = \int_V \phi \frac{\partial C}{\partial t} \, dv. \quad (6.4)$$

Taking into account that the volume is arbitrary and transforming the area integral on the left-hand side of the above expression to a volume integral, the following expression for mass conservation is obtained:

$$-\left[ \frac{\partial}{\partial x} (\bar{V}_x C) + \frac{\partial}{\partial y} (\bar{V}_y C) + \frac{\partial}{\partial z} (\bar{V}_z C) \right] = \frac{\partial C}{\partial t}, \quad (6.5)$$

where  $\bar{V}$  = the average linear velocity of the water phase,  $\bar{V} = \frac{U}{\phi}$ . This is the expression that governs the convective mass transport of the contaminant in water. This expression is combined with the dispersion and diffusion mechanisms later in this chapter.

## DIFFUSION

The process of molecular diffusion is based on the Brownian motion of particles and the concentration gradients between neighboring portions of the fluid being considered. As de Marsily (1986) explains, Brownian motion projects particles in all directions in space. If two adjacent points have the same concentration then the average exchange of particles between the points is the same, but if the concentration varies between two adjacent points then the point with the higher concentration sends more particles (on average) than the point with a lower concentration. Lyman et al. (1982) explains that the diffusion of a contaminant is a function of two compounds, in other words diffusion depends on the nature of the compound in question and the medium in which the compound is being transported through. This means of transport occurs until the concentrations at the adjacent points have approximately the same value.

The coefficient of molecular diffusion,  $D_o$ , varies for various contaminants in different mediums and is given by (de Marsily 1986)

$$D_o = \frac{RT}{N} \frac{1}{6\pi\mu r}, \quad (6.6)$$

where

$R$  = the constant for perfect gases,

$N$  = Avogadro's number ( $6.023 \times 10^{23}$ ),

$T$  = the absolute temperature in degrees Kelvin,

$\mu$  = the fluid viscosity, and

$r$  = the mean radius of the diffusing molecular aggregates.

This expression has the dimensions length<sup>2</sup>/time and is only valid for an infinite dilution. Since  $\mu$  is a function of temperature it follows that the diffusion coefficient is also a function of temperature. The change in the diffusion coefficient due to a change in temperature is an exponential function given by (de Marsily 1986):

$$D_o(T_2) = D_o(T_1) \exp[E(T_2 - T_1) / RT_1T_2], \quad (6.7)$$

where E is the activation energy of the ion in the solution.

Recalling the theory of fluid-solid relations, it is noted that molecular diffusion occurs not only in the free phase but also in the immobile or adhesive phase, with only solids stopping the Brownian movement of the aggregates. This results in a diffusion coefficient that is lower than the theoretical value and is dependent on the porous media (de Marsily 1986). The range of values of the actual diffusion is from 0.1 (clays) to 0.7 (sands) times the theoretical value, as reported by de Marsily (1986).

The actual diffusion coefficient is often estimated based on the tortuosity of the porous medium. This can be described by  $D_d = \tau D_o$ , where  $\tau$  is the tortuosity of the porous medium (EPA 1989). The tortuosity is the factor that accounts for the increased distance a diffusing ion must travel in a porous media (EPA 1989). Typical values for granular media range from 0.6 to 0.7. Gillham (1984) found that tortuosity factors, in sand-clay mixtures, results in diffusion values equal to 0.59 to 0.84 times the theoretical value for  $\text{Cl}^{36}$ , and 0.33 to 0.70 times the theoretical value for tritium.

## EQUATION DEVELOPMENT FOR DIFFUSION

Fick's law states that the mass flux of fluid particles for a fluid at rest is proportional to the concentration gradients between two points in the fluid. A description of this movement is given as (de Marsily 1986):

$$-D_o \frac{\partial C}{\partial x} - D_o \frac{\partial C}{\partial y} - D_o \frac{\partial C}{\partial z} \quad (6.8)$$

Applying the principle of mass balance, the following equation for diffusive transport is obtained:

$$\left[ \frac{\partial}{\partial x} \left( D_o \frac{\partial C}{\partial x} \right) + \frac{\partial}{\partial y} \left( D_o \frac{\partial C}{\partial y} \right) + \frac{\partial}{\partial z} \left( D_o \frac{\partial C}{\partial z} \right) \right] = \frac{\partial C}{\partial t} \quad (6.9)$$

This is the second means mode used to describe the mass transport equation. Later in this chapter the previously presented equation for convection and the above expression for diffusion will be combined with the expression for mechanical dispersion. It is important to note that diffusion is often neglected in coarse soils due to the much larger convection and dispersion terms, but may be significant in fine grained soils have slow ground water velocities.

## MECHANICAL DISPERSION

The phenomenon of dispersion refers to the non steady irreversible mixing action that takes place as a result of two miscible or partially miscible fluids displacing each other in a porous media (Schwartz 1977). This complex reaction caused by both microscopic, macroscopic and megascopic subsurface conditions causes great difficulty in providing effective numerical models. This is a result of the nonlinearities involved in parameter estimation and the heterogeneous nature of the subsurface environment. The heterogeneity of the microscopic velocities results in a mixing phenomenon on a macroscopic scale and this mixing results in plume movements that are not uniform. This non uniform movement is referred to mechanical dispersion.

There are three main reasons mechanical dispersion is needed in estimating mass transport (de Marsily 1986). (1) The velocity profile assumed in pores, considered a network of cylindrical pipes, is parabolic rather than uniformly distributed. This is shown in Figure 6.4. This causes a progressive spreading of the transported substance that differs from the contaminant movement described by either convection or diffusion theory. This spreading is caused by the faster propagation of the fluid in the central region of the pore space (along the axis of a given structure of pores) as compared to the fluid nearest to the solid phase. (2) Spreading of contaminants at up to  $90^\circ$  from the direction of macroscopic flow is caused by differences in aperture and travel distance from one pore to another. Microscopic differences in pore channels such as the sizes of the channels, surface area, and roughness also create different mean velocities and cause fluid flow paths to mix, resulting in dilution of the contaminant over time and space (Freeze and Cherry 1979). (3) Macroscopic heterogeneity in the subsurface also contributes to mechanical

dispersion. This can be caused by lenses of fine grained material, inter layered deposits, and broken or fractured zones. Therefore, mechanical dispersion is considered to be a mixing phenomenon that approximates the errors related to modeling porous media using the simplifying assumptions for advection and diffusion and for using the macroscopic estimation of to determine velocity vectors, namely Darcy's velocity.

Mechanical dispersion can be estimated using lab tests, tracer tests, or pumping well tests. However, the values obtained from these tests may differ according to the scale at which the tests are conducted. It has been observed that small scale lab tests underestimate the value of dispersion that is observed in the field. The EPA (1989) notes that researchers attribute these discrepancies to mechanisms that include immobile zones of water within experimental columns, solution-solid interface processes, anion exchange, and diffusion in and out of aggregates. These mechanisms result in an apparent scale dependency for dispersion, as shown in Table 6.1. The EPA (1989) notes that even experiments involving a single tracer result in an increase in recorded dispersion constants with an increases in distance from the source. This indicates that the assumptions used in convective-dispersive transport theory are not applicable to natural geological settings.

The scale dependent nature of the dispersion coefficient is a function of the scale of the subsurface environment that is considered in the problem. This can be broken down into three different scale relations: (1) microscopic, (2) macroscopic, and (3) megascopic. A listing of these relations and the causes of dispersivity for each of the three scale effects is outlined as follows (Schwartz 1977):

(1) microscopic or pore to pore heterogeneity:

- (a) pore size distribution,
- (b) pore geometry,

- (c) dead-end pore space;
- (2) Macroscopic heterogeneity:
  - (a) Stratification characteristics such as: non uniform stratification, stratification contrasts, stratification continuity, and insulation to cross-flow;
  - (b) Permeability characteristics such as: non uniform permeability, permeability trends, and directional permeability;
- (3) Megascopic heterogeneity, either field wide or regional heterogeneity:
  - (a) reservoir geometry: overall structural framework (faults, dipping strata, etc.) and overall stratigraphic framework (bar, blanket, channel fill, etc.);
  - (b) hyper permeability-oriented natural fracture systems.

Table 6.1 Longitudinal dispersivity values from various scale experiments

Type of Test	Longitudinal Dispersivity (m)
Laboratory Tests	0.0001-0.01
Natural Gradient Tracer Tests	0.01-2
Single Well Tests	0.03-0.3
Radial and Two Well Tests	0.5-15
Model Calibration of Contaminant Plumes	3-100

(After Gillham and Cherry 1982)

Schwartz (1977) explains that the most limiting factors of mass transport analysis based on dispersion are a result of the lack of understanding concerning macroscopic and megascopic factors. He goes on to explain, that the scale considered important in the problem determines what type of testing procedure should be utilized in determining



dispersion coefficients. If the scale being considered for the dispersion of a tracer is only a few meters from the source than microscopic features may be predominant in determining the dispersion. On the other hand for cases involving kilometers of movement, these microscopic heterogeneities may have little to no effect on the dispersion as compared with the macroscopic or megascopic considerations.

On a macroscopic scale Schwartz (1977) shows that there are three factors which effect the dispersivity of a given contaminant. These include the contrasts in permeability values between elements comprising a porous media, the number of low-conductivity inclusions, and the mode of aggregation in the medium (random, clustered, etc.). The first of these three factors is the most significant. Schwartz shows that determining a unique value of dispersivity, from situations involving clustered or continuous zones of low-conductivity, is very difficult. This is because of the progressive change in the hydraulic conductivity as a function of space. This limits models which characterize the dispersivity as a constant value over discrete regions of a porous medium. Therefore, without a complete understanding of the geological system and the relative conductivities in space, the dispersivity coefficients lose their meaning and result in an inaccurate representation of plume movements.

## **EQUATION DEVELOPMENT FOR MECHANICAL DISPERSION**

The equation development for the dispersive component of mass transport is analogous to Fick's first law, used to explain molecular diffusion through the phenomena of mixing (Freeze and Cherry 1979). Therefore, considering conservation of mass, the dispersive flux is given as

$$\left[ \frac{\partial}{\partial x} \left( D \frac{\partial C}{\partial x} \right) + \frac{\partial}{\partial y} \left( D \frac{\partial C}{\partial y} \right) + \frac{\partial}{\partial z} \left( D \frac{\partial C}{\partial z} \right) \right] = \frac{\partial C}{\partial t} \quad , \quad (6.10)$$

where the coefficient  $D$  is referred to as the coefficient of dispersivity. This coefficient is usually a combination of both the dispersive and diffusive modes of transport when used in the convection-dispersion model. de Marsily explains that the dispersion coefficient can be simply characterized by three assumptions:

- (1) the tensor is symmetric and of the second order;
- (2) the tensor has two principle directions: (a) a longitudinal direction which is in the same direction as the velocity vector, and (b) a transverse direction which is perpendicular to the direction of flow; and
- (3) the tensor coefficients are dependent on the average linear velocity.

The anisotropic dispersion tensor is expressed in matrix form as

$$D = \begin{bmatrix} D_L & 0 & 0 \\ 0 & D_T & 0 \\ 0 & 0 & D_T \end{bmatrix} \quad , \quad (6.11)$$

where

$D_L$  = the dispersion tensor in the longitudinal direction, and

$D_T$  = the dispersion tensor in the transverse direction.

The value of the dispersion coefficients varies with the absolute value of average linear velocity. Bear (1972) explains that there are two approaches commonly used in estimating the dispersion coefficient. In the first method, the porous medium is replaced

by a fictitious model which is analyzed using exact mathematical models. It is noted that this approach greatly simplifies the problem. Models such as this may comprise a single capillary tube, a bundle of capillaries, or an array of cells (Bear 1972). The second method involves constructing a model based on a statistical model of the microscopic motion of the fluid particles which is used to estimate the macroscopic movements. Bear (1972) emphasizes that mathematical models are estimates that should be verified by a final test experiment.

The first approach combines the modes of mechanical dispersion with those of molecular diffusion as (Bear 1972)

$$D_h = D + D_o \quad (6.12)$$

where

$D_h$  = the hydrodynamic dispersion,

$D$  = the mechanical dispersion, and

$D_o$  = the molecular diffusion.

Models used to approximate  $D_h$  based on simplified models are outlined by Bear (1972). The hydrodynamic dispersion, as previously discussed, is broken up into a longitudinal and transverse component.

Saffman's work, as explained by Rose (1977), considers a porous bed of randomly distributed networks of capillaries of a length  $l$  and a radius  $a$ , where  $l \ll a$ . This model considers two processes in describing the dispersion tensor: (1) Brownian motion and (2) variations in velocity across the capillary cross-section. Estimates of the longitudinal and

transverse components of dispersion, based on the Peclet number ( $P_e$ ), are presented by Saffman (1960) as:

$$D_{hL} = D_o \left( m + \frac{P_e^2}{15} \right), \quad \text{and}$$

$$D_{hT} = D_o \left( m + \frac{P_e^2}{40} \right), \quad \text{for } P_e \ll 1.0 \quad (6.13)$$

or

$$D_{hL} \approx \left[ \left( \frac{P_e}{6} \right) \ln(1.5P_e) - \left( \frac{17P_e}{72} \right) - (R/l)^2 \frac{P_e^2}{48} + m + \frac{4}{9} \right] D_o, \quad \text{and}$$

$$D_{hL} \approx \left[ \left( \frac{3P_e}{10} \right) + (R/l)^2 \frac{P_e^2}{40} + m - \frac{1}{3} \right] D_o \quad \text{for } 1 \leq P_e \leq 8(R/l)^2, \quad (6.14)$$

where the Peclet number,  $P_e$ , is equal to  $\frac{\bar{V}L}{D_o}$ , here  $L$  is the characteristic length of the porous media. In Equation 6.14,  $R=(24K/\phi)^{0.5}$ , where  $K$  and  $\phi$  are the hydraulic conductivity and porosity of the medium, respectively; and the term  $l$  refers to the pore length and  $m$  is an empirical coefficient between  $1/3$  and  $2/3$ .

Correlating the above relation to a porous medium, Saffman considered the length of the pores to be equal to the mean particle diameter and inferred the radius from the permeability of the medium. The work of Saffman is found to accurately predict dispersion coefficients over a wide range of Peclet numbers. Rose (1977) notes that the theory agrees well with the experimental data presented by Hiby (1962), Harleman et al (1963), and Edwards and Richardson (1968).

An example of the second type of model is described by Bear (1972). This model is based on the idea of building a continuum at the macroscopic level by averaging microscopic quantities (Rose 1977). Here the porous medium is modeled as a random network of interconnected channels of varying length, cross-section, and orientation. The mean length and characteristic cross-section are taken to be equal to the mean radius. The relationship is given as

$$D_h = D_o \left[ T_m^* + P \left( 1 + \frac{2}{P} + \frac{4}{P} \left( \frac{l}{a} \right)^2 \right)^{-1} \right], \quad (6.15)$$

where  $T_m^*$  is the tortuosity of the macropores. Rose (1977) explains that this model is sensitive to changes in  $l/a$ , but is valid for all Peclet numbers.

Rose (1977) and de Marsily (1986) explain that the dispersion coefficient can be described to fall under one of five regimes based on the empirical relations between transverse and longitudinal dispersivities and the Peclet number. These five regimes can be described by the following.

- (1) Pure molecular diffusion ( $P < 0.3$ ). This occurs when the velocity is small, and  $D_h/D_o = T_m^*$ .
- (2) Superposition ( $0.3 < P < 5$ ). Convection becomes the same order of magnitude as diffusion.
- (3) Interference ( $5 < P < 400$  to  $10^3$ ). Convective-dispersive process dominates, but diffusion cannot be eliminated and because the transverse molecular diffusion interferes with the longitudinal convection and tends to cause a decrease in dispersion.

- (4) Pure convection-dispersion ( $10^3 < P < 1.5 \times 10^5$ ), provided Darcy's law is still valid. Diffusion can be neglected.
- (5) Convection-dispersion outside the validity of Darcy's law. The effects of inertia cannot be neglected. This regime is unlikely in ground water flow studies.

Dispersion coefficients are usually based on velocities encountered in regions 3 and 4, in which the following relationship is generally admitted:

$$\begin{aligned} D_{hL} &= \alpha_L |U| \\ D_{hT} &= \alpha_T |U| \end{aligned} \quad (6.16)$$

where

$\alpha_i$  = the longitudinal and transverse intrinsic dispersion coefficients, which have dimensions of length; and  
 $U$  = the Darcy velocity.

For regions 1 and 2, where molecular diffusion effects are significant the hydrodynamic dispersion coefficient can be characterized as

$$\begin{aligned} D_{hL} &= \phi D_o + \alpha_L |U| \\ D_{hT} &= \phi D_o + \alpha_T |U| \end{aligned} \quad (6.17)$$

A relationship, not regime dependent, developed by Bear (1979), is given as

$$D_{hij} = \alpha_T \bar{V} \delta_{ij} + (\alpha_L - \alpha_T) \frac{\bar{V}_i \bar{V}_j}{\bar{V}} + D_o, \quad (6.18)$$

where

$\bar{V}$  = the magnitude of the velocity vector,  $(\bar{V}_i^2 + \bar{V}_j^2)^{1/2}$ ;

$\bar{V}_i$  = the average linear velocity in the i-direction;

$\bar{V}_j$  = the average linear velocity in the j-direction; and

$\delta_{ij}$  = Chromicler's delta.

The validity of this expression is a controversial matter, but it is generally accepted as valid for laboratory conditions (Ahmad 1991). For field conditions, it has been observed that the results of Equation 6.18 greatly under predict the dispersion coefficient (Fried 1975, and Bigger and Nielson 1976).

It is important to note, that most of the studies related to defining the dispersion coefficient have been based on saturated conditions and reliable data on unsaturated conditions is scarce, but one might expect that dispersion coefficients will be smaller in unsaturated conditions (Rose 1977). Explanation of this is based on given Peclet number which is a function of the pore water velocities, which are smaller for unsaturated conditions.

## COMBINED EQUATIONS OF CONVECTIVE-DISPERSIVE TRANSPORT

Combining the three modes of mass transport namely advection, diffusion, and dispersion; incorporating the effects of retardation through solute adsorption, chemical reaction, and/or radioactive decay; and including a source-sink term, the following equation is obtained (Huyakorn and Pinder 1983):

$$\left[ \frac{\partial}{\partial x} \left( D_x \frac{\partial C}{\partial x} \right) + \frac{\partial}{\partial y} \left( D_y \frac{\partial C}{\partial y} \right) + \frac{\partial}{\partial z} \left( D_z \frac{\partial C}{\partial z} \right) \right] - \left[ \frac{\partial}{\partial x} (\bar{V}_x C) + \frac{\partial}{\partial y} (\bar{V}_y C) + \frac{\partial}{\partial z} (\bar{V}_z C) \right] - \bar{F}C + \bar{Q} = R \frac{\partial C}{\partial t}, \quad (6.19)$$

where:

$D_i$  = the hydrodynamic dispersion coefficient in the x-, y-, and z-directions, this is a combination of mechanical dispersion and molecular diffusion;

$C$  = the concentration of the solute, defined as the mass of solute per unit volume of solution;

$\bar{V}$  = the average linear velocity, which is obtained by dividing the specific discharge by the porosity;

$\bar{F}$  = the first order radioactive decay coefficient, defined in terms of a given chemical's half-life;

$\bar{Q}$  = the zero order source or sink term, and

$R$  = the retardation factor, defined as a measure of the ratio of the velocity of water flow to the velocity of the contaminant.

Equation 6.19 is the general form of the convection-dispersion equation. In Chapter 7 this equation is extended to each phase in the three-phase system and combined with relations for the partition coefficients and radioactive decay terms to develop the form of the transport equation used in the weakly-coupled system.



## FINITE ELEMENT FORMULATION FOR DIFFUSION

Now consider the eight-noded solid element, which is the three-dimensional counterpart of the four-noded tetrahedron. The concentration  $C$  given in Equation 6.9 is now approximated as

$$C = N_i C_i = [N] \{q_c\}^T, \quad (6.20)$$

where  $[N]$  is the matrix of the shape functions given by Equation 2.22 and  $\{q_c\}$  is the approximate solution of the nodal concentrations. Applying Galerkin's Method of weighted residuals to Equation 6.9, the following finite element relationship is obtained:

$$[K] \{q_c\} + [K_T] \{\dot{q}_c\} = \{Q_c\}, \quad (6.21)$$

where  $[K]$  is the stiffness matrix given by

$$[K] = \iiint_{XYZ} [B]^T [D] [B] \, dxdydz. \quad (6.22)$$

The  $[B]$  matrix is defined as the derivative of the shape functions and can be represented as

$$[B] = \left[ \frac{\partial N_i}{\partial x}, \frac{\partial N_i}{\partial y}, \frac{\partial N_i}{\partial z} \right], \text{ where } i = 1 \text{ to } 8, \quad (6.23)$$

where s, t, and r refer to the local transformed coordinate system. The constitutive matrix for mass transport is given as

$$[D] = \begin{bmatrix} D_o & 0 & 0 \\ 0 & D_o & 0 \\ 0 & 0 & D_o \end{bmatrix}, \quad (6.24)$$

where the terms  $D_o$  is the isotropic diffusion coefficient. The damping matrix  $[K_T]$ , used in Equation 6.21, is defined as

$$[K_T] = \iiint_{XYZ} [N]^T R [N] dx dy dz, \quad (6.25)$$

where  $R = 1$  for no retardation. The velocity vector for the time dependent portion of the problem,  $\{\dot{q}_c\}$  is given as

$$\{\dot{q}_c\}^T = \left\{ \frac{\mathcal{X}_1}{\mathcal{A}} \quad \frac{\mathcal{X}_2}{\mathcal{A}} \quad \frac{\mathcal{X}_3}{\mathcal{A}} \quad \frac{\mathcal{X}_4}{\mathcal{A}} \quad \frac{\mathcal{X}_5}{\mathcal{A}} \quad \frac{\mathcal{X}_6}{\mathcal{A}} \quad \frac{\mathcal{X}_7}{\mathcal{A}} \quad \frac{\mathcal{X}_8}{\mathcal{A}} \right\}, \text{ and} \quad (6.26)$$

the load vector  $\{Q_c\}$  is given as

$$\{Q_c\} = \frac{\mathcal{X}}{\mathcal{N}} \big|_x \big|_r \big|_z. \quad (6.27)$$

The solution procedure for the given set of equations, first involves calculating the matrices and vectors on an elemental level. These equations are then assembled in a global matrix with application of the boundary conditions. This yields a global set of equations of the following form:

$$[K]\{r\} + [K_T]\{\dot{r}\} = \{R\}. \quad (6.28)$$

The assembled matrix is symmetric and can be solved using a symmetric or unsymmetric matrix solver. Numerical integration is used to approximate the solution using the two-point Gauss-Quadrature rule.

## TIME INTEGRATION METHOD

The time dependent derivative terms in the governing differential equation are solved using the finite difference technique based on the reduced trapezoidal rule. There are many different techniques that can be utilized in the solution of time the dependent problem, based on a weighting factor 'θ.' These include the fully-explicit forwards difference method, the fully-implicit backwards difference method, and the Crank-Nicholson and Galerkin's procedures. The portion of the program that solves the time dependent equation for mass transport is based on the backwards difference method, which is unconditionally stable but may be inaccurate for large time steps. The backwards difference method is given by

$$\left( \frac{[K_T]_{t+\Delta t}}{\Delta t} + [K]_{t+\Delta t} \right) \{r\}_{t+\Delta t} = \left( \frac{[K_T]_{t+\Delta t}}{\Delta t} \right) \{r\}_t + \{R\}_{t+\Delta t}. \quad (6.29)$$

### EXAMPLE 6.1

The following example problem is presented to test the validity of the three-dimensional finite element formulation based on the previously validated two-dimensional formulation. The problem consists of a hypothetical rectangular column of soil, 20 cm high and 5 cm square. A contaminant species is applied to the top of the soil domain but a no flow condition exists. The concentration of the contaminant, at the top of the soil sample, represents the boundary condition for the problem which is set equal to 25 mg/l for all times levels. The only mode of contaminant transport is by means of diffusion. The diffusion coefficients in the x-, y-, and z-directions are equal to  $1 \text{ cm}^2/\text{s}$ , which corresponds to a hypothetical and very volatile organic fluid. Figure 6.4 shows the three-dimensional finite element mesh used in the analysis. The domain is discretized into 32 elements and 81 nodal points. A similar domain of 16 elements and 27 nodal points is used for the two-dimensional simulation. The time step used in the simulation is 0.10 days, with one output time levels at 0.10, 1.0, and 10 days.

A comparison of the average concentrations within each element layer is presented in Tables 6.2 and 6.3. The first column in these tables, labeled element layers, corresponds to the layer of elements in the vertical direction of the domain. Therefore, layer 1 represents the bottom layer of the domain, which consists of elements 1-4. Similarly, layer 8 represents the upper most layer of elements in the domain, which contain elements 34-36.

Tables 6.2 and 6.3 show that for the given example problem, simulations for the two-, and three-dimensional formulations give the same results at all layers for all time output levels considered. It is concluded that the three-dimensional finite element formulation for diffusion is valid based on the previous two-dimensional formulation.

Table 6.2 Comparison of concentrations from 2-D and 3-D simulations for 1.0 days.

Element layers	2-D Simulation (mg/l)	3-D Simulation (mg/l)
1	19.58	19.58
2	10.23	10.23
3	4.21	4.21
4	1.34	1.34
5	0.77	0.77
6	0.51	0.51
7	0.01	0.01
8	+0.0	+0.0

Table 6.3 Comparison of concentrations from 2-D and 3-D simulations for 10 days.

Element layers	2-D Simulation (mg/l)	3-D Simulation (mg/l)
1	23.31	23.31
2	20.00	20.00
3	16.88	16.88
4	14.09	14.09
5	11.73	11.73
6	9.89	9.89
7	8.62	8.62
8	7.98	7.98

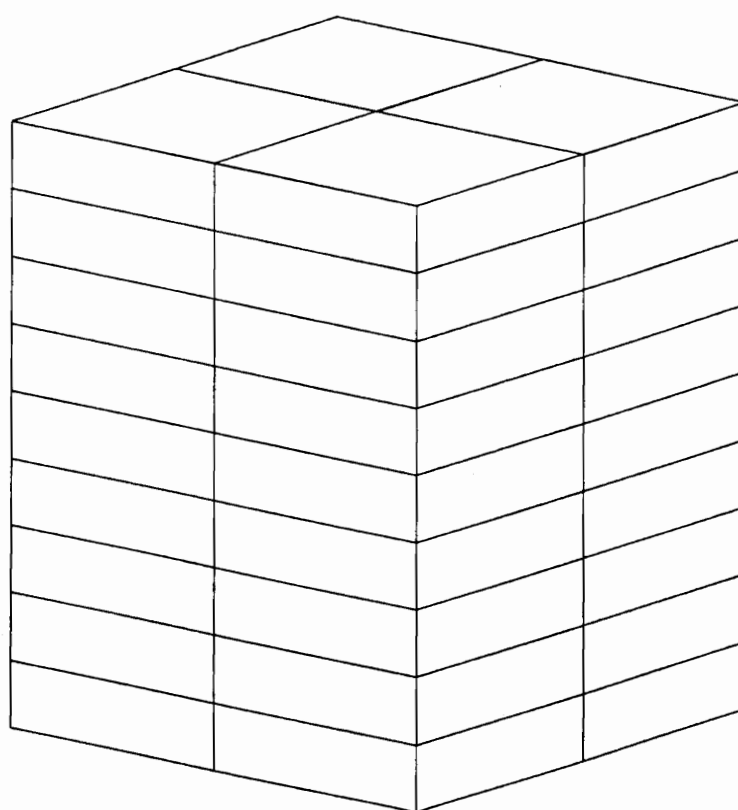


Figure 6.4 Three-dimensional finite element mesh (example 6.1).

## CONCLUSIONS

Chapter 6 introduces the convective-dispersive theory used in mass transport analyses. This theory is based on a combination of three transport components: (1) convection or advection, (2) molecular diffusion, and (3) mechanical dispersion. A description of each of these three components is presented and the equation derivation of each of the components is presented. The components are then combined in one comprehensive transport formulation.

The second part of Chapter 6 presents the three-dimensional finite element analysis for the problem involving molecular diffusion. This includes a discussion of the of the time integration method.

A comparison of the three-dimensional formulation is then made with the previously formulated two-dimensional model. The comparison shows an excellent correlation and thus validates the three-dimensional model.

## **CHAPTER 7**

### **MULTIPHASE FLOW COUPLED WITH MASS TRANSPORT**

#### **INTRODUCTION**

The process referred to as multiphase flow is covered in Chapters 2-5 and the mass transport of contaminants in the aqueous phase is covered in Chapter 6. The objective of this chapter is to provide a single convective-dispersive transport equation to be coupled with the multiphase flow equations presented in Chapter 2. Recall, that equations related to convection, molecular diffusion, and mechanical dispersion are presented in Chapter 6. From these expressions a single convective-dispersive transport model was presented, with the dispersion term referred to as hydrodynamic dispersion. It was explained that this term is a combination of both molecular diffusion and mechanical dispersion and is dependent on the flow conditions present in the subsurface. In this chapter, the general equation for convective-dispersive transport is described for the three-phase system. These equations are then combined assuming equilibrium partition coefficients between adjacent phases resulting in a single convective-dispersive transport model for the three-phase system (Kuppusamy and Lien 1987).

Although most petroleum products are considered immiscible, products such as gasoline contain many compounds that are not absolutely insoluble in water and can be dangerous at low concentrations. In considering gasoline as the contaminant source it is important to understand what type of constituents this involves. As explained by Corapcioglu and Baehr (1987), gasoline is a combination of mostly hydrocarbons, actually several hundred derivatives of hydrocarbons. Obviously, not all of these hydrocarbons can



be modeled effectively, since they all behave differently when exposed to the natural environment. Therefore, only the most important constituents, the ones which provide the greatest risk to the safety of the environment and the community, are modeled.

Constituents such as benzene, which has been labeled a human carcinogen, are the important contaminants that must be tracked and removed. In additions to benzene, the Resource Conservation and Recovery Act has also designated contaminants such as toluene and xylene hazardous materials (Corapcioglu and Baehr 1987). These are also major constituents found in gasoline.

In recent years there has been an increased amount of research in the area of pollutant transport through multiphase flow and mass transport as separate analyses, but few models have been presented that couple the two systems. This is due to the complexity of the equations and computer time needed to investigate meaningful parameters. Parker (1990) outlines the constitutive relations governing multiphase flow coupled with contaminant transport. This is based on the two-dimensional finite element formulation proposed by Kaluarachchi and Parker (1990). This model includes time lagged mass transfer and phase densities, with the gas phase gradients assumed to be negligible. Corapcioglu and Baehr (1987) developed a multiphase finite difference model for contaminant transport which included linear partition coefficients between the air, oil, water, and solid phases. Here contamination of the air phase was also considered. Recently, a one-dimensional model for multiphase flow and mass transport was developed by Ryan and Cohen (1991). This immiscible flow portion of the model incorporated a front tracking algorithm to determine the front of the invading NAPL. It was found that the migration of organic chemicals results in significant contamination in the air and aqueous phases in front of the discrete plume. The model presented in this thesis is based on research conducted by Kuppusamy and Lien (1987). This model involves chemical

migration as a result of multiphase flow weakly-coupled with contaminant mass transport. The model uses a time lagged mass transfer term between the contaminant phase and the mass transport equation. The equation for mass transport is developed based on mass transport for each phase in the system, considering linear partition coefficients.

## GOVERNING EQUATIONS FOR MULTIPHASE MASS TRANSPORT

The governing equations for multiphase immiscible flow are given in Chapter 2. After solving these equations for the unknown head terms, the equation related to mass transport is solved to determine the concentrations of a given pollutant in the water phase and the mass transfer term R.

The governing equations related to this phenomenon in the three-phase system are given as (Kuppusamy and Lien 1987):

(1) for the water phase

$$\phi \frac{\partial C_w S_w}{\partial t} = \frac{\partial}{\partial x} \left( \phi S_w D_{xw} \frac{\partial C_w}{\partial x} \right) + \frac{\partial}{\partial y} \left( \phi S_w D_{yw} \frac{\partial C_w}{\partial y} \right) + \frac{\partial}{\partial z} \left( \phi S_w D_{zw} \frac{\partial C_w}{\partial z} \right) - \frac{\partial q_{xw} C_w}{\partial x} - \frac{\partial q_{yw} C_w}{\partial y} - \frac{\partial q_{zw} C_w}{\partial z} - \gamma_w C_w + r_{ow} - r_{ws} \quad (7.1)$$

(2) for the oil phase

$$\phi \frac{\partial C_o S_o}{\partial t} = \frac{\partial}{\partial x} \left( \phi S_o D_{xo} \frac{\partial C_o}{\partial x} \right) + \frac{\partial}{\partial y} \left( \phi S_o D_{yo} \frac{\partial C_o}{\partial y} \right) + \frac{\partial}{\partial z} \left( \phi S_o D_{zo} \frac{\partial C_o}{\partial z} \right) - \frac{\partial q_{xo} C_o}{\partial x} - \frac{\partial q_{yo} C_o}{\partial y} - \frac{\partial q_{zo} C_o}{\partial z} - \gamma_o C_o - r_{oa} - r_{ow} \quad (7.2)$$

(3) for the air phase

$$\phi \frac{\partial C_a S_a}{\partial t} = \frac{\partial}{\partial x} \left( \phi S_a D_{xa} \frac{\partial C_a}{\partial x} \right) + \frac{\partial}{\partial y} \left( \phi S_a D_{ya} \frac{\partial C_a}{\partial y} \right) + \frac{\partial}{\partial z} \left( \phi S_a D_{za} \frac{\partial C_a}{\partial z} \right) - \frac{\partial q_{xa} C_a}{\partial x} - \frac{\partial q_{ya} C_a}{\partial y} - \frac{\partial q_{za} C_a}{\partial z} - \gamma_a C_a + r_{oa} \quad (7.3)$$

(4) for the solid phase

$$\rho_b \frac{\partial C_s}{\partial t} = - \gamma_s \rho_b C_s + r_{ws} \quad (7.4)$$

The terms

$C_w$ ,  $C_s$ ,  $C_o$ , and  $C_a$  = the mass concentrations of the contaminant per phase volume;

$\gamma_i$  = the first order decay coefficient, where the subscript i represents the phase;

$\rho_b$  = the mass of the solid phase per volume of porous media;  
 $S_i$  = the saturation of the given phase, i;  
 $\phi$  = the porosity of the porous media;  
 $q_{ij}$  = the linear velocity in the i-direction for the j-phase;  
 $D_{ij}$  = the dispersion coefficient in the i-direction for the j-phase; and  
 $r_{ij}$  = the rate of mass transfer from phase i to phase j.

In the current model, it is assumed that there is local equilibrium between the different phases in the multiphase system. This is a reasonable assumption but may not be true for extreme situations in which high velocities are encountered (Kuppusamy and Lien 1987). The linear partition coefficients between phases are defined as

$$T_a = \frac{C_a}{C_w} \text{ for the air/water interface,} \quad (7.5)$$

$$T_o = \frac{C_o}{C_w} \text{ for the oil/water interface, and} \quad (7.6)$$

$$T_s = \frac{\rho_b C_s}{C_w} \text{ for the solid/water interface.} \quad (7.7)$$

The above coefficients are described in detail later in this chapter. Kuppusamy and Lien (1987) show that by adding Equations 7.1 and 7.3 and using Equation 7.4, 7.5, and 7.7 the following relationship can be established:

$$\begin{aligned}
B \frac{\partial C_w}{\partial t} = & \frac{\partial}{\partial x} \left( \phi S_w D_{xw}^* \frac{\partial C_w}{\partial x} \right) + \frac{\partial}{\partial y} \left( \phi S_w D_{yw}^* \frac{\partial C_w}{\partial y} \right) + \frac{\partial}{\partial z} \left( \phi S_w D_{zw}^* \frac{\partial C_w}{\partial z} \right) \\
& - \frac{\partial q_{xw} C_w}{\partial x} - \frac{\partial q_{yw} C_w}{\partial y} - \frac{\partial q_{zw} C_w}{\partial z} - A C_w + R
\end{aligned}
\tag{7.8}$$

where

$$A = (\gamma_w + T_s \gamma_s + T_a \gamma_a),$$

$$B = \phi S_w + T_s + \phi S_a T_a, \text{ and}$$

$$D_{ij}^* = \text{the dispersion tensor in the } i\text{-direction for the } j\text{-phase.}$$

$D_{xw}^*$  is defined by Bear (1972) as (incorporating the Millington-Quirk model for tortuosity with a first order correction for nondilute solution effects):

$$D_{xw}^* = \phi^{1.3} S_w^{3.3} D_w + \phi^{1.3} S_a^{3.3} D_a + \alpha_l \frac{q_{xw}^2}{\phi S_w q_w} + \alpha_t \frac{q_{yw}^2}{\phi S_w q_w} + \alpha_t \frac{q_{zw}^2}{\phi S_w q_w},
\tag{7.9}$$

where

$\alpha_l$  and  $\alpha_t$  = the longitudinal and transverse dispersivities, and

$$q_w = (q_{xw}^2 + q_{yw}^2 + q_{zw}^2)^{1/2}, \text{ is the linear velocity.}$$

The dispersion coefficients in the y and z directions are similar. Kuppasamy and Lien (1987) show that by expressing  $C_0$  in terms of  $C_w$  in Equation 7.2, and by using Equation 7.6 and adding Equation 7.8, the following can be obtained:

$$E \frac{\partial C_w}{\partial t} = \frac{\partial}{\partial x} \left( \phi S_w D_{xw}^* \frac{\partial C_w}{\partial x} \right) + \frac{\partial}{\partial y} \left( \phi S_w D_{yw}^* \frac{\partial C_w}{\partial y} \right) + \frac{\partial}{\partial z} \left( \phi S_w D_{zw}^* \frac{\partial C_w}{\partial z} \right) - \frac{\partial q_{xw}^* C_w}{\partial x} - \frac{\partial q_{yw}^* C_w}{\partial y} - \frac{\partial q_{zw}^* C_w}{\partial z} - F C_w, \quad (7.10)$$

where

$$F = (\gamma_w + T_s \gamma_s + T_a \gamma_a + f_o T_o \gamma_o),$$

$$E = \phi S_w + T_s + \phi S_a T_a + \phi S_o T_o f_1,$$

$D_i$  = the diffusion coefficient for each phase,

$\gamma_i$  = the decay coefficients for the i-phase, and

$\alpha_l$  and  $\alpha_t$  = the longitudinal and transverse dispersivities.

The dispersion tensor is defined in the x-direction as

$$D_{xw}^* = \phi^{1.3} S_w^{3.3} D_w + \phi^{1.3} S_a^{3.3} D_a + f_o T_o S_o^{3.3} D_o + \alpha_l \left( \frac{q_{xw}^2}{\phi S_w q_w} + \frac{f_o T_o q_{xo}^2}{\phi S_o q_o} \right) + \alpha_t \left( \frac{q_{yw}^2}{\phi S_w q_w} + \frac{f_o T_o q_{yo}^2}{\phi S_o q_o} \right) + \alpha_t \left( \frac{q_{zw}^2}{\phi S_w q_w} + \frac{f_o T_o q_{zo}^2}{\phi S_o q_o} \right), \quad (7.11)$$

and the following expressions are defined as:

$$q_{xw}^* = q_{xw} + f_1 T_o q_{xo}, \quad (7.12)$$

$$f_o = \frac{1}{1 - \frac{T_o C_w}{r_o}} \quad (7.13)$$

$$f_1 = \frac{1}{1 - \frac{T_o C_w}{r_1}}. \quad (7.14)$$

In Equations 7.13 and 7.14  $T_o$  is the partition coefficient previously described, and  $r_o$  and  $r_1$  are the initial and final densities of the oil phase,

The solution procedure for the previously described coupled problem involves first estimating a value for  $R$  as zero for use in the equation for oil flow. The finite element method is then used to solve for the unknown oil and water heads. From these solutions, the secondary unknowns, velocity vectors, are solved and input into Equation 7.10. Equation 7.10 is then solved for the concentration values in the water phase,  $C_w$ . The interphase mass transfer is then computed by applying the finite difference method to Equation 7.8. As previously discussed, the iterative process used in solving the equations of multiphase flow is the modified Picard's method. The general form of the Picard's method is used in the iteration scheme for the transport problem.

## COMPONENT PROPERTIES

In order to successfully model contaminant transport in a multi-component environment, there are certain chemical properties that should be considered. These components include diffusion coefficients for the air, oil, and water phases (Parker 1992). In the model presented here, diffusion coefficients for the water phase will only be considered since the water phase is the main source of pollution (refer to Chapter 6 for a complete discussion on the convection, diffusion, and dispersion coefficients). Along with the diffusion coefficients, partition coefficients and first order decay coefficients should

also be considered. The partition coefficients used in the previous expression for mass transport in a three-phase system include the oil-water, water-solid, water-air partition coefficients. The first order decay coefficients include the water, oil, air, and solid decay coefficients.

## LINEAR PARTITION COEFFICIENTS

Chemical transfer between phases in the three-phase system can be a major source/sink term. In the current analysis, partitioning is considered to take place between the air and water phases, the oil and water phases, and the water and solid phases. Since the tracking of contaminant in the air phase is not considered in this analysis and the water phase is considered the main mode of contaminant transport, partitioning between the water and adjacent phases are only considered. The easiest way of modeling phase transfer is through linear partition coefficients between adjacent phases. The following discussion provides a brief explanation for each of the partition coefficients presented in the section on equation development for multiphase mass transport.

The only partition coefficient, of those mentioned above, that is well established is the gas/liquid partition coefficient (National Research Council 1990). This partition coefficient is commonly referred to as Henry's Constant. The partition coefficient from Henry's constant is given as (Lyman et al. 1982).

$$T_a = \Gamma_{aa} = \frac{H_a M_a}{RT}, \quad (7.15)$$

where



$H_{\alpha}$  = the Henry's constant for a given contaminant  $\alpha$ ,

$M_{\alpha}$  = the molecular weight of  $\alpha$ ,

$R$  = the ideal gas constant, and

$T$  = the absolute temperature.

The oil-water partition coefficient is commonly referred to a Raoult's constant and can be estimated from the aqueous solubility and the pure phase density as (Parker 1992):

$$T_o = \Gamma_{\omega} = \frac{\rho_{\alpha}}{C_{\omega}^o} \quad (7.16)$$

where

$\rho_{\alpha o}$  = the density of the pure contaminant  $\alpha$ , and

$C_{\omega}^o$  = the aqueous solubility.

Parker (1992) notes that the above expression applies to organics of low solubility at normal temperatures.

For adsorption of hydrophobic compounds, the partition coefficient is given through a relation to the distribution coefficient  $K_p$ , where (de Marsily 1986):

$$K_p = K_{oc} f_{oc} \quad (7.17)$$

where

$K_{oc}$  = is the dimensionless partition coefficient for a hypothetical soil made of 100 % solid organic material. de Marsily (1986) suggested that this value

can be estimated from the octanol-water partition coefficient  $K_{ow}$  as  $K_{oc} = 0.411K_{ow}$ . This partition coefficient can be found in the literature for many compounds.

$f_{oc}$  = the organic carbon mass fraction in the soil.

Now the partition coefficient for adsorption of a given contaminant can be estimated through the following relationship (Parker 1992):

$$T_s = \Gamma_{as} = \rho_b K_p \quad (7.18)$$

where  $\rho_b$  = the bulk density of the porous media. Partition coefficients for some common organic contaminants are given in Table 7.1. A list of physical properties of some common organic chemicals of environmental significance is given in Table 7.2.

Table 7.1 Properties of common organic contaminants

Parameter	Benzene	Toluene	TCE
$\Gamma_{\alpha o}$	494	1674	1336
$\Gamma_{\alpha a}$	0.17	0.26	0.38
$\Gamma_{\alpha s}$	0	0	0
$M_{\alpha}$	780	920	1310

(after Kaluarachchi and Parker 1990)

Table 7.2 Properties of organic compounds at 20° C

Organic Compound	Relative viscosity	specific gravity	Henry's constant	Water solubility (g/m <sup>3</sup> )
Benzene	0.56	0.878	$2.40 \times 10^{-1}$	1780.0
Toluene	0.58	0.867	$2.80 \times 10^{-1}$	512.0
o-xylene	0.81	0.880	$2.20 \times 10^{-1}$	152.0
Ethyl benzene	0.68	0.867	$3.70 \times 10^{-1}$	152.0
Trichloroethylene	0.59	1.464	$4.20 \times 10^{-1}$	1100.0
Tetrachloroethylene	0.90	1.623	$3.50 \times 10^{-1}$	150.0
1,1,1 Trichloroethane	1.20	1.339	$7.70 \times 10^{-1}$	4400.0
1,1 Dichlorethane	0.44	1.176	$2.40 \times 10^{-1}$	5500.0
1,3 Dichlorobenzene	1.48	1.288	$1.10 \times 10^{-1}$	111.0
Carbon Tetrachloride	0.97	1.594	$9.70 \times 10^{-1}$	800.0
1,2,4 Trichlorobenzene	2.77	1.454	$4.30 \times 10^{-2}$	4.8

(after Parker 1992)

## RADIOACTIVE DECAY COEFFICIENTS

Radioactive decay involves the transformation of one element into another element through the loss of atomic particles (de Marsily 1986). In the model presented in this thesis the decay coefficients are input according to the half live of the species. Parker (1992) explains that decay can be expected to occur almost exclusively in the aqueous phase and therefore terms related to radioactive decay in other phases are often disregarded. Laboratory and field studies of chemicals with conditions similar to the ones found in the environment can be used in simulations, but it is noted that without calibration at a specific site the estimated rates are subject to considerable uncertainty.

## FINITE ELEMENT FORMULATION

It is important to note that in dealing with mass transport solutions using the finite element method, oscillations can often develop for situations in which the convection term is large as compared to the dispersion term (Huyakorn 1977, Huyakorn and Nilkula 1978, Jenson and Finlayson 1980). Griffiths and Mitchell (1976) suggests that this is due to the large coefficients in the first order term (advection term) as compared to the second order elliptic equations, resulting in poor accuracy. Researchers have therefore developed upstream weighing functions that are asymmetrical. It is shown that these weighting functions produce solutions that are oscillatory free for many cases (Huyakorn 1977).

The same three-dimensional brick element with trilinear shape functions, used in the multiphase flow and the diffusion analyses, is also used to estimate the solution of the convection-dispersion equations. The unknown concentration of the contaminant present in the water phase is approximated as

$$C_w = [N]\{C_n\}_w^T = [N_1 \ N_2 \ N_3 \ N_4 \ N_5 \ N_6 \ N_7 \ N_8][C_{w1} \ C_{w2} \ C_{w3} \ C_{w4} \ C_{w5} \ C_{w6} \ C_{w7} \ C_{w8}]^T, \quad (7.19)$$

where  $N_i$  are the trilinear shape functions and  $C_{wi}$  are the unknown nodal concentrations of the chemical contaminant in the water phase. By means of Galerkin's method, Equation 7.10 can be derived in matrix form as

$$[K]_w \{C_n\} + [K_T]_w \{\dot{C}_n\}_w = \{Q\}_w, \quad (7.20)$$

where the overdot represents differentiation with respect to time. The conductivity and capacity matrices are as follows:

(1) conductivity matrix

$$[K]_w = \iiint_{xyz} [B]^T [D_{ij}] [B] dx dy dz + \iiint_{xyz} [N]^T [q^*]_w [B] dx dy dz + \iiint_{xyz} [N]^T [F] [N] dx dy dz, \quad (7.21)$$

$$\text{where } [D_{ij}] = [B]^T \begin{bmatrix} D_{xw}^* & 0 & 0 \\ 0 & D_{yw}^* & 0 \\ 0 & 0 & D_{zw}^* \end{bmatrix} \text{ and } [q^*] = [N]^T \begin{bmatrix} q_{xw}^* & 0 & 0 \\ 0 & q_{yw}^* & 0 \\ 0 & 0 & q_{zw}^* \end{bmatrix}. \quad (7.22)$$

(2) The capacitance matrix is

$$[K_T]_w = \iiint_{xyz} E[N]^T [N] dx dy dz. \quad (7.23)$$

Note that Equation 7.21 is unsymmetric due to the velocity (advection) terms and therefore the matrix solver for the multiphase flow portion of the program cannot be utilized.

## TIME INTEGRATION SCHEME

The time integration scheme previously presented in Chapter 2 is the general form of the ' $\theta$ ' algorithm. For a value of  $\theta = 1$  this algorithm reduces to the fully implicit backwards difference method, which is unconditionally stable for all time steps. It is important to note, that although this scheme is always stable, the accuracy of the fully-implicit backwards difference scheme is not as accurate as some of the other schemes previously mentioned. The reduced equation for the fully-implicit backward difference scheme takes the form of

$$\left( \frac{[K_T]_{t+\Delta t}}{\Delta t} + [K]_{t+\Delta t} \right) \{H_n\}_{t+\Delta t} = \frac{[K_T]_{t+\Delta t}}{\Delta t} \{H_n\}_t + \{Q\}_{t+\Delta t}. \quad (7.24)$$

This is the same scheme as that presented in Chapter 6, for the molecular diffusion problem.

## ITERATION TECHNIQUE FOR NON LINEARITY

The iteration method used in the solution of the equations of multiphase flow is accomplished using a modified version of the Picard's method (direct iteration method). The mass transport equations are also nonlinear and therefore also must be solved by an iterative method. The general Picard's method is used in the portion of the program that controls the solution of the concentration values for the transport equation (refer to Figure 3.1. Therefore, the iteration process for mass transport is the same as the iteration process previously described for multiphase flow but the process only uses a relaxation factor of

1.0. The unknown concentration used in the updating process therefore is equal to the last solution in the iterative process. The convergence criteria for the transport iteration is the same as that for the multiphase flow portion of the program.

## **SOLUTION PROCEDURE**

Kaluarachchi and Parker (1989) found that the results, based on a time lagged mass transfer rate and fluid density, have negligible effects during periods of highly transient non aqueous phase migration, but may become important over a long period of time as the effects of dissolution in the water phase and volatilization in the gas (air) phase account for a larger portion of the total mass. The model presented here, IMFTP3D, handles the interphase mass transfer term ( $R$ ), incorporated in the equation for oil flow, by a time lagged method. The time lagged method updates the  $R$ -vector after the solution of the transport equation for every time step. The density of a lighter than water non aqueous phase liquid (LNAPL) greatly effects its movement through the ground water table. IMFTP3D assumes that this movement is effected by a constant value for individual time steps. IMFTP3D considers the effects of initial and final densities based on a constant value, input by the user, for each time step. This effects the interphase mass transfer term used in the solution of the unknown oil and water heads.

The solution process for the coupled problem for each time step proceeds as follows:

- (1) the equations for multiphase flow, previously presented, will first be solved for the unknown head terms ( $R=0$ ).
- (2) These head terms will then be used to solve for the velocity vectors of both the

oil and water phases.

- (3) The velocity vectors are then used in the solution of the mass transport problem (concentration), involving both advection and dispersion.
- (4) The concentration term is then used to update the R-vector (interphase mass transport term) in the equation of oil flow.
- (5) The process is continued for the remaining time intervals.

Note, the solutions to both the multiphase flow and mass transport portions of this process are time dependent and nonlinear. Therefore, an iterative process is incorporated in each of the two coupled solutions.

## CONCLUSIONS

Chapter 7 introduces the mass transport equation for the three-phase system. This equation is derived based on the mass transport in the air, oil, water, and solid phases incorporating linear partition coefficients. A description of the linear partition coefficients as well as the radioactive decay coefficients is also provided.

Chapter 7 also presents the finite element model for the previously described formulation. This model is derived based on Galerkin's method and is weakly-coupled with the multiphase flow formulation given in Chapter 3.



## **CHAPTER 8**

### **VALIDATION OF WEAKLY-COUPLED FORMULATION**

#### **INTRODUCTION**

In this chapter an example problem of a hypothetical tank (Example 2.2) is modeled by both two- and three-dimensional finite element models for multiphase flow and transport. The results of both the models are compared, validating the three-dimensional model. The example problem is then used to investigate the effects of the partition coefficients between the oil and water, and water and air phases on the discrete and dissolved phase plume movements.

#### **EXAMPLE 8.1**

The problem consists of an underground storage tank placed near the center of a 210 meter long by 16 m wide uniform soil domain. The finite element meshes are shown in Figures 8.1 and 8.2. The two-dimensional mesh is discretized into 140 elements and 169 nodes, while the three-dimensional mesh contains 140 elements and 338 nodes. The boundary conditions, for the multiphase flow problem, are the same those previously presented. The difference in this example is that, in addition to solving the equation for multiphase flow, the mass transport of a single component is also estimated. A boundary condition is imposed at the bottom of the tank, corresponding to saturation of all phases with the organic component. The contaminant is assumed to be benzene and the porous media and mass transport properties are given in Tables 8.1 and 8.2. After validating the

three-dimensional formulation with the previously validated two-dimensional formulation, these partition coefficient values are varied in the three-dimensional model and an investigation of their effects on the movement of the discrete contaminant phase and the dissolved plume within the water phase is made.

Table 8.1 Material Properties\Parameters for multiphase flow portion of Example 8.1

Material Properties	Well-Graded Sand
Hydraulic Conductivities in x-, y-, z-directions for water	2 m/day
Hydraulic Conductivities in x-, y-, z-directions for oil	1.5 m/day
Porosity	0.40
Residual saturation for air-water, air-oil, and oil-water systems	0.0
Model Parameters	Value
van Genuchten parameter, $\alpha$	$5.0 \text{ m}^{-1}$
van Genuchten parameter, $n$	1.84
Scaling Factor, $\beta_{ao}$	2.0
Scaling Factor, $\beta_{ow}$	2.2

(After Sheng 1986)

Table 8.2 Coefficients for mass transport in Example 8.1

Material Properties	Benzene
Longitudinal Dispersivity, $\alpha_l$	0.5
Transverse Dispersivity, $\alpha_t$	0.1
Molecular Diffusion to water phase	$9.0 \times 10^{-5} \text{ m/day}$
Molecular diffusion to air phase	$6.3 \times 10^{-1} \text{ m/day}$
Ratio: $\rho_o/\rho_w$	0.899
Partition Coefficient $T_o$	505
Partition Coefficient $T_a$ (Weast 1985)	0.169

(after Sheng 1986)

### Two-Dimensional Finite Element Mesh Used in Analysis



Figure 8.1 Two-dimensional finite element mesh used for the multiphase flow and pollutant transport problem.

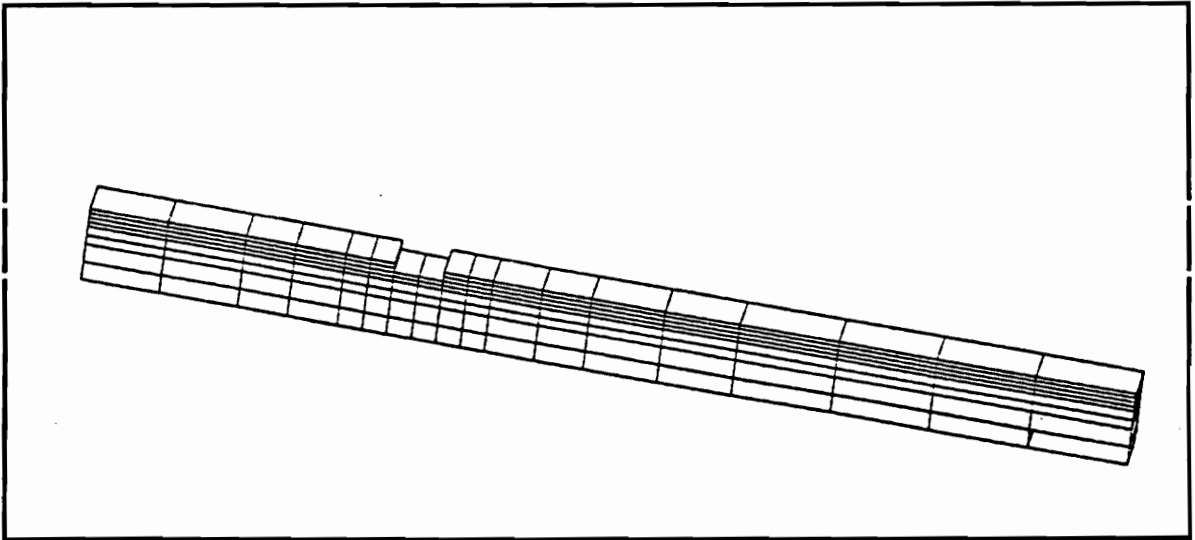


Figure 8.2 Three-dimensional finite element mesh used in the multiphase flow and transport problem.

Figures 8.4 - 8.40 show the results from the two- and three-dimensional finite element simulations. These figures show both the discrete phase plume movement and the dissolved phase plume movement at various time levels. The figures showing discrete phase plume movements differentiate between elements with no oil saturation and those with an oil saturation greater than zero. The figures showing the movements of the

dissolved phase, represent movement through the quantity  $C_w \phi S_w$ , where  $C_w$  is the concentration of the contaminant transferred to the water phase,  $\phi$  is the porosity of the porous media, and  $S_w$  is the saturation of the water phase for that element. The quantity  $C_w \phi S_w$  is the amount of mass transferred from the contaminant phase to the water phase at the center of a given element. Figure 8.3 shows the section view used in selected figures. Note, that the two-dimensional simulation represented by Figure 8.40 has no corresponding three-dimensional simulation, since the mass of contaminant transferred during the 983 day time level was not above 0.6 mg/l for any of the elements in the three-dimensional simulation.

The three-dimensional model again shows slightly slower discrete phase plume movement and a reduced movement in the dissolved phase for low concentrations, but a slightly increased movement of the dissolved phase for higher concentrations at low time levels. The three-dimensional model is considered validate the on the basis of the comparisons made with the two-dimensional simulations.

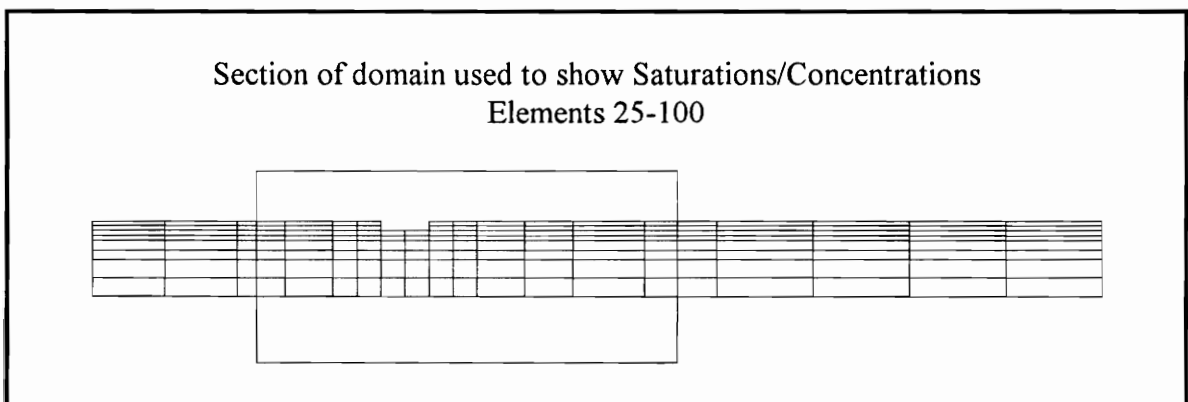


Figure 8.3 Section of the two dimensional domain used in comparing selected two- and three-dimensional simulations.

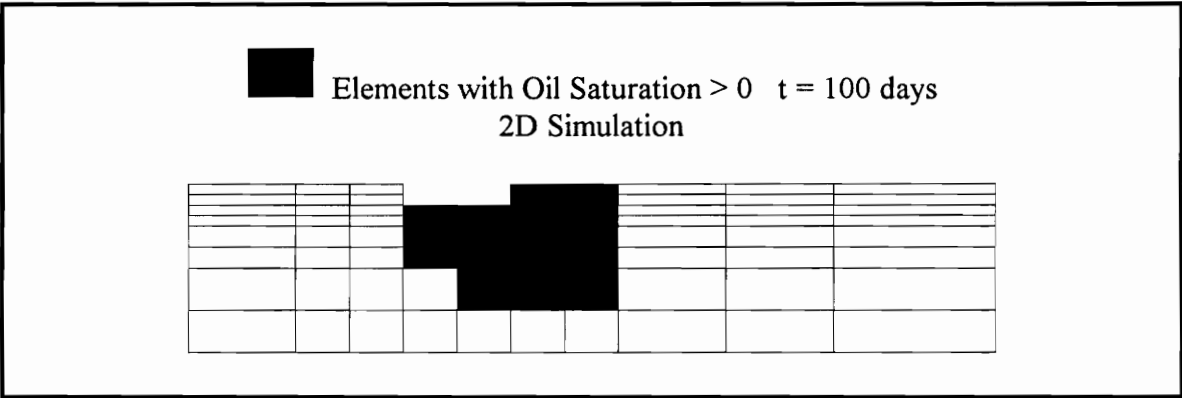


Figure 8.4 Oil plume movement after 100 days.

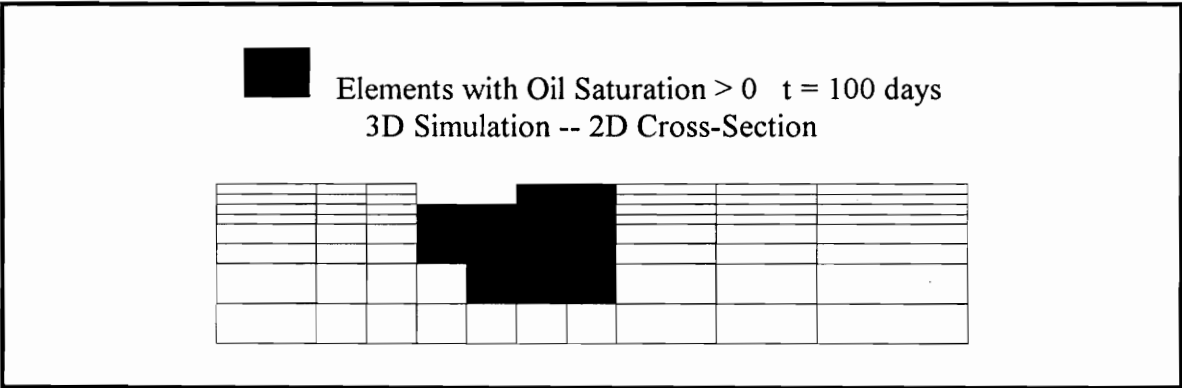


Figure 8.5 Oil plume movement after 100 days (3-D simulation).

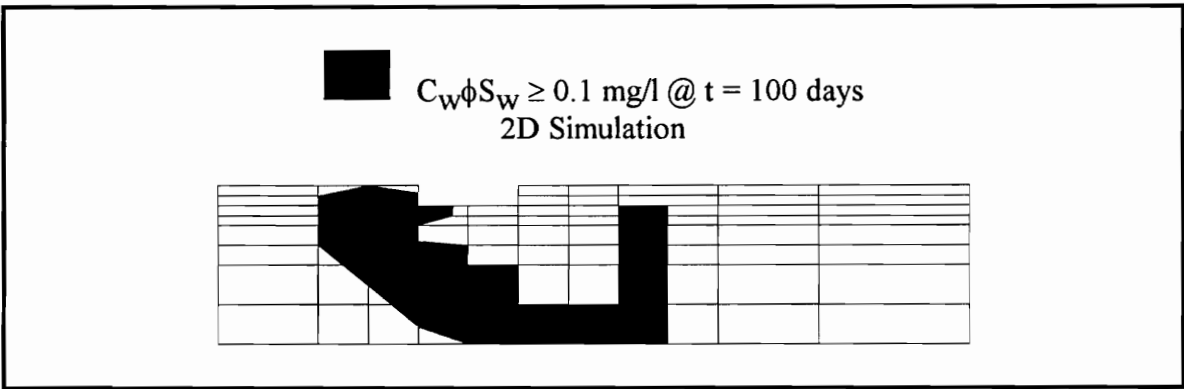


Figure 8.6 Dissolved plume movement after 100 days.

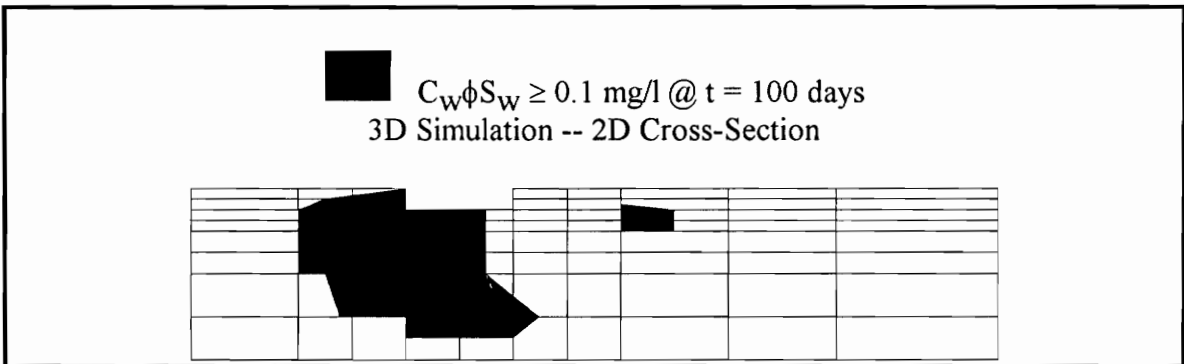


Figure 8.7 Dissolved Plume movement after 100 days (3-D simulation).

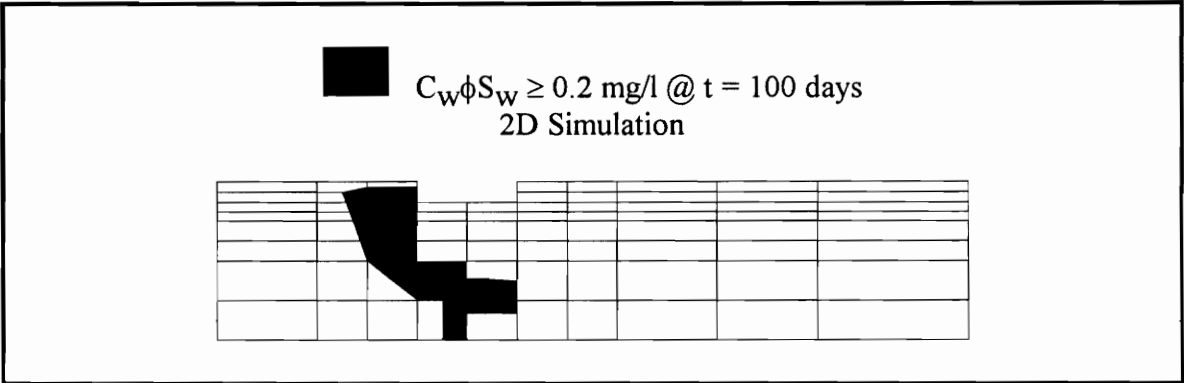


Figure 8.8 Dissolved plume movement after 100 days.

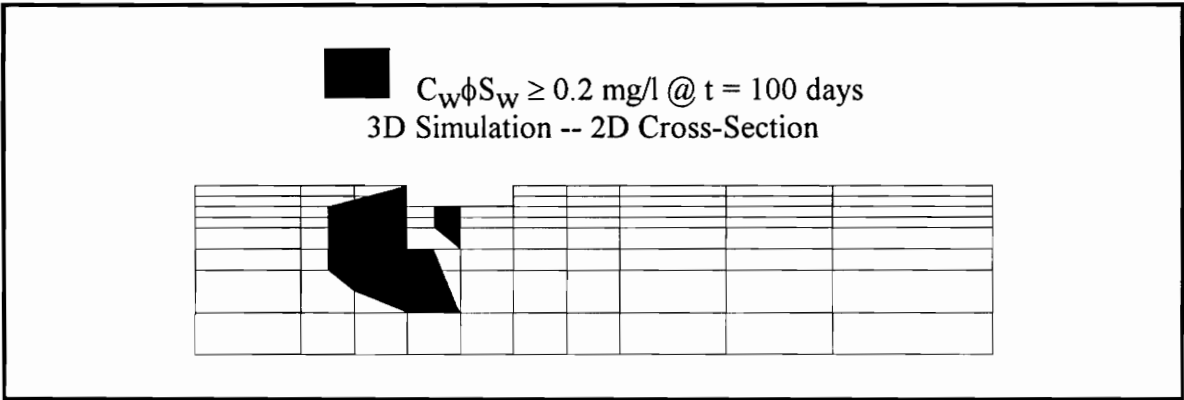


Figure 8.9 Dissolved plume movement after 100 days (3-D simulation).

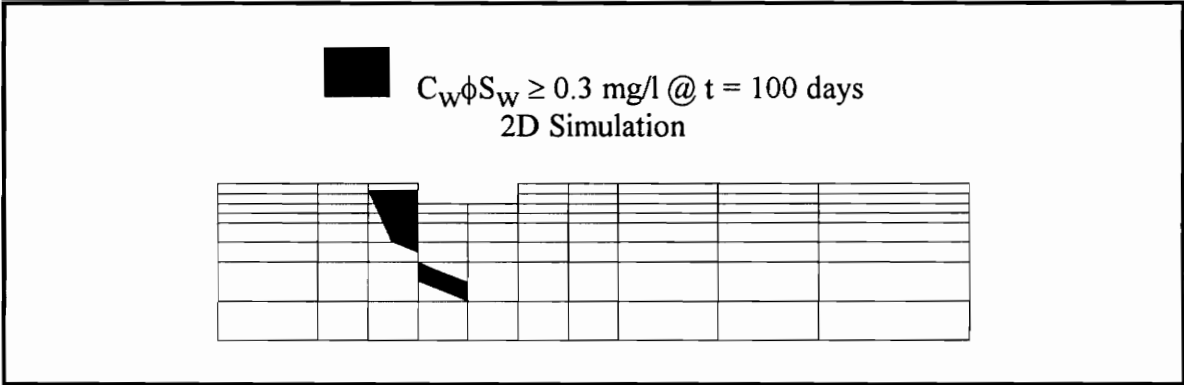


Figure 8.10 Dissolved plume movement after 100 days.

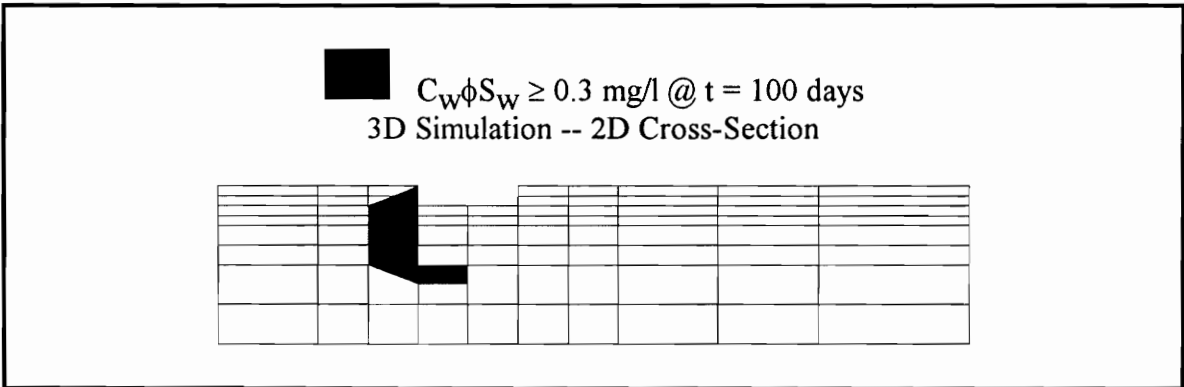


Figure 8.11 Dissolved plume movement after 100 days (3-D simulation)



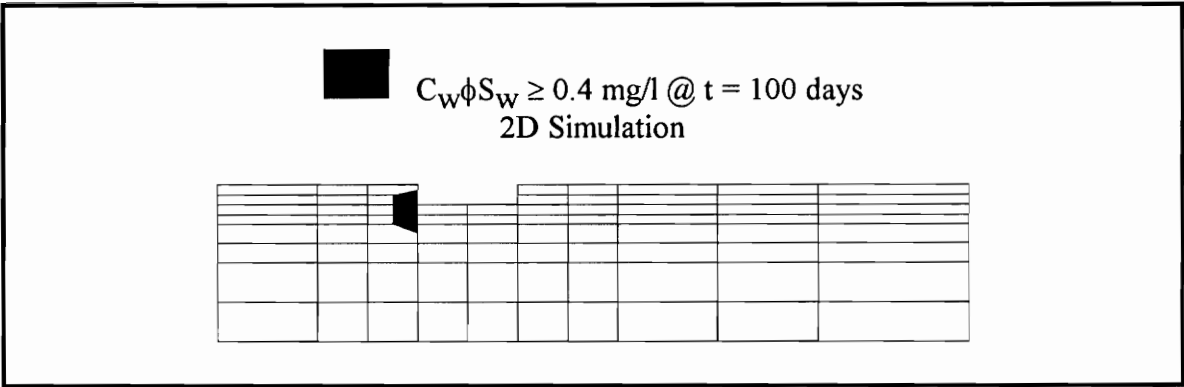


Figure 8.12 Dissolved plume movement after 100 days.

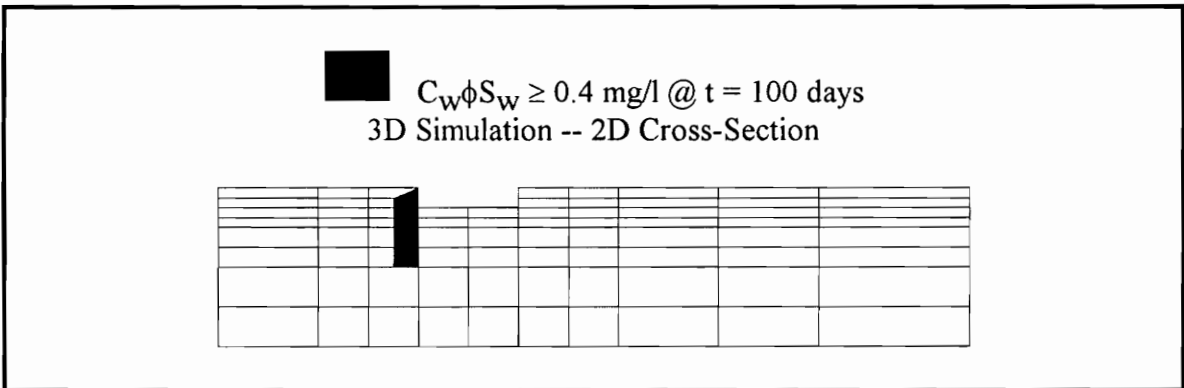


Figure 8.13 Dissolved plume movement after 100 days (3-D simulation).

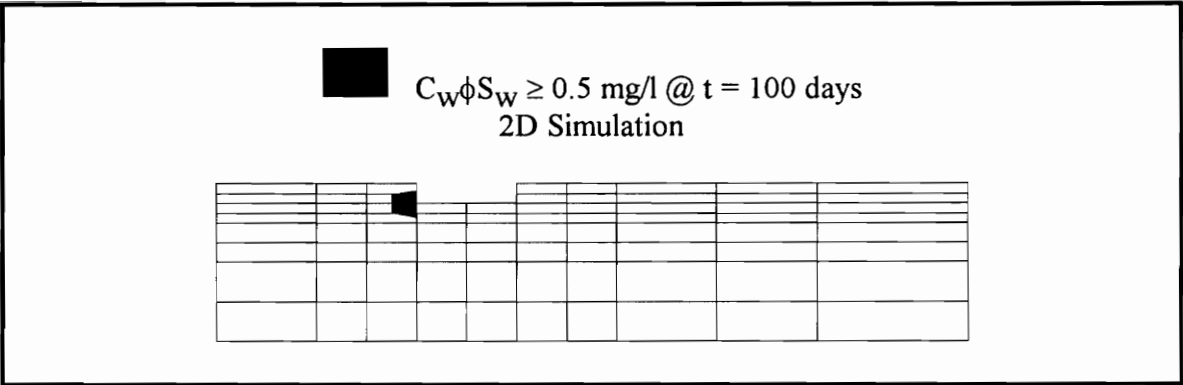


Figure 8.14 Dissolved plume movement after 100 days.

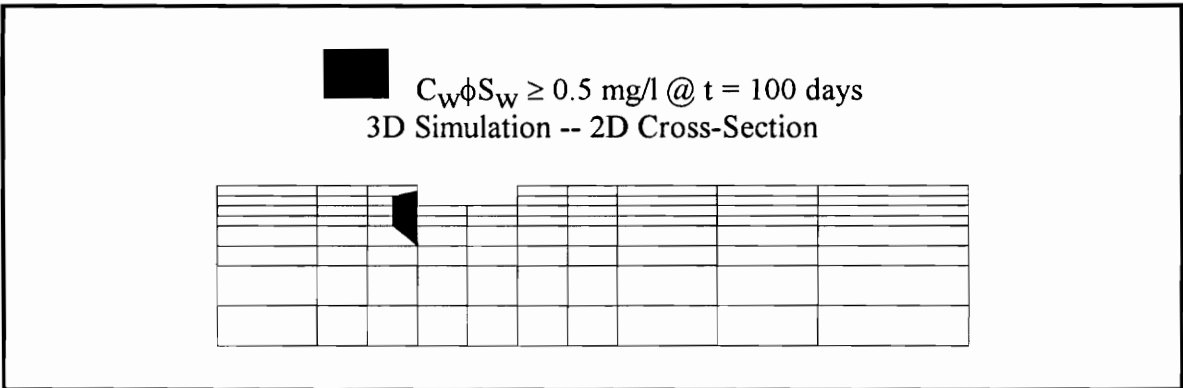


Figure 8.15 Dissolved plume movement after 100 days (3-D simulation).

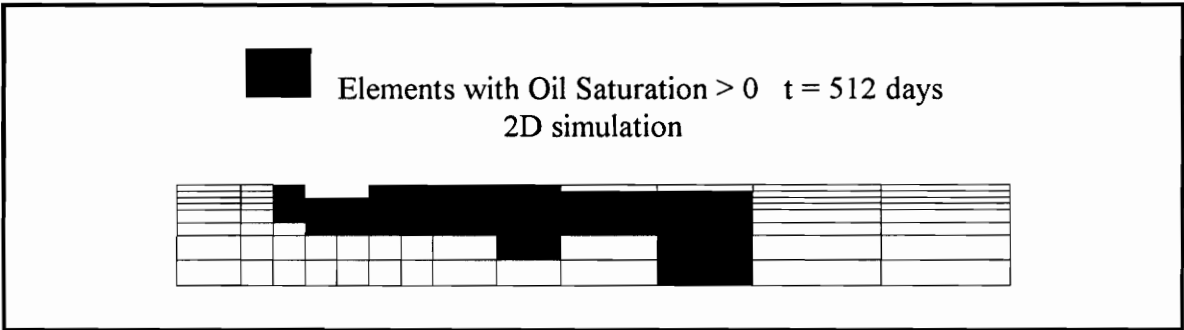


Figure 8.16 Oil plume movement after 512 days.

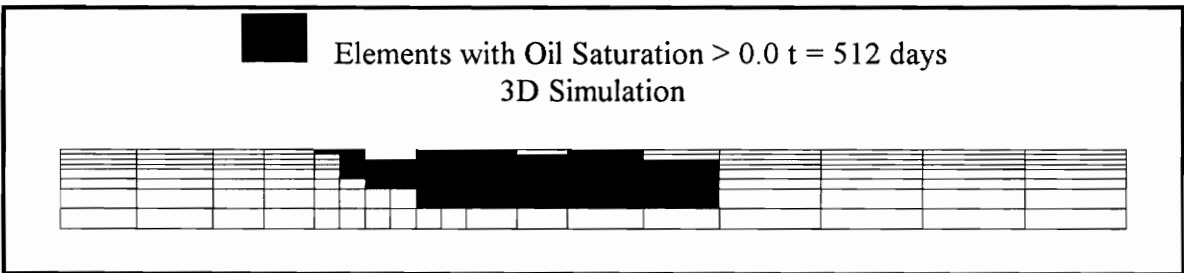


Figure 8.17 Oil plume movement after 512 days (3-D simulation).

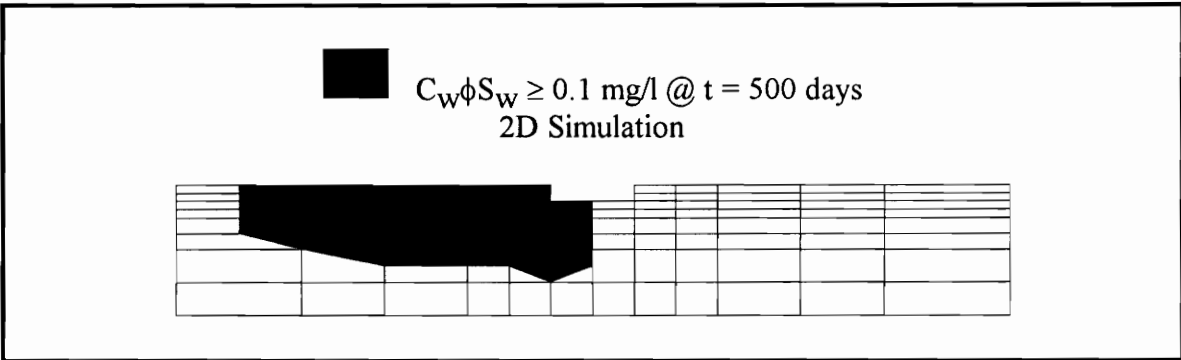


Figure 8.18 Dissolved plume movement after 512 days.

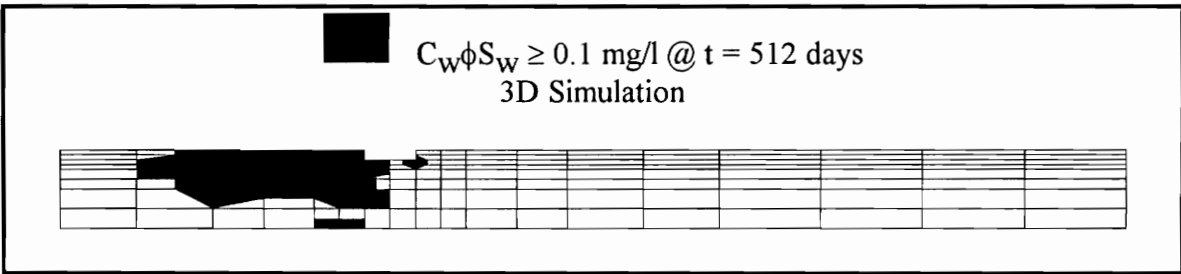


Figure 8.19 Dissolved plume movement after 512 days (3-D simulation).

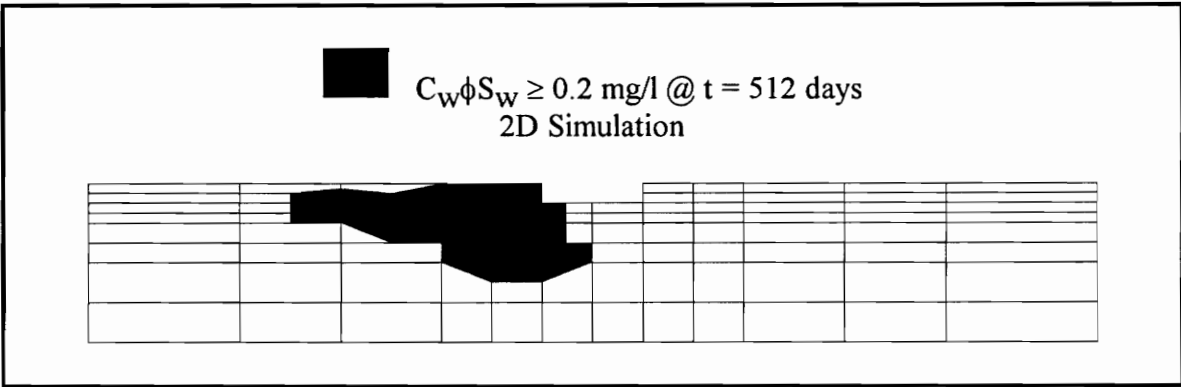


Figure 8.20 Dissolved plume movement after 512 days.

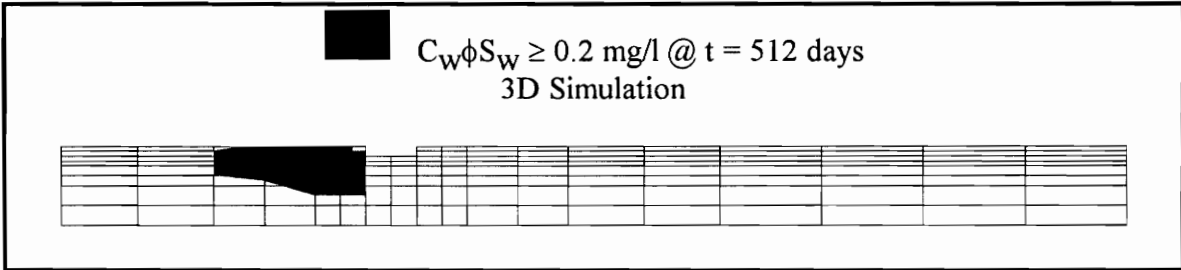


Figure 8.21 Dissolved plume movement after 512 days (3-D simulation).

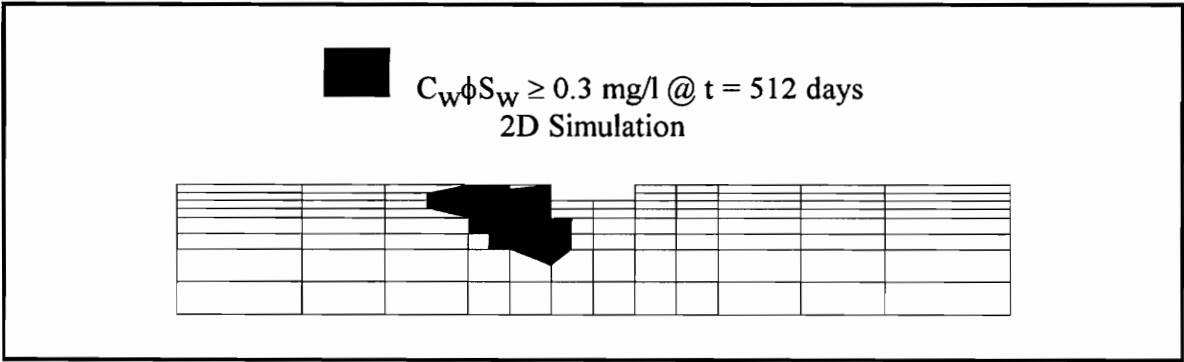


Figure 8.22 Dissolved plume movement after 512 days.

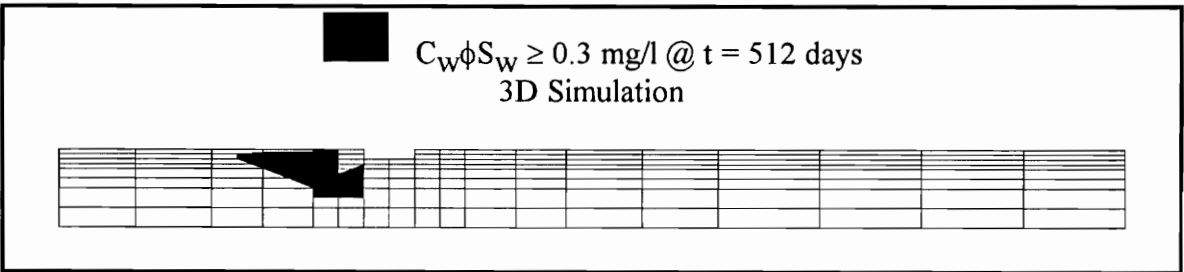


Figure 8.23 Dissolved plume movement after 512 days (3-D simulation).

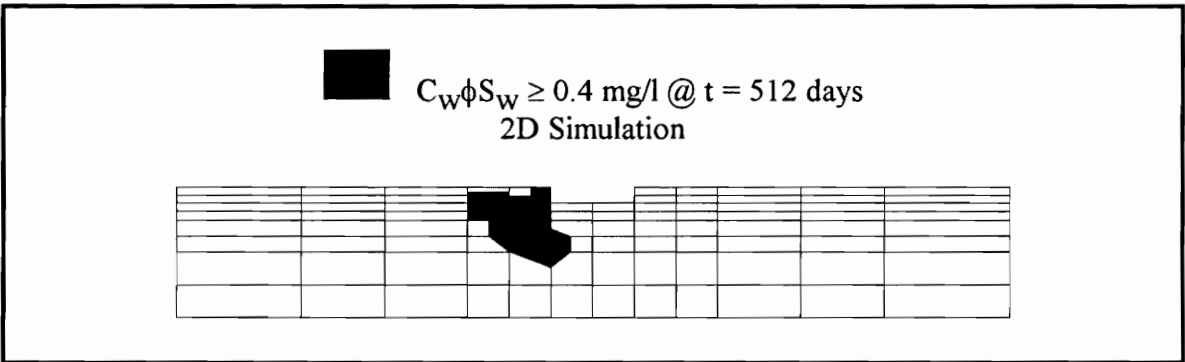


Figure 8.24 Dissolved plume movement after 512 days.

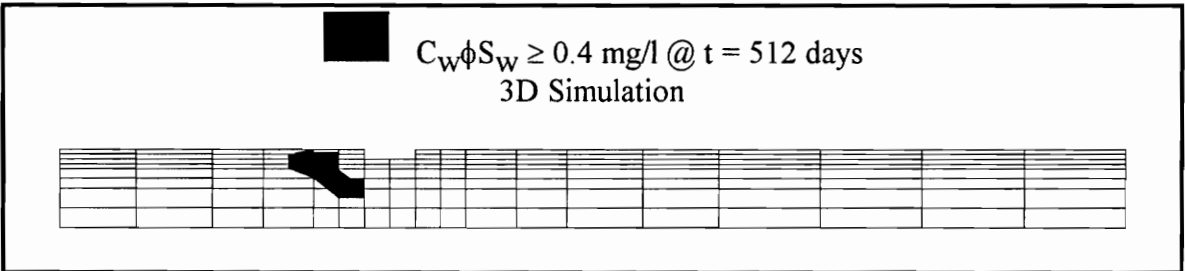


Figure 8.25 Dissolved plume movement after 512 days (3-D simulation).

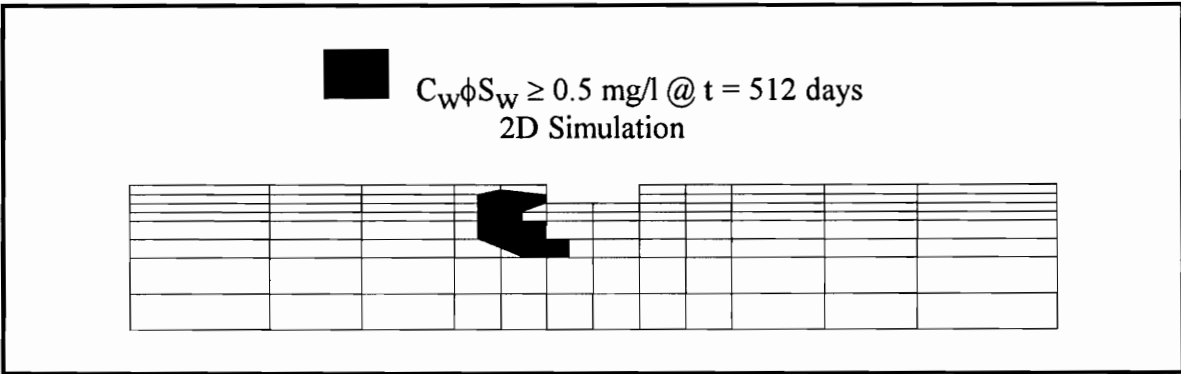


Figure 8.26 Dissolved plume movement after 512 days.

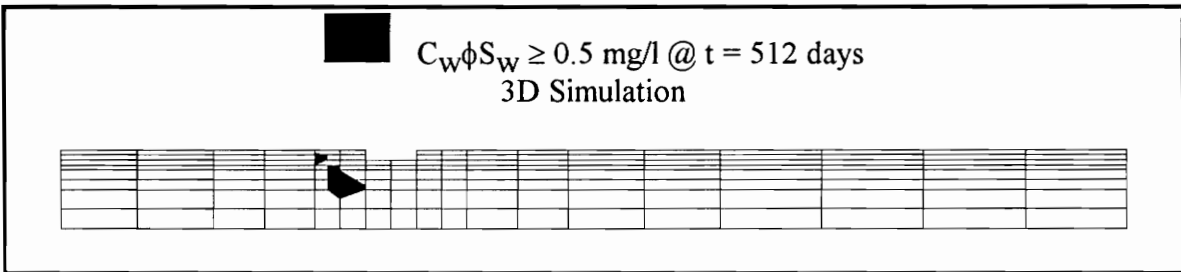


Figure 8.27 Dissolved plume movement after 512 days (3-D simulation).



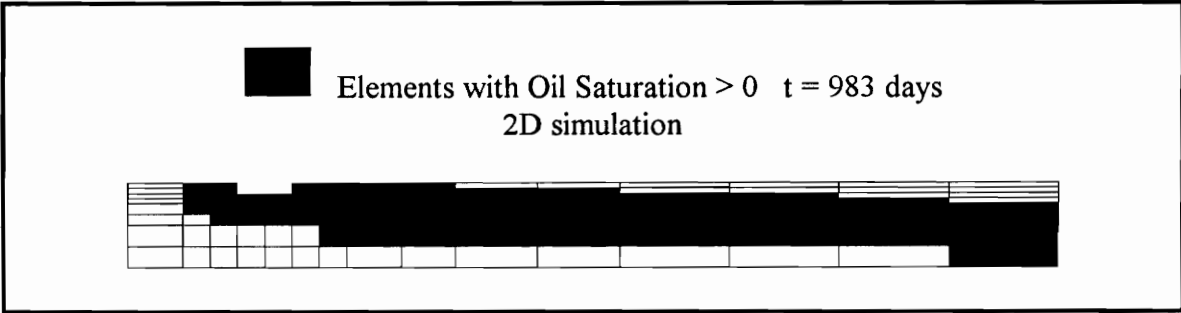


Figure 8.28 Oil plume movement after 983 days.

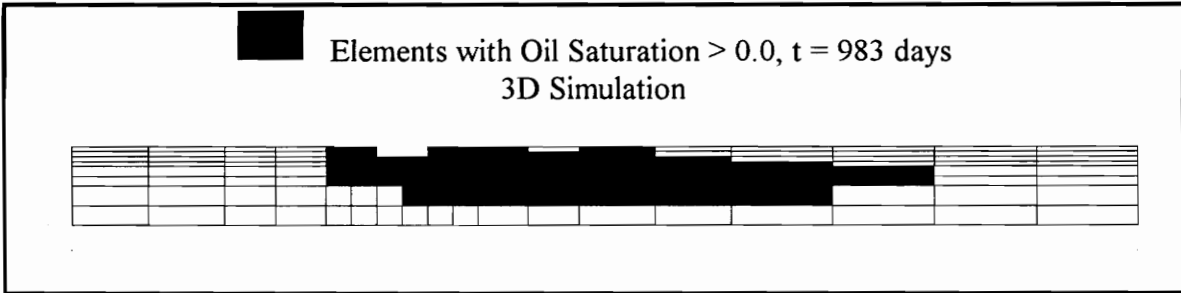


Figure 8.29 Oil plume movement after 983 days (3-D simulation).

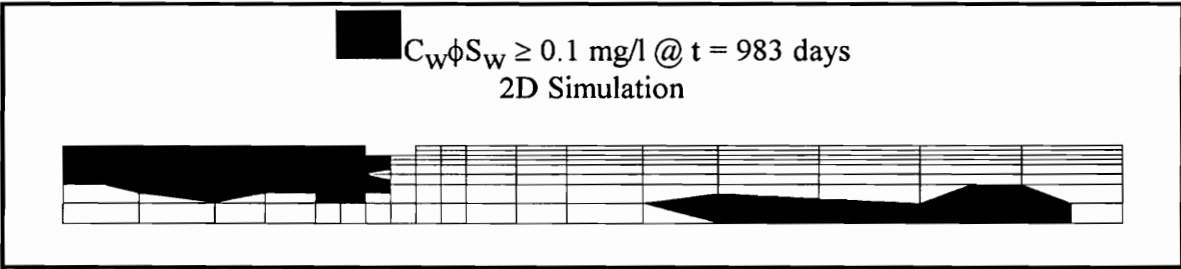


Figure 8.30 Dissolved plume movement after 983 days.

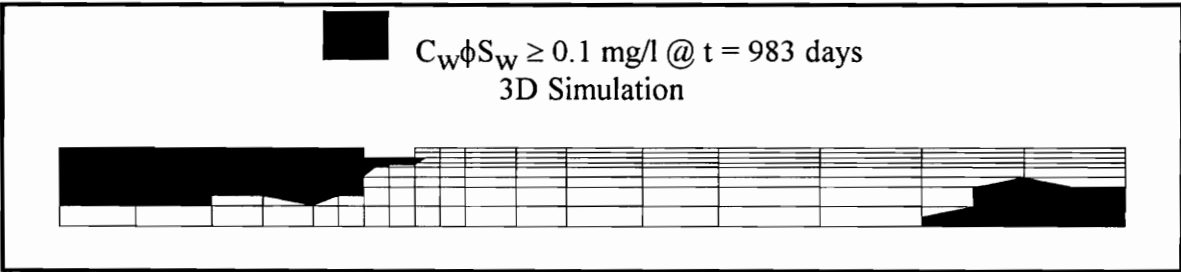


Figure 8.31 Dissolved plume movement after 983 days (3-D simulation).

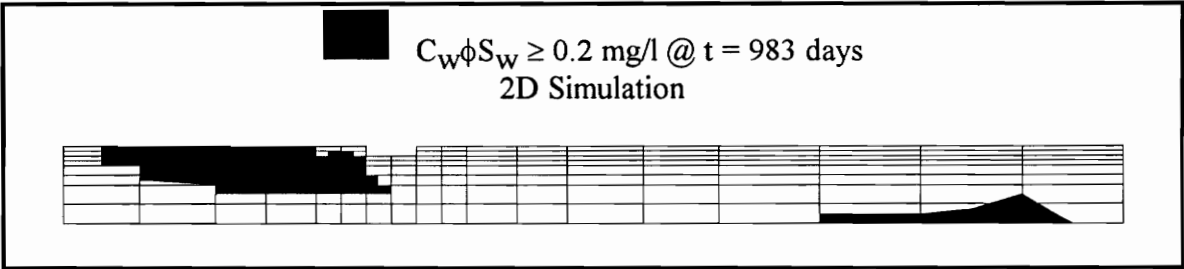


Figure 8.32 Dissolved plume movement after 983 days.

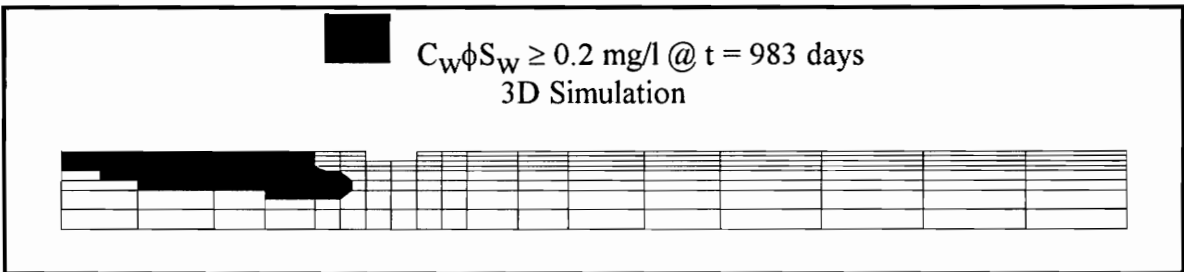


Figure 8.33 Dissolved plume movement after 983 days (3-D simulation).

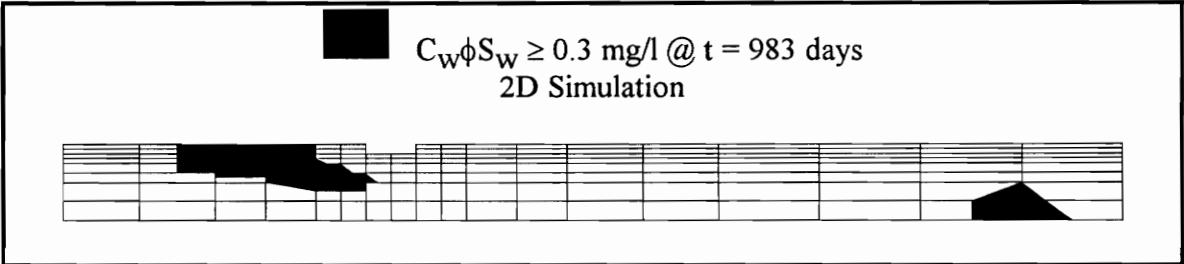


Figure 8.34 Dissolved plume movement after 983 days.

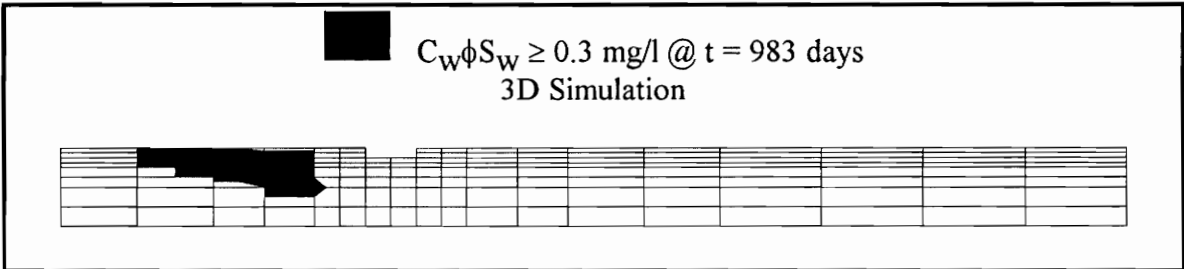


Figure 8.35 Dissolved plume movement after 983 days (3-D simulation).

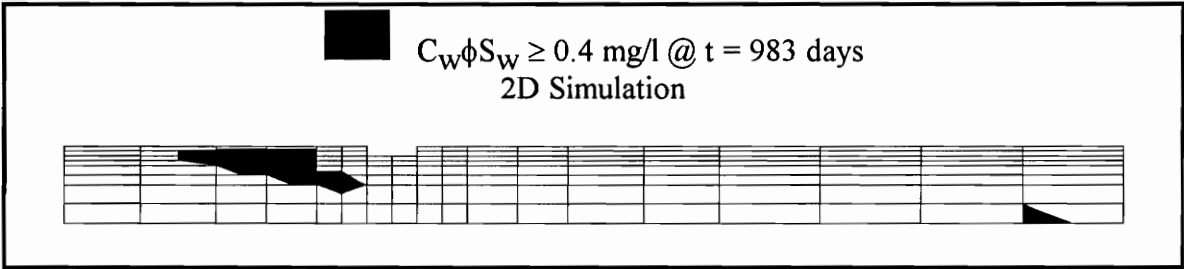


Figure 8.36 Dissolved plume movement after 983 days.

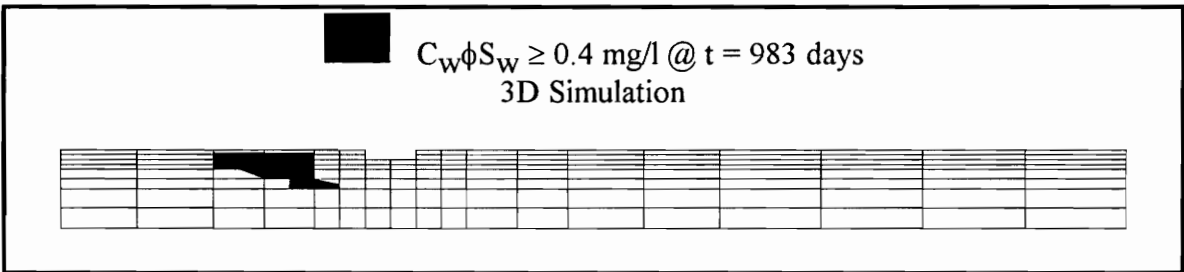


Figure 8.37 Dissolved plume movement after 983 days (3-D simulation).

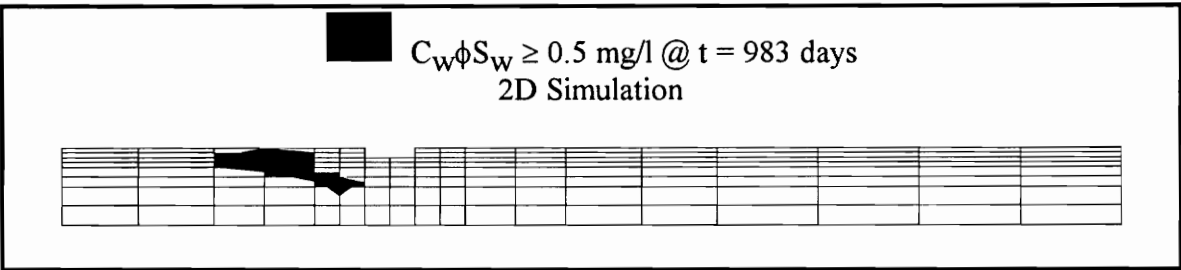


Figure 8.38 Dissolved plume movement after 983 days.

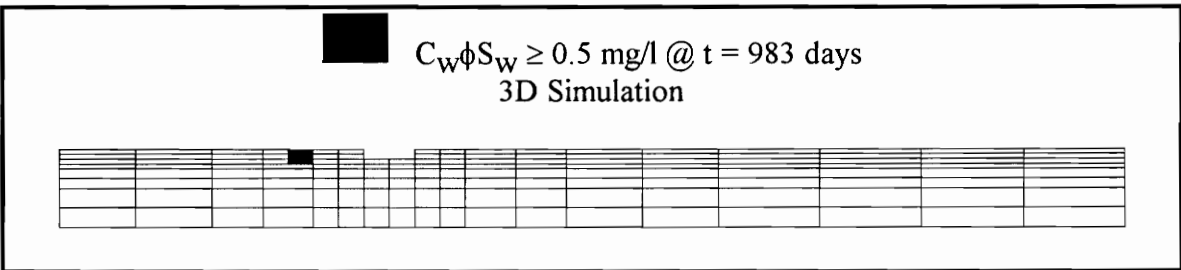


Figure 8.39 Dissolved plume movement after 983 days (3-D simulation).

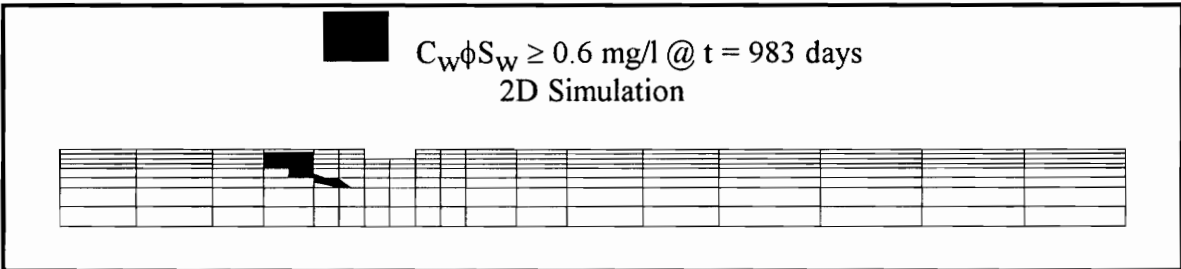


Figure 8.40 Dissolved plume movement after 983 days.

The following three-dimensional simulations are used to investigate the influence the partition coefficients have on the movement of both the discrete oil phase and the dissolved contaminant phase. Figures 8.41-8.53 show the results, in a two-dimensional cross section, of the three-dimensional simulations for a reduced value of the oil-water partition coefficient,  $T_O$ , from  $T_O = 505$  to  $T_O = 105$ . The figures show the movement of oil as a discrete phase as well as a dissolved phase for time levels of 95, 512, and 983 days. Comparing Figures 8.41-8.53 with Figures 8.4-8.40 it is seen that there is less discrete phase and dissolved phase plume movement for a decrease in the oil-water partition coefficient. Along with slowing the plume movement of the dissolved phase, a comparison of the figures also shows a decrease in concentration values within the plume itself. This is true for all the time output levels examined.

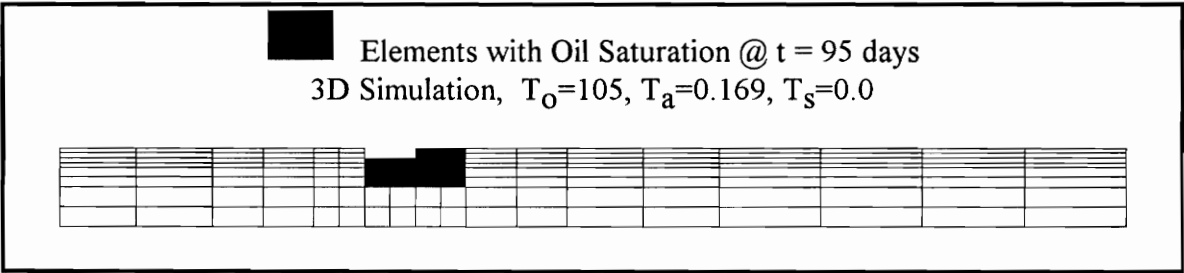


Figure 8.41 Oil plume movement after 95 days.

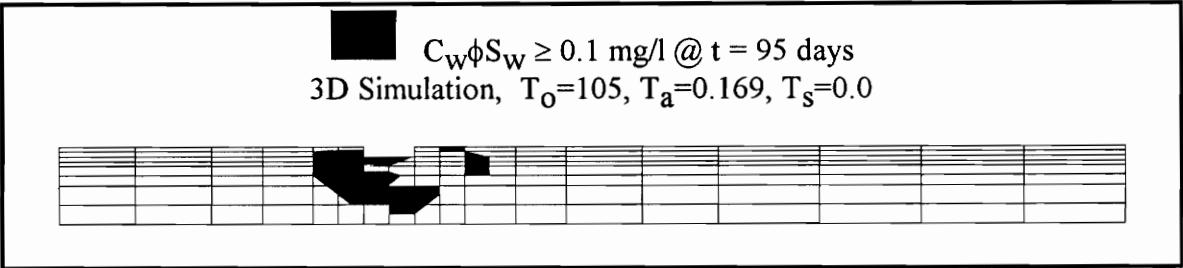


Figure 8.42 Dissolved phase movement after 95 days.

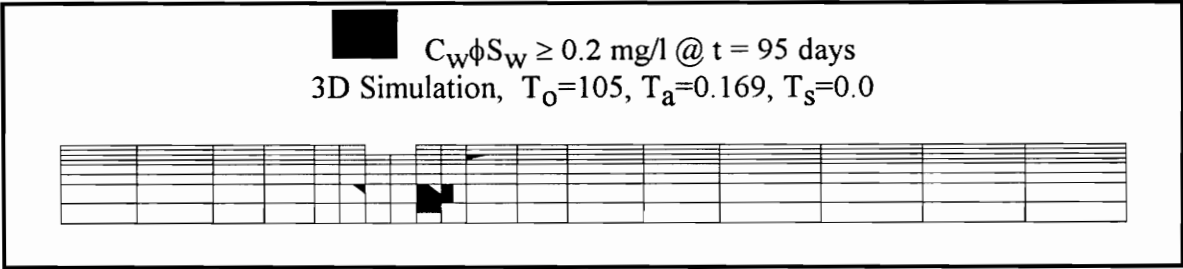


Figure 8.43 Dissolved phase movement after 95 days.

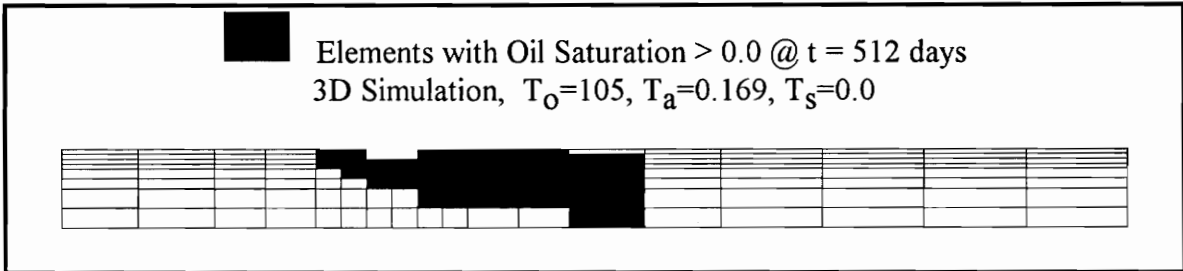


Figure 8.44 Oil plume movement after 512 days.



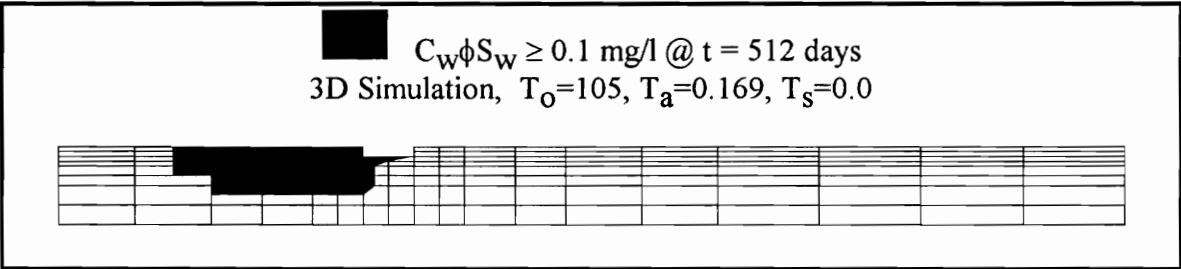


Figure 8.45 Dissolved phase movement after 512 days.

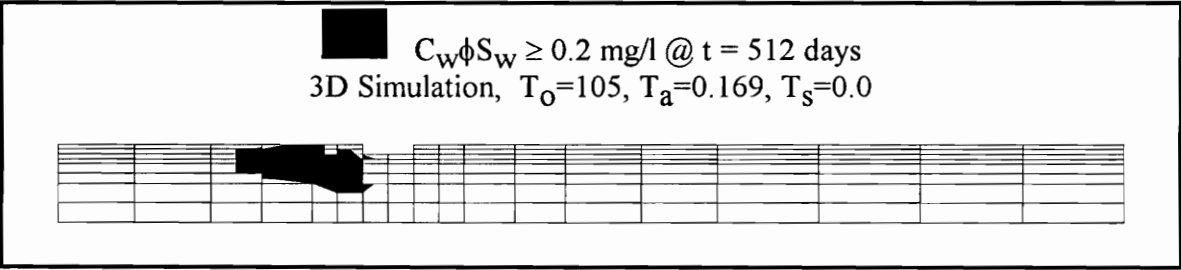


Figure 8.46 Dissolved phase movement after 512 days.

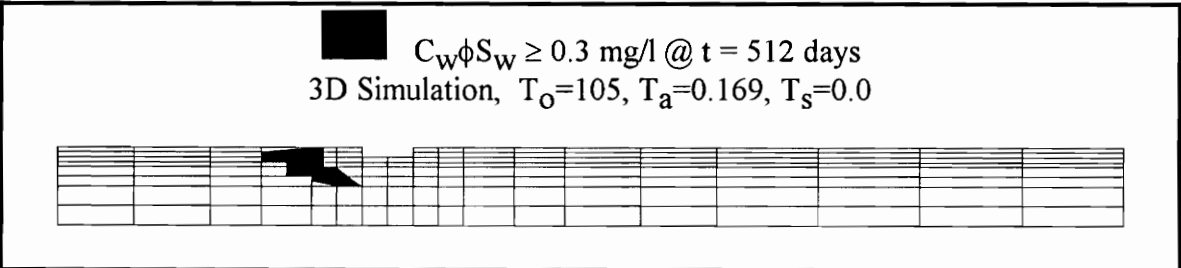
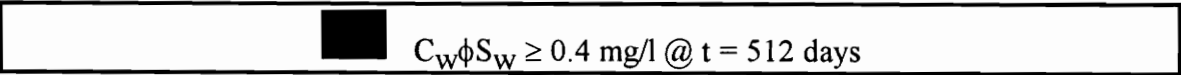


Figure 8.47 Dissolved phase movement after 512 days.



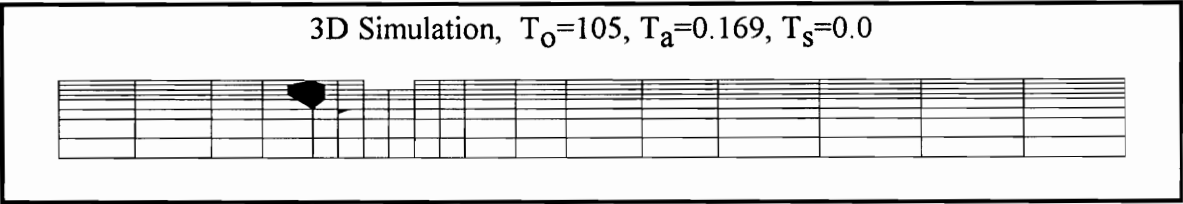


Figure 8.48 Dissolved phase movement after 512 days.

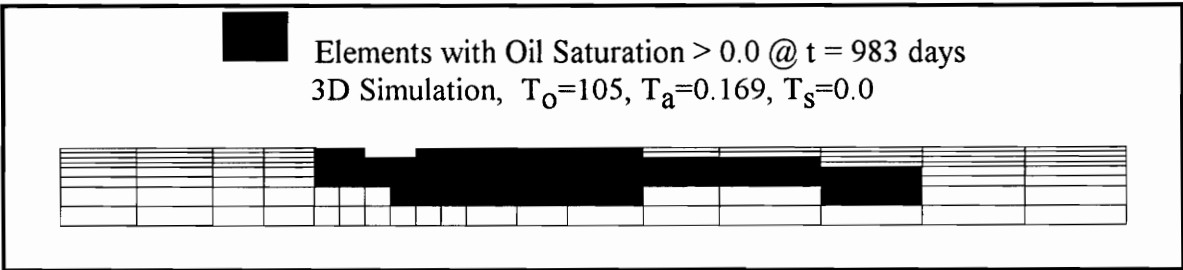


Figure 8.49 Oil plume movement after 983 days.

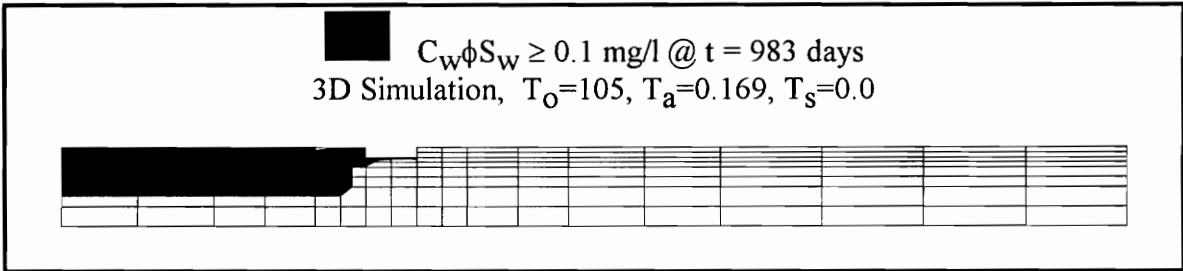
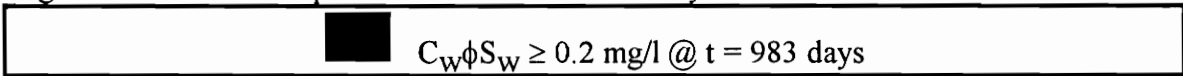


Figure 8.50 Dissolved phase movement after 983 days.



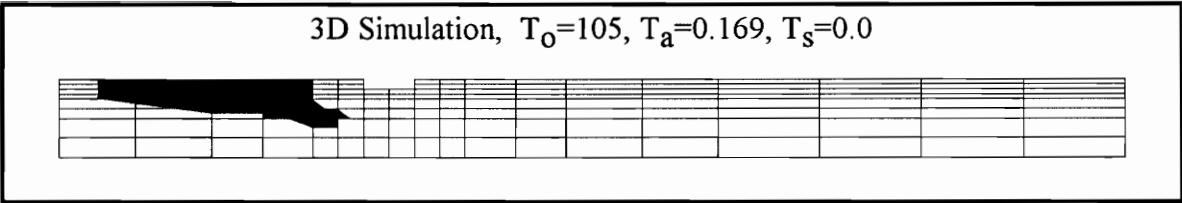


Figure 8.51 Dissolved phase movement after 983 days.

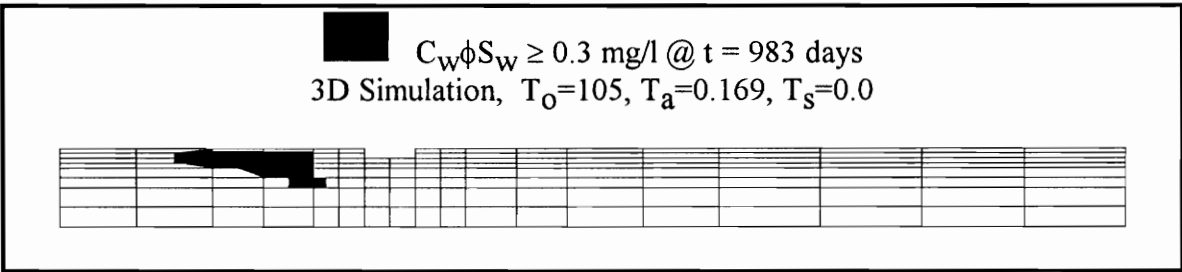


Figure 8.52 Dissolved phase movement after 983 days.

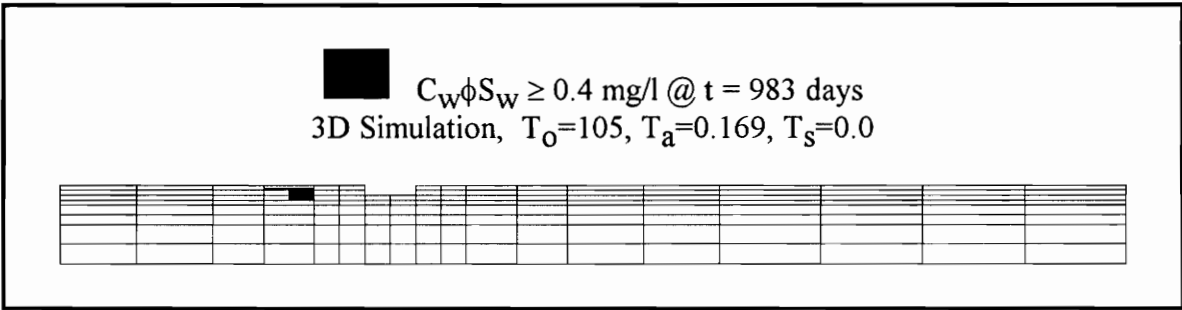


Figure 8.53 Dissolved phase movement after 983 days.

Figures 8.54-8.73 show the results of three-dimensional simulations for an increased air-water partition coefficient,  $T_a$ , with all other partition coefficients kept constant. The partition coefficient for these simulations is increased from  $T_a = 0.169$  to  $T_a = 1.69$ . Comparing Figures 8.54-8.73 with Figures 8.4-8.40, it is seen that increasing the air-water partition coefficient also reduces oil movement in the discrete and dissolved phases, but the decrease in movement shown in these simulations is less than that previously shown for a decrease in the oil-water partition coefficient. This is most prevalent in the concentration values found within the dissolved plume. The simulations resulting from an increase in the air-water partition coefficient of one magnitude resulted in higher concentration values within the dissolved phase as compared to the concentration values found for a decrease in the oil-water partition coefficient of one half a magnitude.

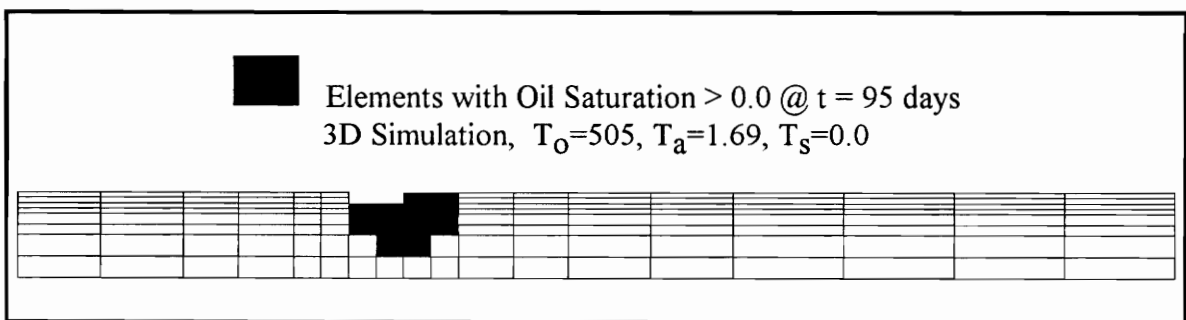


Figure 8.54 Oil plume saturation after 95 days.

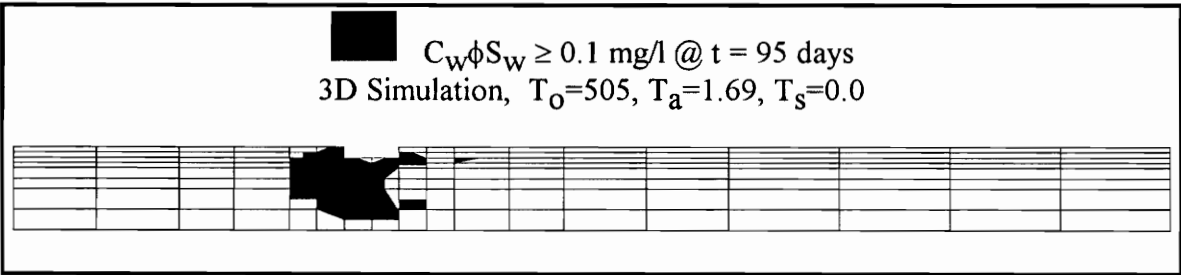


Figure 8.55 Dissolved phase movement after 95 days.

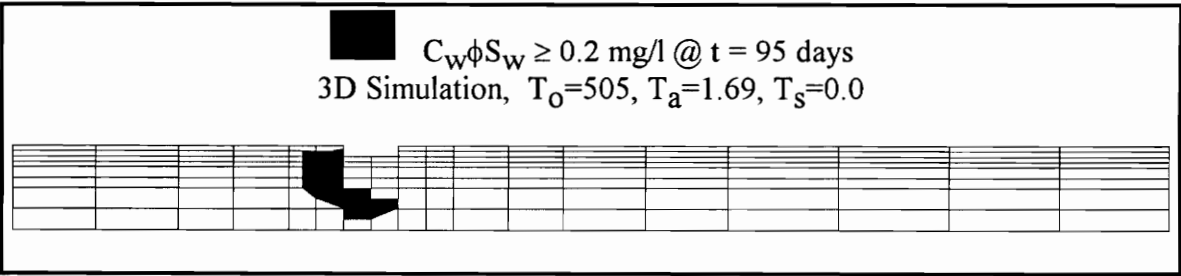


Figure 8.56 Dissolved phase movement after 95 days.

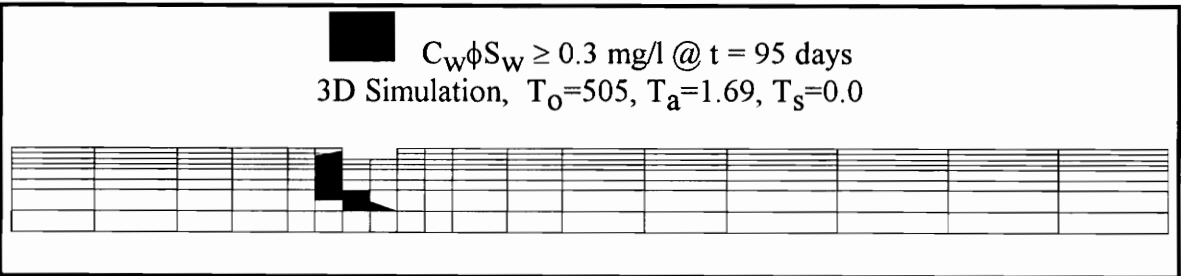


Figure 8.57 Dissolved phase movement after 95 days.

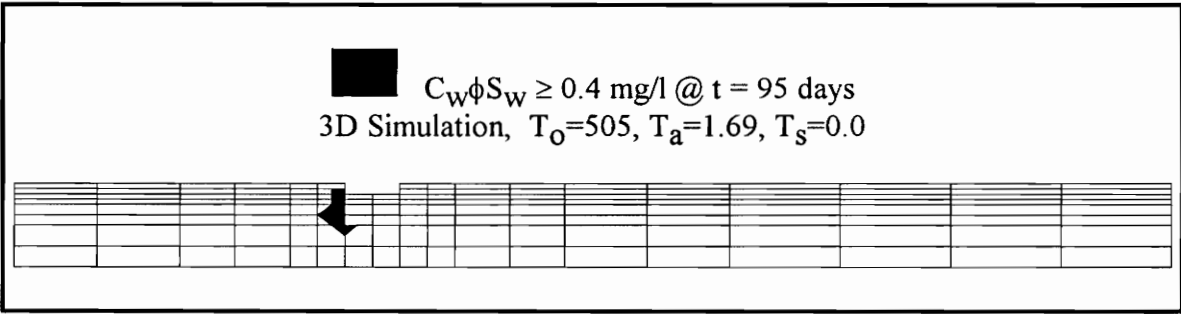


Figure 8.58 Dissolved phase movement after 95 days.

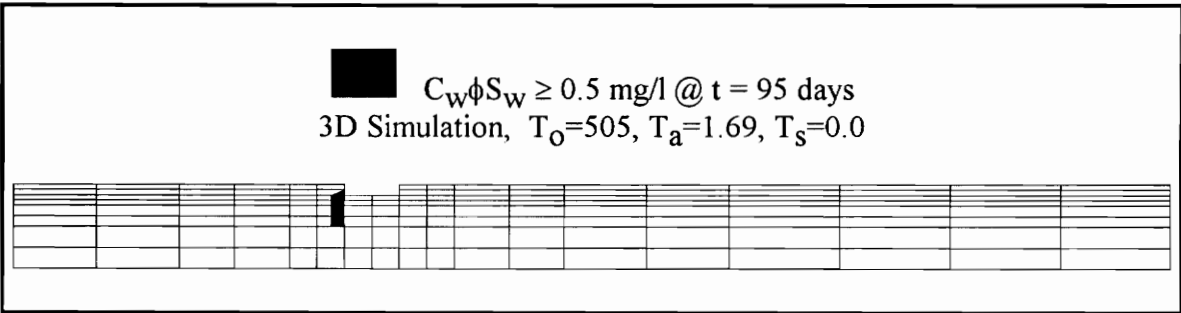


Figure 8.59 Dissolved phase movement after 95 days.

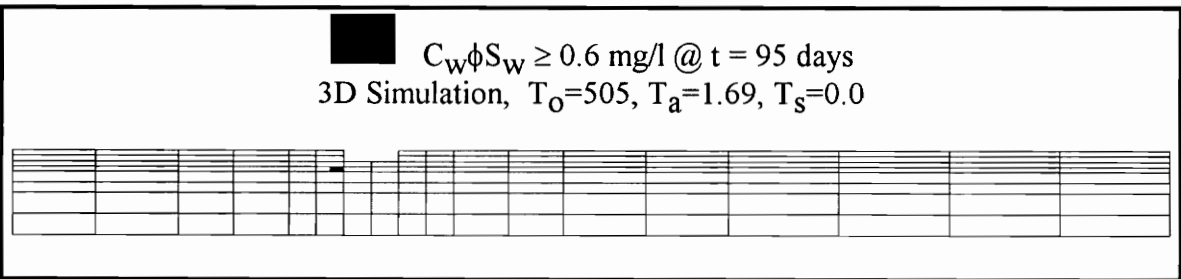


Figure 8.60 Dissolved phase movement after 95 days.

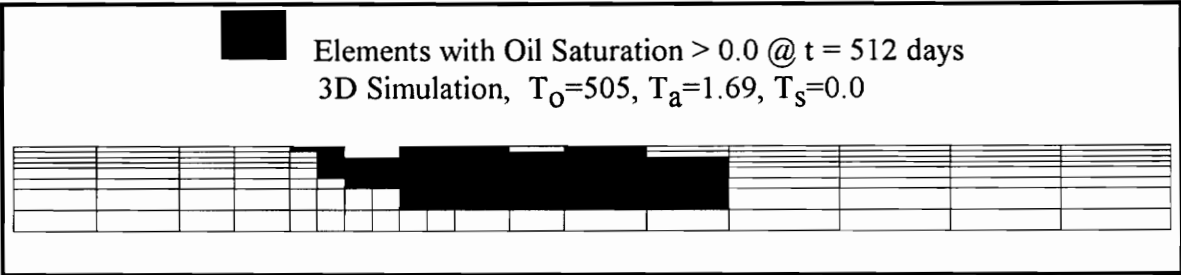


Figure 8.61 Oil plume movement after 512 days.

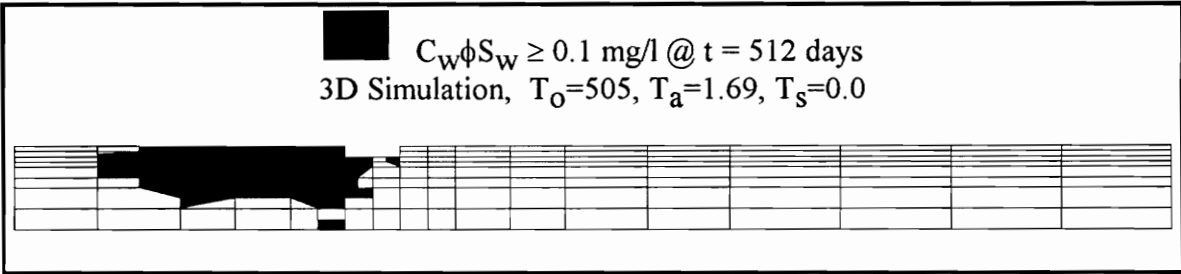


Figure 8.62 Dissolved phase movement after 512 days.

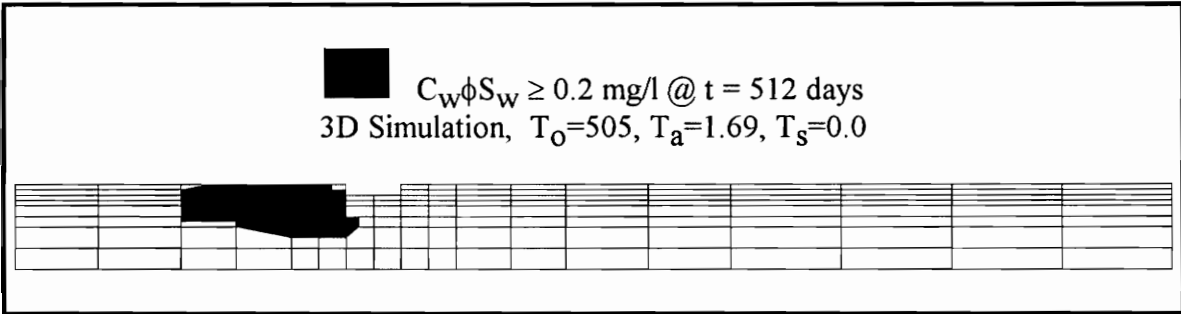


Figure 8.63 Dissolved phase movement after 512 days.

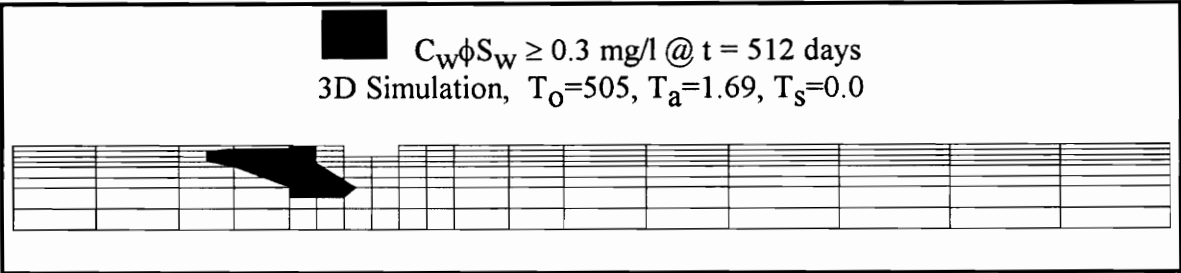


Figure 8.64 Dissolved phase movement after 512 days.

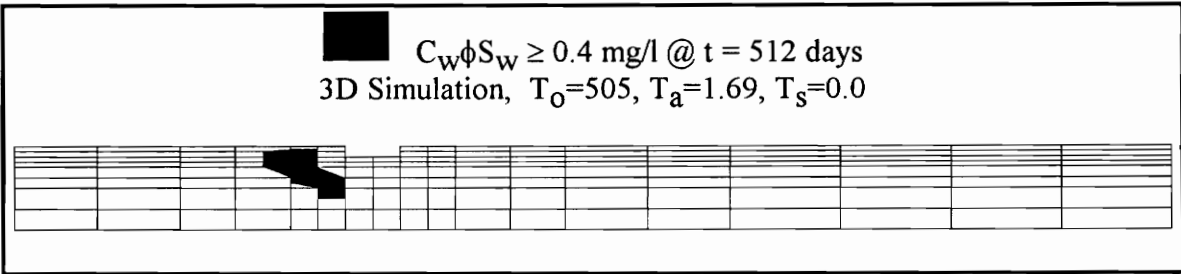


Figure 8.65 Dissolved phase movement after 512 days.

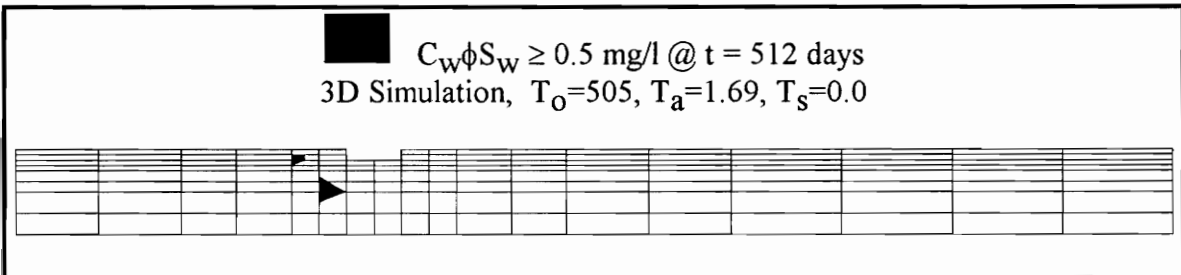


Figure 8.66 Dissolved phase movement after 512 days.



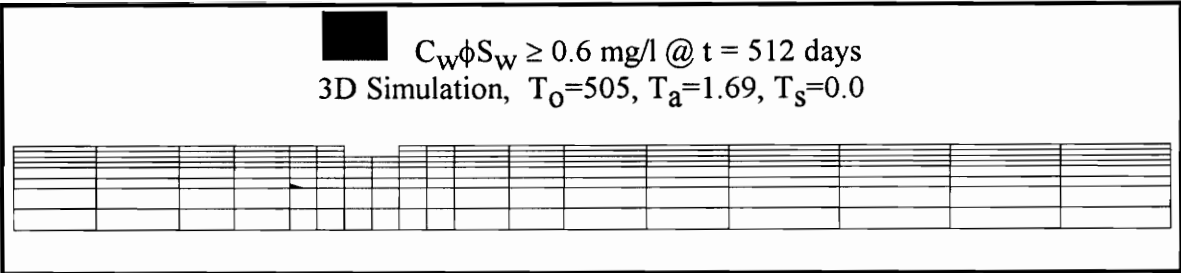


Figure 8.67 Dissolved phase movement after 512 days.

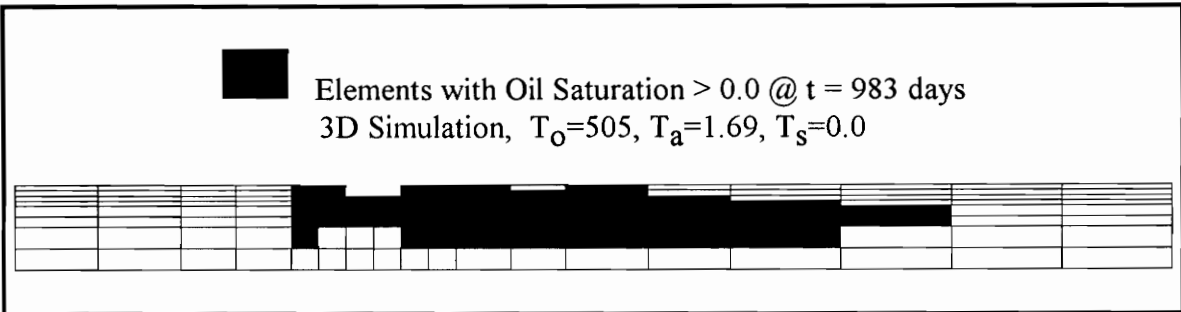


Figure 8.68 Oil plume movement after 983 days.

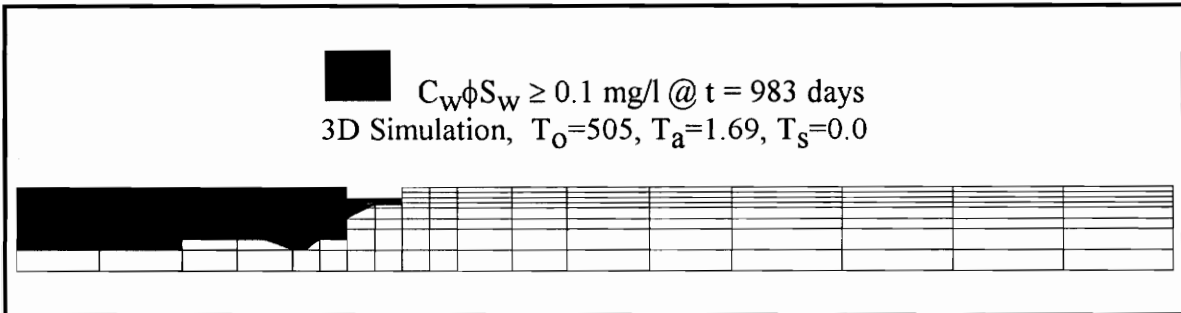


Figure 8.69 Dissolved phase movement after 983 days.

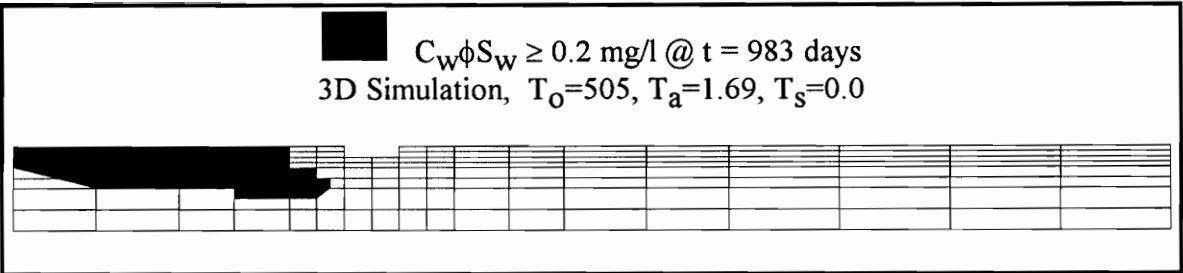


Figure 8.70 Dissolved phase movement after 983 days.

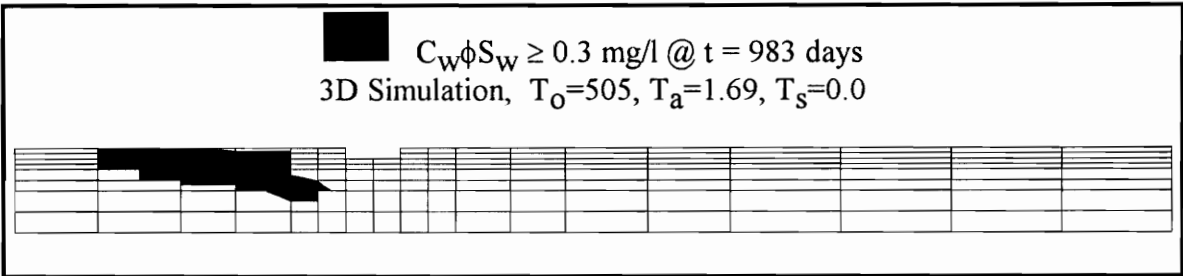


Figure 8.71 Dissolved phase movement after 983 days.

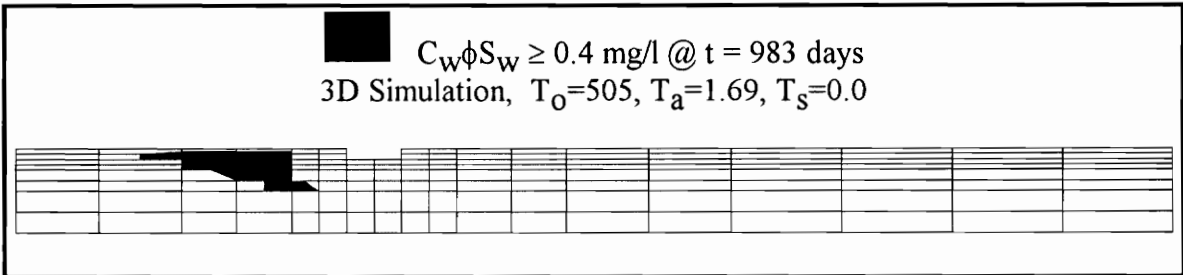


Figure 8.72 Dissolved phase movement after 983 days.

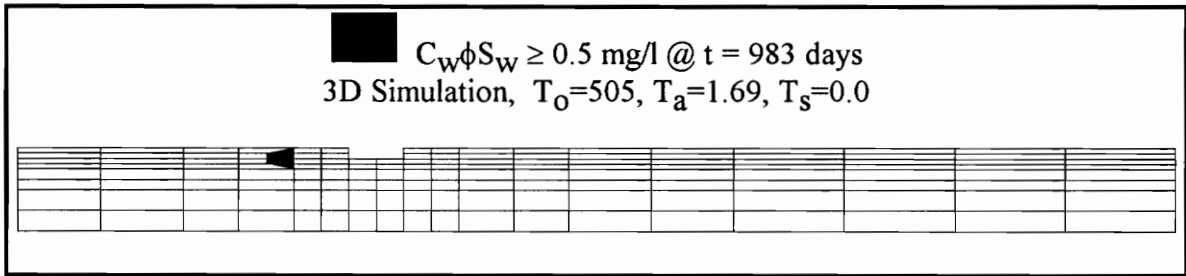


Figure 8.73 Dissolved phase movement after 983 days.

### CONCLUSIONS

Chapter 8 validates the multiphase flow and mass transport finite element formulations presented in Chapters 2, 3, and 7 in a weakly-coupled system. An example problem, similar to the one used in Example 2.2, is used to validate the three-dimensional model for multiphase flow and multicomponent transport based on a comparison with two-dimensional simulations. A comparison of the simulations shows that the three-dimensional model gives similar results to the two-dimensional model in earlier time output levels. The plume movements in the discrete and dissolved phases are both found to be slower in the three-dimensional model, for later time output levels.

The three-dimensional model is then used in to examine the effects of the oil-water and air-water partition coefficients on discrete and dissolved phase plume movements. It is concluded that there is less discrete phase and dissolved phase plume movement for a decrease in the oil-water partition coefficient. In addition to slowing the plume movement of the dissolved phase, a comparison of the figures also shows a decrease in concentration

values within the plume itself. It is also concluded that increasing the air-water partition coefficient reduces oil movement in the discrete and dissolved phases, but the decrease in movement shown in these simulations is less than that previously shown for a decrease in the oil-water partition coefficient. This is most prevalent in the concentration values found within the dissolved plume. The simulations resulting from an increase in the air-water partition coefficient of one magnitude resulted in higher concentration values within the dissolved phase as compared to the concentration values found for a decrease in the oil-water partition coefficient of one half a magnitude

## **CHAPTER 9**

### **SUMMARY AND CONCLUSIONS**

The objective of this thesis is to present and validate a three-dimensional finite element model to be used in solving problems involving multiphase flow and mass transport. The model can be used to simulate three different types of pollution transport problems: (1) multiphase immiscible flow, in underground storage tanks, with the oil phase moving as a discrete plume; (2) dissolved phase movement as a result of diffusion only; and (3) multiphase flow weakly-coupled with mass transport, both discrete and dissolved phase plume movements.

Chapter 2 introduces the concept of multiphase immiscible flow and gives a brief description of the background related to this complex theory that originated in the area of oil exploration engineering. The methodology developed by current researchers (Parker et al. 1987, Kuppusamy et al. 1987, Sheng 1986) is used to develop a three-dimensional finite element model.

The Three-dimensional finite element model is formulated by Galerkin's method. Sections included in this chapter cover the topics of time integration and techniques for non linearity. An evaluation of the effects of convergence on the results of the three-dimensional finite element simulations is made based on the modified Picard's method methods. The modified methods presented in Chapter 3 improved the rate of convergence considerably.

In Chapter 4, the model is compared with a previously validated two-dimensional model and experimental data taken from current literature. The conclusions of these simulations are presented as follows:

- (1) the three-dimensional model shows very similar results to the two-dimensional model for simulations conducted on a one-dimensional column problem;
  - (2) the three-dimensional model shows a reasonable correlation with experimental data from column test results from current literature;
  - (3) the three-dimensional model simulation results are similar to the two-dimensional model simulation results for a two-dimensional UST problem.
- However, slightly slower plume movements for a given time level are observed in the three-dimensional simulation. It is found that this effect tends to increase with an increase in the time output level.

After validation of the three-dimensional model, a fully three-dimensional domain similar to the one used in the two-dimensional simulation (Example 2.2) is used to investigate plume movements in three-dimensions. The simulations show similar but decreased plume movement as compared with the results of the three-dimensional simulations in a two-dimensional setting.

Chapter 5 presents an experimental study using a one-dimensional column test and a two-dimensional flume test. The results of the tests are presented in the initial sections of the chapter, with a comparison made between the multiphase flow column and flume tests and the three-dimensional finite element simulation. The results of the column simulation show a reasonable comparison with the experimental data for the estimated parameters. The differences in estimating the material property parameters are due to the difficulty of effectively and accurately measuring fluid outflow during the testing procedure.

The results of the flume simulations showed a reasonable correlation with the experimental data for the 15 second time output level. Further simulations related to the experimental flume study are being conducted.

The effects on the results of the scaling parameters developed by Parker et al. (1987) is made in the last section of Chapter 5. It is found that as the parameter  $\beta_{ow}$  is increased from 1.2 to 3.2, the value of outflow of water also tends to increase by 30 to 36 %. Similarly, as the parameter  $\beta_{ao}$  is decreased from 4.5 to 2.5, the value of water outflow for the simulations tends to increase by 10 to 30 %.

Chapter 6 introduces the convective-dispersive theory used for mass transport in an unsaturated air-water system. This set of equations is reduced to a system that considers only diffusion. The three-dimensional finite element analysis for mass transport through diffusion is also presented and the solution process is discussed. A comparison of the three-dimensional formulation is then made with the previously formulated two-dimensional model. The comparison shows an excellent correlation, and is the basis for validation of the three-dimensional model.

Chapter 7 presents the three-dimension finite element formulation for multiphase flow and transport, in a weakly-coupled system. The model presented here is derived from van Genuchten's model for unsaturated flow and is based on the saturation-pressure-conductivity relations coupled with pollutant mass transport for the three-phase system.

In Chapter 8, an example problem is used to validate the three-dimensional model based on two-dimensional simulations. A comparison of the simulations shows that the three-dimensional model gives results similar to the two-dimensional model for the time output levels studied. The plume movements in the discrete and dissolved phases are both found to be slower in the three-dimensional model as compared to the two-dimensional model.

The three-dimensional model is then used in to examine the effects of the air-water and oil-water partition coefficients on discrete and dissolved phase plume movements. It is concluded that there is less discrete phase and dissolved phase plume movement for a decrease in the oil-water partition coefficient. In addition to slowing the plume movement of the dissolved phase, a comparison of the relevant figures also shows a decrease in concentration values within the dissolved plume itself. It is concluded that increasing the air-water partition coefficient also reduces oil movement in the discrete and dissolved phases, but the decrease in movement shown in these simulations is less than that shown for a decrease in the oil-water partition coefficient. This is most prevalent in the concentration values found within the dissolved plume. The simulations resulting from an increase in the air-water partition coefficient of one magnitude resulted in higher concentration values within the dissolved phase as compared to the concentration values found for a decrease in the oil-water partition coefficient of one half a magnitude.

Future studies in the area of three-dimensional analysis of multiphase flow and mass transport should focus on a formulation that models the equations in a fully-coupled system. This will involve solving for the unknown head and concentration terms simultaneously. Further studies should also involve investigating the effects of the model parameters, as well as, introduction of biodegradation terms into the constitutive model. Modifications involving both pre- and post-processing systems would also be useful in evaluation of the three-dimensional model.



## REFERENCES

- Abriola, L. M., and Pinder, G. F., "A Multiphase Approach to the Modeling of Porous Media Contamination by Organic Compounds 1. Equation Development," *Water Resources Research*, Vol. 21, No. 1, pp. 11-18, January, 1985a.
- Abriola, L. M., and Pinder, G. F., "A Multiphase Approach to the Modeling of Porous Media Contamination by Organic Compounds 2. Numerical Simulation," *Water Resources Research*, 21, No. 1, pp. 19-26, January, 1985b.
- Acar, Y. B., Hamidon, A. B., Field, S. D., and Scott, L., "The effect of organic fluids on hydraulic conductivity of compacted kaolinite, Hydraulic Barriers in Soil and Rock," *ASTM Spec. Tech. Publ.*, 874, 171-187, 1985.
- Ahmad, F., Numerical Modeling of Transport of Pollutant Through Soils. Thesis for Master of Science degree, Published by Virginia Tech, 1991.
- Baehr, A. L., and Corapcioglu, Y. M. "A Compositional Multiphase Model for Ground water Contamination by Petroleum Products 2. Numerical Solution," *Water Resources Research*, vol. 23, no. 1, pp. 201-213, January, 1987.
- Baker, L. E., "Three-phase relative permeability correlations," *Pap. SPE/DOE 17369*, pp. 539-554, *Soc. of Pet. Eng.*, Dallas, Tex., 1988.
- Bear, J., Dynamics of Fluids in Porous Media. Elsevier, New York, 1972.
- Bear, J., Zaslavsky, D., and Irmay, S., Physical Principles of Water Percolation and Seepage, UNESCO, Paris, 1968.
- Belytschko, T and Liu, W. K. "Computational Methods for Analysis of Transient Response," *Recent Advances in Engineering Mechanics and Their impact on Civil Engineering Practice*, Ed. by Chen, W. F. and Lewis, A. D. M., Vol. 1, *Purdue University*, May, 1983.
- Biggar, J. W. and Nielson, D. R., "Spatial Variability of the Leaching Characteristics of a Field Soil," *Water Res. Research*, Vol. 12, 1967.
- Biot, M. A., "Consolidation Settlement Under a Regular Load Distribution," *Journal of Applied Physics*, Vol. 12, pp. 426-430, 1941.

- Bolt, G. H., and Groenevelt, P. H., "Coupling Phenomena as a Possible Cause for Non-Darcian Behavior of Water in Soil," *Bull. IASH*, No. 2, Vol. 14, pp. 17-26, 1969.
- Brooks, R. H., and Corey, A. T., "Hydraulic Properties of Porous Media," *Hydrology Paper no. 3*, Civil Engineering Dept., Colorado State University, Fort Collins, Colo, 1964.
- Burdine, H. T., "Relative Permeability Calculations From Pore-size Distribution Data," *Trans. Soc. Pet. Eng. AIME*, 198, pp. 71-77, 1953.
- Burnett, R. D., and Frind, E. O., "Simulation of Contaminant Transport in Three-Dimensions 1. The Alternating Direction Galerkin Technique," *Water Resources Research*, Vol. 23, No. 4, pp. 683-694, April, 1987a.
- Burnett, R. D., and Frind, E. O., "Simulation of Contaminant Transport in Three-Dimensions 2. Dimensionality Effects," *Water Resources Research*, Vol. 23, No. 4, pp. 695-705, April, 1987b.
- Collins, R. E., Flow of Fluids Through Porous Materials. Reinhold, NY, 1961.
- Corapcioglu, Y. M., and Baehr, A. L. "A Compositional Multiphase Model for Ground Water Contamination by Petroleum Products 1. Theoretical Considerations," *Water Resources Research*, vol. 23, no. 1, pp. 191-200, January, 1987.
- Corey, A. T., Mechanics of Immiscible Fluids in Porous Media. Water Resources Publications, Littleton, Colo., 1986.
- Corey, A. T., Rathjens, C. H., Henderson, J. H., and Wyllie, M. R. J. "Three-Phase Relative Permeability," *Trans. Soc. Pet. Eng. AIME*, Vol. 207, pp. 349-351, 1956.
- de Marsily, G., Quantitative Hydrology, Academic Press, Inc., 1986.
- EPA, "Transport and Fate of Contaminants in the Subsurface," Seminar Publication, Center for Environmental Research Information, Cincinnati, OH, 1989.
- Edwards, M. F., and Richardson, J. F., "Gas Dispersion in Packed Beds," *Chem. Eng. Sci.*, 23, pp. 67-85, 1968.
- Faust, C. R., "Transport of Immiscible Fluid within and Below the Unsaturated Zone: A Numerical Model," *Water Resources Research*, Vol. 21, pp. 587-596, 1985.
- Freeze, R. A. and Cherry, J. A., Ground water. Prentice-Hall, Englewood Cliffs, NJ, 1979.

- Fried, J. J., Ground water Pollution. Elsevier, New York, NY, 1975.
- Gibson, I. "Procedures and Results of Seepage Column and Tank Tests," paper on experimental study at Virginia Tech involving flow characteristics of gasoline and water, Dec., 1992.
- Gillham, R. W., "The Capillary Fringe and Its Effect on Water-table Response," *Journal of Hydrology*, Vol. 67, pp. 307-324, 1984.
- Gillham, R. W., and Cherry, J. A., "Contaminant Migration in Saturated Unconsolidated Geologic Deposits," *Recent Trends in Hydrology*, T. N. Narasimhan, Editor. Geological Society of America Special Paper 189, pp. 31-62, 1982.
- Griffiths, C. D. F., and Mitchell, A. R. "Finite Element Methods for Second Order Differential Equations with Significant First Derivatives," *International Jour. for Numerical Meth. in Eng.*, Vol. 10, pp. 1389-1396, 1976.
- Havercamp, R., and Parlange, J. Y., "Prediction of water retention curve from particle size distribution, 1. Sandy soils without organic matter," *Soil Science*, 142, pp. 325-339, 1986.
- Harleman, D. R. F., Mellhorn, P. F., and Rumer, R. R. "Dispersion-Permeability Correlation in Porous Media," *Journal of Hydraulics Div., Amer. Soc. Civil Eng.*, 89, pp. 67-89, 1963.
- Hiby, J. W., "Longitudinal and Transverse Mixing During Single-Phase Flow Through Granular Beds," *Interaction between fluids and particles*. Institute of Chemical Engineers, London, Symp. Ser., No. 9, pp. 312-325, 1962.
- Hochmuth, D. P., "Two-Phase Flow of Immiscible Fluids in Ground-water Systems," Thesis presented to Colorado State University, Fort Collins, Colorado in partial fulfillment of the requirements for the degree of Master of Science, 1981.
- Hochmuth, D. P. and Sunada, D. K., "Ground water Model for Two-Phase Immiscible Flow in Course Material," *Ground Water*, 23(5), 617-626, 1985.
- Hughes, T., The Finite Element Method, Linear Static and Dynamic Finite Element Analysis. Prentice Hall Inc., Englewood Cliffs, NJ, 1987.
- Huyakorn, P. S., "Solution of Steady-State, Convective Transport Using an Upwind Finite Element Scheme," *Appl. Math. Modeling*, Vol. 1, pp. 189-195, March, 1977.

- Huyakorn, P. S. and Pinder, G. F., Computational Methods in Subsurface Flow. Academic Press, New York, 1983.
- Huyakorn, P. S., and Nikulha, K., "Solution of Transient Transport Equation Using an Upstream Finite Element Scheme," Appl. Math. Modeling, Vol. 3, February, 1979.
- Jenson, O. K., and Finlayson, B. A., "Oscillation Limits for Weighted Residual Methods Applied to Convective Diffusion Equations," International Journal for Numerical Meth. in Eng., Vol. 15, pp. 1681-1689, 1980.
- Kaluarachchi, J. J., and Parker, J. C., "Effects of Hysteresis on Water Flow in the Unsaturated Zone," Water Resources Research, 23, pp. 1967-1976, 1987.
- Kaluarachchi, J. J., and Parker, J. C., "An Efficient Finite Element Method for Modeling Multiphase Flow," Water Resource Res., 25, pp. 42-54, 1989.
- Kaluarachchi, J. J., and Parker, J. C., "Modeling Multicomponent Organic Chemical Transport in Three-Fluid-Phase Porous Media," Journal of Cont. Hydr., 5, pp. 349-374, 1990.
- Kool, J. B., and Parker, J. C., "Development and Evaluation of Closed-form Expressions for Hysteretic Soil Hydraulic Properties," Water Resources Research, 23, pp. 105-114, 1987.
- Kool, J. B., and Parker, J. C., "Analysis of the Inverse Problem for Unsaturated Transient Flow," Water Resources Research, 24, pp. 817-830, 1988.
- Kool, J. B., Parker, J. C., and van Genuchten, M. Th., "Determining Soil Hydraulic Properties from One-Step Outflow Experiments by Parameter Estimation: I theory and Numerical Studies," Soil Science Society of America Journal, Vol. 49, 1985.
- Kuppusamy, T., Sheng, J., Parker, J. C., and Lenhard, R. J., "Finite Element Analysis of Multiphase Immiscible Flow Through Soils," Water Resources Research, April, 1987.
- Kuppusamy, T and Lien, B. H., IFTP2D -- A Finite Element Program for Two-Dimensional Three-Phase Immiscible Flow and Transport Problem. published in Virginia Tech, August, 1987.
- Kutilek, M., "Non-Darcian flow of water in soils (Laminar Region)," 1st IAHR Symp., Fundamentals of Transport Phenomena in Porous Media, Haifa, Israel, 1969.

- Lehman, John P., "Leaking Underground Storage Tanks," First Public Briefing on the 1984 Amendments of the Resource Conservation and Recovery Act, 1984.
- Lenhard, R. J. and Parker, J. C., "Measurement and Prediction of Saturation-Pressure Relationships in Three-Phase Media Systems," J. Contaminant Hydrol., 1987a.
- Leverett, M. C., "Capillary behavior in porous solids," Trans. Amer. Inst. Min. Metall. Pet. Eng., 142, pp. 152-169, 1941.
- Low, P. F., "Physical chemistry of clay-water interaction," Advan. in Agron., 13, pp. 269-327, 1961.
- Lyman, W. J., Reehl, W. F., and Rosenblatt, D. H. Handbook of Chemical Property Estimation Methods. McGraw-Hill, New York, 1982.
- Milestone, S. B., Influence of Cementation to Liquefaction Resistance, thesis for M.E. Virginia Polytechnic Institute and State University, 1985.
- Mualem, Y., "A New Model for Predicting the Hydraulic Conductivity of Unsaturated Porous Media," Water Resources Research, Vol. 12, No. 3, June, 1976.
- Mull, R., "Migration of Oil Products in the Subsoil with regard to Ground water Pollution by Oil," in Advances in Water Pollution Research, pp. 1-8, Pergamon, New York, 1971.
- National Research Council, Ground Water Models: Scientific and Regulatory Applications, National Academy Press, Washington, D.C., 1990.
- Osborne, M. and Sykes, J., "Numerical Modeling of Immiscible Organic Transport at the Hyde Park Landfill," Water Resources Res., 22(1), pp. 25-33, 1986.
- Parker, J. C., "Multiphase Flow and Transport in Porous Media," Reviews of Geophysics, 27, 3, pp. 311-328, August, 1989.
- Parker, J. C. Unpublished information received during a conversation with Dr. Parker by the Author during the fall semester of 1992, Virginia Polytechnic Institute and State University, 1992.
- Parker, J. C., Kool, J. B., and van Genuchten, M. Th., "Determining Soil Hydraulic Properties from One-Step Outflow Experiments by Parameter Estimation: II Experimental Studies," Soil Science Society of America Journal, Vol. 49, No. 6, November-December, pp. 1354-1359, 1985.

- Parker, J. C., and Lenhard, R. J., "A Model for Hysteretic Constitutive Relations Governing Multiphase Flow, 1. Saturation-Pressure Relations," *Water Resource Res.*, 23(12), pp. 2187-2196, 1987.
- Parker, J. C., and Lenhard, R. J., "A Model for Hysteretic Constitutive Relations Governing Multiphase Flow, 2. Permeability-Saturation Relations, *Water Resource Res.*, 23(12), pp. 2197-2206, 1987.
- Parker, J. C., Lenhard, R. J., and Kuppusamy, T., "A Parametric Model for Constitutive Properties Governing Multiphase Flow in Porous Media," *Water Resources Research*, pp. 618-624, April, 1987.
- Rose, D. A., "Hydrodynamic Dispersion in Porous Materials," *Soil Science*, Vol. 123, No. 5, pp. 277-283, 1977.
- Ryan, P.A., and Cohen, Y., "One-Dimensional Transport of a Non Aqueous Phase Liquid Containing Sparingly Water Soluble Organics: A Front-Tracking Model," *Water Resources Research*, vol. 27, no. 7, pp. 1487-1500, July, 1991.
- Saffman, P. G., "Dispersion Due to Molecular Diffusion and Macroscopic Mixing in Flow Through a Network of Capillaries," *Journal of Fluid Mechanics*, Vol. 7, pp. 194-208, 1960.
- Schwartz, F. W., "Macroscopic Dispersion in Porous Media: The Controlling Factors," *Water Resources Research*, Vol. 13, No. 4, August, 1977.
- Shamir, V. and Dagan, G., "Motion of the sea water interface in coastal aquifers: A numerical solution." *Water Resources Research*, V. 78, no. 3, pp. 655-657, 1971.
- Saraf, D. N., Measurement of Fluid Saturations by Nuclear Magnetic Resonance and its Application to Three-Phase Relative Permeability Studies," Ph.D. thesis, U. of Calif., Berkeley, 1966.
- Sheng, Jopan, "Multiphase Immiscible Flow Through Porous Media," A Ph.D. dissertation published in Virginia Polytechnic Institute and State University, Blacksburg, Va., 1986.
- Snell, R. W., "Three-Phase Relative Permeability in Unconsolidated Sand," *J. Inst. of Pet.* p.80, 1962.
- Stone, H. L., "Probability Model for Estimating Three-Phase Relative Permeability," *J. of Pet Tech.*, pp. 214-218, 1970.

- Stone, H. L., "Estimation of Three-Phase Relative Permeability and Residual Oil Data," J. Can Pet Technol., 12, pp. 53-61, 1973.
- Swartzendruber, D., "Non-Darcy Flow in Liquid-saturated Porous Media," J. Geophysics. Res., No. 13, 67, pp. 5205-5213, 1962.
- Tejada, S., "Underground Tanks Contaminate Ground Water," EPA Journal, Vol. 10, No. 1, January-February, pp. 20-22, 1984.
- USA Today, "Group Warns of Petroleum Danger," Section A3, Wednesday March 17, 1993.
- Van Dam, J., "The Migration of Hydrocarbons in a Water-Bearing Stratum," The Joint Problems of the Oil and Water Industries, edited by P. Hepple, pp. 55-58, Institute of Petroleum, London, 1967.
- van Genuchten, M. Th., "Calculating the Unsaturated Hydraulic Conductivity with a New Closed Form Analytical Model," Research Report 78-WR-08, Water Resources Program, Dept. of Civil Eng., Princeton Univ., Princeton NJ, 1978a.
- van Genuchten, M. Th., "A Closed-form Equation for Predicting the Hydraulic Conductivity of Unsaturated Soils," Soil Science Society of America Journal, Vol. 44, No. 5, September, 1980.
- Von Engelhardt, W. and Tunn, W. L. M., "The Flow of Fluids Through Sandstones," Transl. by P. A. Witherspoon from Heidelberger Beitr. Mineral Petrol., 2, 111, State Geol. Survey, Circular 194, pp. 12-25, 1955.
- Ward, J. C., "Turbulent Flow in Porous Media," Proc. Amer. Society of Civil Eng., No. HY5, 90, pp. 1-12, 1964.
- Weast, R. C., (ed.), Handbook of Chemistry and Physics, CRC Press, Boca Raton, Florida, 1985.

## **Vita**

The author was born on December 14, 1967 in Ridgewood, New Jersey. He attended grade school and high school in Franklin Co., Virginia. After graduating from Franklin Co., High School in May, 1986, he entered Virginia Tech's Civil Engineering program. As an undergraduate, the author co-oped with Roanoke County Utility Department. He received his B.S. in Civil Engineering in May of 1991. The author is currently completing a M.S. in civil engineering under the department of Geotechnical Engineering. He is a member of the ASCE, NSPE, and Chi Epsilon.

A handwritten signature in black ink, appearing to read 'K. E. Epsilon', is centered on the page.